SOFT ROUTES TO INORGANIC FRAMEWORKS *VIA* ASSEMBLY OF MOLECULAR BUILDING BLOCKS

Balamurugan Kandasamy

A Thesis Submitted for the Degree of PhD
at the
University of St Andrews

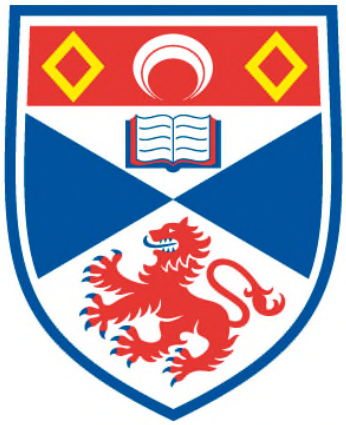

2012

Soft Routes to Inorganic Frameworks *via* Assembly of Molecular Building Blocks

Balamurugan Kandasamy

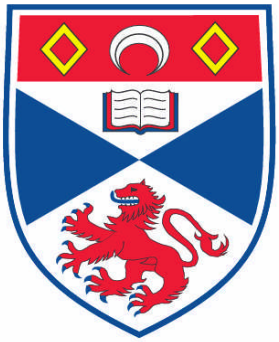

This thesis is submitted in partial fulfilment for the degree of Doctor of Philosophy in the faculty of science of the University of St Andrews

November 2011

1. Candidate's declarations:

I, ……, hereby certify that this thesis, which is approximately ….. words in length, has been written by me, that it is the record of work carried out by me and that it has not been submitted in any previous application for a higher degree.

I was admitted as a research student in [month, year] and as a candidate for the degree of …..…. in [month, year]; the higher study for which this is a record was carried out in the University of St Andrews between [year] and [year].

(*If you received assistance in writing from anyone other than your supervisor/s*):
I, …..., received assistance in the writing of this thesis in respect of [language, grammar, spelling or syntax], which was provided by ……

Date …… signature of candidate …….

2. Supervisor's declaration:

I hereby certify that the candidate has fulfilled the conditions of the Resolution and Regulations appropriate for the degree of ……. in the University of St Andrews and that the candidate is qualified to submit this thesis in application for that degree.

Date …… signature of supervisor …….

3. Permission for electronic publication: (*to be signed by both candidate and supervisor*)

In submitting this thesis to the University of St Andrews I understand that I am giving permission for it to be made available for use in accordance with the regulations of the University Library for the time being in force, subject to any copyright vested in the work not being affected thereby. I also understand that the title and the abstract will be published, and that a copy of the work may be made and supplied to any bona fide library or research worker, that my thesis will be electronically accessible for personal or research use unless exempt by award of an embargo as requested below, and that the library has the right to migrate my thesis into new electronic forms as required to ensure continued access to the thesis. I have obtained any third-party copyright permissions that may be required in order to allow such access and migration, or have requested the appropriate embargo below.

The following is an agreed request by candidate and supervisor regarding the electronic publication of this thesis:

(iii) Embargo on both [all or part] of printed copy and electronic copy for the same fixed period of 2 years (*maximum five*) on the following ground(s):

publication would preclude future publication;

Date 12/1/12 signature of candidate …… signature of supervisor …….

A supporting statement for a request for an embargo must be included with the submission of the draft copy of the thesis. Where part of a thesis is to be embargoed, please specify the part and the reasons.

Acknowledgements

Primarily, I would like thank to my supervisor Dr. John Errington who introduced me to the fascinating field of Polyoxometalates. His guidance, understanding and constant support throughout my time at Newcastle University will never be forgotten.

I sincerely thank to Prof. Peter .G. Bruce FRS, University of St. Andrews for offered me PhD studentship and arranged DHPA award for my three years PhD work.

I thank to School of Chemistry, University of St.Andrews and Newcastle University for giving me permission to commence this thesis, to do the necessary research work and for the use of the departmental facilities.

I thank to Prof. William Clegg and Dr. Ross Harrington, Newcastle University for determining the crystal structures. I also thank Dr. Corrine Wills and Prof. William McFarlane, Newcastle University for their advice regarding NMR spectroscopy, numerous spectra, variable temperature NMR, multinuclear NMR, 2D EXSY NMR and special INEPT experiment.

I also thank Prof. Josep Poblet, Universitat Rovira, Spain for computational studies and my thanks continues to Prof. Andrew Houlton and Dr. Ben Horrocks, Newcastle University for allowing me to carry out surface chemistry work.

I am also thankful to Dr. Corinne Wills for correcting my PhD thesis, Dr. Scott Watson for AFM measurement, Richard Baron for elemental analysis, Dave Dunbar for ESIMS analysis, Gary for mechanical work, and Chris and William for glass blowing work.

I also thankful to my lab mates Mr. Paul Middleton and Dr. Gavin Harle for being extremely helpful and training me in laboratory work, and many masters and bachelor students who have made my time in Bedson Building unforgettable.

Finally, I wish to thank my family particularly my parents Mr. Kandasamy and Mrs. Kasthuri and my loveable sisters Sangeetha Ramesh and Dhanalakshmi Anandan for their continuous encouragement and selfless support. I am also grateful to all my Newcastle friends who stayed with me for past three years.

Last but not least, I thank to my longstanding ever green friend “Lord Ganesh” by dedicating this entire work to him for giving me the continuous blessings.

Contents **Page**

Abbreviations

1. Spectroscopic

FTIR	Fourier Transform Infra Red
s	Small
m	Medium
w	Weak
(br)	Broad
NMR	Nuclear Magnetic Resonance
INEPT	Insensitive Nuclei Enhanced by Polarization Transfer
s	Singlet
d	Doublet
t	Triplet
q	Quartet
m	Multiplet
ppm	Parts per Million
δ	Chemical shift

2. Solvents

MeCN	Acetonitrile
Et_2O	Diethyl ether (ether)
MeOH	Methyl alcohol
THF	Tetrahydrofuran
H_2O*	10% ^{17}O enriched water

3. Chemicals and ligands

TBA	Tetrabutyl ammonium
HMDSO	Hexamethyldisiloxane
HMDS	Hexamethyldisilazane
POM	Polyoxometalate
LDA	Lithiumdiisopropylamide
sal	Salicylaldehyde
DIPA	Diisopropylamine

Abstract

The assembly of mononuclear and polynuclear molecular building blocks has been investigated as a route to extended metal oxide structures. Various $[MX_y]^{n-}$ (X = Cl, OMe, OH) and $[(RO)M'M_5O_{18}]^{3-}$ (R = MeO, M' = Sn, M = W) building blocks have been synthesised. Controlled hydrolysis has been explored for transition and main group metal hexahalides $[MCl_6]^{n-}$ M=Ti, Sn using ^{17}O enriched water.

An attempted synthesis of $[Me_3NCH_2Ph]$ $[Sn(OMe)_6]$ gave the dinuclear product $[Me_3NCH_2Ph]$ $[Sn_2(OMe)_9]$. Variable temperature ^1H NMR studies revealed exchange between terminal and bridging alkoxides and the limiting spectrum is consistent with solid state structure. 2,6-lutidinium hydrochloride was synthesised and used to chlorinate the metal alkoxides $\{M(OR)_n\}$ (M = Nb). A route to monochloro niobium alkoxide $\{NbCl(OMe)_4\}$ was developed and variable temperature ^1H NMR spectroscopy studies of $\{NbCl(OMe)_4\}$ in different solvents revealed exchange between bridging and terminal alkoxides and also suggested the presence of different structural isomers in solution.

A novel heterometallic Lindqvist type of POM containing Sn has been successfully synthesised by using controlled hydrolytic aggregation. A mixture of $(TBA)_2WO_4$, $WO(OMe)_4$ and $\{Sn(O^tBu)_4\}$ was partially hydrolysed in a non-aqueous solvent to give $(TBA)_3[(MeO)SnW_5O_{18}]$ **1**. ^{119}Sn NMR INEPT and selective tin decoupled proton NMR experiments have been carried out to determine the axial and equatorial ^2J $\{^{119}Sn*^{183}W\}$ coupling constants and to estimate $^3J\{^{119}Sn^1H\}$ and $^3J\{^{117}Sn^1H\}$ coupling constants. The electrochemistry of **1** was studied by cyclic voltammetry (CV), and was shown to undergo a reversible one electron reduction close to the solvent limit.

Hydrolysis of $[(MeO)SnW_5O_{18}]^{3-}$ produced $[(OH)SnW_5O_{18}]^{3-}$ **2** which is stable in the solid state but in solution undergoes a condensation reaction to give $[(\mu\text{-}O)(SnW_5O_{18})_2]^{6-}$ **3**.

The chloro stannotungstate $[ClSnW_5O_{18}]^{3-}$ was also obtained during the synthesis of **1** and **2**. Compounds **2** and **4** are crystallographically isostructural and Sn hetero site was disordered over all six metal positions in both anions. The redox properties of **4** were studied by CV and showed an irreversible reduction peak at -1.67 V. Compound **4** is

stable in air and did not react with H_2O or PhOH but did react with MeOH or NaOMe to give **1**. It also reacted with diisopropylamine (DIPA) to produce the H-bonded aggregate $[(Pr^i_2NH_2)_2(\mu\text{-}O)(SnW_5O_{18})_2]^{4-}$. The adduct structure is related to a recently characterised titanium analogue $[(\mu\text{-}O)(TiW_5O_{18}H)_2]^{4-}$, which forms the H-bonded THF adduct $[(\mu\text{-}O)(TiW_5O_{18}H)_2(THF)]^{4-}$.

2D-^{1}H EXSY NMR studies of the mixtures of **1** and MeOH did not show any exchange peaks between **1** and methanol which demonstrates that exchange is slow but reactivity studies of **1** have been carried out with various alcohols and phenols to give substituted products. Sterically smaller alkyl groups gave *trans* disordered structures, but no disorder is present in structures of anion with bulkier aliphatic alkoxide and aryloxide groups. Hydrogen bonding was observed between the POM cage and pendant phenolic OH groups All the alkyl and aryloxido derivatives have been characterised by single crystal X-Ray diffraction, ^{1}H and multinuclear NMR spectroscopy, infrared spectroscopy and CHN analysis.

Preliminary studies to explore the immobilisation of metal alkoxides $[Ti(OPr^i)_4]$ and **1** on ~30% OH functionalised Si(111) surfaces have been carried out. The attempted covalent immobilisation of **1** to Si(111) surfaces appeared to be successful from Atomic Force Microscopy (AFM) measurements.

Chapter 1

Introduction

Aim and general background

The primary objective of this project is to synthesise the extended metal oxide arrays by non-aqueous solution based 'soft' methods in a controlled manner. In order to synthesise extended metal oxides, we adapted a strategy involving the assembly of molecular building blocks. This may open the door between traditional molecular inorganic chemistry and solid state chemistry. Various possible building blocks have been synthesised and used in this project.

The building blocks used can be classified into two types; a) mononuclear, and b) polynuclear. Mononuclear building blocks contain only one reactive metal center whereas polynuclear contain more than one reactive metal center. Mononuclear building blocks are transition and main group metal hexahalides $[MCl_6]^{2-}$, hexa alkoxides $[M(OMe)_6]^{2-}$ and hexahydroxides $[M(OH)_6]^{2-}$ (M=Ti, Sn). The polynuclear building blocks studied in this project were polyoxometalates, and in particular, alkoxo derivatised Lindqvist type heteronuclear polyoxometalates. The synthesis and reactivity of building blocks are discussed in the Chapters 2, 3 and 4.

The assembly of building blocks is an attractive approach to the production of an extended array of oxide materials but is very challenging. Generally, controlling the nature and structure of the building blocks in solution is very difficult and leads to poor correlation between the reactants and products. Yaghi *et.al* [1] reported that controllable, well-defined crystalline solid networks could be synthesised by using molecular building blocks. The building blocks are commonly known as secondary building units (SBU), the structural integrity of which can be maintained throughout the whole process. This is a viable approach, which is completely different from supramolecular and retrosynthetic chemistry because building blocks are strongly linked by chemical bonding in this process and their structures are unaltered for the whole process. This chemistry has yielded materials designed to have predetermined structures, compositions and properties. This process has been termed reticular synthesis. Our interest is initially to synthesise the extended materials in a linear fashion $(M\text{-}O\text{-}M\text{-}O\text{-}M)_x$, by linking the building blocks *via* oxo ligand (O^{2-}) rather than using organic difunctional ligands such as carboxylates.

In addition, the reactivity of molecular precursors on functionalised Si(111) surfaces would be explored. Controlled hydrolytic aggregation processes are to be expected by

anchoring the possible building blocks through inert (poorly labile) linkages where subsequent transformations will be used to generate reactive groups that can then react with further building blocks. Metal oxide network will be formed by reactions between adjacent molecular precursors with water, alcohol or ether elimination which is analogous to Atomic Layer Deposition (ALD).[2]

Chapter 1: Introduction

This chapter provides a general overview of the synthesis of metal oxide networks in solution media, the nature of the possible mononuclear and polynuclear building blocks and their properties. This is followed by a description of the analytical techniques especially for ex: ^{17}O, ^{119}Sn and ^{183}W NMR spectroscopy and cyclic voltammetry (CV) that were used for characterising the precursors discussed in the end of the thesis.

1.1. Soft Routes to metal oxides

Metal oxides are a very important class of materials in various fields of chemistry, physics and materials science and have been the subject of various reviews and books.[3,4,5] The sophisticated techniques developed in the middle of the last century have allowed chemists to understand the true nature of many materials both at the atomic and molecular scales. Livage introduced the concept of *chimie douce* ('soft routes') in the 1970's and the controlled design of novel advanced materials was born, replacing the trial and error tradition which governed the construction of ancient materials. Soft chemistry routes i.e. bottom up approach at low temperatures and pressures are particularly suited to construct new materials with controlled shape and structure. The main advantage of this method is that a variety of precursors, solvents and synthetic conditions is available and we can easily change the reaction parameters i.e pH, concentration, temperatures and counter ions. By changing the reaction parameters, the reaction provides highly assembled molecular networks, yielding solids with significant architecture or morphology. Apparently, the solid properties can also be changed by this method.[6]

The controlled design and synthesis of novel crystalline materials from defined building blocks has received huge attention from the scientific community because these materials have unique properties and potential applications in domains related to sustainable development, energy, health, micro-optics and microelectronics. The soft route technique has opened up new opportunities for the design of new inorganic and hybrid materials to fabricate future functional devices such as nano lasers and optoelectronic devices, nanotransistors, nanosuperconductors, nanophotonics, nanocomputers, nanosensors, gas and energy storage systems, Li-ion batteries, catalyst

etc. In addition to applied research, fundamental studies also such as structural, magnetic, chemical and solution behaviour are also very interesting.[7]

1.2. Over view of Sol-gel process

The Sol-Gel process is a wet chemical technique which has been extensively used for synthesising metal oxides in the fields of material science and ceramic engineering. These methods are mainly used for fabrication of materials starting from colloidal solution (Sol) to an integrated network (Gel) of either metal oxide polymers or particles. The term sol-gel processing typically involves the hydrolysis and subsequent condensation of metal alkoxides $M(OR)_n$ and these alkoxides have commonly been used as precursors for this process.[8] However the chemistry of sol-gel processing is hardly understood and assumed concepts are obtained from early studies on silica.

1.2.1. Sol-gel chemistry of Silica

Silicon alkoxides, alkoxy silanes are very stable to hydrolysis by water and protolytes, acids so bases are used to initiate the reaction. The hydrolysis of silicon alkoxides can be influenced by either base or acid catalysis and leads to the formation of reactive Si-OH groups. However, the latter one is preferred because of the formation of stable cationic species during hydrolysis.

A three step S_N2 mechanism is generally proposed for base catalysed hydrolysis of Si alkoxides. Nucleophilic addition of a hydroxide anion to the positively charged Si atom, leads the central atom (Si) to a transition state, where the coordination number of Si has been increased by one. The second step involves a charge transfer within the intermediate state leading to release of an alkoxide anion, which in turn reacts with water regenerating the hydroxide catalyst. Acid catalysed hydrolysis shows a different reaction pathway. The cationic species are formed in the first step upon addition of an acid to Si alkoxides. Acids can easily coordiante to the oxygen atom in the alkoxide ligand leading to the formation of the reactive cationic species. This step is rate-determining, which results in an S_N1-type mechanism. The cation thus formed is attacked by a water molecule, which leads again to formation of a Si–OH bond, release of an alcohol molecule (better leaving group) and regeneration of a proton catalyst. [9]

1.2.2. Metal alkoxides

The metal alkoxides $[M(OR)_x]_n$ (M = metal or metalloid of valance x, R = alkyl, substituted alkyl and alkenyl, n= degree of molecular association) are formed by the replacement of alcoholic (ROH) hydrogen atoms by metal or metalloid atom. The systematic investigation of all periodic table metal alkoxides began in the early 1950's. The term metal alkoxides has always been confused with the term orthoester which relates only to the oxyacid elements. If the electronegativity difference between the metal and the derivatives of the metal is greater than 2 on the Pauling scale they are considered as a orthoesters.[10] With respect to all metal alkoxides with an electronegativity less than 2, the term alkoxide applies.

Metal alkoxides are moisture sensitive and rapidly react with water in the absence of catalysis. The reaction rates for hydrolysis of titanium alkoxides and zirconium alkoxides [11] are 10^5–10^8 times faster than silicon alkoxides.[12] Main group and transition metal alkoxides strongly favour acid catalysed hydrolysis rather than base catalysis and easily form stable cationic intermediates during hydrolysis. The mechanism for the formation of cationic species with suitable diagram is discussed in Chapter 2.

Condensation is also a very complex process, it occurs rapidly as soon as a the hydroxo species generated. Three types of mechanisms have been proposed so far for sol-gel process leading to metal oxide formation. 1) alkoxolation 2) oxolation 3) olation.

Alkoxolation

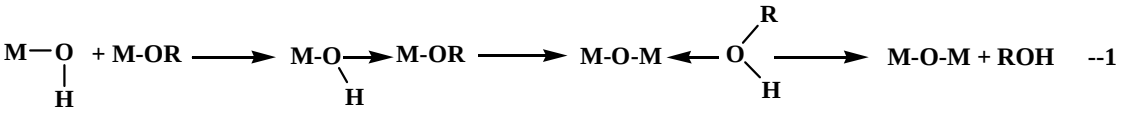

Oxolation:

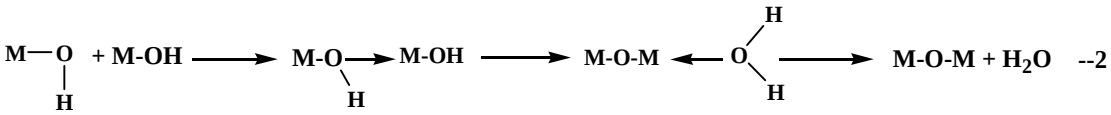

The alkoxlation and oxolation mechanisms are very similar except for the leaving group. In the earlier case, the oxo bridge is formed by the elimination of an alcohol molecule, while in the latter one, a water molecule is eliminated. Olation can occur when the full coordination of a central atom is not achieved and bridging hydroxo groups can be formed through the elimination of a solvent molecule. Metal centers may have coordination numbers higher than their valance, i.e, Zr, Hf alkoxides prefer olation reaction pathways. The use of mixed metal precursors can result in the formation of homogeneous species in solution during hydrolysis, as a result of differential hydrolysis and condensation rates. However addition of stabilising ligands alters the alkoxide functionality and the structure of the hydrolysed products.

Olation

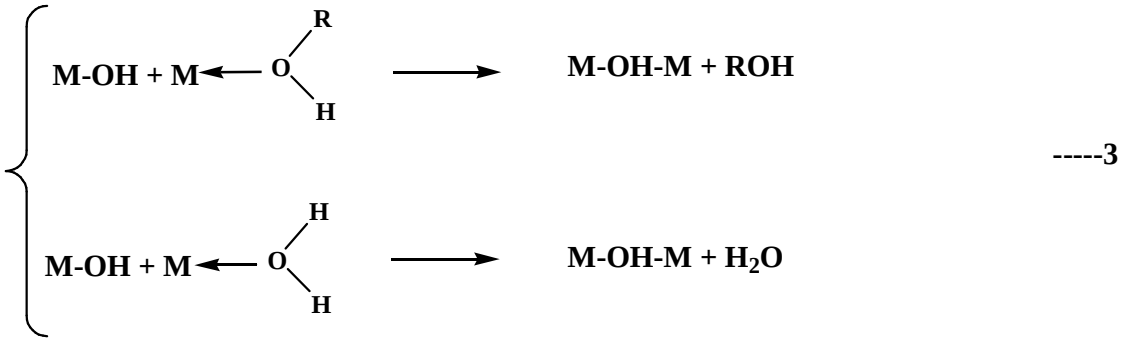

-----3

These four reactions (hydrolysis, alcoxolation, oxolation and olation) may be influenced in the transformation of a molecular precursor into an oxide network. These contributions can be controlled by carefully changing the experimental conditions which are related to both internal (nature of the metal atom and alkyl groups, structure of the molecular precursor) and external (water/alkoxide ratio, catalyst, concentration, solvent, temperature) parameters.[13]

1.2.3. Chemical modification of metal alkoxides

Sol-gel processing mainly involves the use of metal alkoxides as a starting material and because of the high reactivity towards water results in uncontrollable products. Initially scientists believed that chemical modification of metal alkoxides by using different acidic ligands such as carboxylic acids, β-diketonates [10], functional alcohols etc. might help to control the rate of hydrolysis. After an addition of water to modified alkoxides, clear sol was obtained rather than formation of precipitates. Lacks of

significant evidence, initially scientists were assumed that modifying – mostly chelating reduces the rate of hydrolysis. The proposed explanation was

1) Blocking the coordination sites of the metal atoms

2) Not changing significantly the charge distribution in the molecules.

3) Shielding the metal atoms from polycondensation by non-hydrolysable and thus not removable ligands.

These three postulates were believed and accepted previously and reproduced in recent books written by U.Schubert *et.al*, [12] V.Kessler and N.Turova *et.al*.[14] Recently V.Kessler *et.al* [9] studied the reactivity of various modified metal alkoxide complexes i.e. β-diketonate complexes such as $Sr_2Zr(thd)_4(OPr^i)_4(Pr^iOH)$ (thd = 2,2,6,6-tetramethylheptanedion) $Ni_2Ti_2(acac)_4(OEt)_8$, $Ni_5TiO(acac)_6(OEt)_6$ (acac = acetylacetonate). Crystallographic analysis, bond length and calorimetric measurements revealed that chemical modification is not slowing down the hydrolysis and polycondensation reactions. Based on this strong theoretical evidence, they proposed the following principles

1) Chelating ligands are not blocking the coordination sites

2) Chelating ligands are increasing charge distribution

3) Chelating ligands are accelerating hydrolysis and condensation

4) Chelating ligands are highly mobile and do not hinder the condensation.

Modification with acetylacetone is most commonly used for the isopropoxide derivatives of titanium, zirconium and aluminium alkoxides, which means that the entering ligand is much smaller than the isopropoxide or *n*-propoxide ligands it is replacing. From the above principles and kinetic measurements, it was revealed that modification of metal alkoxides does not lead to a decreased rate of hydrolysis and polycondensation reaction. However, it does help to slow down or even prevent the gelation and strongly favours the acid catalysed S_N1 hydrolysis route.

1.3. M-O-M formation

The main limitation of the sol-gel process is controlling the rate of hydrolysis and condensation process, because metal centers are very reactive and undergo hydrolysis very rapidly in the absence of catalyst, followed by condensation yielding a rigid network of metal oxides. However, hydrolysis and condensation can be controlled in non-aqueous media. In many molecular approaches to extended solids, metal alkoxides or modified metal alkoxide derivatives are either invoked as starting materials or used as the intermediates. The systematic construction and assembly of molecular metal oxo clusters or building blocks offers a number of distinct advantages over other methods to prepare mixed metal oxides. In the molecular building block approach, it should be possible to build hierarchical structures with particular stoichiometry and as a result control many of the physical and chemical properties of the final material such as pore structure, density and crystallinity.

Aprotic condensation reactions

In this approach, aprotic conditions are preserved by the use of hetero functional condensation reactions excluding hydroxyl groups. Generally oxo bridges are formed by a condensation reaction between two different functional groups which are bonded to two different metal centres by eliminating a small molecule like ether, ester or alkyl halide. Although ether elimination has been postulated in the formation of some μ-oxoalkoxides, it has not been developed so far as sol-gel processing, unlike the two other ways, ester and alkyl halide eliminations.[15]

1.3.1. Ester elimination

In the case of metal oxide chemistry, the elimination of an ester between metal alkoxides and metal carboxylates has been observed in many cases; however, the mechanism of this reaction has not been well understood. The choice of beta-diketonate or carboxylate ligands depends on the basicity of the ligand, or the pK_a of the conjugate acid. In general, beta-diketonates are likely to form chelates whereas carboxylates have a strong propensity to form bridged species. In addition, beta-diketonates are more labile compared with metal carboxylates.[16]

Hampden smith *et.al* proposed the ester elimination mechanism reaction between metal alkoxides and metal carboxylates by non- hydrolytic methods. [17] They also have observed that incomplete ester elimination takes place in the formation of $Sn_6O_6(OBu^t)_6(OAc)_6$ and leads to molecular cluster intermediate. For example, ester elimination between Sn tert-tetrabutoxide and tin carboxylate also leads $Sn_6O_6(OBu^t)_6(OAc)_6$. It can used as a building block to synthesise pure metal oxides. This cluster can be considered a small molecular fragment of the cassiterite phase SnO_2.

$$M(OR)_n + M'(O_2CR')_n \longrightarrow MM'(O)_x(OR)_{n-x}(O_2CR')_{n-x} + x\ RO_2CR' \qquad \text{-----4}$$

$$MM'(O)_x(OR)_{n-x}(O_2CR')_{n-x} \longrightarrow MM'(O)_n + (n-x)\ RO_2CR$$

Further studies were performed on the ester elimination reactions between Si carboxylate and Sn alkoxide compounds and were monitored by NMR Spectroscopy in different solvents. In one experiment the reaction could be monitored by ^{17}O NMR spectroscopy by labelling the alkoxide oxygen with ^{17}O. The labelled alkoxide oxygen was transferred to the ether oxygen in the ester. From this observation, they have proposed that the transition state of this reaction is similar to transesterfications where the carbonyl oxygen coordinates to an alkoxide metal centre, which allows the nucleophilic attack of the alkoxide oxygen on the carbonyl carbon, and is solvent dependent. Coordinating solvents such as pyridine hinder the ester elimination reaction.[18]

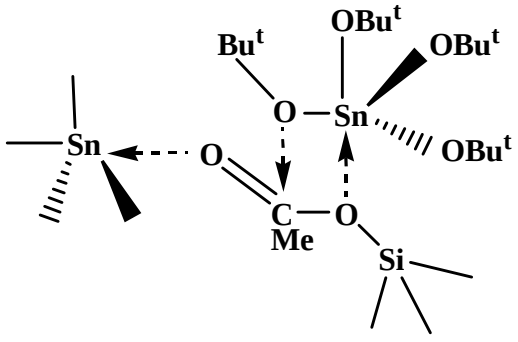

Fig 1.1: Four membered cyclic transition state.

Ester elimination reactions were also observed in some mixed metal oxo cluster syntheses. Hampden smith *et.al* [19] reported that the reaction between $Pb(OAc)_4$ and

$Sn(OBu^t)_4$ yields $PbSn_2(O)(OBu^t)_4(OAc)_4$ and they have studied the mechanism thoroughly in solution, but the detail of the mechanism is not well understood.

1.3.2. Alcohol elimination

The use of acetylacetone as a modifier of metal alkoxide hydrolysis is now well established.[8,20] Errington *et.al* first systematically studied and characterised that hydrolysis of titanium acetylacetonato alkoxides by ^{17}O enriched water and the elimination of alcohol molecules has been observed in the formation of $[\{TiO(acac)_2\}_2]$. [21] In addition these reactions are solvent dependent, elimination reactions are significantly slower in polar solvents compared to non-polar solvents such as benzene and toluene. A proposed mechanism for the formation of $[\{TiO(acac)_2\}_2]$ is shown in the equation.

$$(RO)_2Ti(acac)_2 + H_2O \longrightarrow (HO)(RO)Ti(acac)_2 + ROH \qquad \text{-----5}$$

$$(HO)(RO)Ti(acac)_2 \longrightarrow 1/2\ [OTi(acac)_2]_2 + 2\ ROH$$

1.3.3. Alkyl halide elimination

The alkyl halide elimination route is another possible way to synthesise metal oxides. It is based on a non-hydrolytic method and aprotic reaction conditions preserved throughout the whole reaction.

Nucleophilic S_N2 attack of an alkoxy group to the metal center of the second molecule, is followed by the release of an alkyl halide molecule leading to an oxide linkage. This reaction results in the nucleophilic cleavage of an OR bond, and, therefore, the electronic effects on the carbon center are critical.

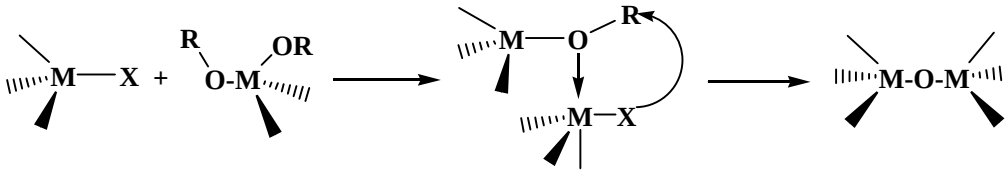

---6

Yuh *et.al* [22] proposed that the alkyl halide elimination reaction can take place *via* a two step process.

In the first step, an organic oxo compound coordinates to the active metal center forming the intermediate alkoxy species by elimination of alkyl halide or hydrogen

halide. The alkoxy intermediate subsequently reacts with other metal halides and produce the M-O-M bridges.

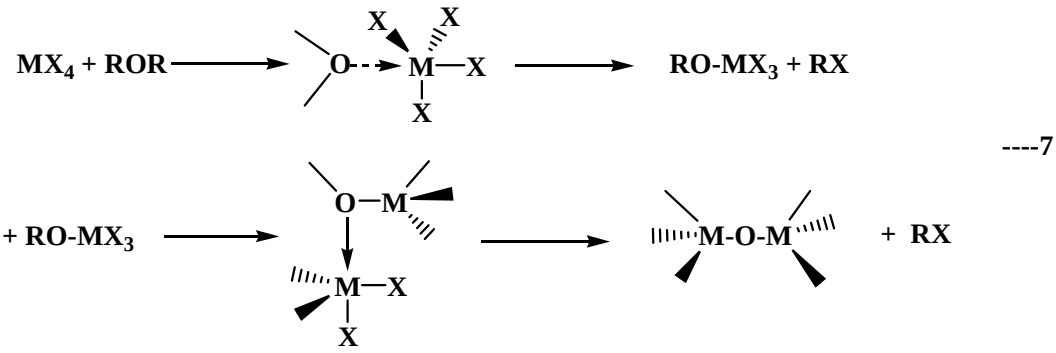

Etherolysis of transition metal (Ti) halides by using possible oxide source materials such as diethyl ether (Et_2O), diisopropyl ether ($Pr^i{}_2O$) and HMDSO is more interesting and leads to metal oxide formation with HX, Me_3SiX elimination. The main limitation of this method is that it forms stable intermediate metal chloroalkoxide species. For example, in the presence of $(Pr^i)_2O$, alkoxylation of $TiCl_4$ forms intermediate $Ti(OPr^i)_3Cl$ which is stable in solution and adopts an equilibrium with starting precursors.

We assumed that controlled hydrolysis of transition and main group metal halides by using either ^{17}O enriched hexamethyldisiloxane or H_2O as oxygen donors leads to M-O-M linkage and the product could be easily monitored by ^{17}O NMR spectroscopy. Transition metal halides are more readily available than parent alkoxides and the oxo bridge might be formed possibly with elimination of trimethylsilyl chloride. (TMS-Cl) The stepwise hydrolysis of $[TiCl_6]^{2-}$ and $[SnCl_6]^{2-}$ by using ^{17}O-enriched HMDSO and H_2O is discussed in Chapter 2.

1.3.4. Ether elimination

Etherolysis of transition metal halides is one of the versatile routes to sol-gel synthesis of metal oxides. Diethyl and diisopropyl ether elimination may occur and it is postulated in some of the oxoalkoxide formation but this chemistry has not been developed so for in the sol-gel process. [23,24].

For this project work, we have synthesised and used various mononuclear and polynuclear building blocks. The polynuclear building blocks studied in this project

were polyoxometalates, and in particular, alkoxo derivatised Lindqvist type heteronuclear polyoxometalates, and polynuclear metal oxoalkoxides. A general overview POMs and functionalisation of POMs to extended materials is discussed in the following section.

1.4. Polyoxometalates

POMs are discrete oxygen cluster anions that are structurally complex and diverse with interesting and unique multifaceted chemistry. Transition metals such as V, Nb, Ta, Mo and W readily form discrete oxoanion clusters in their highest oxidation states. Since the 1800's, many scientists have developed the POM field and research is still active in this area.

POMs can be classified into two distinct types (i) isopolyoxoanions, $M_nO_y^{p-}$ and (ii) heteropolyoxoanions, $X_xM_nO_y^{q-}$ (x< n). Isopolyoxoanions contain only one type of transition metal cation along with oxide anions. Heteropolyoxoanions contain one or more p or d block elements referred to as a heteroatom located at a well defined site within the transition metal oxide framework. More than 65 elements in the periodic table can be found as heteroatoms incorporated into polyoxoanions. The ability of POM complexes to accommodate such a diverse range of heteroatoms allows for a large variety in structure and composition.

History

Jons Jacob Berzelius initiated POM work and he isolated the first well known polyoxometalate ammonium phosphomolybdate $(NH_4)_3[PMo_{12}O_{40}]$ which can be easily obtained by reacting $MoO_x.H_2O$ with phosphate. [25] $[PMo_{12}O_{40}]^{3-}$ anion is generally yellow in colour and when reduced by Na/Hg amalgam, it quickly turns blue, however, the electron transfer mechanisms are not well understood.[49] Subsequently in 1862, Marignac [26] carried the research work on POMs and successfully achieved synthesis and characterisation of the α and β isomers of 12-tungstosilicic acid, $H_4SiW_{12}O_{40}$ along with a number of its salts.

In the period 1908-1933, several hundred POMs were prepared by various research groups but their structures were not understood. Werner,[27] Miolati,[28] Rosenheim,[29] and Pauling [30] all proposed structures for POMs based upon sharing metal-oxygen polyhedra. Based upon the rules, they proposed that 12-tungsto anion was based upon a central PO_4 or SiO_4 tetrahedron surrounded by twelve WO_6 octahedra. In this proposed structure, three of the oxygen atoms on each octahedra share electrons with three neighbouring octahedra. As a result, 18 oxygen atoms were used as bridging

atoms between the metal atoms. The remaining oxygen atoms were bonded to protons, resulting in the formula $[(PO_4)W_{12}O_{18}(OH)_{36}]^{3-}$.

Using X-Ray diffraction techniques, J.F. Keggin [31] structurally characterised the first POM with a molecular formula $[XM_{12}O_{40}]^{n-}$ where M = W or Mo and X = P have cage structures with one central atom X bonded to four oxygen atoms. The hetero atom might be a main group element such as P(V), Si(IV) and B(III). These POMs are now called Keggin polyoxometalates and are extensively investigated by various groups around the world.

1.5. Types of polyoxometalates

1.5.1. Keggin polyoxometalates

The Keggin structure $[XM_{12}O_{40}]^{n-}$, is one of the best known and characterised POMs to date. Keggin or Keggin type POM structures have the molecular formula $[XM_{12}O_{40}]^{n-}$ with a heteroatom in the center of the structure with a tetrahedral environment. A central XO_4 tetrahedron is surrounded by 12 MO_6 octahedra arranged in four M_3O_{13} groups. Each M_3O_{13} group is composed of three edge-shared MO_6 octahedra. Four M_3O_{13} groups corner-shared to the XO_4 tetrahedron.

There are many possibilities for geometrical isomerism in Keggin POM complexes, and designated by the prefixes α, β, γ, δ and ε. For example, The Keggin structure contains four M_3O_{13} addenda group and these isomers were derived by 60^o rotations of M_3O_{13} units around their 3-fold axes. Rotation of one of the M_3O_{13} units results in the β isomer. Rotation of two, three or all four of the M_3O_{13} units produces the γ, δ, ε isomers respectively.[32] The α-Keggin structure has T_d symmetry and these rotations lower the symmetry of the overall structure.

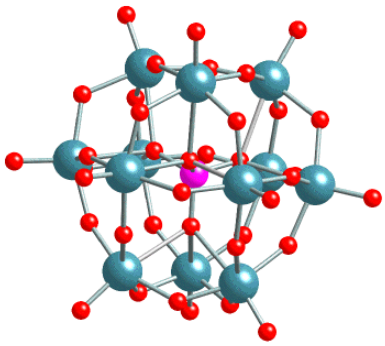

Fig.1.2. Ball and stick representations of $[XM_{12}O_{40}]^{n-}$. The colour codes are as follows: M (pale blue), O (red), X (purple).

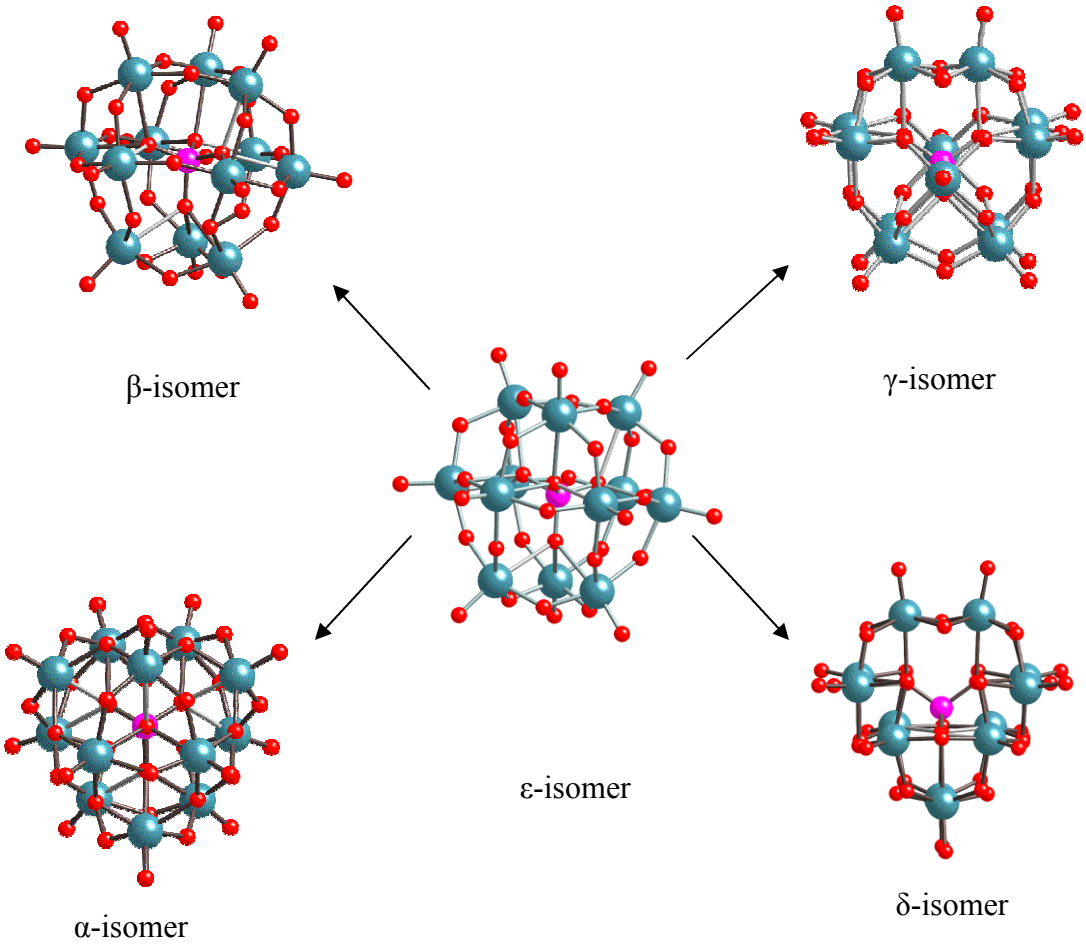

Fig. 1.3: Ball and stick representations of the Keggin structure, $[XM_{12}O_{40}]^{n-}$ and its four constitutional isomers. The M_3O_{13} groups have been rotated with reference to the α-Keggin structure. The colour codes are as follows: M (pale blue), O (red), X (purple).

1.5.2. The Lindqvist hexametalate structure

The hexametalate Lindqvist POM structure is comparatively simple, and consists of a central oxyanion surrounded in an octahedral cage formed by six metal and eighteen oxygen atoms. Besides the central oxygen atoms, they each coordinate triply to one terminal oxygen atom, forming a terminal metal-oxo group, and share an additional four doubly-bridging (μ_2-O) oxygen atoms with neighbouring metal atoms. The structure has O_h symmetry.

Most of the late transition metals (Mo, W, Nb, Ta) tend to form hexametalate structures. In 1955, Lindqvist [33,34] solved the hexametalate structures of $Na_7[HNb_6O_{19}].15H_2O$ and $K_8[Ta_6O_{19}].16H_2O$. Since then various other molecular and, extended metal oxide structures such as $[Mo_6O_{19}]^{2-}$,[35] $[W_6O_{19}]^{2-}$,[36] $[MW_5O_{19}]^{3-}$ [37] (M = Nb, Ta), $[Nb_2W_4O_{19}]^{4-}$ [38] have been identified. Fuchs *et.al* were the first to investigate the non-aqueous synthesis of polyoxometalates by hydrolysis of metal alkoxides or dissolution of metal oxides in the presence of organic bases. Their interest was to synthesise POMs with addenda atoms like Mo, V and W, for example, $[M_6O_{19}]^{2-}$ (M = Mo^{VI} and W^{VI}), $[W_{10}O_{32}]^{4-}$, $[H_2W_{12}O_{40}]^{6-}$, and $[HV_4O_{12}]^{3-}$.[39,40.] $[W_6O_{19}]^{2-}$ was synthesised according to the following reaction.

$$\mathbf{6\ WO(OEt)_4 + 12\ H_2O + 2OH^- \longrightarrow [W_6O_{19}]^{2-} + 24EtOH} \qquad \textbf{----8}$$

Subsequently Errington *et.al* [41] reported that controlled hydrolysis of mononuclear tungstate WO_4^{2-} and metal alkoxides leads to highly stable Lindqvist POM structures. The rigid stability of this hexametalate anion in non-aqueous media allowed them to investigate the reactivity of Lindqvist POMs (Mo and W) using functionalisation. This could be achieved either by using organic nitrogenous bases or incorporation of heterometals with surface alkoxido ligands.

$$\mathbf{WO_4^{2-} + 5WO(OMe)_4 + 10H_2O \longrightarrow [W_6O_{19}]^{2-} + 20MeOH} \qquad \textbf{----9}$$

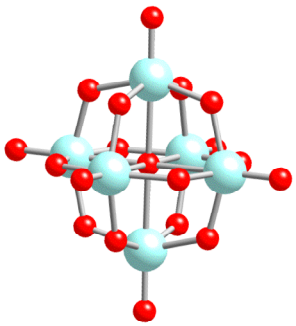

Fig 1.4: Ball and stick and representations of $W_6O_{19}^{2-}$. The colour codes are as follows: W (pale blue), O (red).

For the work mainly presented within this thesis is on synthesising extended metal oxide (M-O-M) structures using the building block approach. Because of their high stability and accessibility, we considered heterometallic Lindqvist type POMs $[(RO)MW_5O_{18}]^{3-}$ as one of the possible building blocks.

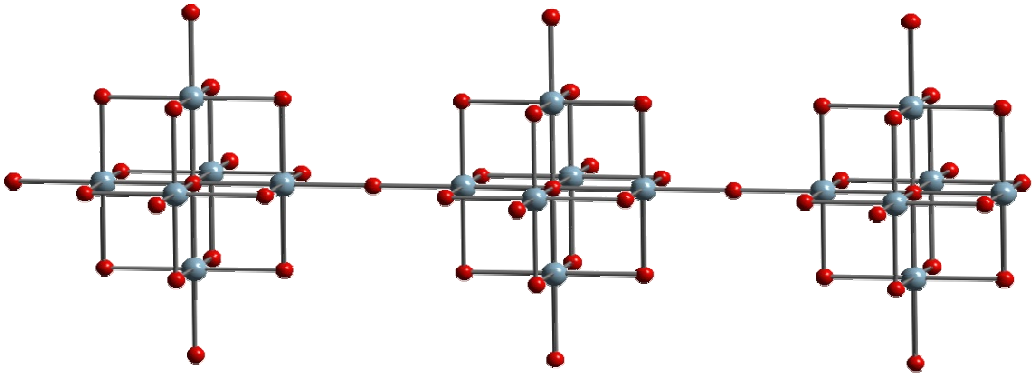

Fig.1.5: M-O-M linkages by using polynuclear building blocks.

Yaghi *et.al* [1] demonstrated that controlled extended solid crystalline materials could be synthesised by using secondary building block units. Secondary building blocks were prepared by chelating the metal ions using a carboxylate ligand and readily directionality, rigidity and controllability for crystalline materials were readily obtained. Functionalisation of Lindqvist (Mo) POMs and assembly of POMs using organic ligands is discussed in the following section **1.6.1** and reveals how

functionalised Lindqvist POMs could be used as building blocks but we mainly focused to linking the metals through oxo ligands rather than organic moities.

1.6. Functionalisation of Lindqvist POMs

1.6.1. By using organic ligands

$[M_6O_{19}]^{2-}$ (M=W, Mo) isopolyanions have d^0 electronic configuration and it is generally observed that polyoxomolybdates are labile while polyoxotungstates are inert, and much more stable. [42,43] This may be attributed to the slightly larger force constant of the W=O compared to Mo=O. Functionalisation of Keggin and larger polyoxometalates through organic ligands is well known and Lindqvist type POMs can also be functionalised by using organic ligands.

For the $[Mo_6O_{19}]^{2-}$, the terminal Mo=O bonds are reactive towards nitrogenous species and these oxygen atoms are replaced by these bases. J. Zubeita *et.al* [44] initiated this type of work and were followed by E. A. Maatta *et.al* [45,46,47,48] who reported many monosubstituted organodiimido and organodiimido-bridged bis(hexamolybdate) derivatives. Errington *et.al* [49,50] successfully synthesised the same organoimido derivatives of $[Mo_6O_{19}]^{2-}$ by using aromatic amines ($H_2NC_6H_4NH_2$, $AdNH_2$; Ad=adamantyl). At elevated temperatures, these reactions provided amino derivatised organoimido species. However assembling of POM by using NH_2 functionalities has not been successful because metal oxide fragments apparently deactivate these amines towards electrophiles.

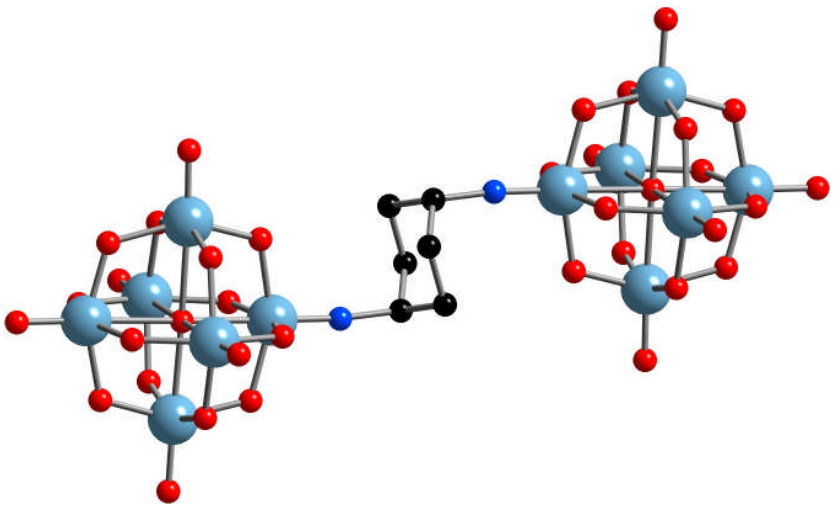

Fig 1.6: structure of the *trans*-1,4-cyclohexyldiimidobis(hexamolybdate) tetraanion. The colour codes are as follows: Mo (pale blue), O (red), N (dark blue), C (black). [46]

Proust *et.al* [51] also reported the highly functionalised p-tolylimido derivative of $[Mo_6O_{19}]^{2-}$ i.e. $[Mo_{10}(NC_6H_4Me\text{-}p)_{12}O_{18}(py)_2]^{4-}$. Recently, Peng *et.al* published a variety of papers about the functionalisation of isopolyanions. They also demonstrated that organoimido derivatives of $[Mo_6O_{19}]^{2-}$ can be synthesised by using aromatic amines [52] and the rate of these reactions has influenced by using a catalyst; i.e. dicyclohexylcarbodiimide (DCC). Bifunctionalisation of the same isopolyanion provides mixtures.[53] Later, they extended the same approach and synthesised the mono or bifunctionalised iodo derivatives of organoimido POMs. These kinds of POMs allowed reactions with terpyridine, followed by metal halides ($FeCl_2$) to synthesise extended POM materials.[54]

1.6.2. By using heterometals

Non-aqueous studies of POM revealed that the tungstate hexametalate $[W_6O_{19}]^{2-}$ is more inert compared to its Mo analogue. However, the $[W_6O_{19}]^{2-}$ species is not stable in basic media and is very easily degraded by concentrated bases. The mechanisms of the degradation involve attack by OH^- ions and a change of the addenda's coordination number is not clearly understood. The natural stability of these hexanuclear structures in acidic conditions are allowed the synthesis of heteronuclear Lindqvist type POM structures $[M'M_5O_{18}]^{n-}$. The activation of the tungsten oxide framework by the introduction of heterometal atoms or surface alkoxide ligands is another fascinating approach to functionalise the POMs.

In 1985, Klemperer *et.al* [55] reported the surface functionalisation method in the preparation of thio-derivatives $[MW_5O_{18}S]^{3-}$, (M = Ta and Nb). Their contribution involved the synthesis of polyoxomolybdates and tungstates, especially the heterometal-hexanuclear complexes in solution and characterisation of structures by ^{17}O NMR spectroscopy. In the same period, Errington and his co-workers, also developed a new technique involving controlled hydrolysis for the synthesis of TBA salts of alkoxido derivatised heteronuclear Lindqvist type POMs $[(L)M'M_5O_{18}]^{n-}$ (M' = Ti, Zr, Hf, V, Nb, Ta, Co, Fe and Sn. M = Mo^{6+} and W^{6+}) in non-aqueous medium from various metal alkoxides and tungstate precursors. These POMs are structurally characterised by ^1H NMR, multinuclear NMR, micro analysis and single crystal X-Ray diffraction methods. They have successfully synthesised a wide range of transition and main group metal heterometallic Lindqvist type POMs such as

$[(MeO)TiW_5O_{18}]^{3-}$ [56], $[(Pr^iO)TiMo_5O_{18}]^{3-}$ [57],$\{(MeO)ZrW_5O_{18}\}_2]^{6-}$ [58] and $[(MeO)SnW_5O_{18}]^{3-}$ [59] by controlled hydrolysis.

The M-O-M linkage would be formed if we hydrolyse the alkoxido derivatised heterometallic Lindqvist type POMs in non-aqueous media and the products can be investigated by ^{17}O NMR spectroscopy. Incorporation of many surface alkoxide ligands i.e. increasing the reactive sites in the POM cage, followed by hydrolysis, may lead to extended metal oxide structures.

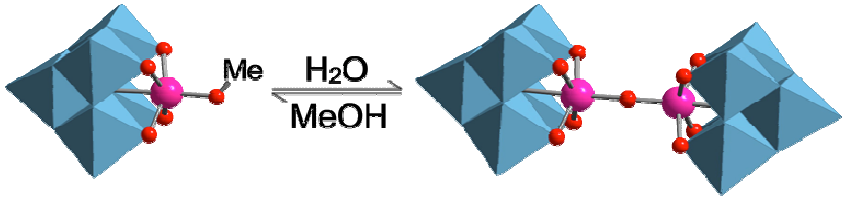

Fig.1.7: Formation of M-O-M linkage by hydrolysis of $[(RO)MM'_5O_{18}]^{3-}$ Where R=MeO or Pr^iO, M=Ti, Nb M'= W. The colour codes are as follows: Ti or Nb (pink), O (red), W or Mo (pale green).

Errington and his co-workers have attempted to synthesise the dimethoxo functionalised titanium POMs $[(MeO)_2Ti_2W_4O_{17}]^{4-}$. [60] Initial attempts at this work were successful. However, it leads to *cis*-di hetero Lindqvist type POMs with three alkoxide groups rather than *trans*- di hetero POM with two alkoxide groups.

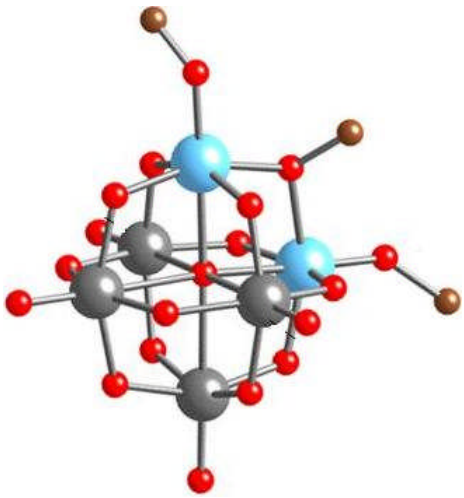

Fig.1.8: Structure of the anion *cis*-$[(MeO)_3Ti_2W_4O_{17}]^{3-}$ The colour codes are as follows: Ti (blue), O (red), C (brown), W (black).

To best of our knowledge, no one has used alkoxido functionalised heterometallic Lindqvist type POMs as building blocks in non-aqueous media. Controlled hydrolytic synthesis of $[(MeO)SnW_5O_{18}]^{3-}$, its family of structures and the attempted synthesis of extended M-O-M structures using POMs in non-aqueous medium are discussed in Chapters 2 and 3.

1.7. Metal oxide thin films on functionalised surfaces

Part of our project concerns the synthesis of extended metal oxide structures using building blocks on functionalised Si(111) surfaces. Metal oxide (M-O-M) linkage formation was expected by anchoring the building blocks and subsequent hydrolysis on surfaces. We are expecting that metal alkoxides would react more slowly compared to solution phase reactions.

Surface sol-gel process

1.7.1. Metal alkoxides

Controlled synthesis of metal oxide thin films on functionalised surfaces is still very challenging and it has received huge attention from the scientific community recently because of its potential applications in the field of electronics. Many thin films are prepared by sol-gel processing conducted under mild experimental conditions. Controlled growth of metal oxide thin films with atomic precision has been accomplished by sequential surface chemical reactions using the Chemical Vapour Deposition (CVD) technique.[61] Atomic Layer Deposition (ALD) is also one of the processes used for the formation of oxide thin films on surfaces. The precursor molecule mostly metal alkoxides and metal halides, chemisorbs or reacts with surface groups saturatively and further exposure to a second precursor leads to controlled growth of metal oxide thin films.[62,63] Recently T. Kunitake *et.al* [64,65] reported a novel method to fabricate metal oxide thin films by means of stepwise adsorption of metal alkoxides from solution., monitoring the reactions by quartz crystal microbalance (QCM). This has been termed as surface sol-gel process and contains four major steps; chemisorptions of alkoxide, rinsing, hydrolysis of chemisorbed alkoxide and drying. In addition they found that polyhydroxyl compounds, polymers and small molecules strongly adsorb onto metal oxide layers formed by surface sol-gel process.

In our efforts, we are trying to synthesise metal oxide thin films by anchoring the possible precursor i.e. metal alkoxides or metal halides to ~30% hydroxyl functionalised Si (111) surfaces.[66] The preliminary studies carried out with metal alkoxides on functionalised Si(111) surfaces and the details of reactivity studies are discussed in Chapter 5.

1.7.2. Polyoxometalates

Our approach with regards to synthesising extended metal structures on the functionalised surfaces is to attach the diheterometallic (especially *trans*) Lindqvist type POMs initially, followed by subsequent reactions with another POM leading extended metal oxide structures. Errington *et.al* attempted to synthesise the diheteroemetallic Lindqvist POMs and as discussed in section **1.6.2**.

Multilayer films of polyoxometalate ions have been assembled by using electrostatic alternate adsorption techniques. Klemperer *et.al* started the surface chemistry technique to construct monolayers of POMs on various surfaces e.g. Ag(111) and Au(111). [67] Keggin POM monolayers were prepared by immersion of Ag(111) and Au(111) in to acidic solutions of silicotungstate $[SiW_{12}O_{40}]^{4-}$. This was followed by Errington and his co-workers, who have successfully attached alkoxido derivatised heterometallic Lindqvist type POMs $[(RO)M'M_5O_{18}]^{3-}$ (M'=Ti, Zr, Nb, Ta, Hf and Sn) to functionalised Si(111) surfaces. These surface alkoxido groups are readily accessible to attach to functionalised silica surfaces and they have successfully attached the novel TiW_5 polyoxometalate to undecanol derivatised silicon (Si) surfaces. This was the first demonstration of the covalent surface immobilisation of polyoxometalates.[68] The basic principle being that a reacting group is erected on the surface, which binds to the POMs and then these surfaces are then studied by AFM, XPS or by FTIR techniques.[69]

Several techniques such as Langmuir-Blodgett, sol-gel processing and layer-by-layer self assembly have been employed to produce hybrid inorganic-organic materials. Decher *et. al* [70,71,72,73] originally developed the layer-by-layer assembly technique to prepare multilayer assemblies of organic polymers and this technique is simply based on adsorption of oppositely charged species from dilute solutions. This method allows the use of various inorganic building blocks. Hu *et.al* [74] reported the first organic-inorganic composite films of a rare earth containing POM, $Na_9\{EuW_{10}O_{36}]$ and

poly(allylamine hydrochloride) by the layer- by- layer self assembly method. Cabuil *et.al* [75,76] have successfully demonstrated the covalent attachment of thiol derivatised $[\gamma\text{-}SiW_{10}O_{36}(RSi_2)O]^{4-}$ ($R=HSC_3H_6$) POM on gold nanoparticles. The organic part R plays a critical role which easily makes covalent link to gold particles through the thiol group and covalent links with polyanion through the trimethoxy silane group.

Currently, we are aiming to synthesise diheterometallic alkoxido derivatised Lindqvist type POMs and reactivity studies with ~30% -OH functionalised Si (111) surfaces will be developed in future. The reactivity of tin Lindqvist type POM anions $[(MeO)SnW_5O_{18}]^{3-}$ with 30% functionalised Si(111) surfaces is discussed in Chapter 5.

1.8. Applications of sol-gel process

1.8.1. Reversible cathodes for Li Batteries

Transition metal chalcogenides have been extensively used as reversible cathodes for Li ion batteries especially V_2O_5, which exhibits a three dimensional layer structure rather than being van der Waals host. It is hoped that better reversibility can be achieved with amorphous oxides for which structural changes should be limited and thus vanadate glasses have been suggested as reversible cathodes for lithium batteries.[77,78]

1.8.2. Catalysts

The sol-gel process offers many advantages for making catalysts. Since the homogenous mixing can be achieved at the molecular scale, the chemical reactivity of the oxide surface can be greatly increased and usually provides powders with specific pore dimensions and large surface area. The average size of the particles can be varied in the range 30-120 Å by diluting the alkoxide precursor during the synthesis. If drying is performed in hypercritical conditions, a highly porous material called an aerogel is obtained. Aerogels exhibit better catalytic properties in terms of selectivity, activity. etc than xerogels.[79,80]

1.8.3. Materials

The Sol-gel process is widely used to make multi-component ceramics or glasses. Metal alkoxides are usually used for initial precursors and various ceramic synthetic routes and their applications are listed in the following table.

Ceramics	Initial precursors	Uses
$BaTiO_3$	$Ba(OEt)_2$ or $Ba(OPr^n)_2$ [81,82] $Ti(OEt)_4$ or $Ti(OPr^i)_4$	Ferroceramics
$PbTiO_3$	$Pb(OAc)_2$ and $Ti(OPr^i)_4$ [83,84,85]	High dielectric constant capacitors.
$NiFe_2O_4$	Fe (II), Ni(II) hydroxides [86]	Ferromagnetic films.
$LaYO_3$	$La(OEt)_3$ and $Y(OEt)_3$ [87]	Thermomechanical ceramics.
$Y_3Al_5O_{12}$	$Y(NO_3)_3$ and $Al(OPr^i)_3$ [88]	Translucent gel.

Table 1: Applications of various meral oxides in ceramics field.

1.8.4. Bio-Applications

The sol-gel method was first used for the powderless processing of glasses and ceramics. The encapsulation of fragile bio molecules within sol-gel glasses has been recently addressed and cells, antibodies and enzymes are safely trapped by the sol-gel materials where they retain the bioactivity or sometimes enhance their activity. The increased activities of enzymes in sol-gel materials may be explained in terms of structural changes which are observed in enzymes and the sol-gel matrix cage upon heating. Therefore a real burst of interest in biological applications of sol-gel materials has occurred during recent years and now scientists around the world have been working on bio-sensors or bio-catalysts.[89]

1.9. Applications of Polyoxometalates

1.9.1. 'Blue electron reduction'

Polyoxometalates act as oxidising agents. The low-lying empty d-type orbitals of addenda atoms can accept numerous electrons with no major changes in geometry. Sometimes reduction disintegrates the POM cage and it forms lower oxidation state atoms. These extra electrons, located in d-orbitals are called metallic or *blue electrons*.[90] For example, Mo^{1V} and W^{1V} have d^0 electronic configuration and have vacant non-bonding orbitals. These POMs exhibit reversible reduction which depends on the applied potential, and the pH. The molybdenum hexametalate anion $[Mo_6O_{19}]^{2-}$

is more easily reduced compared to the tungsten analogue $[W_6O_{19}]^{2-}$ as confirmed by cyclic voltammetry technique.

Usually Mo and W Lindqvist POMs do not produce the 'blue colour' after reduction unlike Keggin POMs. This characteristic "blue" colour consists of a very large group of POM complexes known as the "heteropoly or the POM blues". The added "blue" electrons are delocalised over certain atoms or the parts of the structures. These delocalised electrons might be used for electrical conduction however the mechanism is not clearly understood. Errington *et.al* [91] have found that Keggin $[PMo_{12}O_{40}]^{3-}$ structures can be easily reduced by using Na/Hg amalgam and the structure of the POM remains in solution after an addition of 6 e^-'s. However the application of these POMs in terms of conductivity and magnetism have yet to be developed.

1.9.2. Photocatalyst

Another tungstate structure $[W_{10}O_{32}]^{4-}$ shows a very strong LMCT band at λ 323 nm in the UV spectrum and two quasi-reversible reduction peaks at -0.85 V and -1.35 V in non-aqueous solvents. The relatively low energy value of the LMCT makes these isopolytungstate useful as photo catalyst for solar energy conversion and the oxidation potential of the one electron- reduced species is highly negative compared to the redox potential of H^+/H_2, which indicates that $[W_{10}O_{32}]^{4-}$ is a simple photocatalyst for H_2 production from a variety of substrates with or without the heterogeneous catalysts Pt and RuO_2.[92]

1.9.3. Medical applications

Generally, POMs are relatively non-toxic compared to organic moieties and this makes them suitable to use in medical research. They have been used for anti tumour and antiviral agents. C.Hill *et.al* [93] systematically reviewed the various iso and heteropolyoxoanions in antiviral and antitumoral studies. Isopolyoxoanions, e.g. $[Mo_6O_{19}]^{2-}$ and $[W_6O_{19}]^{2-}$ are potentially less active on to HIV-I cells compared to heteropolyoxoanions. Certain POMs have a characteristic to adhere to different tissues with varying tenacity, and polyoxotungstates are valuable as electron microscopy stains. POMs are attached to the organic side chains of the tissues effecting in staining the tissues.

Besides the applications of POM in medicine and catalysis, POMs are useful in various other fields and the main applications has been reviewed by Katsoulis [94] and these are listed in the following table.

No	Main applications of POMs	POM
1	Coatings	Si-Molybdates
2	Electrolytic capacitors	Mo, W Keggin POMs
3	Wood Pulp bleaching	Vanadotungstates and molybdates.
4	Electrochromic–ion conducting gels, films.	$H_3PW_{12}O_{40}$
5	Liquid H_2-O_2 fuel cell	$H_3PW_{12}O_{40}$
6	Separations	α-$Li_xNa_{4-x}Si$-tungstates
7	Electrode for NO determination	$PW_{11}O_{39}Fe^{III}(OH_2)^{4-}$
8	Planographic printing plates	$H_3PMo_{12}O_{40}$, $H_3PW_{12}O_{40}$
9	dopant in polypyrrole	$[(C_4H_9)_4N]_4[PW_{11}O_{39}Fe^{III}(OH_2)]$
10	flame retardant materials	$(NH_3)_6[H_2W_{12}O_{40}]$, $H_3PW_{12}O_{40}$

Table 2: Applications of POMs in various fields.

1.10. Synthesis of POMs in non-aqueous media

For the work we discuss in this thesis, we mainly focus on synthesis of mononuclear and polynuclear building blocks and subsequent reactions with regards to attempted synthesis of extended metal oxide structures in non-aqueous media. In addition, $[W_6O_{19}]^{2-}$ and alkoxido functionalised Lindqvist type heterometallic POMs are stable in non-aqueous media. Before taking into consideration the building block synthesis, we turned our attention to choosing the particular solvents and characterisation techniques. The solvent systems and characterisation techniques we used in this thesis are discussed in the following sections.

Solvent system

Four key factors are to be considered when selecting the solvent. The factors are given below.

1) Solvent must not be reactive with the compound to be examined

2) Solvent must be quite polar otherwise POMs and Polyelectrolytes will not be soluble

3) Solvent should have high boiling point in order to take NMR Spectroscopy at elevated temperatures

4) Solvent should have low viscocity.

The properties of several solvents, commonly employed in polyoxoanion chemistry, are given in Table 3.

Solvent	Viscocity, cP	Bp, ^{o}C
H_2O	1.01	100
1,2-$C_2H_4Cl_2$	0.80	84
$(CH_3)_2NCHO$	0.80	152
$CHCl_3$	0.54	62
CH_2Cl_2	0.39	40
CH_3CN	0.35	82
$(CH_3)_2CO$	0.32	56

Table 3: Physical properties of different solvents.

The aforementioned four factors must be taken into consideration when selecting the solvent. Klemperer *et.al* [95] found that acetonitrile solvent fulfilled the above factors and in addition it has high dielectric constant. So they suggested that it was the best choice for the majority of non-aqueous polyoxometalate reactions. Dimethyl sulfoxide was also used in some cases where acetonitrile failed to dissolve the inorganic frameworks.

1.11. Analytical techniques

Polynuclear building blocks i.e. alkoxido derivatised Lindqvist POMs are moisture sensitive and precautions need to be followed when analysing the starting materials. These POMs are usually synthesised in non-aqueous media using Schlenk line and dry box techniques [96] and characterised by multinuclear NMR spectroscopy techniques. Multinuclear NMR spectroscopy is invaluable in understanding the structures and solution dynamics of these POMs. Generally polyxometalates are characterised by multinuclear NMR spectroscopy methods such as ^{17}O, ^{119}Sn, ^{183}W and ^{31}P.

1.11.1. ^{183}W NMR spectroscopy

The ^{183}W nuclide is the only NMR active natural tungsten isotope with a spin of 1/2 and the natural abundance is 14.35 %. The ^{183}W chemical shifts are very sensitive to their surrounding environment, including the central atom, temperature, the electric charge and the size of adjacent elements, counterions in solution and solvent. Baker and co-workers first applied the ^{183}W NMR technique to iso and hetero polyoxotungstates and it was then developed by various groups around the world. To date, ^{183}W NMR is an important tool for structural characterisation for polyoxotungstates in solution.[97]

Lindqvist POM has a very simple structure with six identical W atoms. They belong to O_h symmetry and the ^{183}W NMR spectrum showed one line. Removing a $\{WO\}^{4+}$ unit from high symmetrical structure, and insertion of $\{M=O\}^{3+}$ would produce $[M'M_5O_{19}]^{3-}$ structure. If only one heterometal atom is present in the polyoxometalate cage, it has equal probability of occupying all the six equivalent sites. For example: Substitution of $\{W=O\}^{4+}$ by $\{V=O\}^{3+}$, produced $[VW_5O_{19}]^{3-}$. Mono substituted hexametallate structures showed two characteristic peaks with 4:1 ratio in the ^{183}W NMR spectrum. Insertion of another heterometal atom to the polyoxometalate cage would produced $[V_2W_4O_{19}]^{4-}$ structure. There are two possibilities available; the heterometal may occupy the trans or cis position. If both heteroemetals occupy the cis position, it exhibits two characteristic peaks with 1:1 ratio whereas trans-$[V_2W_4O_{19}]^{4-}$ shows one line in the ^{183}W spectrum.[98]

Narrow lines in ^{183}W NMR help to observe the indirect spin-spin coupling of $^2J\{W\text{-}P\}$, $^2J\{W\text{-}W\}$, $^2J\{W\text{-}Sn\}$, which provides important information in order to assign the

structural arrangement in solution.[99] Lefebvre *et al.* [99] observed the mononuclear coupling constant $^{2}J\{W–O–W\}$ in Keggin type POMs $[H_2W_{12}FO_{39}]^{5-}$ and $H_4SiW_{12}O_{40}$.They found that the magnitude of the coupling constant $^{2}J\{W–O–W\}$ varied with W–O–W bond angle. The less bent bridging bond results in a greater interaction of the bridging oxygen orbital with the tungsten atoms and therefore the larger values of $^{2}J\{W–O–W\}$. The coupling constants usually observed are 20-22 Hz for corner shared W atoms, and 8-10 Hz for edge shared W atoms. $^{2}J\{W\text{-}W\}$ coupling arising from non-equivalent tungsten atoms are not observable in Chapters 3 and 4 because of the lower concentration of the samples. Various groups around the world found that coupling constant varies with bridging angle and bond distance.

In Chapters 3 and 4, $^{2}J\{^{119}Sn^{183}W\}$ heteronuclear satellite coupling constants are discussed. The $^{2}J\{Sn\text{-}W\}$ coupling constant value is 39 Hz. Computational and simulation studies have been carried out in order to assign the $^{2}J(^{119}Sn^{183}W_{eq})$ and $^{2}J\{^{119}Sn^{183}W_{ax}\}$ coupling constants.[100]

1.11.2. ^{17}O NMR spectroscopy

The ^{17}O nucleus is a difficult nucleus to observe by NMR spectroscopy for a couple of reasons. First it has a spin of 5/2 with an appreciable quadrupole moment which leads to rapid nuclear quadrupole relaxation. A quadrupolar nucleus with shorter relaxation time generally leads to broad signals and hence poor spectral resolution is usually obtained. The second main reason is the low natural abundance of ^{17}O (0.037%) and it is an expensive isotope, so it is usually necessary to use ^{17}O enriched samples.[101]

^{17}O NMR is widely used to investigate polyoxometalates because oxygen is the common element in all iso and hetero polyoxoanions. There are different types of oxygen present in the polyoxometalates. Klemperer and his co-workers [95] have applied the ^{17}O NMR technique to investigate polyoxometalate structures and they concluded the following factors are important for assigning the structure in solution.

1) Chemical shift of oxygen atoms of the same type which are bonded to atoms of various metals differ.
2) The number of lines corresponds to the number of types of O atoms.
3) An increase in screening when the O coordination number increases.

4) The intermediate position of lines of M–O–M' bridges in comparison with M–O–M and M'–O–M' bridges.

The $[M_6O_{19}]^{2-}$ anion contains one metal and all the octahedral atoms are equivalent. The ^{17}O NMR spectrum of isopolyoxometalate (both Mo and W) showed three signals for terminal, bridged and centered oxygens with 6:12:1 intensity. The substitution of one hetero metal atom into Lindqvist POMs complicates the ^{17}O NMR spectrum. If only one heterometal atom is present in the polyoxometalate cage, it has equal probability of occupying all the six equivalent sites. For example: Substitution of $\{W=O\}^{4+}$ by $\{V=O\}^{3+}$, produced $[VW_5O_{19}]^{3-}$. Monosubstituted hexametallate structures showed six characteristic peaks in ^{17}O NMR spectra.

Insertion of another heterometal atom in to the polyoxometalate cage would produced $[V_2W_4O_{19}]^{4-}$. There are two possibilities available, the heterometal may occupy the trans or cis position. If both heterometals occupied the cis position, it exhibits nine characteristic peaks whereas trans-$[V_2W_4O_{19}]^{4-}$ shows only a five line spectrum. Errington *et.al* [56] applied this to alkoxo derivatised Lindqvist type transition and main group hexametalates and all the derivatives showed six characteristic peaks. The alkoxido groups are not enriched and will not appear in the ^{17}O NMR spectrum. The ^{17}O NMR spectrum of $[(MeO)TiW_5O_{18}]^{3-}$ is shown in the Figure 1.9.

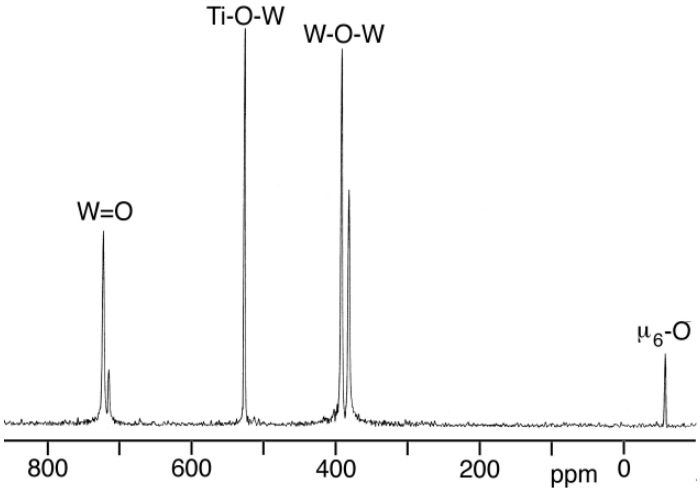

Fig. 1.9: ^{17}O NMR of $[(MeO)TiW_5O_{18}]^{3-}$

We have also applied this technique for hydrolytic studies of POMs, metal alkoxides and oxoalkoxides as well to understand the solution behaviour of these materials. We have further studied the hydrolysis of metal hexahalide anions by ^{17}O NMR spectroscopy. (see Chapter 2).

1.11.3. ^{119}Sn NMR spectroscopy

^{119}Sn NMR spectroscopy has already proven to be useful in the NMR spectroscopy field. Three types of tin nuclei are present in nature. Usually ^{119}Sn is selected since its receptivity is greater than that of ^{117}Sn. ^{115}Sn is not usually preferred by spectroscopists because of the low natural abundance. A large body of data is now available which demonstrates that ^{119}Sn NMR studies provide accurate, relatively easily obtainable information on the bonding to the tin atom. In many cases, the coordination chemistry of tin atom was proved by chemical shift of the tin atom in solution.[102]

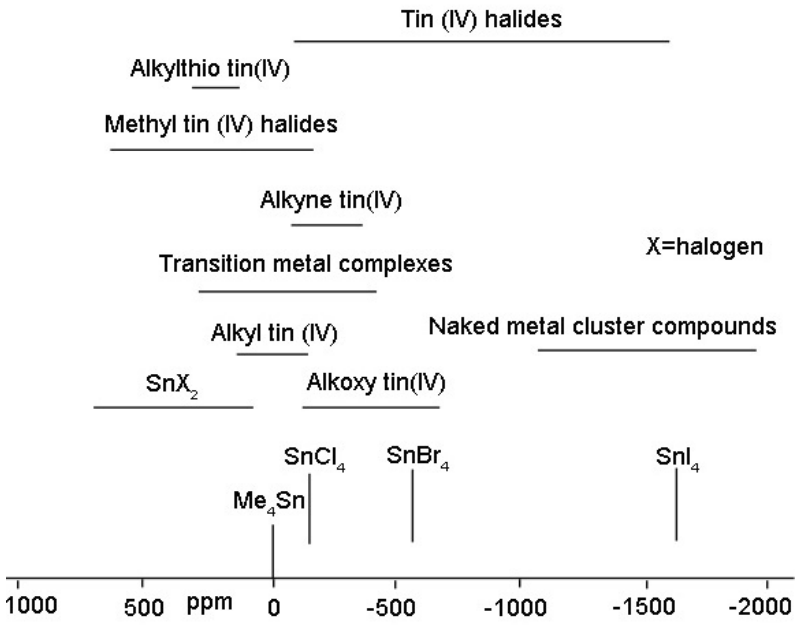

Fig 1.10: Chemical shift ranges for ^{119} Sn NMR.[103]

From the chemical shift value of tin, possibly we could presume the coordination chemistry and oxidation state of the tin heterometal atom. Hampden Smith and his coworkers had used ^{119}Sn NMR as a major tool to understand the solution behaviour of tin alkoxides and its reactions.[104,105] Errington *et.al* extended ^{119}Sn NMR

spectroscopy as a tool to investigate the tin heteronuclear lindqvist type POMs. The $^{n}J\{^{119}Sn^{1}H\}$ (n = 2,3,4), $^{n}J\{^{119}Sn^{13}C\}$(n = 2, 3), $^{2}J\{^{119}Sn^{183}W\}$couplings are discussed in the Chapters 3 and 4 in detail.[106]

1.11.4. Cyclic Voltammetry

Cyclic voltammetry is a type of poteniometric electrochemical measurement and is used to study the redox properties of POM complexes. In this experiment the working electrode potential is raised linearly versus time starting from a potential where reduction or oxidation of the polyoxometalates $[M_6O_{19}]^{2-}$ (M = Mo, and W) occurs. When cyclic voltammetry reaches a set potential, the working electrode's potential ramp is inverted and electrode reactions of products along with the intermediates formed during the forward scan, can be detected.

A one electron redox potential wave is detected for $[Mo_6O_{19}]^{2-}$ but whereas $[W_6O_{19}]^{2-}$ anion exhibit two one electron redox potential wave in CV. From these studies, we have confirmed that, $[Mo_6O_{19}]^{2-}$ POMs are more easily reducible than $[W_6O_{19}]^{2-}$.The technique is characterised by several important parameters, (a) the cathodic (E_{pc}) and anodic (E_{ac}) peak potentials, the cathodic (i_{pc}) and ionic (i_{pa}) peak currents, (b) the reduction potential (E_{red}), and the oxidation potential (E_{oxi}), and (c) the half-wave potential ($E_{1/2}$).[107]

The supporting electrolyte tetra-n-butyl ammonium tetrafluoroborate (QBF_4) (50 cm^3, 0.005 M) in acetonitrile was freshly prepared and used as supporting electrolyte. The solution of $[W_6O_{19}]^{2-}$ (25 cm^3, 0.005 M) in QBF_4/ CH_3CN was prepared. To study the redox properties of $[W_6O_{19}]^{2-}$, the forward scan was begun at the initial potential of 0 V and first redox wave was observed at –0.63 V. A further one-electron redox peak also observed at -1.64 V which is close to the solvent limit though careful control of solvent purity is required for observation of this second reduction wave. The first reversible redox peak was observed for $[W_6O_{19}]^{2-}$at -0.63 V for $[W_6O_{19}]^{2-}/[W_6O_{19}]^{3-}$ and second redox peak at -1.64 V for $[W_6O_{19}]^{3-}/[W_6O_{19}]^{4-}$.

$$\mathbf{[W_6O_{19}]^{2-} + e^- \underset{k_{-1}}{\overset{k_1}{\rightleftharpoons}} [W_6O_{19}]^{3-} + e^- \underset{k_{-2}}{\overset{k_2}{\rightleftharpoons}} [W_6O_{19}]^{4-}} \qquad \textbf{----10}$$

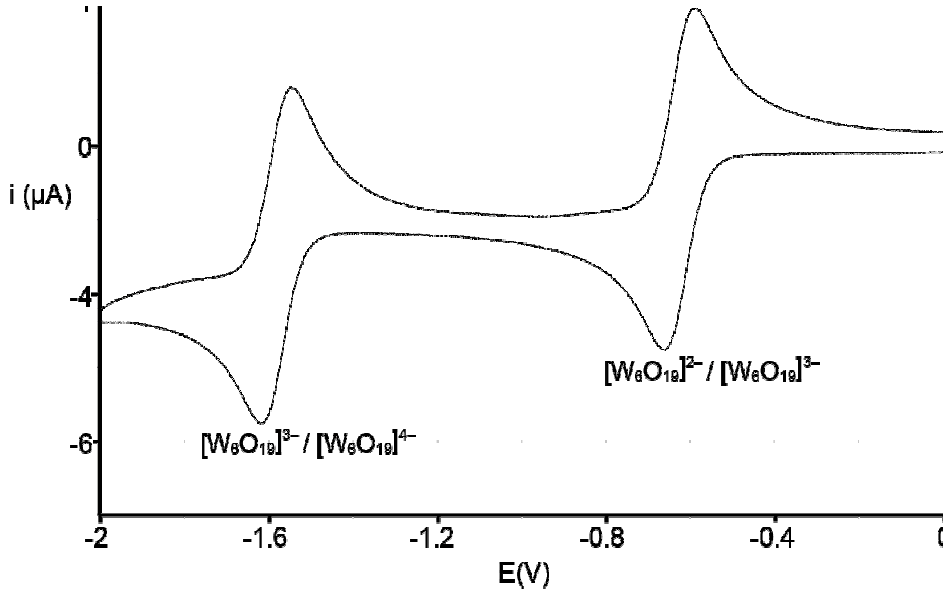

Fig.1.11: Cyclic voltammogram (CV) of $[W_6O_{19}]^{2-}$ (0.005 M) in acetonitrile.

A solution of ferrocene (0.005 M) was used as an internal standard and was added at the end of an experiment. Ferrocene easily undergoes a reversible redox reaction, forming the ferrocenium ion, which at 0.445 V.

Summary

The field of metal oxide chemistry in solution and on functionalised surfaces has received huge attention from the scientific community because of the continuing grow in size particularly with regard to their potential applications. Assembling of polynuclear building blocks using organic ligands has been addressed. However inorganic bridging ligand i.e. O^{2-} and mechanisms are yet to be explored.

This thesis mainly deals with the synthesis of mononuclear and polynuclear building blocks and the reactivity studies in non-aqueous medium. Chapter 2 mainly focuses on the possible mononuclear building blocks and hydrolytic studies of these substances have investgated by ^{17}O NMR spectroscopy. Chapters 3 and 4 mainly discuss about non-aqueous synthesis of alkoxo derivatised Lindqvist type POMs and reactivity studies with various protic reagents have investigated. Finally, Chapter 5 takes a different approach to synthesise the single molecule metal oxide network on 30%-hydroxy functionalised Si(111) surfaces by using surface sol-gel and covalent immobilization techniques.

1.14. References

1) O. M. Yaghi, M. O'Keeffe, N. W. Ockwig, H. K. Chae, M. Eddaoud and J. Kim, *Nature*, **2003**, 423, 12, 705-714.

2) E. Rauwel, G. Clavel, M. G. Willinger, P. Rauwel and N. Pinna, *Angew.Chem.Int.Ed.* **2008**, 47, 3592-3595.

3) The Chemistry of Nanomaterials Synthesis, properties and application, C.N.R.Rao, A.Muller and A.K. Cheetham, *Wiley-VCH publications*, **2004**, Vol.1.

4) Nanomaterials chemistry. Recent developments and new directions, C.N.R.Rao, A.Muller and A.K. Cheetham., *Wiley-VCH publications*, pp 119-135.

5) Nanoscale materials in chemistry, K. J. Klabunde., *Wiley- VCH publications.* **2001**, pp- 85-120.

6) C. Sanchez , L. Rozes, F. Ribot, C. Laberty, R. D. Grosso, C. Sassoye, C. Boissiere, L. Nicole., *C. R. Chimie*, **2010**, 13, 1–2.

7) L. Vayssieres, *Pure Appl.Chem*, **2006**, 78**,** 1741-1747.

8) C. J. Brinker and G. W. Scherer, *Sol-Gel Science*, Academic Press, New York, **1990**, 53-59.

9) V. G. Kessler, G. I. Spikjsma, G. A. Seisenbaeva, S. Hakansson, D. H. Blank, H. J. M. Bouwmeester, *J.Sol-gel Techn*, **2006**, 40, 163-179.

10) D. C. Bradley, R. C. Mehrotra and D. P. Gaur, Metal alkoxides, Academic Press, New York, 1978.

11) M. T. Harris, A. Singhal, J. L. Look, J. R. S. Kristensen, J. S. Lin, L. M. Toth, *J. Sol-Gel Sci.Techn*, **1997**, 41, 8

12) U. Schubert U. N. Husing, Synthesis of Inorganic Materials, **2000**, Wiley-VCH, Weinheim.

13) J . Livage, M. Henry and C. Sanchez, *Prog.Inorg.Chem*, **1997**, 46, 239.

14) N. Turova, E. P. Turevskaya, V. G. Kessler, M. I. Yanovskaya, The chemistry of metal alkoxides, **2002** , Kluwer AP, Boston

15) A. Vioux, *Chem. Mater*, **1997**, 9 (11), 2292-2299.

16) R. J. Ridland, PhD thesis, **1998**, Newcastle University.

17) J. Caruso and M. J. H. Smith, *J.Sol-gel sci.Techn*, **1997**, 8**,** 35-39.

18) J. Caruso, C. Roger, F. Schwertfeger, M. J. H. Smith, A. L. Rheingold and G. Yap, *Inorg.Chem*, **1995**, 34, 449-453.

19) J. Caruso, M. J. H. Smith and E. N. Duesler, *J.Chem.Soc. Chem. Commun*, **1995**, 1041-1042.

20) L. G. Hubert-Pfalzgraf, *Appl.Organomet.Chem*, **1992**, 6, 627-643.

21) R. J. Errington, J. Ridland, W. Clegg, R. A. Coxall and J. M. Sherwood. *Polyhedron*, **1998**, 17, 657-674.

22) S. K. Yuh, E. P. Bescher, F. Babonneau, J. D. Mackenzie, *Mater. Res. Soc. Symp. Proc*, **1994**, 346, 803.

23) K. G. Caulton, L. G. Hubert-Pfalzgraf, *Chem. Rev*, **1990**, 90, 969. (b) Hubert-Pfalzgraf, L. G. *Polyhedron*, **1994**, 13, 1181

24) S. Daniele, R. Papiernik, L. G. Hubert-Pfalzgraf, *Inorg. Chem*, **1995**, 34, 628.

25) J. J. Berzelius, *Poggendorffs Ann. Phys. Chem*., **1826**, 369, 380.

26) C. Marignac, *Ann. Chim*., **1862**, 25, 362.

27) A. Werner, *Ber. Dtsch. Chem. Ges*., **1907**, 40, 40.

28) A. Miolati, R. Pizzighelli, *J. Prakt. Chem*., **1908**, 77, 417.

29) A. Rosenheim, *Handbuch der Anorganischen Chemie*; R. Abegg, F. Auerbach (Eds), Hirzel Verlag: Leipzich, **1921**, vol 4, Part 1, ii, 997.

30) L. Pauling, *J. Am. Chem. Soc*., **1929**, 52, 2868.

31) J. F. Keggin, *Nature*, **1933**, 131, 908.

32) L. C. W. Baker, J. S. Figgis, *J. Am. Chem. Soc*., **1970**, 92, 3794.

33) I. Lindqvist, *Ark.Kemi*, **1953**, 5, 247.

34) I. Lindqvist and B. Aronsson, *Ark.Kemi*, **1955**, 7, 49.

35) H. R. Allock, E. C. Bissell and E. T. Shawl, *Inorg.Chem*, **1973**, 12, 2963.

36) J. Fuchs, W. Freiwald and H. Hartl, *Acta Crystallogr., Sect B*, **1978**, 34, 1764.

37) C. J. Bescker, W. G. Klemperer, D. J. Maltbie and D. A. Wright, *Inorg.Chem*, **1985**, 24, 1027.

38) M. Dabbabi and M. Bower, *J. Inorg. Nucl. Chem*, **1976**, 38, 1011.

39) K. F. Jahr, J. Fuchs, *Angew. Chem. Int. Ed. Eng.* **1966**, *5*, 689.

40) J. Fuchs, *Z. Naturforsch. B* **1973**, *28*, 389.

41) W. Clegg, M. R. J. Elsegood, R. J. Errington, J. Havelock, *J.Chem.Soc., Dalton Trans*, **1996**, 681-690.

42) K. H. Lee, Doctoral dissertation, Georgetown University, 1970. *Diss. Abstr. Int.* **1971**, *31B*, 5240.

43) N. Casañ-Pastor, P. R. Gomez, G. B. Jameson, L. C. W. Baker, *J. Am. Chem. Soc.* **1991**, 113, 5658.

44) H. Kang, J. Zubieta, *Chemical Communications*, **1988**, 17, 1192.

45) J. B. Strong, R. Ostrander, A. L. Rheingold and E. A. Maataa, *J.Am.Chem.Soc*, **1994**, 116, 3601.

46) J. L. Stark, A. L. Rheingold and E. A. Maataa, *Chem.Commun*, **1995**, 1165.

47) J. L. Stark, V. G. Young, Jr and E. A. Maataa, *Angew.Chem.Int.Ed*, **1995**, 34, 2547.

48) J. B. Strong, G. P. A. Yap, R. Ostrander, L. M. Liable-Sands, A. L. Rheingold, R. Thouvenot, P. Gouzerh and E. A. Maataa, *J.Am.Chem.Soc*, **2000**, 122, 639.

49) W. Clegg, R. J. Errington, K. Fraser, C. Lax, D. G. Richards, *Polyoxometalates: from Platonic Solids to Anti-Retro*V*iral Acti*V*ity*; M. T. Pope, A. Muller, Eds; Kluwer: Dordrecht, **1994**, pp 113.

50) W. Clegg, R. J. Errington, K. Fraser, S. A. Holmes, A. Schafer, *J. Chem. Soc., Chem. Commun*, **1995**, 455-456.

51) A. Proust, S. Tauiner, V, Artero, F. Robert, R. Thouvenot and P. Gouzerh, *Chem.Comm*, **1996**, 2195.

52) Y. Wei, B. Xu, C. L. Barnes,and Z. Peng, *J. Am. Chem. Soc.* **2001,** 123, 4083-4084.

53) L. Xu, M. Lu, B. Xu, Y. Wei, Z. Peng, and D. R. Powell, *Angew. Chem. Int. Ed. Eng.* **2001**, 40, 12, 2290.

54) L. Xu, M. Lu, B. Xu, Y. Wei, Z. Peng, and D. R. Powell, *Angew. Chem. Int. Ed. Eng.* **2002**, 41, 21, 4129.

55) V. W. Day, W.G. Klemperer, C. Schwartz, *J. Am. Chem. Soc.* **1987**, 109, 6030.

56) W. Clegg, M. Elsegood, R. J. Errington, J. Havelock, *J. Chem. Soc., Dalton. Trans.*, **1996**, 681.

57) R.J. Errington, L. Coyle, P. S. Middleton, C. J. Murphy, W. Clegg, R. W. Harrington, *Journal of Cluster Science*, **2010**, 21, 503-514.

58) R. J. Errington, S. S. Petkar, P. S. Middleton, W. McFarlane, W. Clegg, R. A. Coxall, R. W. Harrington, *J. Am. Chem. Soc.*, **2007**, 129, 12181.

59) R. J. Errington *et.al*., Unpublished results.

60) R. J. Errington *et.al*., Unpublished results.

61) I. Ichninose, H. Senzu and T. Kunitake, *Chemistry Letters*, **1996**, 831-832.

62) M. Leskela and M. Ritala, *Angew.Chem.Int.Ed*, **2003**, 42, 5548-5554.

63) M. Leskela and M. Ritala, *Thin Solid Films*, **2002**, 138-146.

64) I. Ichinose, T. Kawakami and T. Kunitake, *Chem.Mater*, **1997**, 9, 1296-1298.

65) I. Ichinose, T. Kawakami and T. Kunitake, *Adv.mat*. **1999**, 10, 7, 535-539.

66) D. J. Michalak, S. R. Amy, A. Esteve and Y. J. Chabal, *J.Phys.Chem.C*, **2008**,112, 11907-11919.

67) W. G. Klemperer and C. G. Wall, *Chem. Rev*, **1998,** 98, 297-306.

68) R .J. Errington, S. S. Petkar, B. R. Horrocks, A. Houlton, L. H. Lie, and S. N. Patole, *Angew. Chem. Int. Ed*, **2005**, 44, 1254 –1257.

69) A. R. Pike, B. R. Horrocks, A. Houlton, *Angew. Chem. Int. Ed.* **2002**, 41, 4.

70) a) G. Decher and J. D. Hong, *Makromol.Chem.Makromol.Symp*, **1991**, 46, 321.

71) G. Decher,, J. D. Hong, *Thin Solid films*, **1992**, 210/211, 831.

72) Y. Lvov, F. Essler and G. Decher, *J.Phys.Chem*, **1993**, 97, 13773.

73) G. Decher, *Science*, **1997**, 277, 1232.

74) Y. Wang, X. Wang, C. Hu, C. Shi., *J. Mater.Chem,* **2002**, 12, 703-707.

75) C. R. Mayer, S. Neveu, V. Cabuil, *Angew. Chem*. **2002**, 114, 519;

76) C. R. Mayer, S. Neveu, V. Cabuil, *Angew. Chem. Int. Ed*. **2002**, 41, 501.

77) D.W. Murphy, F.A. Christian, F.J. Disalvo and J.V. Waszeak, *Inorg. Chem.,* **1979**, 18, 2800

78) D. W. Murphy and P. A. Christian, *Science*, **1979**, 205, 651.

79) S.J. Teiehner, G.A. Nicolaon, M.A. Vicarini and G.E.E. Gardes, *Adv. Colloid Interface Sci.,* **1976**, 5 245. (1976).

80) S. J. Teichner, *ProE. in Phys.*,**1986**, 6, 22.

81) J. L. Rehspringer, P. Poix and J.C. Bernier, *J. Non-tryst. Solids*, **1986**, 82, 286

82) E. Wu, K. C. Chen and J. D. Mackenzie, p.169, in ref.14.

83) Y. Hayashi and J. B. Blum, *J. Mater. Sci*, **1987**, 22, 2655.

84) S. R. Gurkovich and J. B. Blum, p.152, in ref.ll.

85) J. B. Blum and S. R. Gurkovich, *J. Mater.* Sci, **1985**, 20, 4479.

86) K. C. Chen, A. Jana and J. D. Mackenzie, p.731, in ref.15.

87) O. Yamaguchi, H. Kawabata, H. Ahashimoto and K. Shlmin, *J. Amer. Ceram. Soc*, **1987**, 70, C131.

88) C. Vedney, R.A. Condrate, W. B. Crandall and M. E. Washburn, *Mat. L*ett, **1986**, 4, 470.

89) D. Avnir, T. Coradin, O. Lev and J. Livage, *J. Mater. Chem*, **2006**, 16, 1013–1030.

90).M. T. Pope, *Heteropoly and Isopoly Oxometalates*, Springer-Verlag, berlin, 1983.

91) R. J. Errington *et.al*., Unpublished results

92) T. Yamase, *Chem. Rev.* **1998,** *98*, 307-325.

93) J. T. Rhule, C. L. Hill, D. A. Judd and R. F. Schinazi, *Chem. Rev.* **1998,** 98, 327-357.

94) D. E. Katsoulis, *Chem. Rev.* **1998,** 98, 359-387.

95) M. Filowitz, K.C.Ho, W. Klemperer and W.Shum, *Inorg. Chem*, **1979**, 18, 1, 93-103.

96) R. J. Errington, *Advanced practical inorganic and metalorganic chemistry*: Blackie Academic and Professional, London, **1997**.

97) Y. G. Chen, J. Gong, L.Y. Qu, *Coordination Chemistry Reviews*, **2004**, 248, 245–260.

98) M. A. Fedotov and R. I. Maksimovskaya, *Journal of Structural Chemistry*, **2006**. 47, 5, 952-978.

99) F. Lefebvre, F. Chauveau, P. Doppelt, C. Brevard, *J. Am. Chem.Soc*, **1981**, 103, 4589.

100) R.J. Errington *et.al.*, Unpublished results.

101) I. P. Gerothanassis, *Progress in Nuclear Magnetic Resonance Spectroscopy*, **2010**, 56, 2, 95-197.

102) Multinuclear NMR, J.Mason, **1987**, Plenum press, pp 305-333.

103) http://Chem.Ch.hujj.ac.il/nmr/techniques/1d/row5/sn.html.

104) M. J. H.Smith, T. Wark, A. Rheingold, J. C. Huffman, *Can. Chem.*, **1991**, 69, 121-129.

105) C. D. Chandler, J. Caruso, M. J. H. Smith and A.Rheingold., *Polyhedron*, **1995**, 14, 17-18,2491-2497

106) R. J. Errington *et.al*, Uunpublished results

107) D. H. Evans, K. M. O'Connell, R. Peterson, M. Kelly, J. Cyclic Voltammetry. *J. Chem. Educ.*, 290.

Chapter 2

Synthesis and Hydrolysis of Metal Halide and Alkoxide Building Blocks

Chapter 2: Synthesis and Hydrolysis of Metal Halide and Alkoxide Building Blocks

2.1 Introduction

This chapter will mainly focus on the synthesis of molecular precursors and the attempted synthesis of extended metal oxide structures in non- aqueous solution. As we discussed in the previous chapter with regard to synthesis of extended oxide materials, a strategy has been followed involving the assembly of molecular building blocks[1] *via* oxo bridge formation in solution. This provides an attractive approach to inorganic frameworks.

The possible mononuclear molecular precursors are metal hexahalides, hydroxides and alkoxide anions which have the general formula $[MX_m]^{n-}$ where M = Sn, Ti, Nb and X = Cl, OH, OMe. These molecular precursors are expected to be very reactive in solution and extended inorganic metal oxide structures can be obtained by hydrolysis. Hydrolytic studies of mononuclear building blocks i.e. transition and main group metal halides could be monitored by ^{17}O NMR and other multinuclear NMR spectroscopy. Controlled hydrolytic studies of transition and main group metal halides by ^{17}O NMR spectroscopy, variable temperature ^{1}H NMR studies and 2D exchange spectroscopical (EXSY) studies of transition metal alkoxides and niobium chloroalkoxides are discussed towards end of this chapter.

Polynuclear building blocks i.e. alkoxo derivatised Lindqvist type heterometallic polyoxometalates (POMs) $[(RO)M'M_5O_{18}]^{n-}$ where M' = Ti, Nb, Sn, M = W and R = Me can also be used to synthesise the extended metal oxide structures. These POMs can be synthesised by a hydrolytic aggregation route. Reactivity of tin POMs was investigated with water, alcohols and various monohydric and dihydric phenols. The synthesis and reactivity of a tin POM is discussed in following Chapters 3 and 4. An interesting feature of this and upcoming chapters is that ^{17}O enriched water has been used for hydrolytic studies. Thus, we were able to investigate the species formation and follow the reaction pathways by ^{17}O NMR spectroscopy.

2.2. Background

Various research groups around the world have been working in the field of metal oxides since the 1950's. Metal alkoxides may be described by the formula $[M(OR)_x]$

and can either be considered to be the derivatives of alcohols in which the hydrogen has been replaced by a metal or derivatives of metal hydroxides, $[M(OH)_x]$ which act as bases or oxyacids according to the electronegativity of the central element.

Metal alkoxide hydrolysis and condensation reactions are interesting to study from a structural point of view and a wide range of metal alkoxides has been studied by D.C. Bradley and R.C. Mehrotra. Hydrolysis of metal alkoxides leads to the formation of strongly nucleophilic metal hydroxyl groups which undergo condensation reactions with alkoxide further to give metal oxide $(-M-O-M-O-)_x$ networks. Uncontrollable metal oxide networks have usually been obtained by traditional sol-gel methods based on hydrolysis, and the condensation reaction of the molecular precursors such as metal alkoxides is very fast in solution.

Metal alkoxides are extremely moisture sensitive and the rate of hydrolysis is governed by the nature of the alkoxy groups. The lower alkoxides are rapidly hydrolysed by moist air but as the chain length increases the susceptibility to hydrolysis decreases, [3] the mechanism for the hydrolysis and condensation reactions may be presumed to follow that of alcohol exchange, reported to be either S_N2 type by increasing the coordination by one or S_N1 type involving proton assisted cationic species formation. Metal alkoxides are strong Lewis bases compare to silicon alkoxides and these rapidly react with water in the absence of catalysts but the non-metallic silicon alkoxides, alkoxysilanes are very stable towards hydrolysis. The major difference in the chemistry of metals and non or semi metals lies in their ability to easily form relatively stable cationic complexes. This feature in combination with the well-acknowledged high Lewis basicity of metal alkoxides facilitates the ligand exchange through a proton-assisted S_N1 reaction mechanism.[4] According to the experimental kinetic measurements, the ligand exchange, i.e. both hydrolysis and chemical modification, start with the protonation of a negatively charged alkoxide oxygen atom.[5] The generated reactive cationic species coordinates then an additional donor ligand and releases an alcohol molecule. (Reaction 1, M = metals)

The three step S_N2 mechanism is generally proposed for the base- catalysed reaction by involving a nucleophilic addition of hydroxide anion to the metal or non–metal followed by an increase in their coordination number by one and a hypervalent transition state metallic center is achieved. The second step involves a charge transfer

within an intermediate state leading to release of an alkoxide anion, which in its turn reacts with water regenerating the hydroxide catalyst. (Reaction 2) Steric properties of alcohol and the coordination behaviour of alcohol or solvents mainly affect these reactions. Intermolecular association will also act to stabilise the metal centers and it would decrease the reaction rate, in particular for the oligomeric polybutyl titanates.[6] Metal oxide formation can also be influenced by acidic and bascity factors.

2.2.1. Acidic hydrolysis

Under acidic conditions, the hydrolysis reaction is more accelerated than the condensation reaction. For example, in reaction the metal alkoxide has basic sites to accept the proton from mineral acids and makes a better alcohol leaving group by the formation of a hypervalent transition state. Subsequently, the basic M-OH moiety reacts with a protanated transition state species leading to branched chain oligomers.

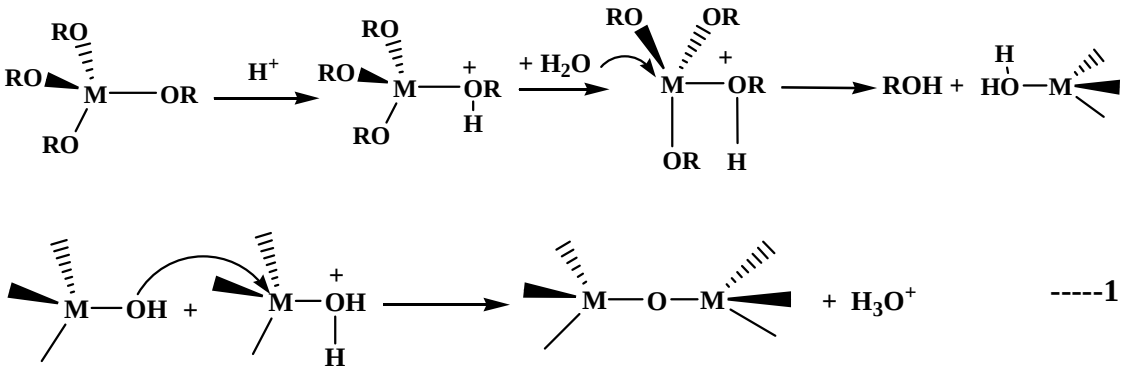

2.2.2. Basic hydrolysis

Under basic conditions, hydrolysis and condensation reaction occur simultaneously. For example, in reactions with non-metal alkoxides, M = Si, both hydroxyl anions and deprotanated silionol species are better nucleophiles than water. The condensation reaction involves attack of a deprotanated silanol on a neutral siloxane species.

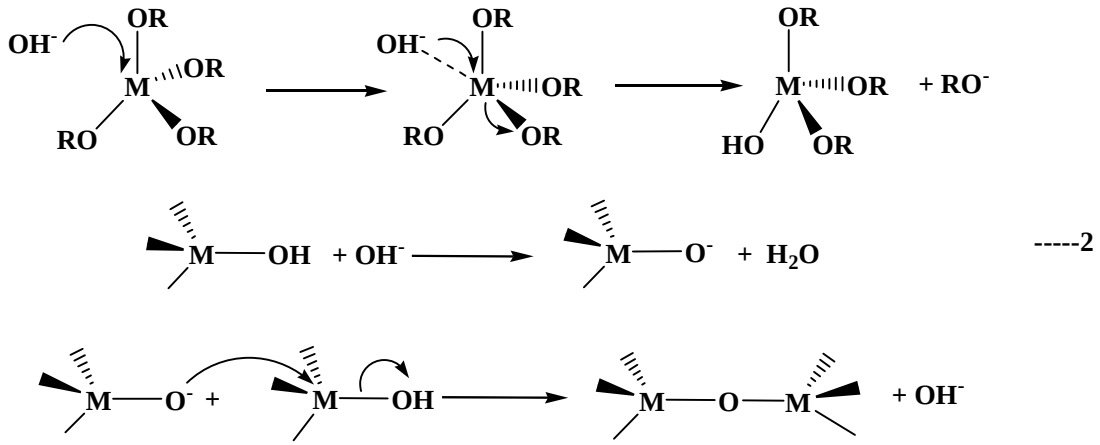

Brown *et.al* [5] recently determined that 600 kJ/mol energy is required for replacing the alkoxide ligand *via* an S_N2 mechanism, while only 20-30 kJ/mol (20 times lower) is required replacing the same alkoxide ligand *via* a proton assisted S_N1 mechanism. It clearly suggests that metal alkoxides undergo hydrolysis *via* a proton assisted S_N1 mechanism. Hydrolytic rates of these metal alkoxides can be controlled by using nucleophilic additives such as carboxylates and beta-diketonates. The alternative strategy is to synthesise the metal oxide networks by non-hydrolytic sol-gel methods in which the oxo bridge is formed by the condensation reaction between two metal centers which is connected to two different metal centers with small molecule elimination. The building block contains reactive functional groups which are expected to react with each other in a controlled fashion both spatially and kinetically.[7]

For this purpose, we have synthesised kinetically labile, thermodynamically stable functional group containing mononuclear building blocks. Various molecular precursors have been prepared namely metal alkoxides such as $Sn(OBu^t)_4$[8], $[\{WO(OMe)_4\}_2]$ [9] and $[\{Nb(OMe)_5\}_2]$ [10] according to the literature.

2.3. Results and discussion

Synthesis of molecular precursors

The molecular precursors for this project are transition metal (Ti, Nb) and main group (Sn, Sb) metal halides, metal alkoxides, metal chloroalkoxides and Polyoxometalates.

2.3.1. Synthesis of metal hexahalides $[MCl_6]^{2-}$

2.3.1.1. Synthesis of $[TiCl_6]^{2-}$

The titanium hexachloride anion was synthesised from direct reaction between dry tetra n-butyl ammonium chloride (TBACl) and $TiCl_4$ in dichloromethane (15 cm^3). Yellow crystals were obtained from slow diffusion of ether upon cooling at -30 ^oC. Elemental analysis supports the formation of $[TiCl_6]^{2-}$ anion.

$$\mathbf{2\ n\text{-}[(C_4H_9)_4N]\text{-}Cl\ +\ TiCl_4 \xrightarrow{\text{Dry DCM}} n\text{-}[(C_4H_9)_4N]_2TiCl_6} \qquad \mathbf{\text{-----}3}$$

2.3.1.2. Synthesis of $[SnCl_6]^{2-}$

$SnCl_4$ was reacted with an equimolar amount of dry TBACl leading to the single product, $TBA_2[SnCl_6]$. Colourless crystals were obtained from slow diffusion of ether in DCM upon cooling at -30 ^oC and were used for further characterisation.

$$\mathbf{2\ n\text{-}\ [(C_4H_9)_4N]\text{-}Cl\ +\ SnCl_4 \xrightarrow{\text{Dry DCM}} [(C_4H_9)_4N]_2\ SnCl_6} \qquad \mathbf{\text{------}4}$$

The product is extremely moisture sensitive and gave one single peak at δ -732 ppm in the ^{119}Sn NMR Spectrum. This clearly suggests that one type of tin species exists in solution, further, the tin exhibits six coordination octahedral geometry. No ^2J $\{^{119}Sn^{117}Sn\}$ satellite coupling was observed in solution, which suggests that in solution tin behaves as a single molecule and is not associated with any other octahedral tin site. Elemental analysis also supports the formation of $TBA_2[SnCl_6]$.

2.3.1.3. Synthesis of $[NbCl_6]^-$

$[NbCl_6]^-$ anion was also synthesised by the same procedure and recrystallised from acetonitrile and ether at room temperature. Elemental analysis supports the formation

of $[NbCl_6]^-$. Niobium NMR is not very informative because of the quadrupolar nature of the nucleus; it has very short spin relaxation time leading to very broad lines.[11]

$$\text{n-}[(C_4H_9)_4N]\text{-Cl} + NbCl_5 \xrightarrow{\text{Dry } CH_3CN} \text{n-}[(C_4H_9)_4N]\,NbCl_6 \quad \text{--------5}$$

2.3.1.4. Synthesis of ^{17}O enriched hexamethyldisiloxane (HMDSO)

^{17}O enriched hexamethyldisiloxane (HMDSO) was prepared by hydrolysis of chlorotrimethylsilane (TMSCl) by using mixture of ^{17}O enriched water (64 µl, 3.27 mmol) and normal distilled water (64 µl, 3.27 mmol) in the presence of 2,6-lutidine in dry ether. The precipitate was identified as 2,6-lutidinium hydrochloride and was separated by filtration. All the volatile impurities were removed by normal distillation and further microdistillation was performed in order to obtain the pure colourless liquid.

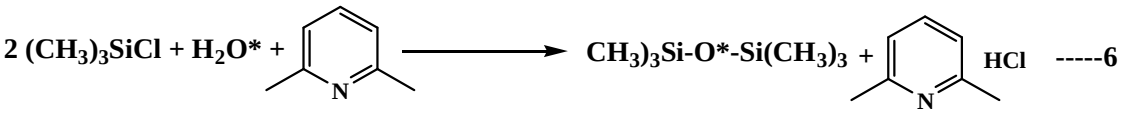

^1H NMR and ^{17}O NMR Spectra showed one single peak at δ 0 ppm and 423 ppm respectively which were assigned to the trimethylsilyl group and the natural abundance of hexamethyldisiloxane. The side product 2,6-lutidinium hydrochloride was used further for acidification reactions.

2.3.2. Hydrolytic studies of $[MCl_6]^{2-}$ (M= Ti, Sn)

^{17}O NMR spectra obtained during the stepwise pseudo hydrolysis of $[TiCl_6]^{2-}$ in DCM are listed in Table 1. It should be noted that in this and all the subsequent tables describing details of the spectra, the molar ratio is the ratio of HMDSO or water: metal added.

2.3.2.1. Stepwise pseudo hydrolysis of $[TiCl_6]^{2-}$ with ^{17}O enriched HMDSO

If an acid (H^+) is present in certain concentration throughout the reaction in solution, it may be found to decrease the concentration of one of the reactant (*via* hydrolysis) and according to chemical kinetics the term is called acid catalysis. If the substance does not provide H^+ in solution, at the same time it performs like acid catalysis and decrease the reactant concentration then the term is called as pseudo-hydrolysis.

Upon pseudo-hydrolysis, one new signal in the ^{17}O NMR spectrum was obtained at δ 493 ppm along with the reactant [$(Me_3Si)_2O$*] at 43 ppm which remain until a HMDSO:Ti ratio of 3:1 is reached. (Fig. 2.1) At lower concentration, the new signal intensity was gradually increased upon addition of HMDSO but at higher concentration, the intensity of the new peak was not changed as much. It is noteworthy that at higher concentration, the HMDSO peak intensity was increased significantly. Initially, we were trying to replace one of the active halide functional group by using HMDSO. These types of reactions are termed as pseudo hydrolysis. We had expected to observe the monomer Cl_5Ti-$OSiMe_3$ which would possibly be reactive in solution. The monomer is likely to interact very rapidly with other molecular precursors, and the product is expected to form μ_2-OTi_2 bridged species. Klemperer *et.al* [12] identified that in Ti oxoalkoxides, μ_2-OTi_2 and μ_3-OTi_3 species are usually observed in the region between δ 850-650 and 650-450 ppm in ^{17}O NMR spectra. The new signal was obtained at δ 493 ppm was compared with the Ti oxoalkoxides chemical shift as earlier reported. It clearly indicates that some μ_3-OTi_3 species should have formed in solution. Yellow crystals were formed upon cooling at -30 ^oC in a DCM/Toluene mixture but the crystals were very thin and did not diffract well in an X-ray diffractometer. Based on these results we proposed the possibility of a triply bridged species (Fig 2.2) forming in solution rather than a doubly bridged species.

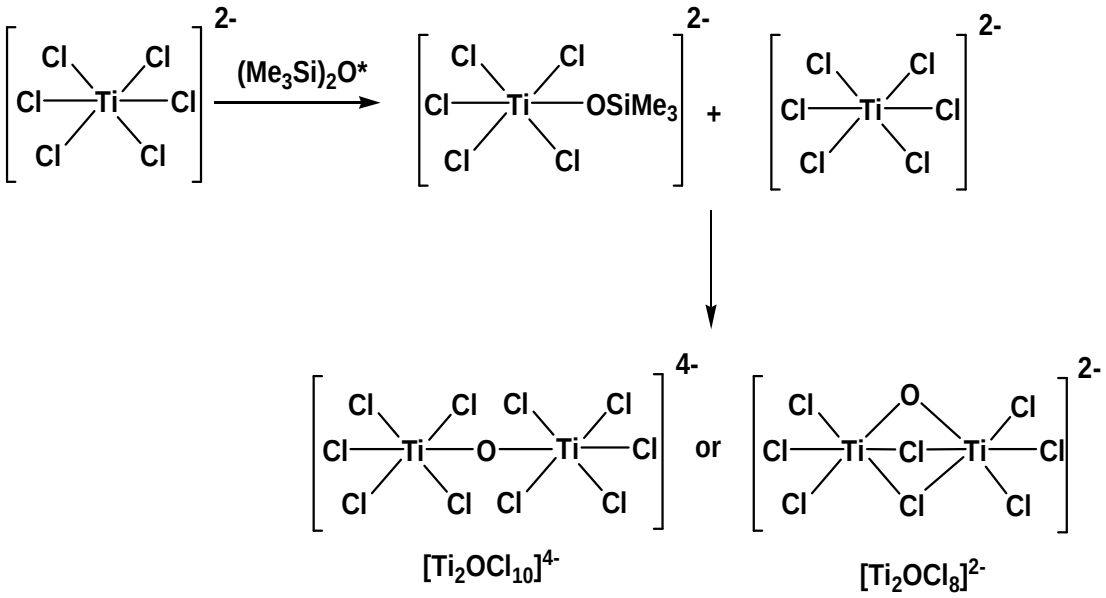

Fig. 2.1: Proposed mechanism of hydrolytic studies of $[TiCl_6]^{2-}$ by using HMDSO.

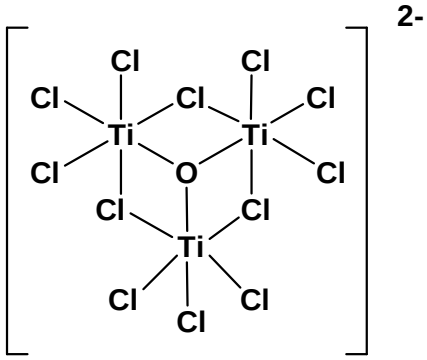

Fig. 2.2: Proposed structure of triply bridged species $(Ti_3OCl_{12}]^{2-}$

Attempted recrystallisation in various solvents was unsuccessful and at room temperature the crystals melt very quickly and turn to yellow oil.

Experiment	HMDSO(µl)	Molar Ratio	Results (ppm)
1	6	0.1	492 (s), 43 (s)
2	12	0.2	493 (s), 43(s)
3	30	0.5	492 (bs), 42.4 (s)
4	42	0.7	493 (bs), 43 (s)
5	60	1	493 (bs), 43 (vs)

Table 2.1: Reaction between $[TiCl_6]^{2-}$ and HMDSO in DCM at 293K.

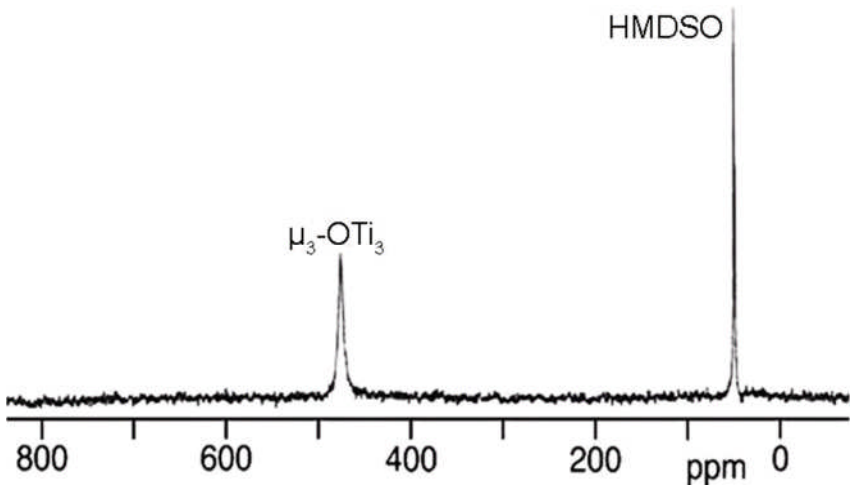

Fig. 2.3: ^{17}O NMR spectrum of reaction between 3 eq. of HMDSO and $[TiCl_6]^{2-}$

2.3.2.2. By using ^{17}O enriched water

The stepwise hydrolysis of $[TiCl_6]^{2-}$ was done by using ^{17}O enriched water rather than HMDSO. The rate of hydrolysis of this reaction was expected to be very rapid and observe many possible doubly and triply bridged species.

Upon initial hydrolysis i.e. H_2O:Ti ratio is 0.125:1, one broad major signal was obtained at δ 837 in the ^{17}O NMR spectra. At this point, we were not able to observe the water signal in ^{17}O NMR. After addition of 0.5 equivalents of water to the reaction mixture, one new signal appeared at δ 40 ppm. Upon increasing the concentration of water further, i.e. 0.5 to 1.5, a new peak appeared at δ 738 ppm. At higher concentration, i.e 2:1, another new peak appeared at δ 787 ppm. The major signals at 837, 787 and δ 738 fall within the μ_2-OTi_2 regions previously identified, but do not match those of known oxoalkoxides. In spite of this, it is apparent from the line widths that many solution species may exist in dynamic equilibrium, all with doubly and triply bridging oxo ligands. The most interesting observation in this reaction after an addition of excess water, was that there was no gelation or precipitated in this reaction. We have concluded that hydrolysis of titanium hexahalides produces various doubly and triply bridging oxo species and ligand re-distribution in solution is very fast.

The reaction mixture gave yellow crystals in DCM/hexane but unfortunately the crystals were very thin and did not diffract well in the diffractometer. Attempted preparation to isolate large crystals in various solvents was unsuccessful.

Experiment	Water (µl)	Molar Ratio	Results (ppm)
1	1	0.125	837 (bs)
2	2	0.25	834, 40 (bs)
3	4	0.5	825(s), 36 (bs)
4	5	0.625	822, 738, 43
5	6	0.75	825, 738, 36
6	8	1	823 (bs), 731(s), 30
7	10	1.25	820, 735, 37
8	12	1.5	820, 731, 45
9	14	1.75	820, 786 (bs), 731(s) and 37
10	16	2	816, 789 (bs), 731(s) and 45

Table 2.2: Hydrolysis of $[TiCl_6]^{2-}$ in DCM at 293K

2.3.2.3. Hydrolysis of $[SnCl_6]^{2-}$

Hydrolysis of hexachloro titanate $[TiCl_6]^{2-}$ has been discussed in the section, **2.3.2.2** and we are proposing that triply bridged species might be formed in solution. We have applied the same approach to main group metal hexahalides i.e. $[SnCl_6]^{2-}$. We had expected to observe the formation of $[Cl_5Sn\text{-}OH_2]^-$ reactive species in solution rather than observe the hydrolytic product $[Cl_5Sn\text{-}OH]^{2-}$. M.J.Taylor *et.al* [13] thoroughly studied the tin(IV) halide especially $SnCl_4$ hydrolysis in aqueous medium and found the chemical shifts of complexes $[SnCl_5(H_2O)]^-$, $[SnCl_4(H_2O)_2]$ and $[SnCl_6]^{2-}$ appeared at -648, -677 and -720 ppm in the ^{119}Sn NMR. These results were expected to be replicated in non-aqueous medium also but stepwise hydrolytic studies of $[SnCl_6]^{2-}$ spectra did not show any new characteristic peaks in ^{119}Sn NMR. The TBA salts of $[SnCl_6]^{2-}$ appeared at δ -732 ppm in the ^{119} Sn NMR spectrum in CD_2Cl_2. After addition of two equivalents of water, precipitates were immediately formed but no significant peaks were observed in the ^{119}Sn NMR. However, a small shoulder peak was observed at 6.8 ppm in the ^{17}O NMR spectrum when the water to metal ratio was 2:1. Upon increasing the concentration of water, the multinuclear NMR spectra were not affected significantly.

2.3.4. Synthesis of $Ti(OSiMe_3)_4$

Titanium tetrakis(trimethylsiloxide) was prepared by the direct reaction between titanium alkoxide and trimethylsilylacetate according to the literature. [14]

$$Ti(OPr^i)_4 + 4\,(CH_3)_3SiOAc \longrightarrow Ti(OSi(CH_3)_3)_4 + 4\,{}^iPrOAc \quad \text{----7}$$

Trimethylsilylacetate was added very slowly by using a time controlled syringe pump to the hot titanium tetraisopropoxide in cyclohexane. Simultaneously isopropyl acetate was removed by azeotropic distillation at room temperature. The remaining residue was further distilled in *vacuo* at a pressure of 7 mm/Hg at 110 ^oC. Pure light greenish liquid was obtained and used in subsequent reactions.

The ^1H and ^{17}O NMR spectra depict one single peak at 0 and 289 ppm for the trimethylsilyl group. IR showed characteristic Ti-O vibration band at 527 cm^{-1}.

2.3.4.1. Hydrolytic studies with ^{17}O enriched water

The ^{17}O enriched H_2O showed one single peak at δ -0.2 ppm and we assigned it to the natural abundance peak for H_2O. Upon hydrolysis of $Ti(OSiMe_3)_4$ with water at low concentrations, the spectra showed two strong signals at δ 553 and 292 ppm. After hydrolysis, no gelation or precipitate was observed. Based on the previous literature reports of the Ti oxoalkoxides, we propose that it may be a doubly bridged species. However, we cannot definitely discuss the product formed in this stage until the crystals obtained from the solution.

2.4. Attempted synthesis of hexaalkoxometalates $[M(OMe)_6]^{2-}$ (M=Ti, Sn)

An attempted synthesis of metal hexaalkoxides from various synthetic routes has not been successful. Initially, hexachloro anion precursors were treated with sodium methoxide in excess methanol to prepare the corresponding alkoxo derivatives of the metal.

$$n\text{-}[(C_4H_9)_4N]_2\,[MCl_6] + 6\,NaOMe \xrightarrow{\text{Dry MeOH}} n\text{-}[(C_4H_9)_4N]_2\,[M(OMe)_6] + 6\,NaCl \quad \text{-----8}$$

$$M=Ti,Sn$$

At room temperature, this aforementioned reaction produced only an oily material. No peaks were observed for the methoxide group in the ^1H and ^{13}C NMR spectra

respectively. Hexaalkoxotitanates did not produce any single crystals at room and low temperatures but attempted synthesis of hexaalkoxostannates gave only tetrabutyl ammonium chloride at -30 ^{o}C, which was confirmed by single crystal x-ray diffraction.

In an alternative route, we tried to prepare alkoxide precursors from the parent halides but this method also gave only oily products. The oily materials have been characterised by ^{1}H NMR spectroscopy. The proton NMR showed only tetrabutyl ammonium peaks and no methoxide peak was observed for all the compounds. However, attempted synthesis of $[Me_3NCH_2Ph]$ $[Sn(OMe)_6]$ from the parent alkoxide $Sn(O^tBu)_4$ and benzyl trimethyl ammonium methoxide leads to the dinuclear product $[Sn_2(OMe)_9]^-$. The solid state structure of the anion $[Sn_2(OMe)_9]^-$ is depicted in Fig.2.4

In the crystal structure, both tin atoms are connected through the three methoxide bridges and are six coordinate.

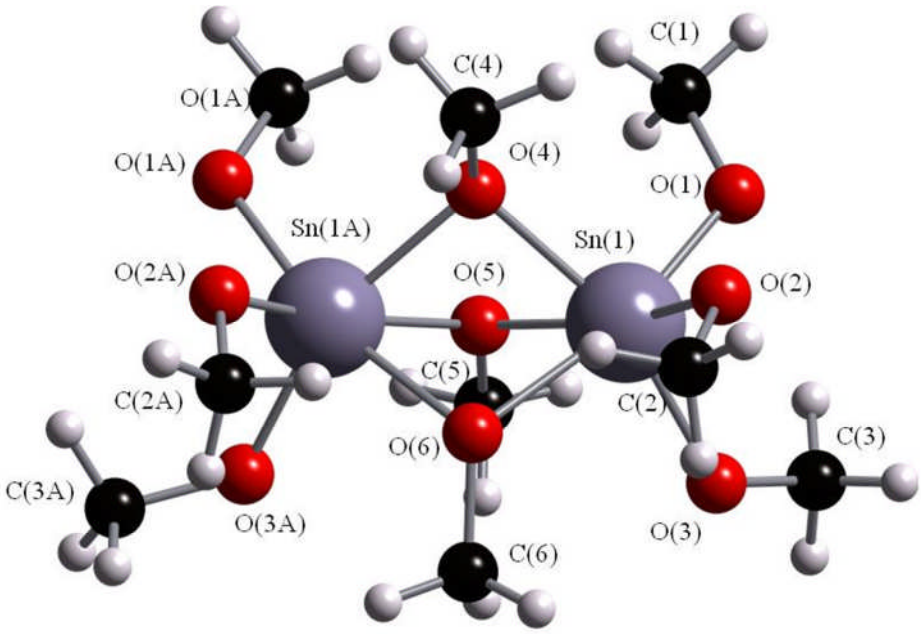

Fig. 2.4: Structure of the anion $[Sn_2(OMe)_9]^-$. The colour codes are as follows. Sn(Grey), O(red), C(black) and H(grey)

Sn(1)-O(1)	1.980	Sn(1A)-O(1A)	1.982
Sn(1)-O(2)	1.990	Sn(1A)-O(2A)	1.988
Sn(1)-O(3)	1.987	Sn(1A)-O(3A)	1.976
Sn(1)-O(4)	2.121	Sn(1A)-O(4)	2.128
Sn(1)-O(5)	2.137	Sn(1A)-O(5)	2.118
Sn(1)-O(6)	2.126	Sn(1A)-O(6)	2.169
Sn(1)-Sn(1A)	3.102	Sn1(A)-O(4)-Sn(1)	101.077
Sn(1A)-O(5)-Sn(1)	98.591	Sn(1A)-O(6)-Sn(1)	92.472
Sn(1)-O(1)-C(1)	122.293	Sn(1)-O(2)-C(2)	120.184

Table 2.3: Selected bond lengths (Å) and bond angles (^{o}) of $[Sn_2(OMe)_9]^-$ anion.

Based on the solid state structure, $[Sn_2(OMe)_9]^-$ was expected to give two methoxide peaks in the ^{1}H NMR spectrum but at room temperature only a single peak at δ 3.3 ppm was observed. This indicates a rapid exchange process between the bridging and terminal methoxide groups. Variable temperature ^{1}H NMR Spectroscopy was performed and showed two peaks with 6:3 ratio at -60^{o}C which is consistent with the solid state structure. In addition, we have clearly identify the $^3J\{^{119}Sn^1H\}$ coupling constant for terminal methoxide groups from the low temperature ^{1}H NMR spectrum. The coupling constant value was measured and the value is 65 Hz.

2.4.1. Variable Temperature ^{1}H NMR studies

The product is dynamic in solution with the observation of one set of ^{1}H NMR signals for the methoxide groups at ambient temperature (a). In order to probe the solution structures of $[Sn_2(OMe)_9]^-$, the sample were subjected to VT ^{1}H NMR studies in CD_2Cl_2 and selected spectra are shown in Fig. 2.5. At 0 ^{o}C (b), the methoxide peak was slightly broadened and some satellite peaks were observed. It was not as well resolved as we had expected at this temperature.

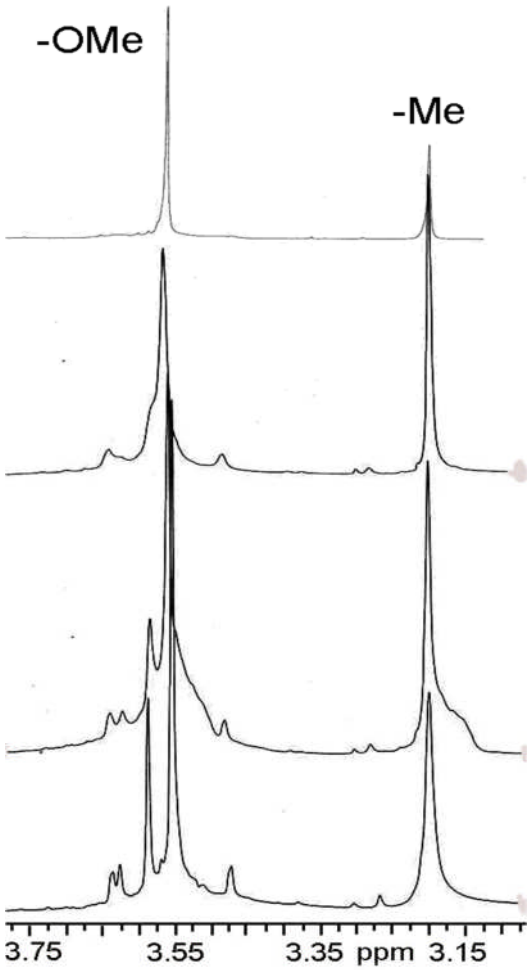

Fig. 2.5: Variable ^{1}H NMR spectra of $PhCH_2NMe_3$ $[Sn_2(OMe)_9]$ a) 23 ^{o}C b) 0 ^{o}C c) -10 ^{o}C, d) -50^{o}C.

When the temperature was lowered to -10^{o}C (c), two peaks were seen in the methoxide region at δ 3.58 and 3.62 ppm and these were assigned to the bridging and terminal methoxide peaks respectively. However the integration was not good enough to assign the counter cation. When the temperature was lowered to -50 ^{o}C (d), the methoxide peak was completely resolved and it showed two sets of peaks with 3:1 ratio. In addition, we also measured $^{3}J\{^{119}Sn^{1}H\}$ coupling constant for methoxide protons at this temperature. Further reduction of the temperature did not affect the resolution of the spectrum. The above variable temperature (VT) ^{1}H NMR studies suggest that the anion remains dimeric in solution, at least at low temperatures, as well as in the solid state.

2.4.2. Variable temperature ^{13}C NMR studies

At ambient temperature, anion $[Sn_2(OMe)_9]^-$ showed a single peak at 69 ppm in the ^{13}C NMR Spectrum which corresponds to a methoxide carbon. Attempted low temperature ^{13}C NMR studies to differentiate bridging and terminal carbons have not been successful because the product was fairly soluble in CD_2Cl_2. At -60 ^oC, the cation i.e. benzyl trimethyl ammonium ($PhCH_2NMe_3$) peaks overlapped with anion $\{[Sn_2(OMe)_9]^-\}$ peaks and were not well resolved at this temperature. The low temperature ^{13}C NMR spectrum were not sufficiently resolved to differentiate the two types of carbon. ^{119}Sn NMR spectrum showed one single peak at -598 ppm, which suggest that anion $[Sn_2(OMe)_9]^-$ contains only one type of tin center and exhibits six coordination in solution.

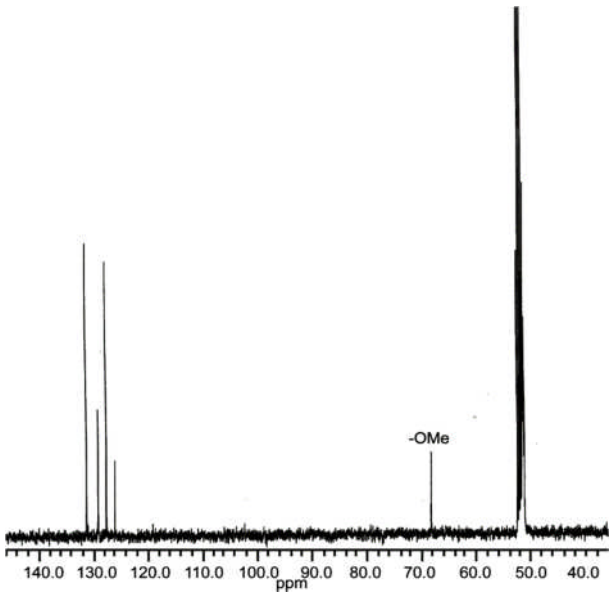

Fig. 2.6: ^{13}C NMR spectrum of $Q[Sn_2(OMe)_9]$ $Q=BzNMe_3$ $Bz=PhCH_2$

2.4.3. Infra red spectroscopy

The Infra – red spectrum of $[Sn_2(OMe)_9]^-$ showed a very strong band at 728 cm^{-1} which is assigned to the Sn-O-Sn stretching frequency, [15] and this value is consistent with a heteronuelcar Lindqvist type tin polyoxometalate dimer which are discussed in Chapter 3. The spectrum also showed very strong bands at 1060 and 1029 cm^{-1} along with counter cation stretching bands. These strong bands are assigned for C-H deformation for both bridging and terminal methoxide groups. Hampden smith *et.al* [8] performed isotopic labelling experiments in order to assign the M-O stretching

frequency and assigned the Sn-O stretching frequency at 605 cm^{-1} but the crystal structure $[Sn_2(OMe)_9]^-$ does not shown any band near 550-700 cm^{-1}. Elemental analysis supports the formulation as Me_3NCH_2Ph $[Sn_2(OMe)_9]$

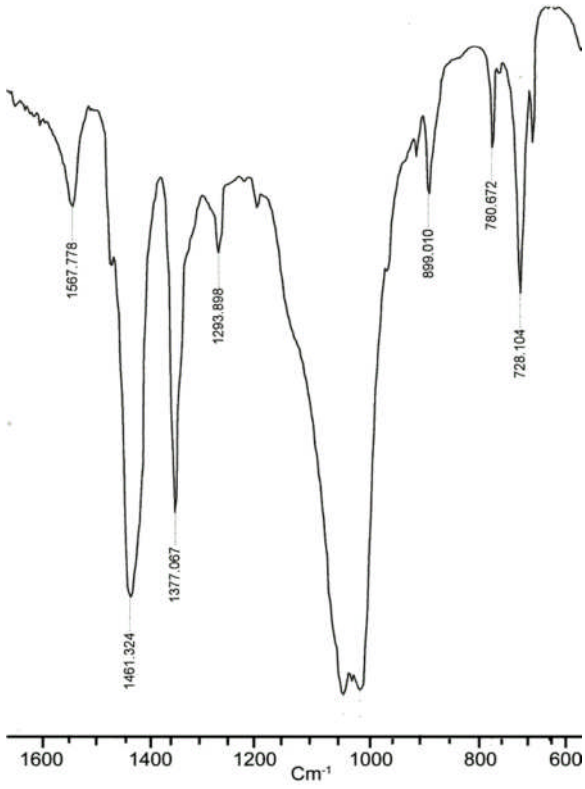

Fig. 2 7: Infra red spectrum of anion $[Sn_2(OMe)_9]^-$

2.5. Attempted synthesis of hexahydroxometalates $[M(OH)_6]^{2-}$

Attempted synthesis of metal hexahydroxo anion from transition and main group metal halides in water produced oily products. Initially, the reaction between metal halides and tetrabutyl ammonium hydroxide (TBA OH) had been expected to give possible mononuclear precursors $[M(OH)_6]^{2-}$. Attempted recrystallisation by various methods has not been successful.

$$\mathbf{MCl_4 + 2\ TBAOH\ in\ H_2O \xrightarrow{Dry\ DCM} TBA_2[M(OH)_6]} \qquad \mathbf{M=Ti,\ Sn} \qquad \mathbf{-----9}$$

$[Ti(OH_2)]^{2+}$, $[Ti(OH)_3]^+$, $Ti(OH)_4$, $[Ti(OH)_5]^-$ have been proposed as intermediate products in sol-gel methods in the synthesis of TiO_2 and the solution chemistry was investigated by Sugimato *et.al.*[16] Recently M. Veith *et.al* [17] reported that hydrolysis of $Ti(OPr^i)_4$ in [BMIM] BF_4 in ethanol produced $[BMIM]_2$ $[Ti(OH)_6]$ as was confirmed

by single crystal X-Ray diffraction and ^{1}H NMR Spectroscopy. In addition, they found that the attempted synthesis of the Bu_4N^+ and Bu_4P^+ salts $[Ti(OH)_6]^{2-}$ leads only to oily products which is consistent with our results.

2.6. Synthesis of niobium pentamethoxide

Niobium pentamethoxide was obtained by simple methanolysis of niobium pentachloride. Excess dry methanol was added to a solution of niobium pentachloride in toluene and was allowed to stir at room temperature until the solution was clear then excess ammonia was passed through the solution. The mother liquor was carefully separated and evaporated under vacuum. Colourless crystals were obtained from the crude product upon cooling at -30 ^{o}C in dry hexane.

^{1}H NMR spectra showed that two single peaks are observed at δ 4.3 and 4.5 ppm. Based on the molecular structure, three singlet peaks are expected in a ratio 2:2:1 ratio as a result of the different environments experienced by the hydrogen atoms in the methyl groups and dimerisation of niobium alkoxide occurs through asymmetric alkoxo bridges which are coplanar with three different types of methoxide groups. Riess *et.al* [10] reported that niobium exhibits octahedral coordination geometry and the crystal structure shows two different conformers are presented in the single asymmetric unit cell.

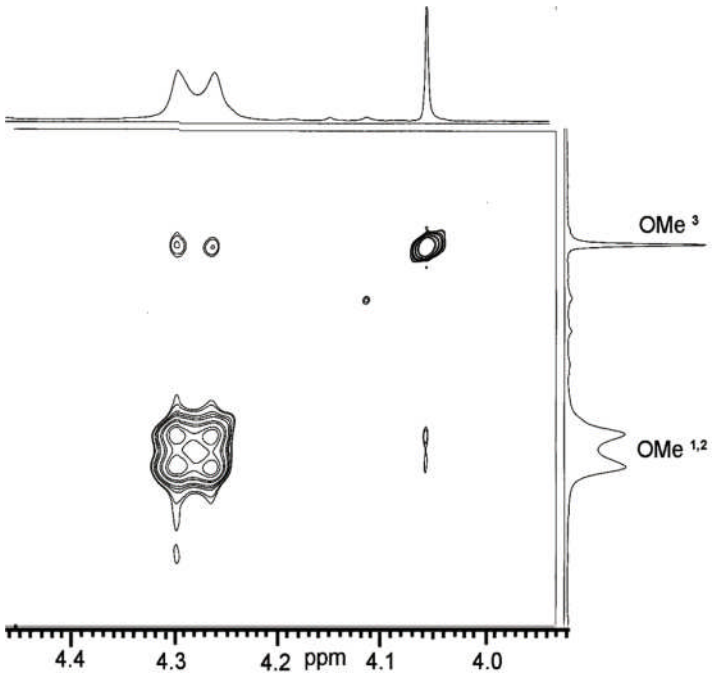

Fig. 2.8: 2D EXSY spectrum of $\{Nb(OMe)_5\}_2$ in Tol-d_8.

VT ^{1}H NMR studies suggest us that bridged, terminal methoxide protons are dynamic in nature and involved in exchange at room temperature. We were interested to carry out low temperature ^{1}H EXSY studies of $\{Nb(OMe)_5\}_2$ in order to establish whether a stepwise exchange process could be observed. The spectrum in the Fig. 2.8 was taken at -36^{o}C with 500 ms mixing time. It clearly indicates that at low temperature, the terminal, axial methoxide groups exchanged with bridged methoxide groups. Currently we are investigating the exchange rate of the methoxide groups.

2.7. Synthesis of niobium chloroalkoxides

M. Schoenherr *et.al* [18] first reported that methanol (MeOH) slowly reacted with $NbCl_5$ in CCl_4 at 20^{o}C and produced $NbCl_n(OMe)_{5-n}$ (n=1-3), and all compounds exist as a dimer in hydrocarbon solvents. However this method leads mixture of products. Errington *et.al* [19] successfully prepared the $Nb(OMe)_4Cl$ by reacting $\{Nb(OMe)_5\}_2$ with 2,6-lutidinum hydrochloride. 2,6-lutidinum hydrochloride was used to chlorinate the nioboium methoxide. Hot 2,6- lutidine hydrochloride in dichloromethane was added to $\{Nb(OMe)_5\}_2$ in DCM. Immediately a cloudy solution was formed which turned into a clear solution upon heating. The expected side products are 2,6- lutidine and methanol were easily removed under vacuum and colourless crystals were obtained from the crude product in saturated toluene upon cooling to -30 ^{o}C. These crystals were used for further characterisation.

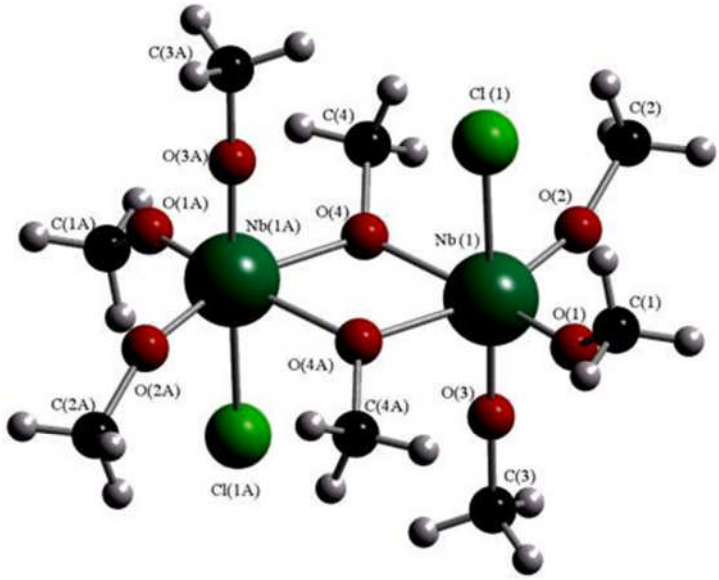

Fig. 2.9: Crystal structure of $\{Nb(OMe)_4Cl\}_2$ The colour codes are as follows Nb(dark green), Cl(pale green), O(red) and C (black)

Nb(1)-O(1)	1.873	Nb(1)-O(4)-Nb(1A)	109.775
Nb(1)-O(2)	1.856	Nb(1)-O(2)-C(2)	153.495
Nb(1)-O(3)	1.849	Nb(1)-O(1)-C(1)	146.888
Nb(1)-O(4)	2.099	Nb(1)-O(3)-C(3)	176.379
Nb(1)-O(4A)	2.122	Nb(1)-O(4)-C(4)	123.229
Nb(1)-Cl(1)	2.481	Nb(1)-O(4A)-C(4A)	120.594

Table 2.4: Selected bond lengths (Å) and bond angles (^{o}) of $\{Nb(OMe)_4Cl\}_2$

The product $[Nb(OMe_4)Cl]_2$ was recrystallised from hot toluene upon cooling to -30^{o}C. An X-Ray crystallographic determination revealed that the asymmetric unit consists of $\{Nb(OMe)_4Cl\}_2$ with the dimer being centrosymmetric around a crystallographic inversion center. The two niobium atoms are asymmetrically bridged by two methoxide groups, with Nb-O bond lengths of 2.099 Å and 2.122 Å respectively. The Nb-O bond lengths are comparatively smaller than in the previously reported complex (Nb-O) 2.104 Å and 2.157 Å in [NbCl(μ-OMe)[$N(SiMe_3)_2$]($NSiMe_3$)]$_2$.[20] Steric effects may play a considerable role in determining the Nb-O bond lengths. Niobium exhibits a distorted octahedral coordination geometry in $\{Nb(OMe_4)Cl\}_2$.

Solution studies of $[\{Nb(OMe)_4Cl\}_2]$

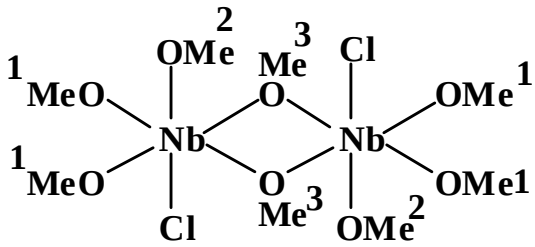

Fig. 2.10: Structure of $\{Nb(OMe)_4Cl\}_2$

2.7.1. ^{1}H NMR in tol-d_8 and CD_2Cl_2

^{1}H NMR spectroscopy was used to analyse the colourless crystals of $[\{Nb(OMe)_4Cl\}_2]$ as a solution in d_8-toluene. Based on the solid state structure, at ambient temperature the product was expected to show three sets of peaks with a 4:2:2 ratio but we observed only two sets of peaks with a 3:1 ratio at δ 4.09 and 4.26 ppm. We assigned the peak observed at δ 4.26 ppm to terminal methoxide (**1** and **2**) and the other peak

observed at δ 4.09 ppm to bridged methoxide (**3**) protons. The terminal methoxide peaks are slightly broad compared to bridging one suggesting us that these protons are dynamic, involving exchange in solution at room temperature.

During the course of the study, we found that [{$Nb(OMe)_4Cl$}$_2$] was fairly soluble in deutrated dichloromethane (CD_2Cl_2) and the ^{1}H NMR spectrum of [{$Nb(OMe)_4Cl$}$_2$] at room temperature was observed to be slightly different from that in deutrated toluene- d_8 ($C_6H_5CD_3$). In CD_2Cl_2, the same product showed two sets of peaks with a 3:1 ratio at δ 4.09 and 4.33 ppm. The observed chemical shifts in CD_2Cl_2 are slightly deviated from the previous one. The different dielectric constants of the solvents may affect the chemical shifts of the product, however, the reason is not clearly understood and further work is needed to understand the complete solution behaviour of this novel compound in various solvents. It is noteworthy to analyse the niobium chloroalkoxide compound by variable temperature ^{1}H NMR and EXSY spectroscopy methods to confirm the solution behaviour at a modest level.

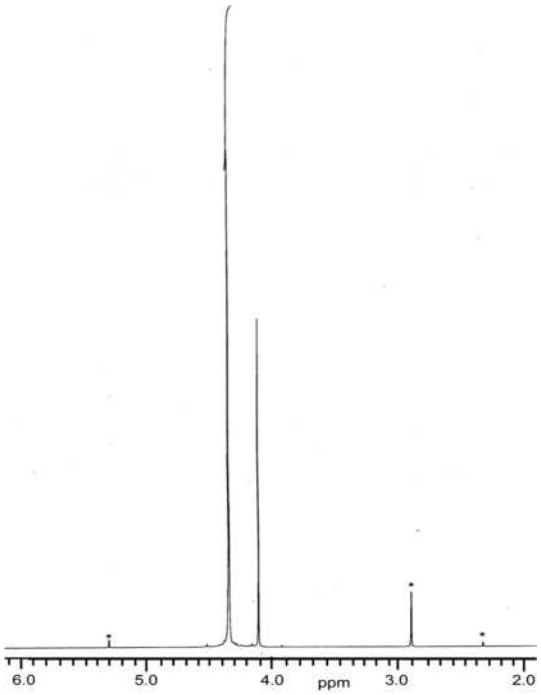

Fig. 2.11: ^{1}H NMR spectrum of {$Nb(OMe)_4Cl$}$_2$ in CD_2Cl_2 at RT.

2.7.2. Variable temperature ^{1}H NMR studies

At ambient temperature, the ^{1}H NMR spectrum of [{$Nb(OMe)_4Cl$}$_2$] in CD_2Cl_2 showed two peaks in the ratio of 3:1. The peak observed at δ 4.33 ppm is slightly

broadened suggest us that the haloalkoxo species is not static in solution. A low temperature ^{1}H NMR spectroscopy study of $[\{Nb(OMe)_4Cl\}_2]$ in CD_2Cl_2 was performed and the results are shown in Fig. 2.12.

We confirmed that the peak at δ 4.33 ppm is temperature dependent giving a broad peak at room temperature, but being well resolved at low temperature. At room temperature, two different terminal methoxide (**1** and **2**) protons are involved in exchange and gave a broad peak. However at low temperature (-80 ^{o}C) the major peak has split into two and in total three different kinds of peaks were observed. The peaks observed at δ 4.29, 4.27 and 4.04 ppm are assigned for trans (**2**), terminal (**1**) and bridged (**3**) methoxide protons, respectively. In addition, some very less intense peaks were also observed at this temperature and because of the low intensities of these minor peaks, we could not able to integrate and relate them to the haloalkoxide completely.

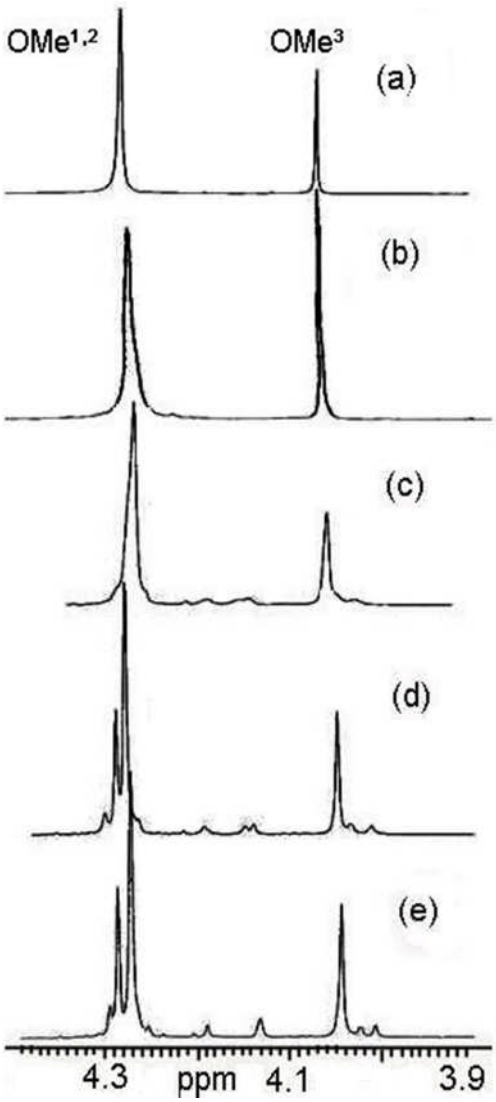

Fig. 2.12: Variable temperature ^{1} HNMR studies of $\{Nb(OMe)_4Cl\}_2$ in CD_2Cl_2 a) 23 ^{o}C, b) 0 ^{o}C c) -50 ^{o}C d) -60 ^{o}C e) -80 ^{o}C.

From low temperature NMR spectroscopy studies, we confirmed that the two different types of terminal methoxide (**1** and **2** in Fig 2.10) groups are exchanging in solution. However, because of the solvent temperature limitation, we were not able to obtain EXSY spectrum using CD_2Cl_2 solvent at high temperature. NMR spectra of $\{Nb(OMe)_4Cl\}_2$ at higher temperatures clearly revealed ligand exchange.

2.7.3. High temperature ^{1}H NMR studies

Toluene-d_8 was the best choice to explore the exchanging phenomena of $\{Nb(OMe)_4Cl\}_2$ at higher temperature in solution. At room temperature, the haloalkoxide compound showed two sets of peaks with 3:1 ratio, however the peak

observed at δ 4.26 ppm was quite broad compared to the other one (See section **2.7.1**) When temperature increases, we were expected to observe one single peak for all the three methoxide groups (**1**, **2** and **3** in Fig. 2.10) but we are not observed coalescence resonance in ^{1}H NMR.

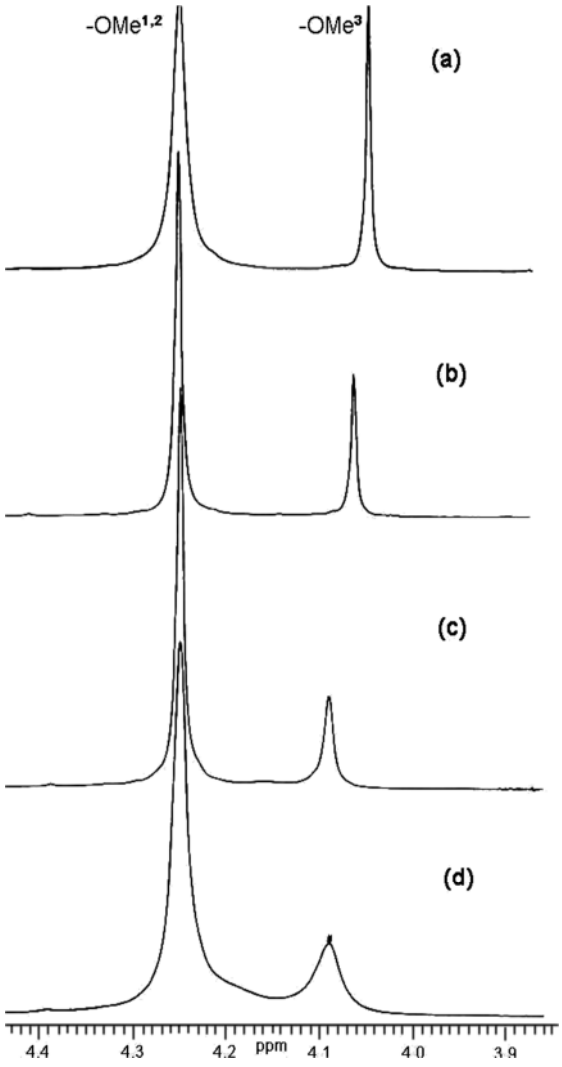

Fig. 2.13: Variable temperature ^{1}H NMR studies of $\{Nb(OMe)_4Cl\}_2$ in Tol-d_8. a) 23 ^{o}C b) 50 ^{o}C, c) 65 ^{o}C, d) 80 ^{o}C.

A 2D EXSY spectrum was taken at 60 ^{o}C with 200 ms mixing time; it showed all the three methoxide protons are involving in the exchange process. It apparently showed that solution studies of $\{Nb(OMe)_4Cl\}_2$ is very similar to its parent alkoxide i.e. $\{Nb(OMe)_5\}_2$ and Group IV alkoxides $[\{M(OR)_4\}_2]$ M = W. Errington *et.al* [21] proposed that a bond dissociation process is taking place in solution and the alkoxide

complexes are present as dimers which undergo facile intramolecular alkoxide exchange, and no monomers being observed. If the same bond dissociation happens to $[\{Nb(OMe)_4Cl\}_2]$ in solution, it possibly would produce many different structural isomers. This can be interpretated, when rotate Nb-OMe^3 bond by small angle, two important exchanges might be expected. Primarily, bridging ($OMe^{\mathbf{3}}$) ligand can exchange the position with axial methoxide lignd ($OMe^{\mathbf{2}}$). Secondly, bridging alkoxide ligand ($OMe^{\mathbf{3}}$) can easily exchange the position with chloride ligand. In addition, the exchange between two terminal methoxide lignads is also expected. When temperature increases further, fast exchange might be expected between three alkoxide ligands (**1**, **2** and **3**) in solution. Due to high energy, Nb-OMe^3 bond breaks and two five coordination Nb atoms might be formed in solution. The 'clock-wise' mechanism is clearly explained with suitable diagram in Fig. 2.14.

We are proposing that 'clock-wise' rotation mechanism happens in solution. At room temperature, bridging alkoxide bond dissociates very easily and high temperature, dimer dissociates completely and both Nb atoms exhibit five coordination due to high energy.

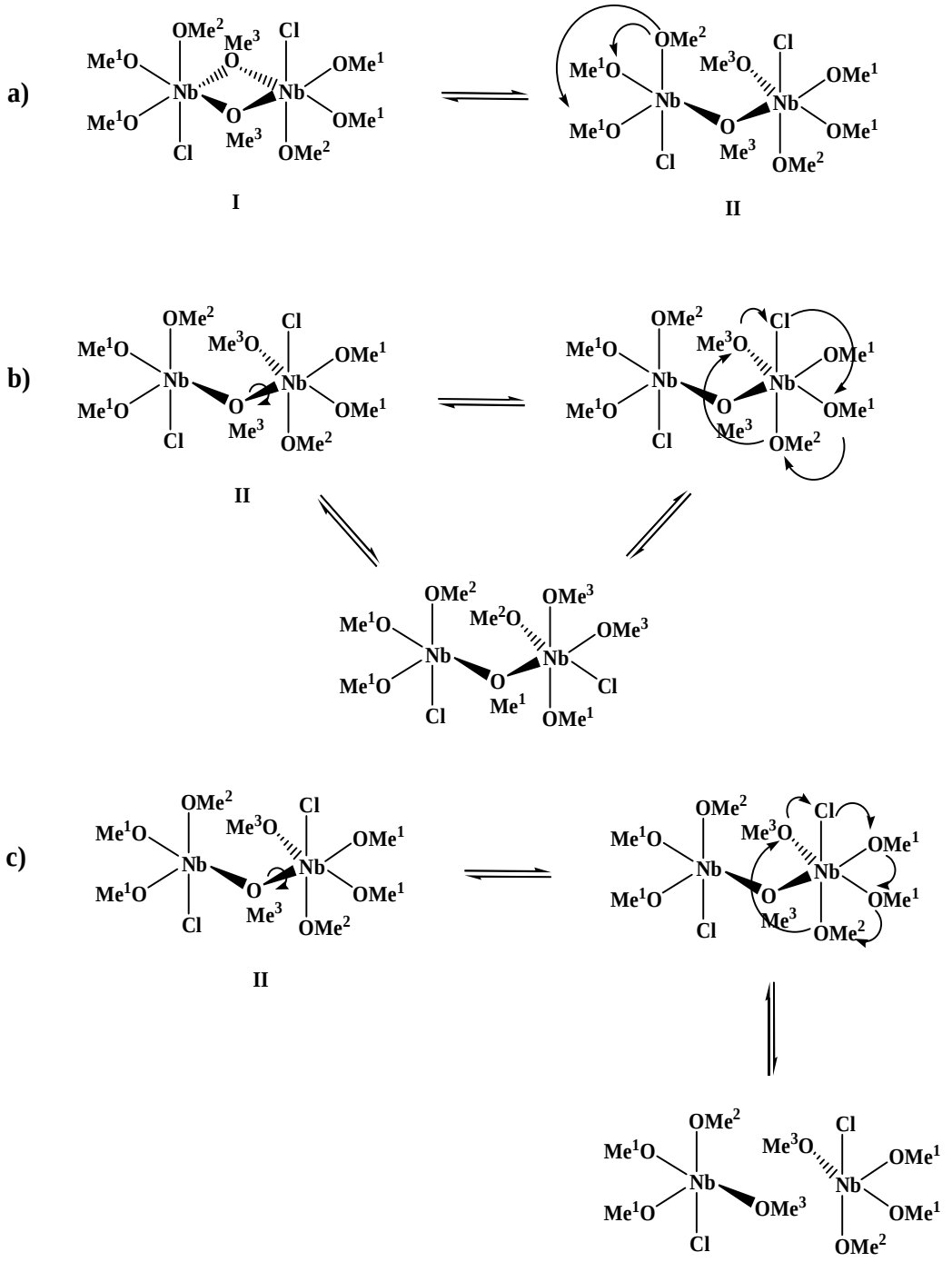

Fig. 2.14: Proposed Clock-Wise mechanism of $\{Nb(OMe)_4Cl\}_2$ in tol-d_8. a) at low energy, b) rotation around Nb-OMe^3 by small angle c) full rotation Nb-OMe^3

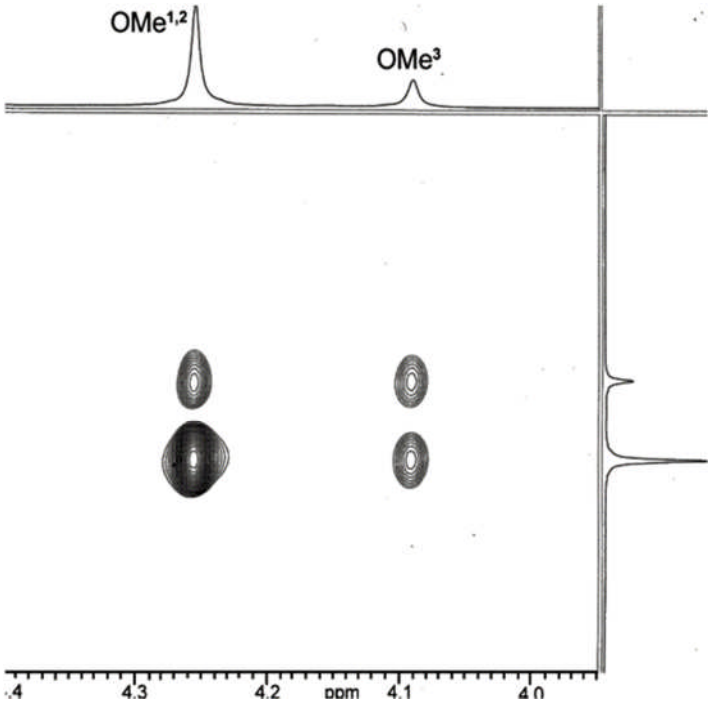

Fig. 2.15: 2D EXSY spectrum of $\{Nb(OMe)_4Cl\}_2$ at 60^oC in Tol-d_8

In conclusion, at room temperature, the haloalkoxide terminal methoxide protons (**1** and **2** in Fig. 2.10) showed broad peaks due to exchange. At high temperature (60^oC to 80^oC), in addition with terminal methoxides, bridged methoxide groups are also involved in the exchange which was confirmed by 2D EXSY ^1H NMR spectroscopy. The ^{13}C NMR Spectrum depicts one single peak at 65.8 ppm due to the alkoxide carbon. Elemental analysis also supports the compound as $\{Nb(OMe)_4Cl\}_2$.

2.8. Attempted synthesis of cationic alkoxoclusters

Cationic metal alkoxide are expected to be highly electrophilic and therefore are of interest for Lewis acid catlaysis, olefin polymerisation, and other potential applications. Jordon *et.al* [22] reported the synthesis and molecular structure of the first example of cationic dinuclear species with the bridging alkoxide group, $[\{(^iPr_2\text{-ATI})Al(\mu\text{-}O^iPr)\}_2]^{2+}$ (ATI= N,N-diisopropylamino-troponiminate ligand), however, interaction of metal alkoxides with metal halides in non-aqueous media is generally very poorly researched area, due in particular to the extreme sensitivity of the formed heterometallic alkoxide halides. Errington *et.al* [23] carried out a reaction between molybdenum oxomethoxide and $BiCl_3$ expecting a molecular aggregation of the heteromolecular alkoxide but the reaction leads to a mononuclear $[Mo(OMe)_5CH_3CN]$ Bi_2Cl_7 cationic alkoxide species in non-aqueous medium. During the course of the

study of niobium haloalkoxides, we were interested to synthesise the mononuclear cationic alkoxides by abstraction of halide from $\{Nb(OMe)_4Cl\}_2$ by using metal halides in non-aqueous medium.

$$\mathbf{2\ \{[Nb(OMe)_4Cl]_2\} + 4SbCl_5 \xrightarrow{Dry\ DCM} [Nb_4(OMe)_{16}](SbCl_6)_4} \qquad \mathbf{-----10}$$

Niobium chlorotetramethoxide was reacted with an equimolar amount of antimony pentachloride ($SbCl_5$) in dichloromethane. It was expected to form niobium alkoxo cationic clusters by removal of Cl^- from $\{Nb(OMe)_4Cl\}_2$ by using highly Lewis acidic halide $SbCl_5$ but this reaction afforded the pale brown needle shaped crystals and the structure is very similar to triethyloxonium salts of antimony hexachloride.[24] We suspect that the solvent diethyl ether easily reacts with antimony pentachloride to produce oxonium salts of the corresponding hexahalide. However, further work is needed to explore this field.

2.9. Synthesis of $[Sb(O^iPr)_5(NH_3)]$

Antimony alkoxide $[Sb(OEt)_5(NH_3)]$ was previously prepared by passing NH_3 through a mixture of $SbCl_5$ and EtOH.[25] We adapted the same alcoholysis synthetic procedure in order to prepare $[Sb(O^iPr)_5(NH_3)]$. Dry isopropanol (39 cm^3) was slowly added to $SbCl_5$ in toluene (80 cm^3) at -30^oC. The yellow solution immediately became colourless and produced two immiscible layers. After stirring for 2 hrs at room temperature, ammonia gas was passed through the resultant solution. Ammonium chloride was filtered off and concentrating the mother liquor produced colourless needle shaped crystals at -30 ^oC.

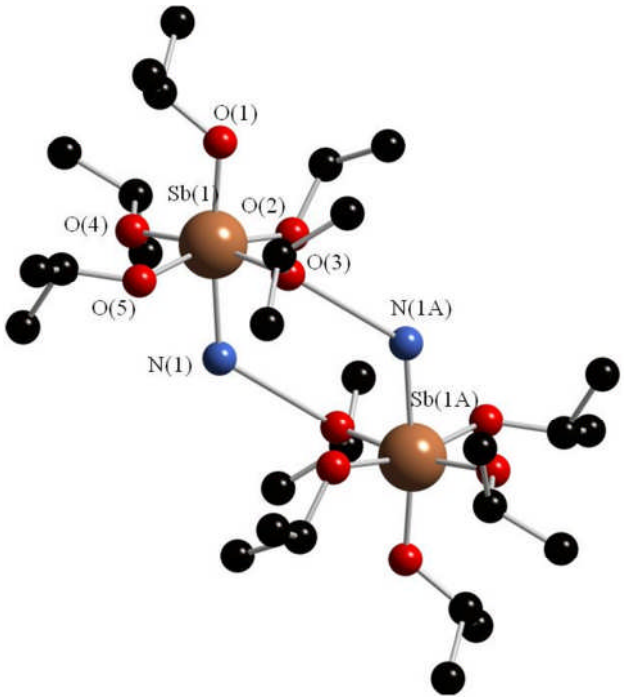

Fig. 2.16: X-Ray crystal structure of $[Sb(O^iPr)_5(NH_3)]$. The colour codes are as follows N(blue), O(Red), H (black) and Sb(saffron)

Sb(1)-O(1)	1.948	Sb(1)-O(5)	1.951
Sb(1)-O(2)	1.971	Sb(1)-N(1)	2.179
Sb(1)-O(3)	1.966	Sb-O-C	121-128
Sb(1)-O(4)	1.952	O(5)-Sb(1)-O(4)	7.577

Table 2.5: Selected bond lengths (Å) and bond angles(^{o}) of $Sb(O^iPr)_5.NH_3$

Recently Kirean *et.al* [26] reported that solid state structures of ethoxo derivatives of mononuclear antimony (V) alkoxides and found that ethoxide groups are non-equivalent in solution, and antimony exhibits octahedral geometry with hexa coordination. The ^1H NMR spectrum of $[Sb(OPr^i)_5(NH_3)]$ showed three broad signals at δ 1.3, 3.5 and 4.6 ppm at room temperature and the broadness of the peaks suggests that the isopropoxide groups are dynamic in solution. Crystals suitable for X-ray crystallography were grown from toluene and these crystals are isostructural with $[Sb(OEt)_5.(NH_3)]$. The asymmetric unit contains two independent molecules with hexa coordination. Each antimony is octahedrally coordinated in a SbO_5N environment. Molecules arrange themselves as a dimer held together by N-H…O-C hydrogen bonds involving all three hydrogen atoms on each ammonia. Sterically demand antimony

(Sb) alkoxides such as $[Sb(OEt)_5(NH_3)]$ and $[Sb(OPr^i)_5(NH_3)]$ are monomeric with six coordination but smaller alkoxides like $Sb(OMe)_5$ are dimeric in nature with μ-OR groups like $\{Nb(OMe)_5\}_2$.[27]

2.9.1. Variable temperature ^{1}H NMR studies of $[Sb(OPr^i)_5(NH_3)]$

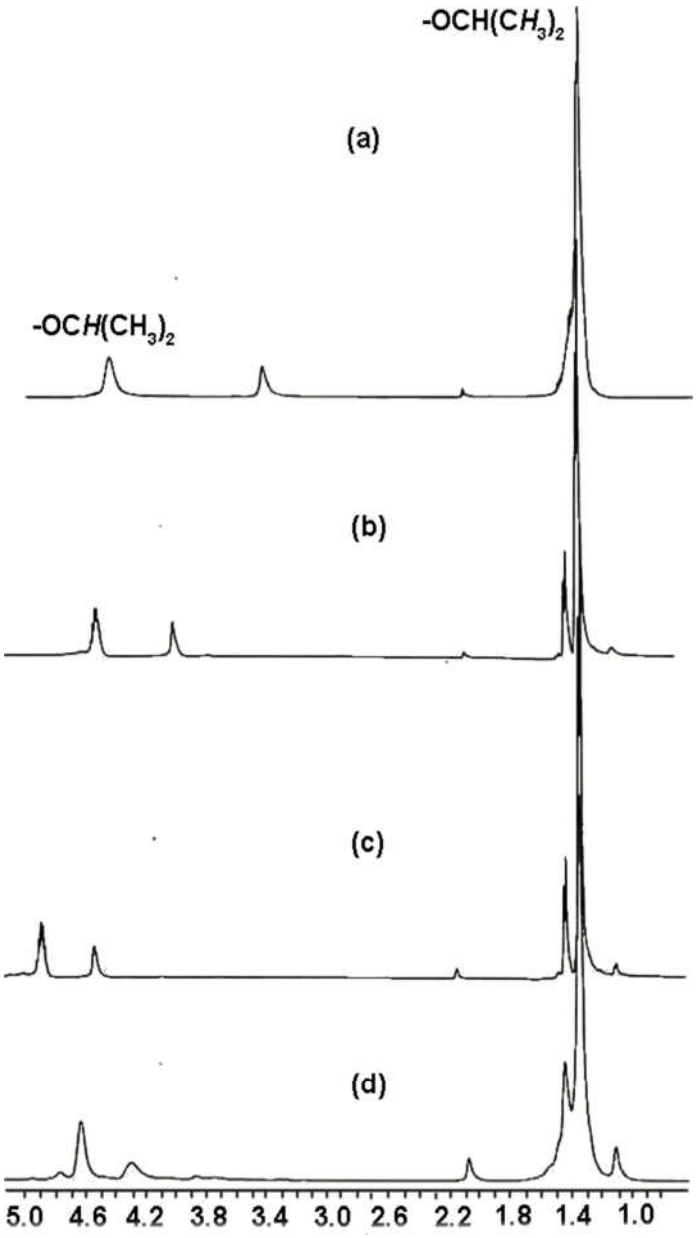

Fig. 2.17: Variable ^{1}H NMR studies of $[Sb(O^iPr)_5.(NH_3)]$. a) 23 ^{o}C b) -20 ^{o}C c) -40 ^{o}C d) -60 ^{o}C

Antimony pentaisopropoxide is dynamic in solution with the observation of two sets of ^{1}H NMR signals for the isopropoxide groups at ambient temperature. One shoulder

peak was also observed at δ 3.5 ppm at room temperature. In order to probe the solution structures of $[Sb(O^iPr)_5(NH_3)]$, the sample was subjected to VT ^1H NMR spectroscopy studies in toluene – d_8 and selected spectra are shown in Fig 2.17. At room temperature (a), the broad peak at δ 1.3 ppm and the peak at δ 4.6 ppm signals are assigned for the methyl and methine protons respectively. Based on the solid state structure, we had expected to observe the two different methyl and methine protons, however, at 0°C (b), the methyl peaks was sharpened and methine proton was clearly identified but splitting of both peaks were not observed. The downfield peak at δ 4.6 ppm is due to methine proton of the isopropoxide ligand and δ 1.3 ppm is due to methyl peak. Still the methyl signals are not well-resolved at this temperature. When the temperature was lowered to -20 °C (c), two sets of doublets at δ 1.40 and δ 1.29 ppm were seen for methyl protons of the isopropoxide but methine proton was not split further. Further reducing the temperature of the same sample (d), led to broadening of the peaks. At all of the temperatures, one single peak was present in the region at δ 4.3 ppm and was assigned to the NH_3 protons. We had expected to observe further splitting of the methyl and methine signals in VT ^1H NMR spectra because the crystal structure showed hydrogen bonding and clearly revealed that the molecular geometry of (Fig 2.16) at low temperature consists of two magnetically inequivalent isopropyl groups, however, further work is needed to completely understand the solution behaviour of antimony alkoxides. The above VT NMR spectroscopy studies suggest that the antimony alkoxide complex partially remains dimeric nature in solution, at least at low temperatures, as well as in the solid state.

We had expected to observe four carbon peaks for the two inequivalent isopropoxide groups in the ^{13}C NMR spectra but it exhibits three signals at δ 20.7, 26.41 and 65.8 ppm. Among these three peaks, the downfield peak at δ 65.8 was much broadened and further analysis is required to understand the solution chemistry of $[Sb(O^iPr)_5(NH_3)]$.

2.10. Synthesis and characterisation of Lindqvist POMs in non-aqueous media

2.10.1. Introduction

In order to synthesise the heterometallic Lindqvist type POMs, the complex dynamic processes involved in aggregation and the factors affecting the relative stabilities of the structural motifs must be well understood in order to provide the basis for reliable

and predictable synthetic methodologies. Fuchs *et.al* [28] reported the first non-aqueous synthesis of Lindqvist POMs $[W_6O_{19}]^{2-}$ by hydrolysing metal alkoxides and by dissolution of metal oxides in the presence of organic bases. Following the initial work, Errington *et.al* [28] developed rational methods for synthesis of heterometallic Lindqvist type POMs involving the controlled hydrolytic strategy and they synthesised a range of alkoxido hexametalates. The solution reactivity has exploited the inherent stability of the Lindqvist hexametalate structure in non-aqueous media.

Precursors

2.10.1.1. Synthesis of $\{WO(OMe)_4\}_2$

Funk *et.al* [29] first reported that synthesis of a range of tungsten oxoalkoxides $WO(OR)_4$ (R= Me, Et, Pr^n, Pr^i, Bu^n, CH_2Ph) from $WOCl_4$ and the respective alcohol in the presence of ammonia. Errington *et.al* [21] thoroughly studied the solid state and solution studies of a range of tungsten oxoalkoxides in non-aqueous medium. The structure of $WO(OR)_4$ alkoxides is very sensitive to the steric bulk of the alkoxide group. $WO(OMe)_4$ exhibits a dimeric structure in the solid state and dimerisation of the oxotetramethoxide occurs through asymmetric alkoxo bridges which are coplanar with terminal oxoligands to form an edge shared bi octahedral structure. In solution, it behaves similarly to group 5 homoleptic alkoxides $\{M(OR)_5\}_2$ M = Nb, Ta and no monomer of $WO(OBu^t)_4$ has observed in solution.

Tungsten (VI) alkoxides can be used as one of the starting precursors in sol-gel processes and Errington has used these alkoxides to synthesise polyoxometallates in non-aqueous medium. Jahr, Fuchs *et.al* [30] reported that the hydrolysis of $WO(OMe)_4$ in alcohol solution containing $[NR_4]$ OH leads to a classical isopoly anion $[W_6O_{19}]^{2-}$. The ^1H NMR depicted three singlet peaks at 4.53, 4.40 and 4.36 ppm as a result of the different environments experienced by the methoxide protons.

2.10.1.2 Oxometalates

A range of tetraalkylammonium oxometalates are commonly used as starting materials for the precursors for non-aqueous POM synthesis. Mononuclear oxometalates $Q_2[MO_4]$ (M = Mo and W) are prepared from the hydrated oxides $MO_3 \cdot H_2O$ and

methanolic Q[OH]. The solid obtained after removal of the solvent was dried under vacuum for an extended period of time.

2.11. Attempted synthesis of $(TBA)_2[(MeO)SbW_5O_{18}]$

$$Sb(OPr^i)_5 + WO(OMe)_4 + Q_2WO_4 + 10\,H_2O \longrightarrow Q_2[(MeO)SbW_5O_{18}] + 21\,ROH \quad \text{---11}$$

R= Me, Pr^i

The mixture was obtained from the reaction between tungsten oxometalates and alkoxides. It was reacted further with antimony isopropoxide, followed by controlled hydrolysis using ^{17}O enriched water. The reaction was carried out in acetonitrile solvent, with overnight heating; the mixture was then heated with excess methanol for about 1 hr at the same temperature to enable the formation of the target product.

The expected side product $Q_2[W_6O_{19}]$ was filtered off. Dry diethyl ether was added to the mother liquor and a very small amount of white solid precipitated. It was characterised by ^{17}O NMR Spectroscopy. ^{17}O NMR spectrum showed mainly the possible side product $[W_6O_{19}]^{2-}$ at δ 776, 415 and -78 ppm. In addition, three peaks were observed at δ 758, 619, 431 ppm. However further work is needed to explore this reaction.

2.12. Attempted synthesis of $Q_3[(MeO)GeW_5O_{18}]$

B. Krebs *et.al* [31] reported that the acidic hydrolysis of $PhGeCl_3$with Q_2WO_4 leads to $[PhGeW_5O_{18}]^{3-}$ in non-aqueous medium. We were interested to synthesise the monoalkoxido derivatised germanium tungstates using non-aqueous hydrolytic aggregation.

$$2Ge(OPri)4 + 7WO(OMe)_4 + 3Q_2WO_4 + 17\,H_2O \xrightarrow{\text{Dry MeOH}} 2Q_3[(MeO)GeW_5O_{18}] + 36\,ROH \quad \text{----12}$$

R= Me, Pr^i

$Ge(OPr^i)_4$ (99%) was purchased from Sigma Aldrich and used for this reaction. A mixture of WO_4^{2-} and $WO(OMe)_4$ in acetonitrile solution was transferred to $Ge(OPr^i)_4$ and allowed to stir for 2 hrs at elevated temperatures. 10% ^{17}O enriched water was added and allowed to stir for overnight at the same temperature. All of the volatile

impurities were removed in *vacuo* then the mixture was heated with excess methanol for about 1 hr at the same temperature.

The expected side product $Q_2[W_6O_{19}]$ was filtered off. Dry diethyl ether was added to the mother liquor and a very small amount of white solid precipitated. It was characterised by ^{17}O NMR Spectroscopy. Five peaks were observed in the region δ 778, 736, 568, 448, 401 but no central oxygen peak was observed however further work is needed to explore this reaction.

2.14. Summary

Various mononuclear and polynuclear building blocks have been synthesised and investigated in non-aqueous solvents. Controlled hydrolysis of metal hexa halide anions $[MCl_6]^{2-}$ where M = Ti, Sn have been carried out by using ^{17}O enriched water. $[TiCl_6]^{2-}$ anion gave an uncharacterised solid product and based on the ^{17}O NMR chemical shift, possibly triply bridged Ti chloro $[Ti_3OCl_{12}]^{2-}$ oxide species may be formed in solution.

The attempted synthesis of TBA salts of $[M(OR)_6]^{2-}$ where M = Sn, Ti and R = H, Me were not successful and led to an uncharacterised oily material and crystalline solid was obtained $[Sn_2(OMe)_9]^-$ by changes the counter cation. Various metal alkoxides have been synthesised according to a literatrure procedure and notably hydrolytic studies has been carried out for $\{Nb(OMe)_5\}_2$ using 2,6-Lutidinum hydrochloride. $\{Nb(OMe)_4Cl\}_2$ has been isolated and structurally characterised by single crystal X-Ray diffraction. Variable temperature ^1H NMR in different solvents has been carried out for niobium chloroalkoxides to understand the complete solution mechanism.

The attempted synthesis of Sb and Ge alkoxo derivatised Lindqvist type polyoxometalates produced parent isopolyanion as a major product and possibly some other species.

Experimental section

All air sensitive reactions and manipulations were carried out under an atmosphere of dry, oxygen-free nitrogen using standard Schlenk and drybox techniques.[32] Air sensitive reactions at elevated temperatures were carried out in sealed, screw-top Schlenk flasks fitted with PTFE screw valves. All other reactions and manipulations were carried out using standard bench top techniques.

Solvents were dried over and distilled from appropriate desiccants. Hydrocarbon and ether solvents were dried over and distilled from sodium and benzophenone. Acetonitrile was dried over and distilled from calcium hydride and methanol was stored over 3 Å molecular sieves and distilled from magnesium methoxide immediately prior to use.

Infrared spectroscopy

Infrared spectra were recorded from crystalline solids or powders on a Varian 800 FT-IR spectrometer fitted with an ATR attachment or using as a liquid on a Varian 800 FT-IR.

NMR spectroscopy

NMR spectra were recorded on a Bruker Avance 300 spectrometer operating at 300.0 MHz (^{1}H) or a Jeol Lamda 500 spectrometer operating at 500.0 MHz (^{1}H), 67.81 MHz (^{17}O) or 20.84MHz (^{183}W). All samples were dissolved in acetonitrile or deuterated acetonitrile purchased from Goss Scientific Instruments, which had been degassed and stored under nitrogen over calcium hydride. ^{17}O enriched experiments were carried out using 10% ^{17}O-enriched water purchased from Goss Scientific Instruments.

Chemical Analysis

Elemental analyses were performed by the Newcastle University Chemical Analysis Service.

X-ray crystallography

X-ray crystallographic data was collected at 150 K on an Oxford Diffraction Gemini A Ultra diffractometer, a Nonius Kappa CCD diffractometer or a Bruker SMART 1K

CCD diffractometer using Mo*Kα* radiation (α = 0.71073 Å) and the graphics were obtained using Crystal Maker.

Synthesis of $(Bu^n_4N)_2\,SnCl_6$

TBACl in CH_2Cl_2 (2.723 g, 9.8mmol) was added slowly down the side of Schlenk flask onto a solution of $SnCl_4$ (1.276 g, 4.9mmol), resulting in a clear solution. The resultant solution was allowed to stir at room temperature at for about 1 hr. All the volatile impurities were removed completely under vacuum.

Recrystallisation: The white colour crude product was redissolved in dry dichloromethane again and dry ether was added. White crystals were formed upon cooling at -30^{o}C and were used for solution characterisation.

Yield: 97%.

Data: ^{119}Sn {^{1}H} NMR (186.5 MHz, $C_6D_5CD_3$) δ -733 ppm. FTIR (Nujol mull): 2729 s, 1153 m, 1108 m, 1066 m, 1030 m, 882 s, 745 m. Elemental analysis: Found C, 47.48; H, 7.86; N, 3.74. $C_{32}H_{72}N_2SnCl_6$ requires C, 47.0; H, 8.88; N,3.43 %.

Synthesis of $(Bu^n_4N)\,NbCl_6$

The compound was prepared from direct reaction between $NbCl_5$ and TBACl. Dry tetrabutyl ammonium chloride (1.014 g, 3.65mmol) in dichloromethane was transferred into $NbCl_5$ (0.986 g, 3.65 mmol). The resultant yellow colour solution was allowed to stir at room temperature for about 1 hr. All the volatile impurities were removed completely under vacuum.

Recrystallisation: The white coloured crude product was redissolved in dry dichloromethane again and dry ether was added. White crystals were formed upon cooling at -30^{o}C and were used for solution characterisation.

Yield = 94 %.

Data: Elemental analysis: Found C, 35.96; H, 7.36; N, 2.54. $C_{16}H_{36}N_1NbCl_6$ requires C, 35.06; H, 6.619; N, 2.55 %.

Synthesis of $((CH_3)_3Si)_2O$*

^{17}O enriched water (118 μL) was added to 2,6-Lutidine (1.399 g, 13.06 mmol) in a clean, dry Schlenk flask and allowed to stir to make a homogenous solution. Once the clear solution was obtained, chlorotrimethylsilane was added to the reaction mixture. White colour precipitate was formed immediately and precipitated product was identified as 2,6- lutidinium hydrochloride. The side product was filtered using a sintered filter and the mother liquor was separated carefully. Microdistillation was performed again in order to prepare hexamethyldisiloxane (HMDSO). Colourless liquid was distilled off exactly at 101^oC, and it was stored under nitrogen.

Yield: 59%

Data: ^1H NMR (500 MHz, $CDCl_3$): δ 0 (s, 18H), 7.23(s, $CDCl_3$). (2,6- Lutidine = 2, 6-dimethyl pyridine)

Reaction between $[TiCl_6^{2-}]$ and ^{17}O enriched HMDSO

Solutions of $[TiCl_6]^{2-}$ compound (200 mg, 0.27 mmol) were placed in a 10 mm NMR tube fitted with a teflon rubber tube. ^{17}O enriched HMDSO aliquots (6 μl, 0.27 mmol) were added to the sample using a micro syringe. The ^{17}O NMR spectrum was obtained if possible, after each addition of oxygen enriched HMDSO. The sample was shaken vigorously for 10-15 seconds before insertion into the spectrometer. All the data was collected at ambient temperature and referenced against water at 0 ppm.

The resultant solution was transferred into a Schlenk flask and all the volatile impurities were removed under vacuum.Thin yellow colour thin crystals were obtained from DCM/toluene mixture upon cooling to -30 ^oC.

Data: ^{17}O NMR (67.81 MHz, CD_2Cl_2): δ 423 ppm and δ 493 ppm.

Hydrolysis

Solutions of $[MCl_6]^{2-}$ (M = Ti, Sn) and $Ti(OSiMe_3)_4$ (approximately 3 cm^3) were placed in a 10 mm NMR tube fitted with a teflon rubber cap. A natural abundance ^{17}O NMR spectrum was obtained if possible then aliquots of 10 % enriched water were injected into the sample using a micro syringe. The samples were shaken vigorously for 10-15 seconds before insertion into the spectrometer.

S. No	Compound	Weight (g)	Mmol Ti	Solvent	Temperature (K)
1	$[TiCl_6]^{2-}$	200 mg	0.270	DCM	298
2	$[SnCl_6]^{2-}$	731 mg	0.896	DCM	298
3	$Ti(OSiMe_3)_4$	100 mg	0.247	DCM	298

Synthesis of $PhCH_2N(CH_3)_3[Sn_2(OMe)_9]$

Benzyl trimethyl ammonium methoxide. supplied as a 40% wt solution in methanol, (1.198 g, 6.606 mmol) was added with rapid stirring to tin (IV) t-butoxide (1.358 g, 3.303 mmol). The reaction mixture was allowed to stir overnight at room temperature. All volatile components were removed in *vacuo* to yield a hazy oil which was treated with acetonitrile (20 cm^3), then filtered, mixed with diethyl ether and stored at -30 ^oC over a month. Some uncharacterised white coloured compound precipitated was filtered off, then decreased the mother liquor further by 50% of its own volume and added dry ether for recrystallisation. Colourless crystals were formed and used for characterisation.

Yield: 32%.

Data: ^1H NMR (500MHz, CD_2Cl_2): δ 3.47 (s, 9H), 3.74 (s, 27H), 4.69 (s, 2H), 5.35 (s, CD_2Cl_2), 7.55 (s, 2H) and 7.67 (s, 2H). ^{13}C NMR (100.53 MHz, CD_2Cl_2): δ 69.1 ppm. ^{119}Sn NMR (186.5 MHz, CD_2Cl_2): δ -598. Elemental analysis: found C, 32.02; H, 5.81; N, 2.13. $C_{19}H_{43}Sn_2O_9N$ requires C, 34.2; H, 6.4; N, 2.1%.

Synthesis of $Ti[OSi(CH_3)_3]_4$

Titanium tetraisopropoxide (8 g, 28.14 mmol) was diluted with dry cyclohexane (33 cm^3) in schlenk flask and transferred into a two-neck round bottom flask. After being refluxed at 100-110 ^oC, a time controlled syringe pump was fitted to the RB flask. Trimethylsiliyl acetate (14.89 g, 112.56 mmol) was added slowly drop wise to $Ti(OPr^i)_4$, and simultaneously isopropyl acetate (11.49 g, 112.56 mmol) was removed by azeotropic distillation. The crude product was then again distillated under reduced pressure (7mm/Hg). The pure colourless product had collected in the new receiver, and was stored under nitrogen.

Yield: 88.3%.

Data: ^{1}H NMR (500 MHz, $CDCl_3$): δ 0 (s, 36H), 7.23 (s, $CDCl_3$). FTIR: 2959 s, 1937 w, 1435 m, 1253 vs, 921 s, 873 s, 764 s, 526 s. ^{17}O NMR (67.81 MHz, $C_6D_5CD_3$): δ 289 ppm.

Synthesis of [{Nb(OMe)$_4$Cl}$_2$]

A hot solution of 2,6-lutidine hydrochloride (1.172 g, 8.16 mmol) in DCM was transferred into another schlenk flask containing {Nb(OMe)$_5$}$_2$ (2.025 g, 8.16 mmol). A Cloudy solution was formed initially then it turned into a clear solution upon heating. After stirring at room temperature for about 1 hr, all volatile impurities were removed in *vacuo*. The crude product was washed with diethyl ether (3 x 20 cm^3) to ensure the complete removal of free 2,6-lutidine. White colour crystals were obtained from the crude product in hot toluene upon cooling to -30 ^{o}C and were used for characterisation.

Yield: 93%

Data: ^{1}H NMR (500 MHz, CD_2Cl_2): δ 4.11 (s, 6H), 4.33 (s, 18H). ^{1}H NMR (500 MHz, $C_6D_5CD_3$): δ 4.11 (s, 9H), 4.33 (s, 9H). ^{13}C NMR (100.53 MHz, CD_2Cl_2): δ 65.8 ppm. Elemental analysis calculated for $C_4H_{12}O_4NbCl$ is C=19.02%, H= 4.78%. Found C=18.78% H=5.01%

Attempted preparation of {Nb$_4$(OMe)$_{16}$}[SbCl$_6$]$_4$

Nb(OMe)$_4$Cl (222 mg, 0.88 mmol) was dissolved in dichloromethane (15 cm^3) and transferred to $SbCl_5$. (263 mg, 0.88 mmol) After stirring at room temperature for overnight, all the volatile impurities were removed in *vacuo*. The crude product was recrystallised by vapour diffusion of diethyl ether in dichloromethane. Pale brown crystals were obtained from the crude product and it was used characterisation.

Data: Single crystal X-ray crystallographic studies revealed that the product is very similar to triethyloxonium salts of antimony hexachloride.

Preparation of $(Bu_4N)_2WO_4$

$WO_3.H_2O$ (15.0 g, 0.0600 mol) was placed in a 500 ml round bottomed flask. A 1.0 M solution in methanol of Bu_4NOH (120 cm^3, 0.120 mol) was added gradually with stirring to the tungstic acid and the solution was left to stir at room temperature for 30 minutes with the solution gradually forming a white suspension. Acetonitrile (20 cm^3) was added to the solution and it was then left to stir for 12 hours. The stirring was then stopped to allow the white solid to settle out. The solution was filtered into a Schlenk flask using a cannula filter stick and all volatiles were then removed under reduced pressure. The sticky white solid was then trituated with ether (5 x 40 cm^3) and left under vacuum at 60-70 ^oC for 12 hours. Further scratching with ether (2 x 40 cm^3) resulted in a white solid which was dried under vacuum for 12 hours.

Yield: 83.3 %.

Data: FTIR (Nujol mull): 2961(m), 2932 (w), 2874 (w), 1463 (m), 1378 (m), 1165 (w), 1107 (w), 1054 (m), 1020 (w), 922 (w), 893 (m), 879 (w), 820 (m), 737 (w), 667 (w).

Synthesis of $\{WO(OMe)_4\}_2$

$WOCl_4$ (20.0 g, 58.4 mmol) was placed in a dual 500 cm^3 round bottomed flask separated by a sintered frit filter. The solid was dissolved with stirring at -30 ^oC in tetrahydrofuran (200 ml) to give a red solution. Once all the $WOCl_4$ had dissolved the solution was allowed to return to room temperature and the flask was fitted with a glass tube connected by hosing to a nitrogen supply and an ammonia cylinder. Methanol (9.50 ml) was added gradually to the solution with vigorous stirring and the solution was left stirring for 5 min, during which time the colour changed from red to a pale yellow. The glass tube was then submerged in the solution and nitrogen was bubbled through for 5 minutes. The nitrogen supply was then switched off and ammonia was bubbled through for 5 minutes resulting in the formation of a white precipitate, NH_4Cl. The ammonia supply was stopped and nitrogen was bubbled through the suspension for a further 10 minutes in order to remove any excess ammonia present. The glass tube was removed from the apparatus. The dual round bottomed flask was inverted and the apparatus sealed in order to allow the white solid to settle on the frit filter. The solution was then filtered for 12 hours under nitrogen

with a slight vacuum in the receiving flask. The white solid which collected was washed with THF (100 ml) and again allowed to filter. A dark amber brown solution was obtained. This volume of the dark brown solution was reduced sufficiently to transfer the solution to a Schlenk flask. The volume of the solution was reduced further and the flask was then place in a freezer at -30 ^{o}C in order to crystallise. Off-white crystals of $WO(OMe)_4$ were formed. These crystals were isolated by filtration and dried under vacuum for 12 hours Yield: 54.8 %.

Data: ^{1}H NMR (500 MHz, $C_6D_5CD_3$): δ 4.45 (s, 6H), 4.55 (s, 6H), 4.70 (s, 12H).

Synthesis of $[Sb(OPr^{i})_5(NH_3)]$

$SbCl_5$ (10.16 g, 34mmol) was placed in a dual 500 cm^3 round bottomed flask separated by a sintered frit filter. The liquid was diluted with stirring at -30 ^{o}C in dry hexane (80 cm^3) to give two layers. Once all $SbCl_5$ had dissolved the solution was allowed to return to room temperature and the flask was fitted with a glass tube connected by hosing to a nitrogen supply and an ammonia cylinder. Dry isopropyl alcohol (39 cm^3) was added gradually to the solution with vigorous stirring and the solution was left stirring for 5 min, during which time the colour changed from red to a pale yellow. The glass tube was then submerged in the solution and nitrogen was bubbled through for 5 minutes. The nitrogen supply was then switched off and ammonia was bubbled through for 5 minutes resulting in the formation of a white precipitate, NH_4Cl. The ammonia supply was stopped and nitrogen was bubbled through the suspension for a further 10 minutes in order to remove any excess ammonia present. The glass tube was removed from the apparatus. The dual round bottomed flask was inverted and the apparatus sealed in order to allow the white solid to settle on the frit filter. The solution was then filtered for 12 hours under nitrogen with a slight vacuum in the receiving flask. The white solid collected was washed with dry hexane (50 cm^3) and again allowed to filter. A pale yellow colour solution was obtained. This volume of the pale yellow solution was reduced sufficiently to transfer the solution to a Schlenk flask. The volume of the solution was reduced further and the flask was then place in a freezer at -30 ^{o}C in order to crystallise. Off-white sticky crystals of $[Sb(OPr^{i})_5(NH_3)]$ were formed. These crystals were isolated by filtration and dried under vacuum for 3-4 hours, and was used for characterisation.

Yield: 68.8 %.

Data: ^{1}H NMR (500 MHz, $C_6D_5CD_3$): δ 1.3 (br, 30H), 3.5 (br, 3H), 4.6 (br, 5H). ^{13}C NMR (100.53 MHz, $C_6D_5CD_3$): δ 20.7, 26.41, 65.8. FTIR (Nujol mull): 3369 s, 3126 m, 1619 s, 1272 s, 1168 s, 1116 s, 975 bs, 844 vs, 739 s, 618 s. Elemental analysis: Found: C, 17.96; H,0.39; N, 1.38. $C_{15}H_3O_{40}NSb$ requires C, 18.78; H, 0.315; N, 1.46 %

Attempted preparation of $(TBA)_2[(MeO)SbW_5O_{18}]$

A mixture of TBA_2WO_4 (0.57 g, 0.781 mmol) and $WO(OMe)_4$ (1.005 g, 3.102 mmol) were dissolved in acetonitrile (20 cm^3) at room temperature and allowed to stir for 1 hr. The golden yellow colour solution was transferred into $Sb(O^iPr)_5$ (0.339 g, 0.781 mmol) with constant stirring. The resultant solution was stirred for 2 hrs at 85-90 ^oC before addition of water H_2O (10 % ^{17}O enriched H_2O) (141.2 μL, 7.81 mmol). After being heated overnight, excess dry methanol (15 cm^3) was added and the solution was stirred for 1 hr at 85- 90 ^oC. The reaction was then allowed to cool to room temperature. All volatile impurities were removed by in *vacuo* and redissolved in acetronitrile. Significant amount of crystalline $Q_2[W_6O_{19}]$ was removed by filtration before addition of an ether layer. The volume of mother liquor was reduced by about 30% and dry ether was added. The uncharacterised white colour crude product was settled and it was investigated by ^{1}H and ^{17}O NMR Spectroscopy.

Data: ^{17}O NMR (67.81 Hz, 500 MHz): 758, 619, 431 ppm.

Attempted preparation of $(TBA)_3[(MeO)GeW_5O_{18}]$

A mixture of TBA_2WO_4 (1.423 g, 1.942 mmol) and $WO(OMe)_4$ (1.47 g, 4.53 mmol) were dissolved in acetonitrile (20 cm^3) at room temperature and allowed to stir for 1 hr. The golden yellow colour solution was transferred into $Ge(O^iPr)4$ (0.4 g, 1.295 mmol) with constant stirring. The resultant solution was stirred for 2 hrs at 85-90 ^oC before addition of water H_2O (10 % ^{17}O enriched H_2O) (199 μL, 11.01 mmol). After being heated overnight, excess dry methanol (15 cm^3) was added and the solution was stirred for 1 hr at 85- 90 ^oC. Once the reaction stops and allowed to cool to room temperature. All volatile impurities were removed in *vacuo* and redissolved in acetronitrile. A Significant amount of crystalline $Q_2[W_6O_{19}]$ was removed by filtration before addition of an ether layer. The volume of mother liquor was reduced by about

30% and dry ether was added. A white product settled and was investigated by ^{1}H and ^{17}O NMR Spectroscopy.

Data: ^{17}O NMR (67.81 Hz, 500 MHz): δ 778, 736, 568, 448, 401.

References

1) O. M. Yaghi, M.O'Keeffe, N.W.Ockwig, H.K. Chae, M. Eddaoud and J.Kim, *Nature*, **2003**, 423, 12, 705-714.

2) D. C. Bradley, R. C. Mehrotra and D. P. Gaur, Metal alkoxides, Academic press, New York, **1978**.

3) E. Bistan and I. Gomory, Chem. Zvesti, 1956, 10, 91, Chem. Abstr., **1956**, 50, 4509.

4) V. G. Kessler, G .I. Spijksma, G. A. Seisenbaeva, S. Hakansson, D. H. A. Blank and H. J. M. Bouwmeester, *J. Sol-Gel Sci Techn*, **2006**, 40, 163-179.

5) C. K. Fortner, J. P. Bigi, S. N. Brown, *Inorg.Chem*, **2005**, 44, 2803.

6) G. Winter, Oil and Colour chemist's association, **1953**, 36, 689.

7) A. Vioux, *Chem. Mater*, **1997**, 9, 2292-2299.

8) M. J. H. Smith, R. Wark, A. Heingoldam and J. Huffman, *Can. J. Chem*. **1991**, 69, 121.

9) H. Funk, W. Weiss, and G. Mohaupt, *Z. Anorg. Allg. Chem*. **1960**, 302, 238.

10) A. A. Pinkerton, D. Schwarzenbach, L. G. Hubert-Pfalzgraf and J. G. Riess, *Inorg Chem*, **1976**, 15, 1196-1199.

11) M. A. Fedotov and R. I. Maksimovskaya., *Journal of Structural Chemistry*. **2006**, 47, 952-978.

12) W. Day, T. A. Eberspacher, Y. Chen, J. Hao and W. G. Klemperer, *Inorg. Chim. Acta*, **1995**, 229, 391-405.

13) M. J. Taylor and J. M. Coddington, *Polyhedron*, **1992**, 11, 12, 1531-1544.

14) D. C. Bradley and I. M. Thomas, *Journ. of. Chem. Soc.*, **1959**, 3404-3411.

15) R. J. Errington *et.al*., Unpublished results.

16) (a) T. Sugimoto, X. Zhou, A. Muramatsu, *J. Colloid Interface Sci.* **2002**, 252, 339.

(b) T. Sugimoto, X. Zhou, *J. Colloid Interface Sci.* **2002**, 252, 347.

(c) T. Sugimoto, X. Zhou, A. Muramatsu, *J. Colloid Interface Sci.* **2003**, 259, 43.

17) H. Lin, P. W. de Oliveira, V. Huch and M. Veith., *Chem. Mater*., **2010**, 22, 6518-6523.

18) M. Schoenherr and L. Kolditz, *Zeitschrift fuer Chemie*, **1970**, 10, 2, 72.

19) R. J. Errington *et.al* Unpublished results.

20) A. Antinolo, A. Otero, F. Urbanos, S. G. Blanco, S. M. Carrera, J. S. Aparcio, *Journal of Organometallic chemistry*, **1988**, 350, 25-34.

21) W. Clegg, R. J. Errington, P. Kraxner and C. Redshaw, *J. Chem. Soci. Dalton Trans,* **1992**, 1431-1438.

22) C. E. Radzewich, I. A. Guzei, R. F. Jordan, *J.Am.Chem.Soc*, **1999**, 121, 8673.

23) V. G. Kessler, G. A. Seisenbaeva, R. J. Errington, *Inorganic Chemistry Communications*, **2005**, 8, 6, 503-505.

24) R. Rathore, A. S. Kumar, S. V. Lindeman, J.K.Kochi, *J. Org. Chem.*, **1998**, 63, 5847

25) A. T. Bohra, R. C. Mehrotra, *J.Indian Chem.Soc.* **1990**, 67, 535.

26) G. A. Horley, M. F. Mahon, K. C. Molloy ad M. M. Venter., *Inorg.Chem*,**2002**, 41, 6, 1652-1657.

27) V. N. Tempel, W. Schwarz and J. Weidlein., *Z. Anorg. Allg. Chem*, **1981**, 474, 157-170

28) R. J. Errington, G. Harle, W. Clegg, R. W. Harrigton, *Eur. J. Inorg. Chem*, **2009**, 5240-5246.

29) H. Funk, W. Weiss and G. Mohaupt, *Z.Anorg. Allg. Chem*, **1960**, 304, 238.

30) a) K. F. Jahr, J. Fuchs, *Angew. Chem. Int. Ed. Eng.* **1966**, *5*, 689.

b) J. Fuchs, *Z. Naturforsch. B* **1973**, *28*, 389.

31) B. Krebs, R. Klein, in: M.T. Pope, A. Muller (Eds.), Polyoxometalates From Platonic Solids to Anti-retroviral Activity, Kluwer Academic Publishers, Dordrecht, The Netherlands, **1994**, p. 41.

32) R. J. Errington, Advanced Practical Inorganic and Metalorganic Chemistry, Blackie Academic & Professional, London, UK, **1997**.

Chapter 3

Synthesis and Solution Chemistry of $[(MeO)SnW_5O_{18}]^{3-}$

Chapter 3: Synthesis and Solution Chemistry of $[(MeO)SnW_5O_{18}]^{3-}$

3.1 Introduction

This chapter mainly discusses the synthesis of novel main group heterometallic alkoxido derivatised Lindqvist type tin polyoxometalates $[(RO)SnW_5O_{18}]^{3-}$ **1** (where R=Me), and hydrolytic studies of $(TBA)_3$ **1**. We have also obtained $[ClSnW_5O_{18}]^{3-}$ **4** as a major product whilst attempt to synthesise $[(HO)SnW_5O_{18}]^{3-}$ **2** directly from tungstate and metal alkoxide precursors. The systematic surface reactivity studies of Sn-X (X=OMe, Cl, OH) functionality in these polyoxometalates are discussed in Chapter 4. The synthesis and ligand transformation reactions of $(TBA)_3$ **2** are discussed towards the end of this chapter. Our consideration was that when we increase the reactive sites i.e. more than one heterometallic atoms on the polyoxometalic cage, these substances are expected to act as polynuclear building blocks and could possibly synthesise the extended linear array of metal oxides in solution.

The methoxido tin polyoxometalate **1** has been synthesised from a WO_4^{2-} and constituent metal alkoxides by controlled hydrolysis. ^{17}O enriched water was used for hydrolysis so that we were able to monitor the species formation and characterise the starting precursors by ^{17}O NMR spectroscopy.[1] We were also able to use NMR active elements such as ^{119}Sn and ^{183}W to investigate and differentiate the species formed in solution because $(TBA)_3$ **1** contains a tin heterometal atom in the polyoxometalate cage. The Sn atom in $(TBA)_3$ **1** exhibits coordination number of 6 and the oxidation state IV similar to earlier reported compounds $[(MeO)TiW_5O_{18}]^{3-}$ and $[(ArO)ZrW_5O_{18}]^{3-}$, and it opens opportunity to study the reactivity of $(TBA)_3$ **1** with various organic ligands (HX, where X = RO and ArO).

3.2 Background

Errington and co workers have developed a non-aqueous synthetic route for various alkoxo derivatised hetreometallic Lindqvist type polyoxometalates from WO_4^{2-} and constituent metal alkoxides by controlled hydrolysis. The tungstate alkoxide used is $WO(OMe)_4$. These tungstate precursors are allowed to react with the respective metal alkoxide $M(OMe)_x$ and stoichiometric amounts of water are adjusted according to

heterometal M. The titanium methoxide $[(MeO)TiW_5O_{18}]^{3-}$ and has been prepared according to the following equation 1 and the structures are shown below Fig 3.1.[2]

$$3\ WO_4^{2-} + 7\ WO(OMe)4 + 2\ Ti(OMe)_4 + 17\ H_2O \xrightarrow[CH_3CN]{MeOH} 2[(MeO)TiW_5O18]^{3-} + 34\ MeOH \quad \text{----1}$$

It has been observed that the surface methoxido groups in these anions are reactive and can be systematically replaced by a wide variety of active ligands *via* exchange reactions with a choice of protic reagents. This novel TiW_5 polyoxometalate has also been successfully attached to derivatised silicon surfaces, and this was the first demonstration of the covalent surface immobilisation of polyoxometalates.[3]

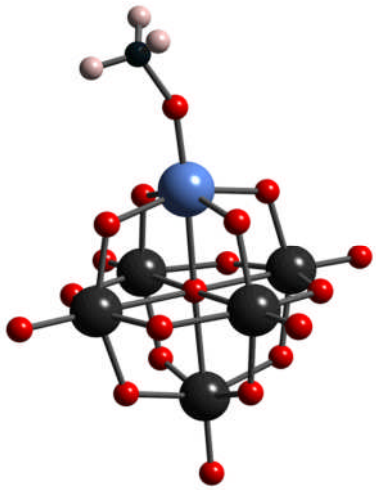

Fig 3.1.Structure of the anion $[(MeO)TiW_5O_{18}]^{3-}$. The colour codes are as follows: W (brown), O (red), Ti (blue), C (black), H (white).[2]

Zirconium $\{[(MeO)ZrW_5O_{18}]_2\}^{6-}$, hafnium $\{[(MeO)HfW_5O_{18}]_2\}^{6-}$ and niobium $[(MeO)NbW_5O_{18}]^{2-}$ analogues also have been prepared by the same controlled hydrolysis route. The zirconium methoxido dimer $\{[(MeO)ZrW_5O_{18}]_2\}^{6-}$ has been prepared according to the following equation and structure is below (Fig 3.2).

$$3\ WO_4^{2-} + 7\ WO(OMe)_4 + 2\ Zr(OPr^n)_4 \xrightarrow[CH_3CN]{MeOH} 2\ \{(\mu\text{-}CH_3O)ZrW_5O_{18}]_2\}^{6-} + 34\ ROH \quad \text{----2}$$
$$R=Me,\ Pr^n$$

The zirconium and hafnium analogues are formed as dimers and the heterometals exhibit seven coordination in e.g. $\{[(MeO)ZrW_5O_{18}]_2\}^{6-}$, $\{[HO)ZrW_5O_{18}]_2\}^{6-}$ and $[(L)ZrW_5O_{18}]^{3-}$ (where L= chelating ligand derived from acetylacetone, acetic acid and

salicylaldehyde) because of the larger atomic radii. The two heterometals are bridged by two methoxide and hydroxide groups. However, zirconium exhibits six coordination in aryl oxido derivatives $[(ArO)ZrW_5O_{18}]^{3-}$ where Ar = Ph, 4-Me-C_6H_4.[4]

Recently, Errington and his co-workers have extended their studies to analogous moylbdates also. They have demonstrated that the alkoxido- titanium pentamolybdate $[(Pr^iO)TiMo_5O_{18}]^{3-}$ could be prepared through hydrolysis using organic-soluble dimolybdate ($Mo_2O_7^{2-}$) and octamolybdate ($Mo_8O_{26}^{4-}$) as a source of polyoxometalate, avoiding the use of molybdenum oxoalkoxide $MoO(OMe)_4$. The $[(Pr^iO)TiMo_5O_{18}]^{3-}$ has been prepared accordingly the following equation.[5]

$$\mathbf{Q_2[Mo_2O_7] + Q_4[Mo_8O_{26}] + 2Ti(O^iPr)_4 + 3H_2O \longrightarrow 2Q_3[(^iPrO)TiMo_5O_{18}] + 6\ ^iPrOH} \quad \text{----3}$$

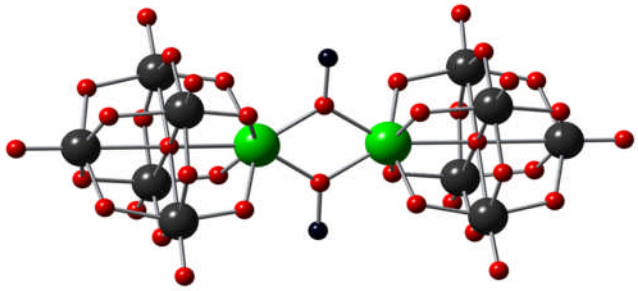

Fig 3.2: Structure of the anion $[\{(\mu\text{-}MeO)ZrW_5O_{18}\}_2]^{6-}$. The colour codes are as follows: W (brown), O (red), Zr (green), C (black).[4]

Errington and co-workers have applied the same strategy to synthesise alkoxido derivatised Lindqvist type of hetero polyoxometalates containing the group 8 and 9 heterometals such as Co and Fe. The attempted synthesis of $[(RO)CoW_5O_{18}]^{5-}$ gave an uncharacterised product rather than the desired alkoxo cobalt pentatungstate because the cobalt(II) methoxide $Co(OMe)_2$ is insoluble in acetonitrile. At high temperature, cobalt methoxide reacts with acetonitrile leading to an uncharacterised product.

The aforementioned hydrolytic approach has also been applied to synthesise 'virtual' polyoxometalate $(^nBu_4N)_6[W_5O_{18}]$ precursor for use in reactions with electrophilic metal complexes and $(^nBu_4N)_3[ClTiW_5O_{18}]$ was obtained by reacting the 'virtual' lacunary precursor with $[TiCl_4(MeCN)_2]$ according to equation 4. [6]

$$\mathbf{3\ (^nBu_4N)_2WO_4 + 2\ WO(OMe)_4 + 4\ H_2O \longrightarrow (^nBu_4N)_6W_5O_{18} + 8\ MeOH}$$

$$\mathbf{(^nBu_4N)_6W_5O_{18} + [TiCl_4(MeCN)_2] \longrightarrow (^nBu_4N)_3[ClTiW_5O_{18}] + 3\ ^nBu_4NCl + 2\ MeCN} \quad \text{----4}$$

The same virtual polyoxometalate precursor had allowed reaction with the group 8 and 9 heterometals iron and cobalt. The attempted synthesis of $(TBA)_5[ClCoW_5O_{18}]$ resulted in the formation of the polyoxometalate $(TBA)_7[\{CoW_5O_{18}H\}_2]Cl$.[7] The 'virtual' precursor reacts with $FeCl_3$ to give dark brown cubic crystals which did not diffract well in XRD but the mass spectrometry and infra red spectroscopy provide for the formation of $[(L)FeW_5O_{18}]^{n-}$ species. In reactions between the 'virtual' precursor and $RhCl_3$ only to the hexametalate $(TBA)_2$ $[W_6O_{19}]$ was obtained. The species $(TBA)_6[\{CoW_5O_{18}H\}_2]Cl$ has been prepared by the following equation 5.

$$\mathbf{2\ "\ (^nBu_4N)_6W_5O_{18}\ "\ + 2\ CoCl_2 + 2\ H_2O \longrightarrow}$$

$$\mathbf{(^nBu_4N)_7[\{CoW_5O_{18}H\}_2].Cl + 3\ (^nBu_4N)Cl + 2\ (^nBu_4N)OH} \quad \text{----5}$$

We therefore extended the same hydrolytic approach to more electrophilic group 14 metals such as tin. To the best of our knowledge, the first non-aqueous synthesis of tin substituted Lindqvist type polyoxometalate was that of the phenyl tin pentatungstate $(TBA)_3[(Ph)SnW_5O_{18}]$, which was synthesised and structurally characterised by B. Krebs *et.al.*[8] It was prepared by acidic hydrolysis of phenyl tin trichloride with WO_4^{2-} and it was recrystallised from acetonitrile and diethylether. In addition Pope *et.al* recently reported on aqueous synthesis of $(TBA)_3[CH_3SnW_5O_{18}]$. Displacement of kinetically metastable $[W_5O_{18}]^{6-}$ anion from 'sandwich' structure $[Ce(W_5O_{18})_2]^{10-}$, by reaction with CH_3SnCl_3 leads to a modest yield of $(TBA)_3[CH_3SnW_5O_{18}]$.[9]

3.3 Results and discussion

3.3.1 Synthesis and Characterisation of $(TBA)_3[(MeO)SnW_5O_{18}]^{3-}$ $(TBA)_3$1

We have successfully synthesised the methoxo derivatised tin pentatungstate by hydrolytic aggregation according to following equation (Eq.6)

$$3Q_2WO_4 + 7WO(OMe)_4 + 2\,Sn(O^tBu)_4 + 17H_2O \xrightarrow{MeOH} 2Q_3[(MeO)SnW_5O_{18}] + 28MeOH + 8\,{}^tBuOH \quad \text{----6}$$

The tungstate precursors TBA_2WO_4 and $WO(OMe)_4$ were reacted in acetonitrile for 1 hr at room temperature to give a clear pale yellow solution. This solution was added to $Sn(O^tBu)_4$ and the mixture was heated to 85-90 ^oC for about 2 hrs. Following addition of water, the solution was heated overnight at the same temperature. All of the solvents were removed in *vacuo* and the remaining product was treated with dry methanol for 1 hr at the same temperature. Volatile impurities were removed in *vacuo*, then the solid was redissolved in acetonitrile. A white precipitate forms when the solution volume is reduced to about 60 %.

The possible side product $Q_2[W_6O_{19}]$ was separated from hot acetonitrile and a colourless solid was precipitated immediately after an addition of dry diethyl ether to the mother liquor, and this solid was investigated by ^{17}O, IR and ^{119}Sn NMR spectroscopy. ^{17}O NMR and IR spectroscopy gives evidence for the target product formation but ^{119}Sn NMR spectroscopy showed four peaks instead of a single peak. The colourless solid was again treated with excess dry methanol in the presence of activated 3Å molecular sieves overnight at 85-90 ^oC in an oil bath. The mother liquor was separated from the molecular sieves and dry diethyl ether was added. Colourless solid was precipitated again and was investigated by ^{119}Sn NMR spectroscopy. It showed one single peak at δ_{Sn} -647 ppm and single cubic shaped crystals were obtained by vapour diffusion of diethyl ether into acetonitrile solution. These crystals were used for X- ray crystal structure determination and microanalysis.

Crystal structure of $(TBA)_3$ **1**

Unit cell Parameters

a = 29.5923(8) Å α = 90°

b = 18.6180(3) Å β = 113.067(3)°

c = 27.2820(7) Å γ = 90°

Crystal system: **monoclinic**

Space group: **C12/c1**

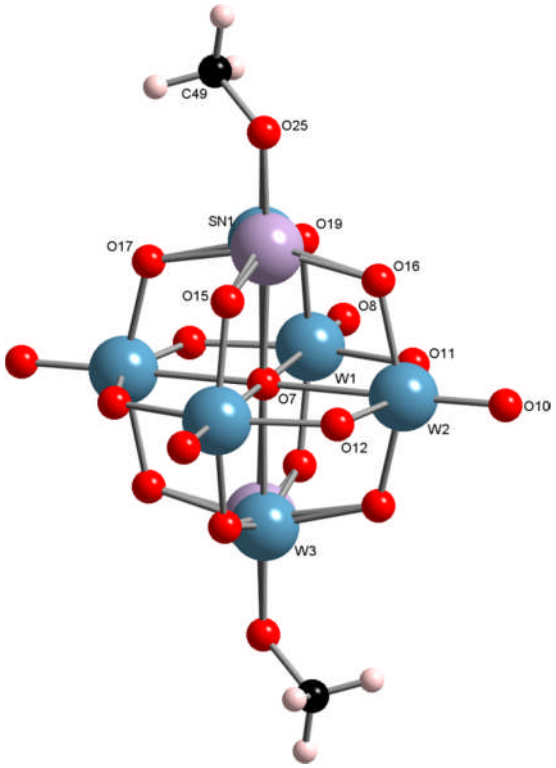

Fig 3.3: Structure of the the anion $[(MeO)SnW_5O_{18}]^{3-}$. The colour codes are as follows: W (pale blue), O (red), Sn (pale grey), C(black).

Single crystal X–ray diffraction studies revealed that $(TBA)_3$ **1** is a hexametalate structure in which the tin heterometal site is disordered over two *trans* positions and the methoxide group is terminally attached to the tin center. There are only three NMR active tin isotopes with natural abundances given in the Table 3.1.

Active tin isotopes	Natural abundance
^{119}Sn	8.59%
^{117}Sn	7.68%
^{115}Sn	0.34%

Table 3.1: Natural abundance of NMR active tin isotopes

Sn(1)-O(25)	1.819	Sn(1)-O(25)-C(49)	144.313
Sn(1)-O(7)	2.314	Sn(1)-O(7)-W(2)	87.819
Sn(1)-W(3)	4.602	Sn(1)-O(7)-W(1)	85.013
O(25)-C(49)	1.123	Sn(1)-O(7)-W(3)	175.737
Sn(1)-C(49)	2.809	Sn(1)-O(16)-W(1)	119.214
O(7)-W(3)	2.291	Sn(1)-O(16)-W(2)	115.636

Table 3.2: Selected bond lengths (Å) and bond angles (^{o}) of $(TBA)_3[(MeO)SnW_5O_{18}]$

3.3.2 Solution studies of $[(MeO)SnW_5O_{18}]^{3-}$

3.3.2.1 ^{119}Sn NMR spectroscopy

In the ^{119}Sn NMR spectrum of the initial product from the attempted synthesis of $(TBA)_3$ **1**, four resonance peaks were observed at δ_{Sn} -610, -633, -647 and -666 ppm with ^{183}W satellites. After treatment with excess methanol, in the presence of activated 3 Å molecular sieves only the δ_{Sn} -647 peak remained. This peak was assigned to $(TBA)_3$ **1** and we found that the δ_{Sn} -610 ppm peak is due to $[ClSnW_5O_{18}]^{3-}$ in which the chloride ion possibly might have come from impurities in the $(TBA)_2WO_4$ or may arise from impure tetrabutyl ammonium hydroxide (TBA OH) in 1M methanol solution. We assigned the other two peaks at δ_{Sn} -633 and -666 ppm to hydrolytic products of $[(MeO)SnW_5O_{18}]^{3-}$ (separately discussed in hydrolysis section).

3.3.2.2. Synthesis of $(TBA)_3$ $[(MeO)SnW_5O_{18}]$

Among the four stannotungstates, the chloride compound $(TBA)_3$ **4** has least solubility and can be easily separated as a single compound by fractional recrystallisation. The $(TBA)_3$ **1** was moisture sensitive and partial hydrolysis of this species was to be expected sometimes during separation of the $(TBA)_3$ **4**. $(TBA)_3$ **1** and its hydrolysed products in acetonitrile were heated with excess methanol in the presence of activated 3Å molecular sieves in order to synthesise pure $(TBA)_3$ **1**. After being heated overnight at 85-90 ^{o}C in an oil bath, the mother liquor was carefully

filtered off and diethyl ether was added. The product was precipitated and recrystallised from saturated acetonitrile. The cubic shaped colourless crystals showed one single peak at δ_{Sn} –647 ppm in the ^{119}Sn NMR spectrum and we have repeated the same procedure several times and confirmed the chemical shift of $(TBA)_3$ **1**. Further, we observed $^2J_{Sn\text{-}W}$ satellites and the coupling constant was measured as 39 Hz. This can be compared to the values of $^2J_{V\text{-}W}$ = 11.1 Hz for the heterometalate isopolyanion $(^nBu_4N)_3[VW_5O_{19}]$.[10]

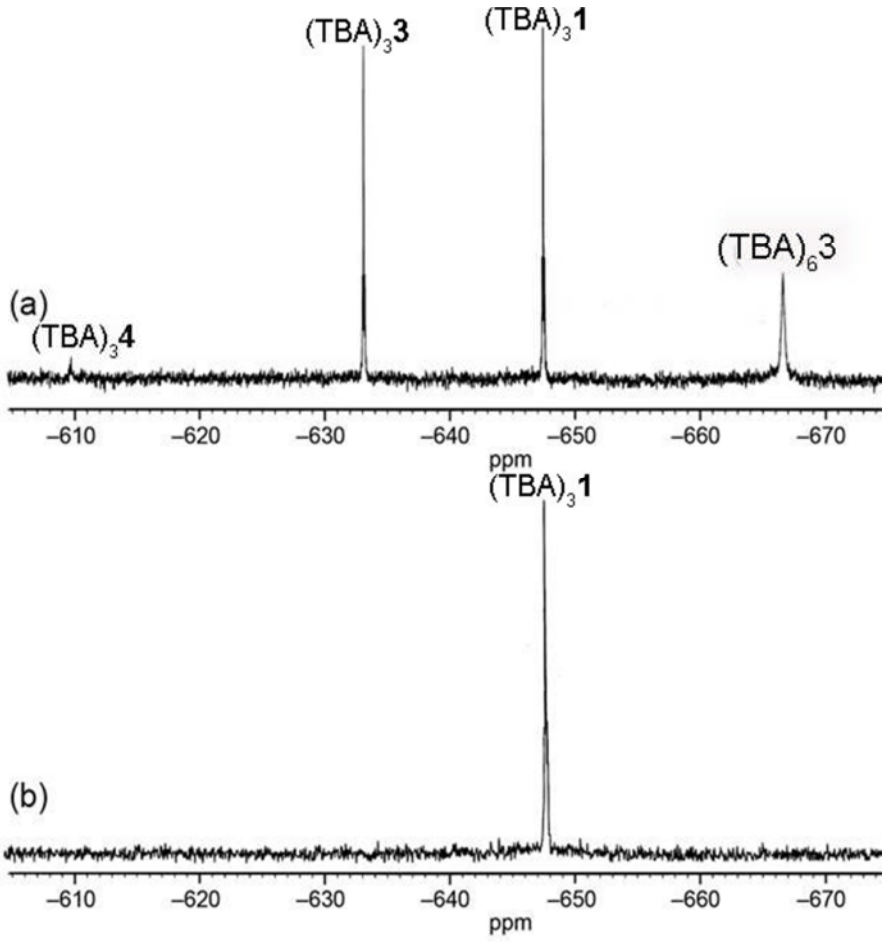

Fig 3.4: (a) ^{119}Sn NMR spectrum of the crude product in the synthesis of $TBA_3[(MeO)SnW_5O_{18}]$. b) ^{119}Sn NMR spectrum of $(MeO)SnW_5O_{18}]^{3-}$

3.3.2.3 Detailed ^{119}Sn NMR studies of $[(MeO)SnW_5O_{18}]^{3-}$

In $(TBA)_3$ **1**, tin heterometal exhibits six coordination and is directly bonded to tungsten through oxygen atoms in the polyoxometalate cage. Broad $^2J\{^{119}Sn^{183}W\}$ satellite coupling peaks are observed in normal ^{119}Sn NMR spectra, so we were not able to assign two different $^2J\{^{119}Sn^{183}W\}$ couplings by normal ^{119}Sn NMR methods.

In order to differentiate two types of $^{2}J_{Sn\text{-}W}$ coupling, a special ^{119}Sn NMR spectroscopy experiment was performed using Insensitive Nuclei Enhanced Polarisation Transfer (INEPT) method. The INEPT spectrum was better resolved and showed satellite peaks consistent with theoretical ^{183}W isotopologue calculations. Simulated axial and equatorial satellite coupling patterns were compared to the experimental INEPT spectrum. The INEPT coupling pattern was exactly matched by the simulated spectra with $^{2}J\{^{119}Sn^{183}W_{ax}) = 12.2$ Hz and $^{2}J\{^{119}Sn^{183}W_{eq}) = 38.4$ Hz.

^{183}W is the only NMR active nucleus for tungsten and the relative natural abundance is 14.31 %. We know that five tungstens are present in the compound $(TBA)_3$ **1** confirmed by the X-ray crystallography and ^{17}O NMR spectroscopy. Four tungstens are occupied in the equatorial position and one tungsten is present in the axial position.

If only one ^{183}W nucleus is present in the polyoxometalate cage, it has equal probability of occupying both sites i.e., equatorial (cis, **a**) or axial (trans, **b**) position. In both positions, the active tin ^{119}Sn nucleus would couple with ^{183}W giving tungsten satellite peaks with 1:1 ratio, however, the intensities of these (**a** and **b**) peaks are different due to number possibilities of the ^{183}W existing at these sites. All equatorial positions are chemically equivalent in $(TBA)_3$ **1** which was confirmed by ^{17}O NMR spectroscopy and the ^{183}W nucleus can occupy one of 4 positions, so the intensity of the later cis position is greater than the trans position. The various possibilities of ^{183}W active nuclei arrangements and the corresponding intensities are shown in the Table 2.

Note:

In Fig 2.5, (a) one ^{183}W nucleus in equatorial position, (b) one ^{183}W nucleus in axial position. (c) two ^{183}W nuclei in equatorial position, (d) one ^{183}W nucleus in equatorial and another in the axial position.

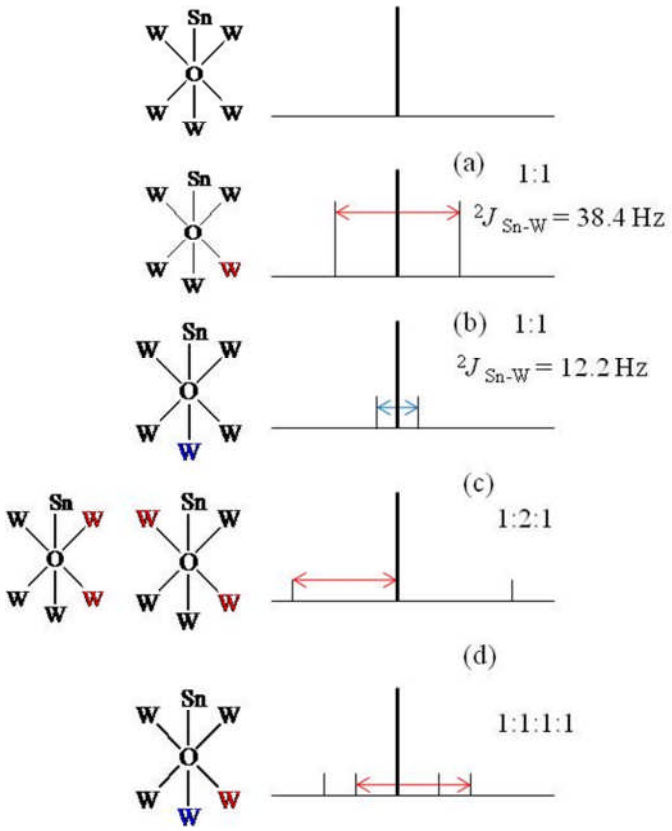

Fig. 3.5: Theoretical modelling of ^{183}W isotopologues and assignment of ^2J $\{^{119}Sn^{183}W\}$ W represents equatorial and W represents axial position.

Trans	Cis		Intensity
W^0	W_4^0	$0.86 * 0.86^4$	0.47043
W^0	$W_3^0W_1^{183}$	$0.86 * 0.86^3*0.14*4$	0.30632
W^0	$W_2^0W_2^{183}$	$0.86 * 0.86^2*0.14^2*6$	0.07480
W^0	$W_1^0W_3^{183}$	$0.86 * 0.86*0.14^3*4$	0.00812
W^0	W_4^{183}	$0.86*0.14^4$	0.00033
W^{183}	W_4^0	$0.14 * 0.86^4$	0.07658
W^{183}	$W_3^0W_1^{183}$	$0.14 * 0.86^3*0.14*4$	0.04987
W^{183}	$W_2^0W_2^{183}$	$0.14 * 0.86^2*0.14^2*6$	0.01218
W^{183}	$W_1^0W_3^{183}$	$0.14 * 0.86*0.14^3*4$	0.00132
W^{183}	W_4^{183}	$0.14*0.14^4$	0.00005

Table 2. Isotoplogues for SnW_5 and their intensities. **(Note:**W^0 =NMR inactive tungsten. W^{183}= NMR active tungsten. Sum of intensities =1.0)

Isotoplogues with two ^{183}W nuclei in the POM cage would produce six possible ways (i.e. two trans and four cis) if both tungsten nuclei are present in the equatorial positions. Both ^{183}W nuclei are chemically equivalent in this stage and the active tin ^{119}Sn metal would couple with two ^{183}W, and it gives tungsten satellite peaks with a 1:2:1 ratio (**c**). There is another probability if ^{183}W tungsten active nuclei occupied equatorial and axial positions, both tungsten nuclei are not chemically equivalent and tin metal center would couple separately with two different ^{183}W nuclei, and it gives tungsten satellite peaks with 1:1:1:1 ratio (**d**)

To emphasise the difference between axial and equatorial tungsten coupling constants, we have assumed the Sn-W(eq) coupling constant is 39 Hz, which was confirmed by most intense doublet of the peak. Then we varied the Sn-W(ax) coupling constant parameter from 50 Hz to 10 Hz in the simulation. These values were chosen from inspection of the relative intensities of ^{119}Sn spectrum. Pope *et.al* [11] have already identified that in organotin 'sandwich' keggin type polyoxometalates, an increased Sn-O-W bond angle is accompanied by an increasing Sn-O-W coupling constant for $[(C_6H_5Sn)_3\text{-}P_2W_{15}O_{59}]^{9-}$ ($^2J_{Sn\text{-}w}$ = 78 Hz, Sn-O-W = 147-158°) and $[(C_6H_5SnOH)_3(PW_9O_{34})_2]^{12-}$ ($^2J_{Sn\text{-}W}$ = 33 Hz, Sn-O-W = 139-142°).

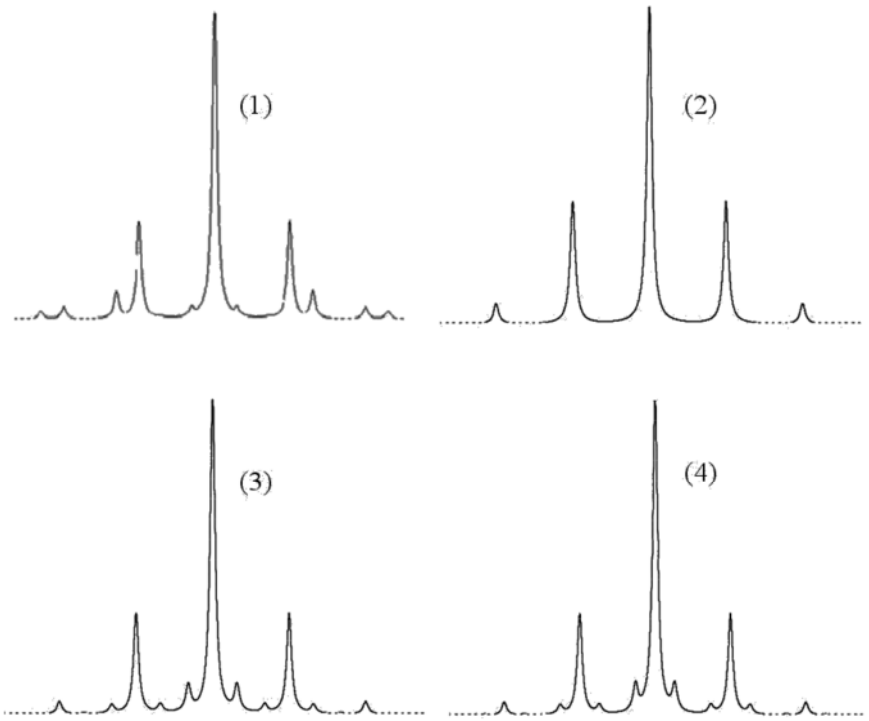

Fig 3.6: ^{119}Sn NMR simulation spectrum of $[(MeO)SnW_5O_{18}]^{3-}$ $^2J_{Sn\text{-}Wax}$ coupling constants of 1) 50 Hz 2) 38.4 Hz 3) 12. 2 Hz 4) 10 Hz

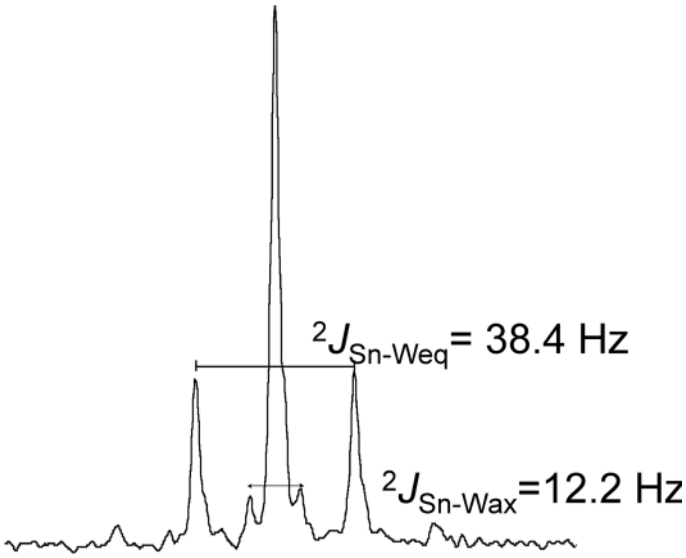

Fig 3.7: ^{119}Sn NMR spectrum of $[(MeO)SnW_5O_{18}]^{3-}$ by INEPT method.

To summarise, we varied the axial coupling constant value from 50 Hz to 10 Hz. The simulated spectrum exactly matched with the original spectrum at 12.2 Hz and therefore assigned Sn-W(ax) coupling constant value is to be 12.2 Hz.

Based on the literature, we had expected to see the axial $^2J_{Sn\text{-}Wax}$ coupling constant to be larger than the equatorial $^2J_{Sn\text{-}Weq}$ but we observed couplings in reverse order. Recently Kortz *et.al* reported the very large $^2J_{Sn\text{-}W}$ = 96 Hz coupling constant for $[(C_6H_5Sn)_2As_2W_{19}O_{67}(H_2O)]^{8-}$ as the Sn-O-W bond angle ranges from 135° to 140°. The bond angle factor alone does not explain the very large coupling constant but most likely the coordination geometries of the tin atoms play also an important role.[12] To best of our knowledge, no one has reported axial and equatorial $^2J_{Sn\text{-}W}$ coupling constant in Lindqvist type polyoxometalate systems and detailed computational studies of $(TBA)_3$ **1** were carried out and discussed in the following section **3.3.2.7**.

3.3.2.4 ^{1}H Proton NMR

The proton NMR spectrum showed one single peak at δ_H 3.64 ppm for methoxide which exhibited tin coupling as satellite peaks for all the NMR active tin isotopes (^{119}Sn, ^{117}Sn, ^{115}Sn). The ^3J(SnH) coupling constants are 78, 72 and 66 Hz for $^3J\{^{119}Sn^1H\}$, $^3J\{^{117}Sn^1H\}$ and $^3J\{^{115}Sn^1H\}$ respectively. This can be compared to $J\{^{119}Sn^1H\}$ values of 70.8 and 70.3 Hz observed for Sn(TPP)(OCOH)X and $SnTPP(X)_2$ where TPP is 5,10,15,20-tetraphenylporphyrin and X = OCH_3.[13,14] The methoxide and foramide functional groups are trans orientated to the tin center.

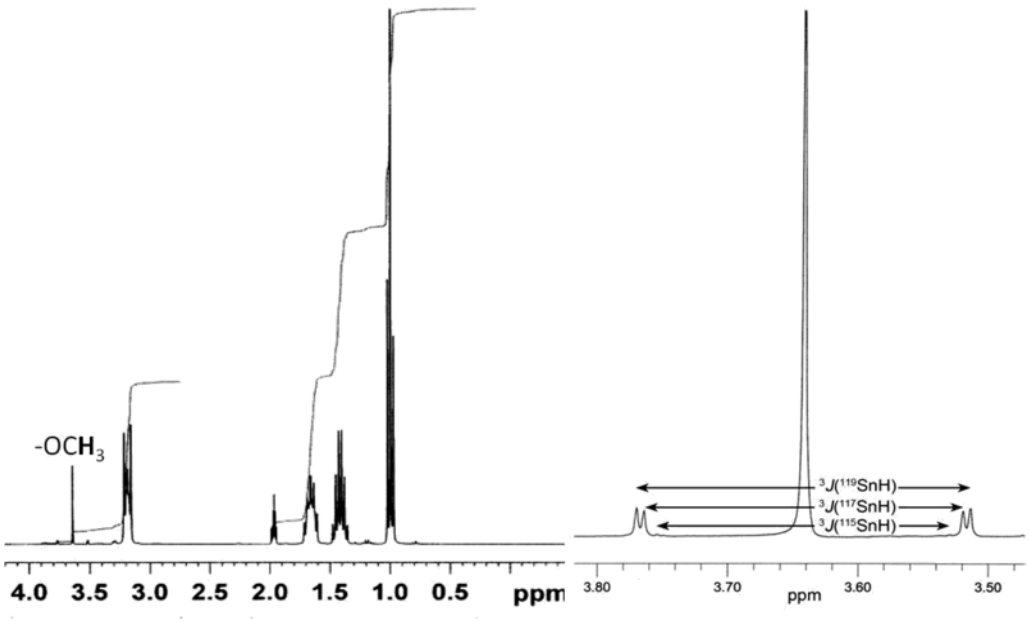

Fig 3.8: ^{1}H NMR spectrum of $(TBA)_3$ $[(MeO)SnW_5O_{18}]$ with an expansion of the methoxide region.

We also measured the $^{3}J\{^{1}H^{119}Sn\}$ and $^{3}J\{^{1}H^{117}Sn\}$ coupling constant value by selective tin (Sn) decoupled proton NMR spectroscopy method. These allowed us to selectively irradiate the ^{117}Sn and ^{119}Sn nucleus. From this, we obtained the following values; ^{1}H {**^{119}Sn**} J_{117SnH}= 75.3 Hz, ^{1}H {**^{117}Sn**} J_{119SnH} = 76.7 Hz and due to the very low abundance ^{115}Sn nucleus, we have not found the $^{3}J\{^{1}H^{115}Sn\}$ coupling constant. The selective Sn decoupled proton NMR spectra is shown in the Fig 3.9. ^{119}Sn spectrum with no proton decoupling was collected, however, even after an overnight collection the signal to noise ratio was still too bad to assign any peaks as being due to $J\{^{117/119}Sn^{1}H\}$.

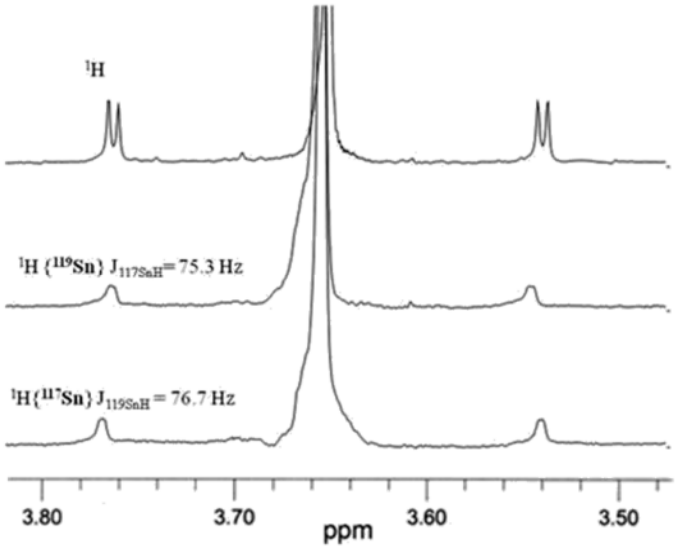

Fig 3.9: Selective tin (Sn) decoupled ^{1}H NMR spectra and assignment of ^3J{SnH} coupling constant.

3.3.2.5 ^{13}Carbon NMR spectroscopy

The ^{13}C NMR spectrum showed one single peak at δ_C 53 ppm for methoxide which exhibited ^{119}Sn coupling. We have measured $^2J\{^{119}Sn^{13}C\}$ = 34.5 Hz for the terminal methoxide group. This can be compared to the values of $^2J\{^{119}Sn^{13}C\}$ = 45 Hz obtained in $Sn(OBu^t)_4$ for terminal butoxide ligands [15] and $^2J\{^{119}Sn^{13}C\}$ = 28 Hz measured for the $TI[Sn(OEt)_6]_n$ where it was demonstrated that the ethoxide ligands were doubly bridging in solution. [16]

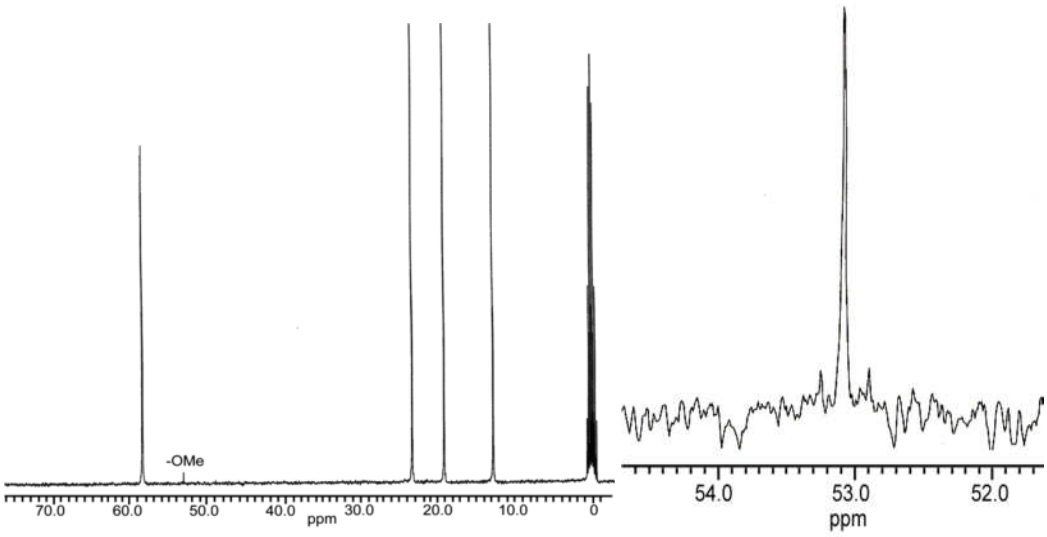

Fig 3.10: ^{13}C NMR spectrum of $(TBA)_3$ $[(MeO)SnW_5O_{18}]$ with an expansion of the methoxide peak.

3.3.2.6 ^{17}O NMR spectroscopy

The ^{17}O NMR spectrum of the $[(MeO)SnW_5O_{18}]^{3-}$ should show six characteristic peaks for the M'M_5 hexametallate structure if the crystal structure is preserved in solution. Based on previously reported $[MW_5O_{18}]^{n-}$ species, we assigned the peaks at 720 and 684 ppm as those due to equatorial (W_{eq}=O) and axial (W_{ax}=O) respectively. The peaks observed between 300 and 400 ppm are in the region that would expected to be μ_2 bridged oxygens. We proposed that the peaks at 395, 383 and 363 ppm are due to Sn-O-W and W-O-W and strong peak observed at 17.4 ppm to be due to the central μ_6- Oxygen. Because of the quadrupole moment of the ^{17}O nucleus, the all observed peaks are slightly broad peaks in ^{17}O NMR.[1]

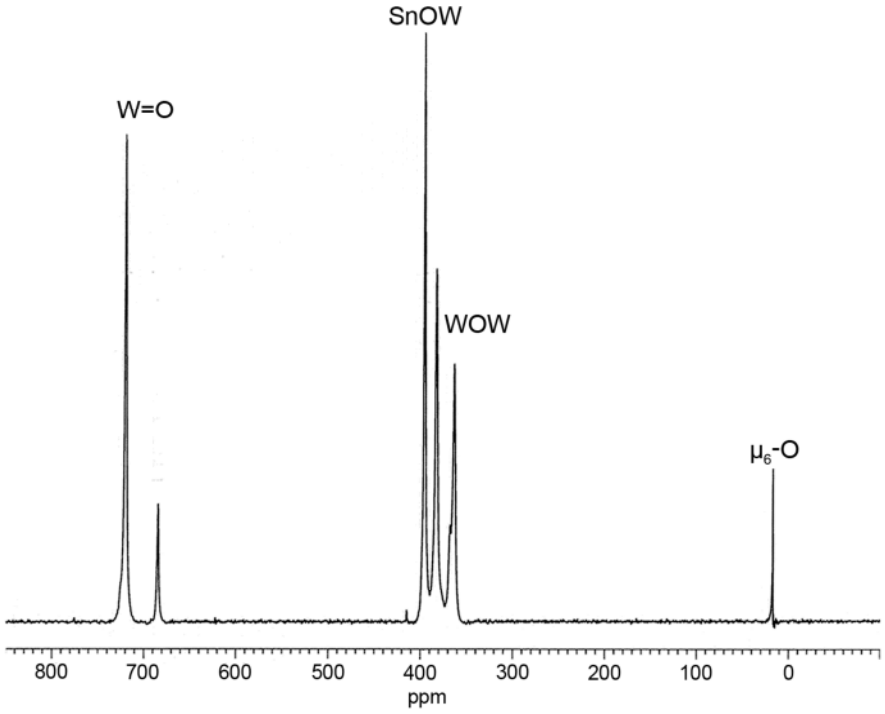

Fig 3.11: ^{17}O NMR spectrum of $[(MeO)SnW_5O_{18}]^{3-}$

The relative intensities of the peaks depend on the relative amounts of ^{17}O enrichment at each site and this is affected by the mechanism of hydrolytic aggregation, which is still not fully understood but it is assumed some sites will be more readily enriched than others.

3.3.2.7. ^{183}W NMR spectroscopy

The ^{183}W NMR spectrum showed two main peaks at δ_W 76.9 and -128.1 ppm with $^2J_{W\text{-}Sn}$ tin satellite peaks. The ^{183}W nucleus has nuclear spin of +1/2 and its natural abundance is 14.31%. The coupling constant value was 39 Hz which exactly matched that measured in the ^{119}Sn NMR spectrum. The tin satellite peaks in the tungsten NMR are quite sharp because of the shorter relaxation time for the tin nucleus. We have observed some other peaks also at δ_W 58.1 ppm in the tungsten NMR. We assigned this peak may due to possible side product $Q_2[W_6O_{19}]$ which is slightly deviated from its previously reported value at 47 ppm. We have assigned the most intensive peaks at δ_W 76.9 and -128.1 as equatorial and axial tungstens, respectively based on intensities. Generally Keggin type polyoxometallates chemical shift values are observed at -100 to -200 ppm in ^{183}W NMR. Recently Pope *et.al* [9] observed a ^{183}W chemical shift at -16 and -20.3 ppm for axial and equatorial tungstens in $[(CH_3)SnW_5O_{18}]^{3-}$, but $(TBA)_3$ **1** and its derivatives all showed chemical shifts at -120 to -130 ppm for axial tungsten (1W) so we believe that $[(CH_3)SnW_5O_{18}]^{3-}$ should be re-investigated.

3.3.2.8 Computational studies of $[(MeO)SnW_5O_{18}]^{3-}$

The electronic structure of $[(MeO)SnW_5O_{18}]^{3-}$ is analogous to that in other non-reduced POMs, with an occupied oxo “band” and a virtual metal “band” with an important HOMO-LUMO gap. Representations of the HOMO and the LUMO are depicted in Figure 3. The HOMO is based on bridging oxido groups, whereas the LUMO is delocalized on the four equatorial W atoms with some contributions on the oxygen atoms.

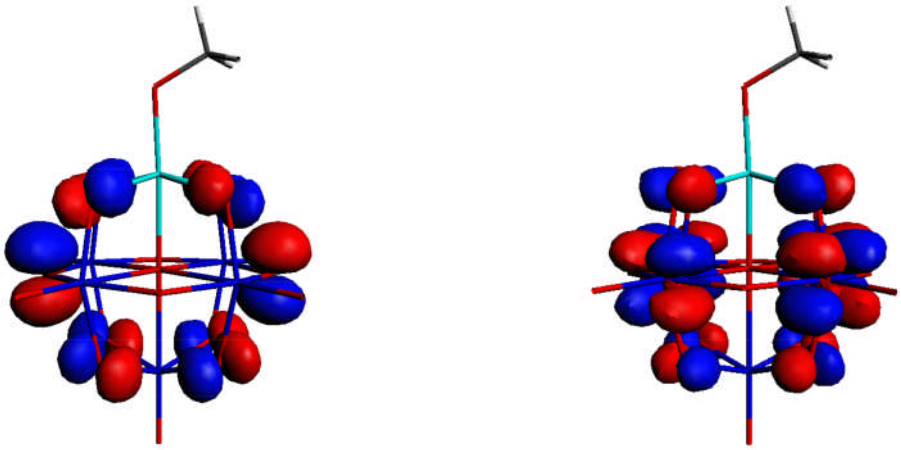

A **B**

Fig 3.12: Representation of the HOMO (A), LUMO (B) orbitals for $[(OCH_3)SnW_5O_{18}]^{3-}$. Colours of the atoms: O, red; W, dark blue; Sn, light blue; C, grey; H, white.

In order to calculate the ^{183}W chemical shift, eclipsed and staggered models have been made with Cs symmetry and dihedral angles of 0^o or 60^o. Simulating the rotation of the -CH_3 group around the O−Sn bond, produced different shielding constants and coupling constants for both models and values are given in the table. Experimentally $(TBA)_3$**1** showed characteristic peaks at 76.9 (4W) and -128.1 (1W). Although the absolute errors in the prediction of the shift are not negligible, −88 *vs* −128 ppm for the axial tungsten and 105 *vs* 77 ppm for the equatorial tungsten, the experimental trend is well reproduced. Moreover, the separation between the two predicted peaks (193 ppm) matches very well that in the experimental spectrum showing that the predicted chemical shifts for the two different types of W atoms (W_{ax} and W_{eq}) are both shifted around 30 ppm from the experimental value. This suggests that the same type of error is present in the prediction of the shielding of the two types of W atoms or in the prediction of the shielding of the reference.

	Eclipsed	Staggered
σ (W_{ax})	2641.18	2647.11
σ ($W_{eq,1}$)	2451.60	2455.20
σ ($W_{eq,2}$)	2443.38	2449.58
σ ($W_{eq,3}$)	2454.54	-
σ $(W_{eq})_{av}$	2449.84	2452.39
δ (W_{ax})	−84.54	−90.47
$\delta_{exp}(W_{ax})$	−128	−128
δ $(W_{eq})_{av}$	106.80	104.15
$\delta_{exp}(W_{eq})$	77	77
$\Delta\delta$ (W_{eq-ax})	191	195
$\Delta\delta$ (W_{eq-ax})	190	190

Table 3: Computed ^{183}W shieldings and chemical shifts for the two models of $[W_5O_{18}Sn(OCH_3)]^{3-}$, along with the experimental values for the shifts (ppm). The computed shielding for the WO_4^{2-} reference is 2556.64 ppm.

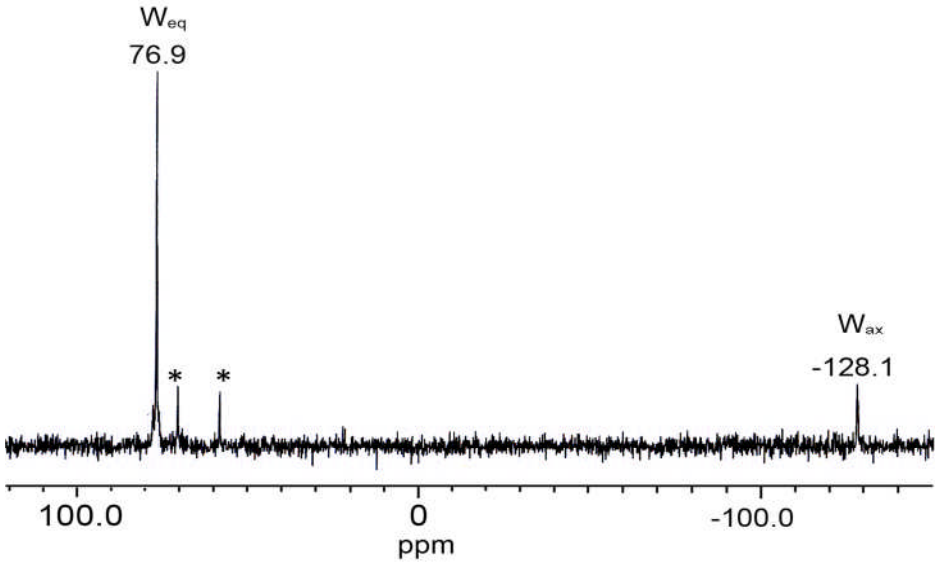

Fig 3.13: ^{183}W NMR spectrum of $[(MeO)SnW_5O_{18}]^{3-}$ [* indicates impurity]

3.3.2.9 Infra red spectroscopy

The crystals of $(TBA)_3$ **1** were investigated by infra red spectroscopy and the spectrum in shown in Figure 3.15. The IR spectrum shows a very strong band *v* (W=O) at 951, 960 cm^{-1} and *v*(W-O-W) band appeared at 790 and 749 cm^{-1}. The highly symmetrical $[W_6O_{19}]^{2-}$ equivalent and terminal oxo bands are found at 974 and 814 cm^{-1}. The higher charge of the anion causes the bathochromic shifts of *v*(W=O) bands leads to lower wave numbers. The *v* (W=O) band is slightly higher than reported derivatives of $[(MeO)TiW_5O_{18}]^{3-}$, $[(Py)CoW_5O_{18}H]^{3-}$.[7] This is due to the more Lewis acidic nature of the tin metal.

The substitution of tin for $[WO]^{4+}$ in the Lindqvist anion $[W_6O_{19}]^{2-}$ also lowers the symmetry from O_h and splits the band due to *v*(W=O), resulting in the observation of a weak band at 960 cm^{-1}. However this splitting was sometimes not distinguishable within the spectrum. This reduced symmetry may also result in the greater number of strong bands associated with bridging vibrations within the spectrum. Characteristic weak bands between 3000 and 1300 cm^{-1} are associated with the tetrabutyl ammonium cations.

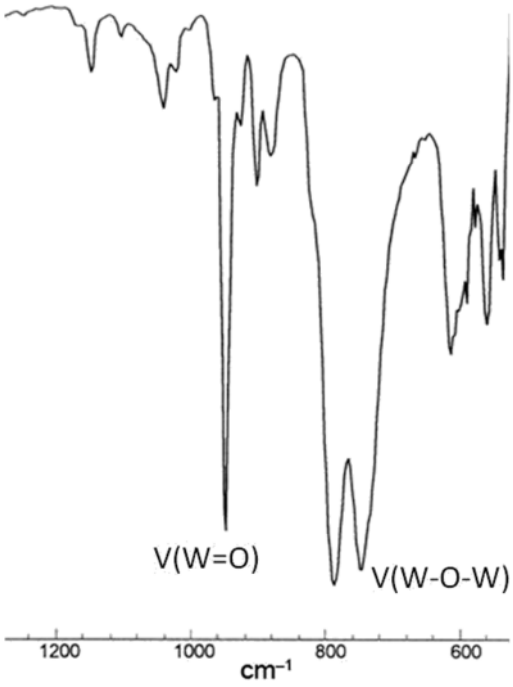

Fig 3.14: Infra- red spectrum of $[(MeO)SnW_5O_{18}]^{3-}$

3.3.2.10 Electrospray Mass spectrometry

Negative ion electrospray ionisation mass spectra (ESI MS), was recorded for ^{17}O un-enriched samples at room temperature. Although we were unable to assign any peaks in the spectrum to the $[(MeO)SnW_5O_{18}]^{3-}$ anion a number of peaks were found to be associated with monomeric SnW_5 clusters as shown in Table 3.

The $[W_6O_{19}]^{2-}$ and $\{QW_6O_{19}\}^{-}$ anion peaks were observed as a some of the most significant peaks in the spectrum of the un-enriched sample and were centred at 1649.83 m/z and 704.28 m/z, respectively. Errington *et.al* [17] reported that the impurity $[W_6O_{19}]^{2-}$ is observed at 703.79 m/z. This may be result from an impurity in the sample or in fact be an indication of the instability of $[(MeO)SnW_5O_{18}]^{3-}$ under electrospray conditions. The major peaks in the spectrum indicate that the sample undergoes hydrolysis very rapidly and produces hydrolytic products. It indicates also that the surface methoxide group is very reactive towards acids.

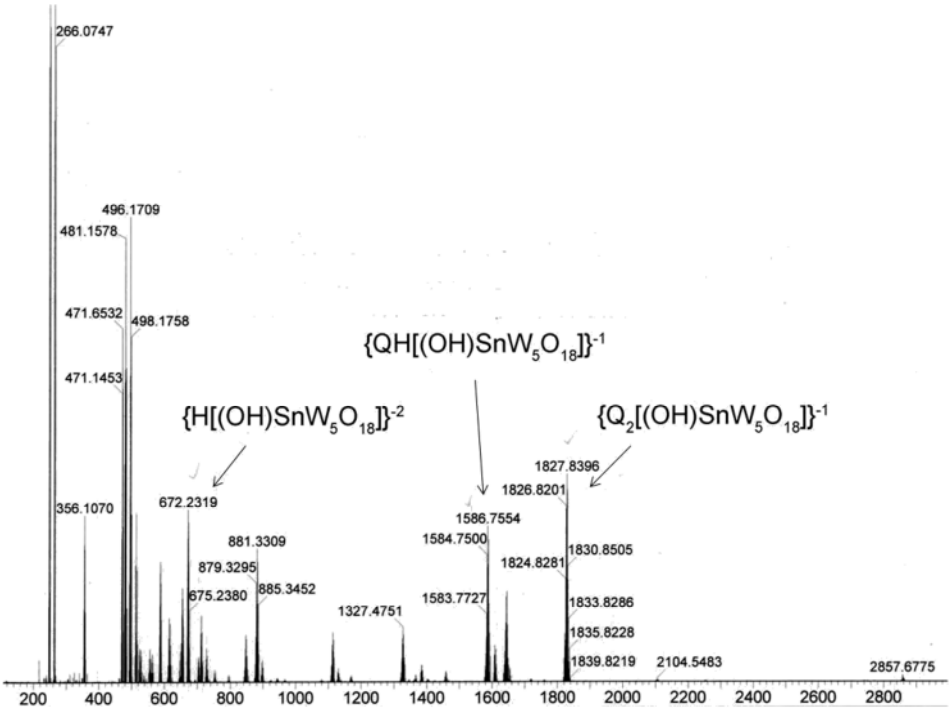

Fig: 3.15. Negative ion electrospray ionisation mass spectrum of $[(MeO)SnW_5O_{18}]^{3-}$.

Anion	Observed *m/z*	Theoretical *m/z*
$\{H[(OH)SnW_5O_{18}]\}^{-2}$	672.238	671.960
$\{Q_2[(OH)SnW_5O_{18}]\}^{-1}$	1827.8396	1827.84
$\{QH[(OH)SnW_5O_{18}\}^{-1}$	1586.7554	1586.38

Table 4: Assignments of peaks to SnW_5 species in the electrospray mass spectrum of $(TBA)_3[(MeO)SnW_5O_{18}]$

3.3.2.11. Electrochemistry of $[(MeO)SnW_5O_{18}]^{3-}$

Cyclic voltammetry (CV) is a powerful technique to study the electrochemical property of POMs. This field has received much attention in recent years because there are possibilities to tune their redox potentials by changing heteroatoms or addenda ions without affecting the structure.

Tetra-n-butyl ammonium tetrafluoroborate (QBF_4) (50 cm^3, 0.005 M) in acetonitrile was freshly prepared and used as supporting electrolyte, The solution of $(TBA)_3$ **1** (25 cm^3, 0.005 M) in QBF_4/ CH_3CN was prepared. The secondary electrode (Ag) was used as a supporting electrode and Pt was used as an auxillary electrode. A solution of ferrocene (0.005 M) was used as an internal standard and was added at the end of an experiment. Acetonitrile was dried by refluxing it under an inert atmosphere in the presence of a drying agent i.e. CaH_2. All the solutions were degassed by the freeze-pump-thaw process.[18]

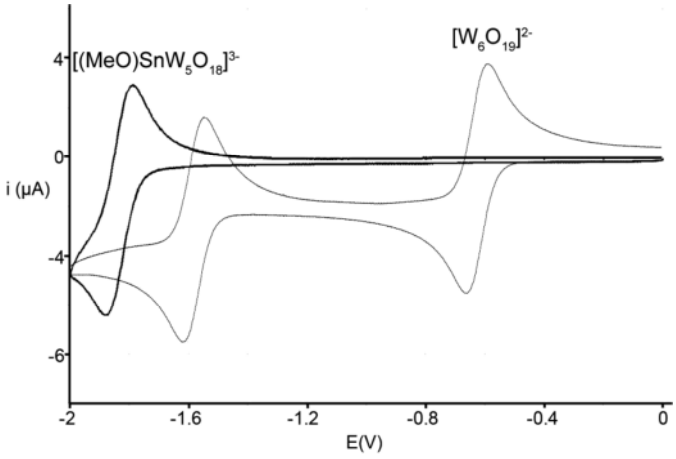

Fig 3.16: Cyclic Voltagram of $(TBA)_3[MeOSnW_5O_{18}]$ and $(TBA)_2$ W_6O_{19} over negative potential range.

The $(^{n}Bu_4N)_2W_6O_{19}$ shows reversible one-electron reduction in acetonitrile at -0.63 V. A further one-electron reduction is also observed at -1.64 V which is close to the solvent limit though careful control of solvent purity is required for observation of this second reduction wave.[18-21] Because of the higher charge associated with the heterometallate, the novel stannotungstate **1** showed reversible redox couple at even more negative potential compared to $[W_6O_{19}]^{2-}$. These reversible redox waves appeared at E_{mid} = -1.84 V where $E_{mid} = (E_{PC} + E_{PA})/2$ (E_{PC} and E_{PA} are the peak cathodic and anodic potentials respectively) significantly more negative potential than both redox couples for $[W_6O_{19}]^{2-}$ at –0.63 V for $[W_6O_{19}]^{2-}$ / $[W_6O_{19}]^{3-}$ and at –1.64 V for $[W_6O_{19}]^{3-}$ / $[W_6O_{19}]^{4-}$. We confirmed this to be a one electron quasi reversible redox process but due to slow electron transfer kinetics, the large E_{pc}-E_{pa} separation was observed. A diffusion coefficient of 3.36 % 10^{-5} cm^2s^{-1} was obtained from chronoamperometry measurements, which were consistent with a one-electron reduction of the anion.

3.4. Hydrolysis of $[(MeO)SnW_5O_{18}]^{3-}$

According to equation 7, hydrolysis of $(TBA)_3$ $[(MeO)SnW_5O_{18}]$ would be expected to form $(TBA)_3$ $[(HO)SnW_5O_{18}]$ and subsequently $(TBA)_6$ $[(\mu\text{-}O)\{SnW_5O_{18}\}_2]$

$$\mathbf{2[(MeO)SnW_5O_{18}]^{3-} + H_2O \rightleftharpoons [(HO)SnW_5O_{18}]^{3-} + [(\mu\text{-}O)SnW_5O_{18}\}_2]^{6-}} \qquad \text{-----7}$$

Crystals of $(TBA)_3$ **1** were dissolved in acetonitrile and hydrolysed with a fifty fold excess of distilled water, with heating for 30 minutes at 85-90 ^{o}C. All the volatiles were removed in *vacuo* and the procedure was repeated twice to ensure complete hydrolysis. To avoid the loss of enrichment in the metal oxide framework, the resultant crude product was treated with small amount of ^{17}O enriched water at 85-90 ^{o}C in acetonitrile. Pale yellow crystals were obtained by slow vapour diffusion of ether in acetonitrile and these were used for multinuclear NMR characterisation, infrared spectroscopy and single crystal X ray determination.

Crystal structure of $(TBA)_3$ **2**

Unit cell parameters

a = 24.1538(3) Å α = 90°

b = 16.9306(2) Å β= 97.6760(10)°

c = 16.6864(2) Å γ= 90°

Crystal system: monoclinic

Space group: $P12_1/c1$

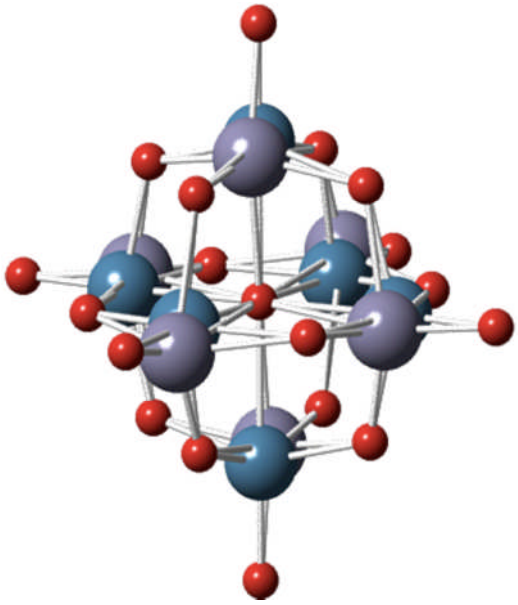

Fig 3.17: Structure of the anion $[OHSnW_5O_{18}]^{3-}$. The colour codes are as follows: W (pale blue), O (red), Sn (pale grey).

In the crystal structure of $[(OH)SnW_5O_{18}]^{3-}$ the Sn-OH group is disordered over all six metal positions. We were not able to assign the OH proton crystallographically but in solution the existence of the hydroxo tin POM has been proven by ^{119}Sn and ^{17}O NMR spectroscopy. $(TBA)_3$ **2** is not stable in solution and the dimer product easily forms by self condensation. These results can be compared with other transition metal Lindqvist polyoxometalates where hydroxo derivatives of the transition metal Llindqvist type POMs have not been observed.

3.4.1. Multinuclear NMR spectroscopy studies

3.4.1.1. ^{119}Sn NMR spectroscopy

$$\mathbf{2\ [(HO)SnW_5O_{18}]^{3-} \rightleftharpoons [(\mu\text{-}O)SnW_5O_{18}\}_2]^{6-} + H_2O} \qquad \mathbf{-----8}$$

After hydrolysis of $[(MeO)SnW_5O_{18}]^{3-}$, the crude product was examined by ^{119}Sn NMR spectroscopy. It exhibited a single peak at δ_{Sn} -633 ppm with $^2J_{Sn\text{-}W}$ satellite coupling. In solution, the condensation reaction takes place readily and leads to the dimer species and water. We have confirmed that $(TBA)_3$ **2** exists in equilibrium with

the dimer species at both room temperature and high temperature. The $^{2}J_{Sn\text{-}W}$ coupling constant value was measured and the value is 37.4 Hz.

Evidence for $[(OH)SnW_5O_{18}]^{3-}$

From the X-ray diffraction, we could not locate the -OH group because hydrogen and oxygen atoms are very small compared to tungsten metal. The electron density of tungsten metal is very high and it completely hides the -OH group electron density. We recorded the ^{119}Sn NMR with no proton decoupling of $[(OH)SnW_5O_{18}]^{3-}$ species in order to prove the OH proton on the tin surface.^{119}Sn NMR spectra with no proton decoupling illustrates the hydroxide proton in $[(OH)SnW_5O_{18}]^{3-}$.

The ^{119}Sn NMR with no proton decoupling of $[(OH)SnW_5O_{18}]^{3-}$ shows a doublet at -633 ppm due to $^{2}J\{^{119}Sn^{1}H\}$ coupling with value 127 Hz. In addition, we also observed $^{2}J\{^{119}Sn^{183}W\}$ coupling with value is 37.4 Hz. (Fig 3.18).

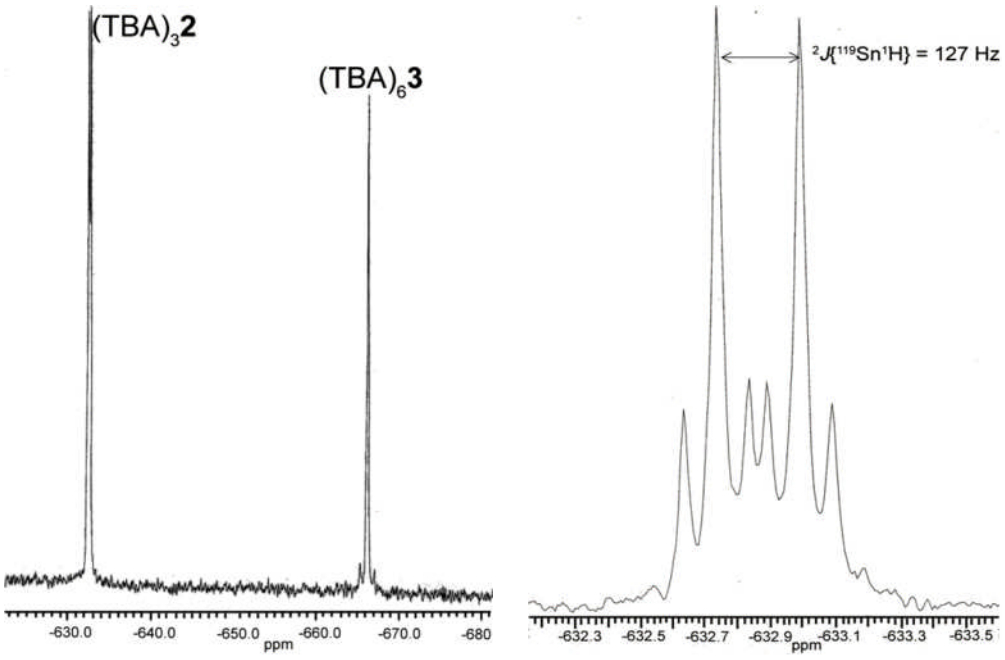

Fig 3.18: ^{119}Sn NMR spectrum of a mixture of $[(OH)SnW_5O_{18}]^{3-}$ and dimer $[(\mu\text{-}O)(SnW_5O_{18})_2]^{6-}$ with no proton decoupling.

3.4.1.2. ^{17}O NMR spectroscopy

It was expected that the ^{17}O NMR spectrum of $[(OH)SnW_5O_{18}]^{3-}$ and $[(\mu\text{-}O)(SnW_5O_{18})_2]^{6-}$ would show six and seven characteristic peaks, respectively, but it showed only six peaks in addition to a peak for water. This clearly suggests that the water molecule arises from a self condensation mechanism which is taking place in solution.

By comparing the chemical shift values of $(TBA)_3$ **2** with the starting material $(TBA)_3$ **1** we assigned the peaks observed at 719 and 683 ppm to the equatorial (W_{eq}=O) and axial (W_{ax}=O) respectively. The peaks observed between 300 and 400 ppm are in the region that expected for μ_2 bridged oxygens. We propose that the peaks at 395, 382 and 367 ppm are due to Sn-O-W and W-O-W. The peak observed at 17.2 ppm is due to the central μ_6- oxygen. We assigned a broad peak observed at -7 ppm to water from the self condensation reaction and we were not able to assign the peak for bridged oxygen (Sn-O-Sn). The ^{17}O NMR spectrum for $[(OH)SnW_5O_{18}]^{3-}$ is shown in Fig. 3.19.

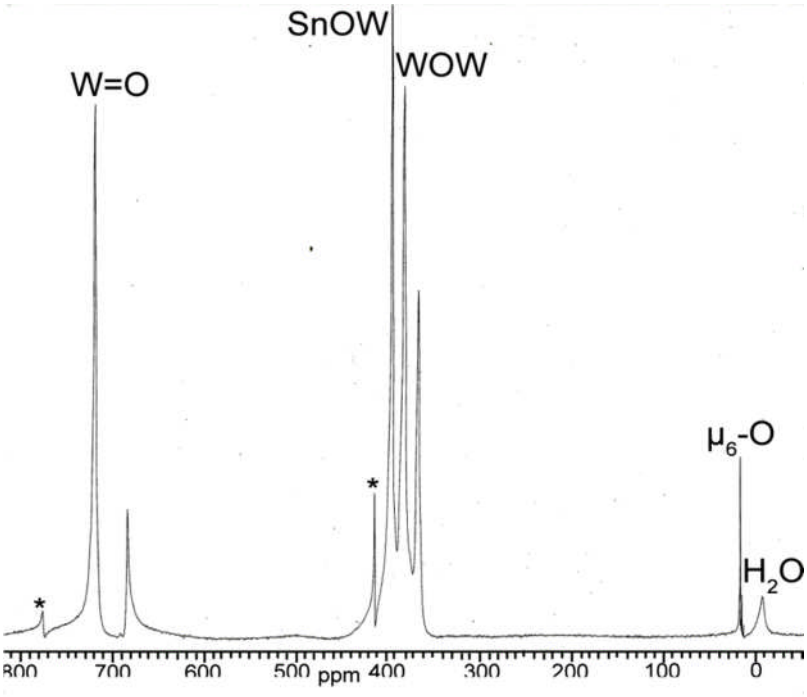

Fig 3.19: ^{17}O NMR spectrum of $[(OH)SnW_5O_{18}]^{3-}$ [* = $(W_6O_{19})^{2-}$]

3.4.1.3. ^{183}W NMR spctroscopy

The ^{183}W NMR spectrum showed four main peaks at δ 72.2, 70.1, -122.2 and -130.8 ppm with $^{2}J_{W\text{-}O\text{-}Sn}$ coupling. The impurity peak at 59 ppm was present in all the derivatives. We assigned the major intense peaks at 72.2 ppm and -122.2 ppm are to the $[(OH)SnW_5O_{18}]^{3-}$ moiety and the less intense peaks to the $[(\mu\text{-}O)(SnW_5O_{18})_2]^{6-}$ species.

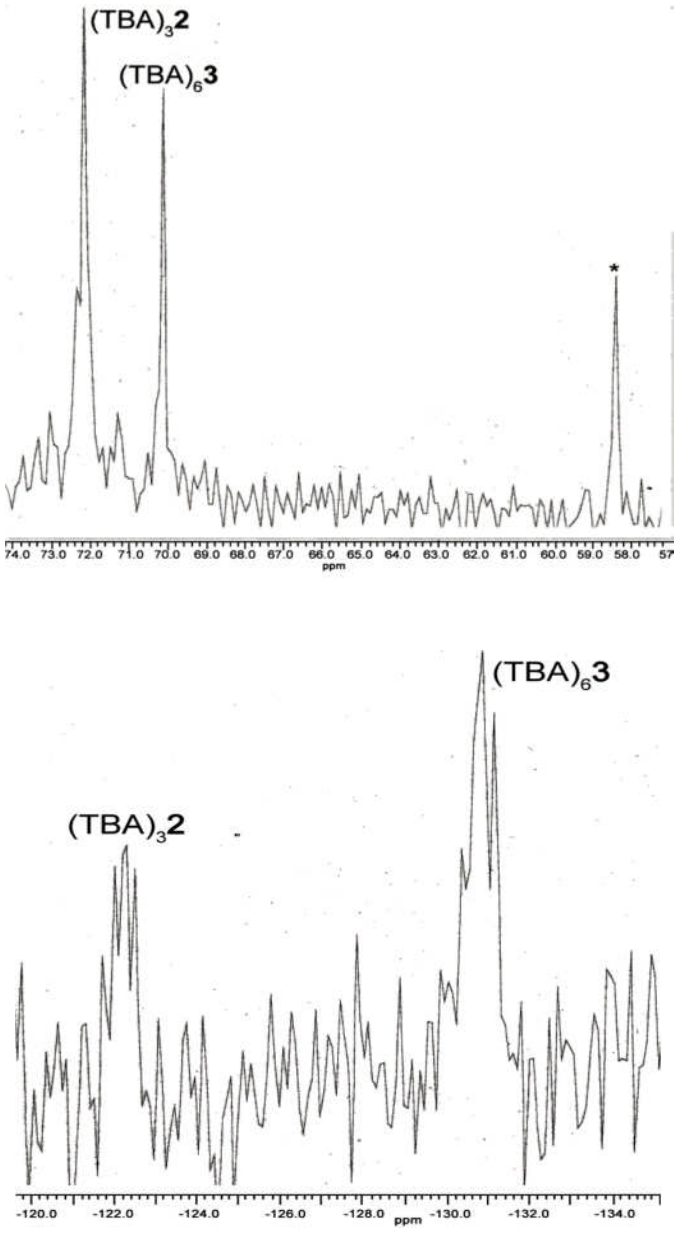

Fig 3.20: ^{183}W spectrum of $[(OH)SnW_5O_{18}]^{3-}$ and $[(\mu\text{-}O)(SnW_5O_{18})_2]^{6-}$ (* due to $[W_6O_{19}]^{2-}$

The coupling constant value for $[(OH)SnW_5O_{18}]^{3-}$ is 36.7 Hz which is comparable with $^{2}J\{^{119}Sn^{183}W\}$ tungsten coupling in ^{119}Sn NMR and because of the shorter relaxation time for tin hetero metal, the tin satellite peaks in the tungsten NMR are sharp. The equatorial and axial regions of the ^{183}W NMR spectrum for a mixture of $[(OH)SnW_5O_{18}]^{3-}$and $[(\mu\text{-}O)(SnW_5O_{18})_2]^{6-}$ are shown Figure 3.20.

3.4.2. Proton NMR

Loss of the Sn-OCH_3 peak δ_H 3.64 ppm from $[(MeO)SnW_5O_{18}]^{3-}$ indicates that the formation of $[(OH)SnW_5O_{18}]^{3-}$. We were unable to observe the OH proton in ^{1}H NMR spectrum because the hydroxide proton is exchanging between OH and H_2O. We have also confirmed that the hydroxide proton is very basic in nature and it easily reacts with acids.

3.4.3. Infra red spectroscopy

The IR spectrum shows a very strong band *v* (W_{ax}=O) at 951 cm^{-1}. In addition the *v* (SnOW) and *v* (WOW) bands appear at 784 and 748 cm^{-1} and a characteristic OH band is observed at *v* (O-H) 3648 cm^{-1}. The W=O, SnOW and WOW stretching frequencies were slightly deviated from the starting precursor $(TBA)_3$ **1** because of the electronic and basic nature of surface groups. The *v* (O-H) stretching frequency can be compared to the fundamental O-H stretching frequency *v* (Sn-OH) of surface groups in SnO at 3640 cm^{-1} which were noted by Harrison *et.al.*[22] The infra red spectroscopy spectrum for $[(OH)SnW_5O_{18}]^{3-}$ is shown in Fig. 3.21.

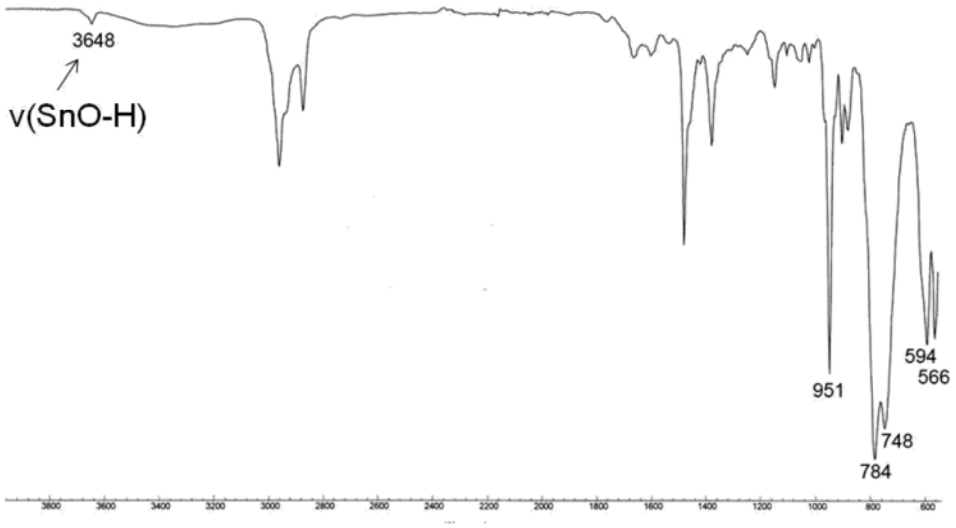

Fig 3.21: Infra red spectrum of $(TBA)_3[(OH)SnW_5O_{18}]$

3.4.4. Electrospray mass spectrometry

The negative ion electrospray ionisation mass spectrum (ESI MS) was recorded for ^{17}O un-enriched samples and the full-spectrum is shown in Figure 3.22.

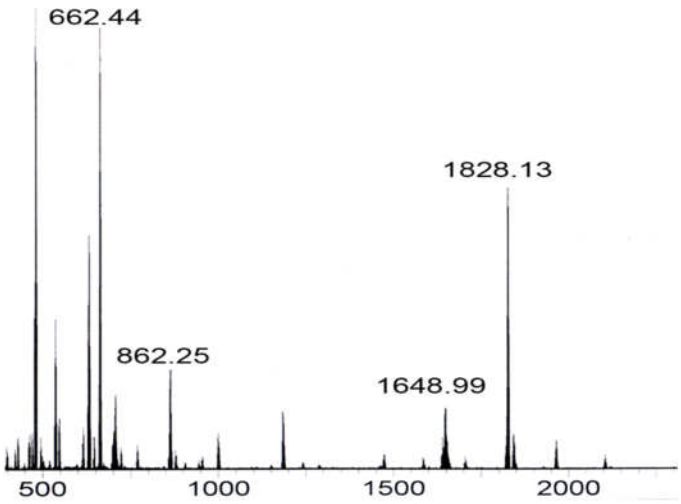

Fig 3.22: Negative ion electrospray mass spectrum of $(TBA)_3[(OH)SnW_5O_{18}]$

Although we were unable to assign any peaks in the spectrum to the $[(HO)SnW_5O_{18}]^{3-}$ anion, a number of peaks were found to be associated with monomeric SnW_5 clusters. The $[W_6O_{19}]^{2-}$ anion peaks were not observed in this mass spectrum but the $\{QW_6O_{19}\}^{-}$ anion cluster peak was observed in the spectrum of the ^{17}O un-enriched sample centred at 1648.99 m/z. This is may be the result of an impurity or an indication of the instability of $[(HO)SnW_5O_{18}]^{3-}$ under electrospray conditions.

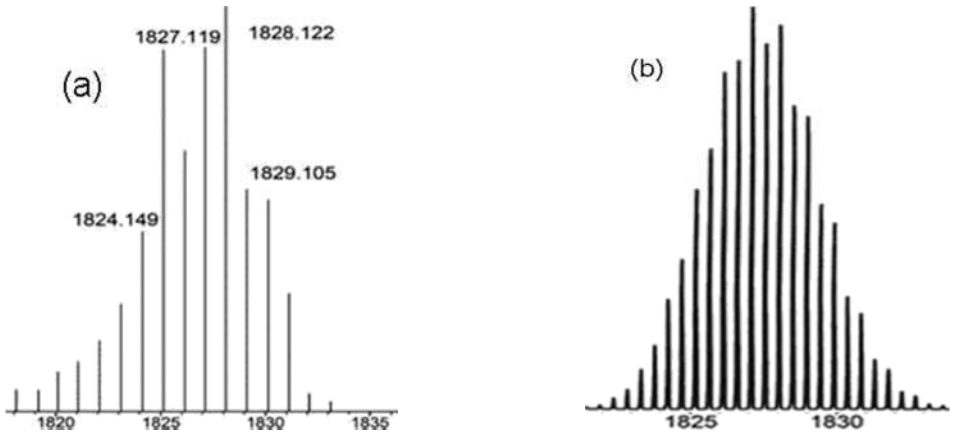

Fig 3.23: a) Peak pattern for the ion cluster assigned to $\{(TBA)_2(OH)SnW_5O_{18}\}^{-}$ in the negative ion electrospray mass spectrum of $(^nBu_4N)_3[OHSnW_5O_{18}]$. b) simulated peak pattern for $\{(TBA)_2(OH)SnW_5O_{18}\}^{-}$ anion.

The major peaks in the spectrum indicate that the sample does not lose the hydroxide group very easily and it remains a monomer in ESI MS conditions. This result was slightly contradictory to the other supporting information because the rest of the data strongly supports the instability of $[(HO)SnW_5O_{18}]^{3-}$ in solution and quickly self-condenses producing a dimer. We did not observe any dimer cluster ion peaks in the mass spectrum, under ESI conditions the dimer anion may dissociate and produce only monomer.

3.5. Equilibrium studies of $[(OH)SnW_5O_{18}]^{3-}$

3.5.1. At room temperature

The $(TBA)_3$ **1** shows a single peak at δ_{Sn} -647 ppm in the ^{119}Sn NMR spectrum but it completely disappears after hydrolysis and simultaneously a new single peak appears at -633 ppm. When we recorded the same sample continuously four days, we have observed the new peak at -667 ppm with $^2J\{^{119}Sn^{117}Sn\}$ coupling and the intensity of the new peak was quite high. This simple experiment indicates that $[(OH)SnW_5O_{18}]^{3-}$ condenses in solution and produces dimer product. The coupling constant value of $^2J\{^{119}Sn^{117}Sn\}$ is 333 Hz. This value can be compared to $^2J\{^{119}Sn^{117}Sn\}$ = 317 and 300 Hz in $[Sn(O^iPr)_4.(HO\text{-}^iPr)]_2$ [15] at -40 ^oC and $[Sn(O^iBu)_4.(HO\text{-}i\text{-}Bu)]_2$ [23] at room temperature. At low temperature, the $[Sn(O^iPr)_4.(HO\text{-}^iPr)]_2$ exhibits a dimeric nature and both tin environments are chemically equivalent. We have also observed $^2J\{^{119}Sn^{183}W\}$ the coupling constant in dimer species and the value was 46.1 Hz. This value was quite high compared with $(TBA)_3$ **1** and $[(OH)SnW_5O_{18}]^{3-}$. This is due to electronic nature of the surface group attached to the tin metal center. The intensity ratio of the two peaks is 1:0.7 which suggests that a dynamic equilibrium is establishing between the hydroxo and dimer species in solution state.

3.5.2. At High temperature

The same equilibrium is observed at high temperatures also. After heating the hydroxide species overnight at 85-90 ^oC in an oil bath, a new peak is observed at -667 ppm. In order to confirm the dimer product, we used activated 3Å molecular sieves to absorb the water, but the equilibrium reaction is not affected very much by this method, so we moved to the traditional azeotropic distillation technique to obtain pure dimer species.

3.6. Attempted synthesis of $(TBA)_6[(\mu\text{-}O)(SnW_5O_{18})_2]$

3.6.1 By using molecular sieves

The $(TBA)_3$ $[(OH)SnW_5O_{18}]$ in acetonitrile was heated at 85-90^oC with activated 3Å molecular sieves for three days. The product was carefully removed by filtration and was used for further characterisation. The intensity of the $[(OH)SnW_5O_{18}]^{3-}$ peak was slightly reduced in ^{119}Sn NMR spectrum.

3.6.2. By azeotropic distillation method

The attempted reaction to remove the water by molecular sieves was not successful so we followed an alternative route to remove the moisture i.e by azeotropic distillation. The $(TBA)_3$ $[(OH)SnW_5O_{18}]$ in acetonitrile was heated under reflux at 85-90 ^oC, then was distilled very slowly over the period of 5-6 hrs, although we were not able to remove the water completely by this method, but we ultimately produced dimer species as a major product. The crude product was used for characterisation.

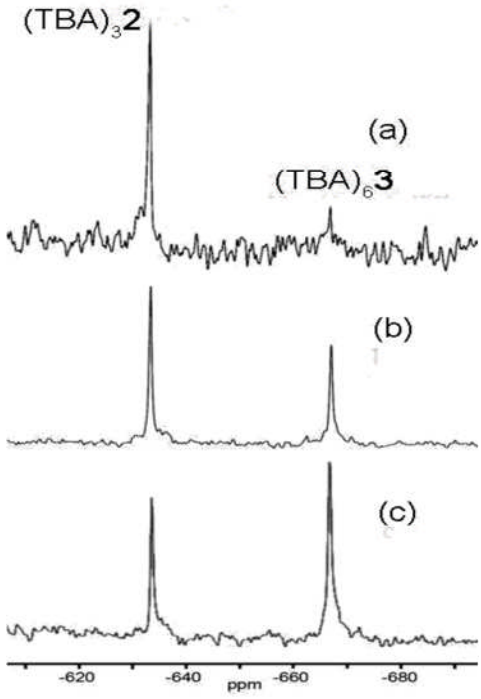

Fig 3.24: Equilibrium studies of $[(OH)SnW_5O_{18}]^{3-}$ a) after hydrolysis b) after heating 2 hrs at 85-90 ^oC c) after treated with 3A^o molecular sieves.

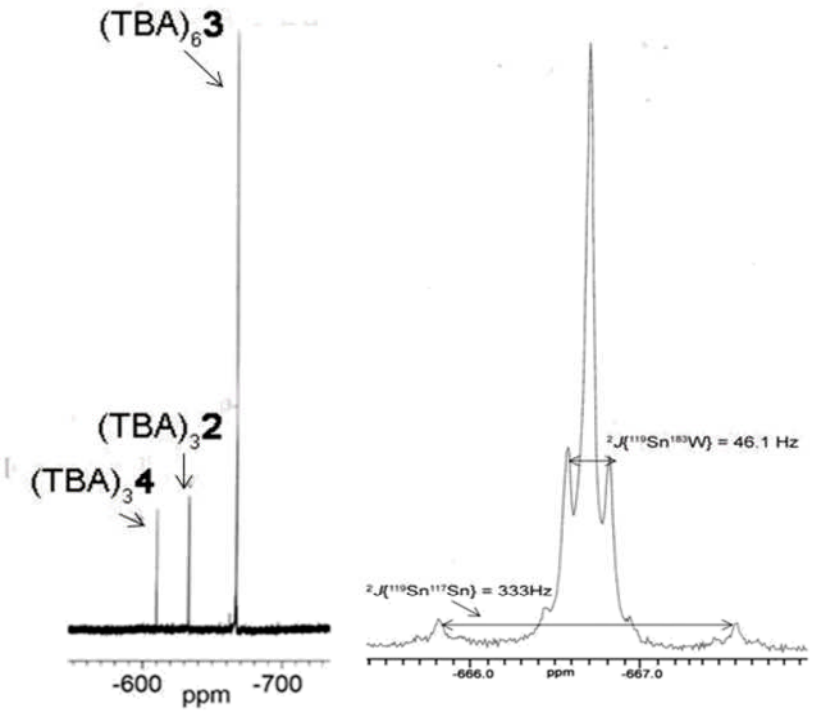

Fig 3.25: ^{119}Sn NMR spectrum of $[(OH)SnW_5O_{18}]^{3-}$ after azeotropic removal of H_2O with an expansion.

3.6.3 Infra red spectroscopy

The Infra red spectrum of the $(TBA)_6$ **3** showed a new band at 720 cm^{-1} in addition to W=O, SnOW and WOW stretching frequencies at 950, 792 and 753 cm^{-1}. The decrease in intensity of the hydroxyl stretching bands can be attributed to condensation of surface hydroxyl groups. Brown *et.al* [24] found that in dimethyltin chloride derivatives, the bands appeared at 570-650 cm^{-1} for Sn-O-Sn asymmetric stretching frequency and Pischtschan *et.al* [25] reported that Sn-O-Sn asymmetric vibrations and symmetric vibrations of $(CH_3)_6Sn_2O$ appear at 740 and 415 cm^{-1}. Recently, Wojciechowski *et.al* [26] found that the Sn-O-Sn asymmetric stretching frequency appeared at 770 cm^{-1} in fluoro and hydroxyfluoro derivatives of tin. Based on the previous literature reports, we have assigned our new band at 720 cm^{-1} to the Sn-O-Sn asymmetric stretching frequency. This value can be compared to earlier reported compounds Ti-O-Ti stretching frequency at 662 cm^{-1} and Nb-O-Nb stretching frequency at 672 cm^{-1}

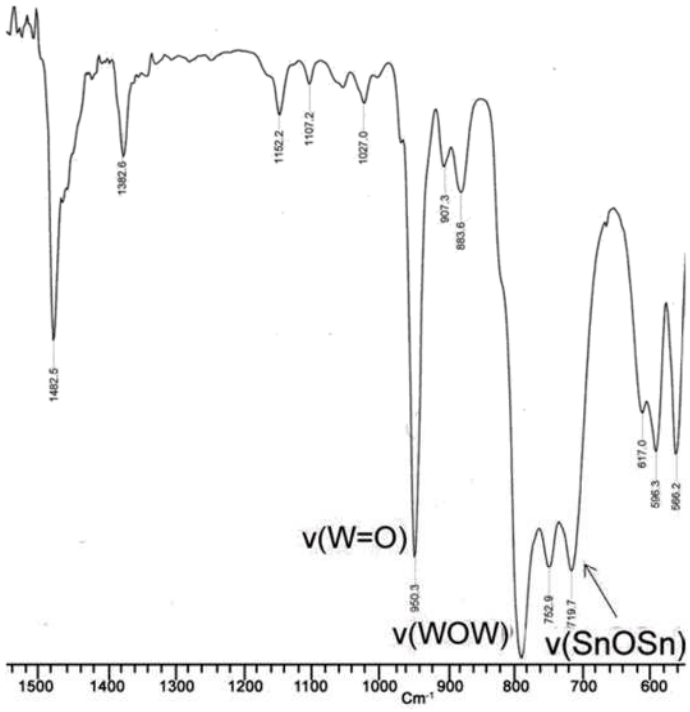

Fig 3.26: Infra red spectrum of $(TBA)_6$ $[(\mu\text{-}O)(SnW_5O_{18})_2]$

3.7. Attempted 'direct' synthesis of $(TBA)_3[(OH)SnW_5O_{18}]$

During direct hydrolysis a new species was found which falls in the region at δ -610 ppm in the ^{119}Sn NMR. This compound has been separated as a single compound although the structure was completely disordered and it was very similar to $[(OH)SnW_5O_{18}]^{3-}$We have completely characterised it by multinuclear NMR and FTIR spectroscopy, electrospray ionisation mass spectrometry and elemental microanalysis. All the characterisation studies revealed that it must be one of the SnW_5 family of structures and some –X functional group should have attached to tin (Sn) hetero metallic site. During the course of the study we have found this new species to be a $(TBA)_3$ $[ClSnW_5O_{18}]$, $(TBA)_3$ **4**. The chloro stannotungstates are formed as major products with reasonable yield when attempting to synthesise $(TBA)_3$ **2** according to the following equation.

$$\mathbf{2Sn(O^tBu)_4 + 3Q_2WO_4 + 7WO(OMe)_4 + 19H_2O \longrightarrow}$$

$$\mathbf{2[(OH)SnW_5O_{18}]^{3-} + 28MeOH + 8Bu^tOH} \quad \textbf{----9}$$

The tungstate precursors WO_4^{2-} and $WO(OMe)_4$ in acetonitrile are allowed to stir for 1 hr at room temperature to give a clear yellow solution. The clear solution was

transferred to $Sn(O^tBu)_4$ and heated to 85-90 ^oC for about 2 hrs. Following hydrolysis of alkoxide mixtures, the solution was allowed to heat overnight at the same temperature. Once reaction stopped, all solvents were removed in *vacuo.* The side product $[W_6O_{19}]^{2-}$ was removed by filtration the volume of the resultant solution reduced to 60% and dry diethyl ether was added. The colourless precipitate was examined by ^{119}Sn NMR spectroscopy. The $(TBA)_3$ **4** has least solubility and could be easily separated as a single compound by fractional crystallisation. Interestingly, the $(TBA)_3$ **4** is inert to moisture and it has been used for solution NMR studies. .

The ^1H NMR and ^{13}C NMR spectra showed only tetrabutyl ammonium peaks along with those for the solvent fully deutriated would not show peaks in the ^1H NMR spectrum.

3.7.1. ^{17}O NMR spectroscopy

The ^{17}O NMR spectrum of $(TBA)_3$ **4** shows six resonance peaks for the proposed compound which arises from the six non-equivalent types of oxygen atoms. These were observed at 725, 691(W=O), 398 (Sn-O-W), 386, 365 (W-O-W) and 14 (μ_6-O) ppm. The chemical shift values are compared with the initial precursor $(TBA)_3$ **1** and observed that the values are slightly deviated from the starting precursor

Errington and co-workers have successfully synthesised $[ClTiW_5O_{18}]^{3-}$ from the reaction between $(TBA)_6[W_5O_{18}]$ and $[TiCl_4.(MeCN)_2]$. The intermediate $[W_5O_{18}]^{6-}$ has never been isolated and characterised and it acts as a virtual lacunary precursor and forms $[LMW_5O_{18}]^{(6-n-)}$ species when treated with $\{ML\}^{n+}$. However, $(TBA)_3$ **4** was not able to be synthesised by this route because $[SnCl_4.(MeCN)_2]$ reacted with the virtual precursor and produced $[SnCl_6]^{2-}$ as a major product. The chemical shift values of $(TBA)_3$ **4** can be compared to $(TBA)_3$ **1** and peaks were clearly observed in the downfield region. This is due to the electronegative chloride ion removing the electron density from the polyoxometalate.

The ^{17}O NMR spectrum of $(TBA)_3[ClSnW_5O_{18}]$ is shown in the figure 3.27.

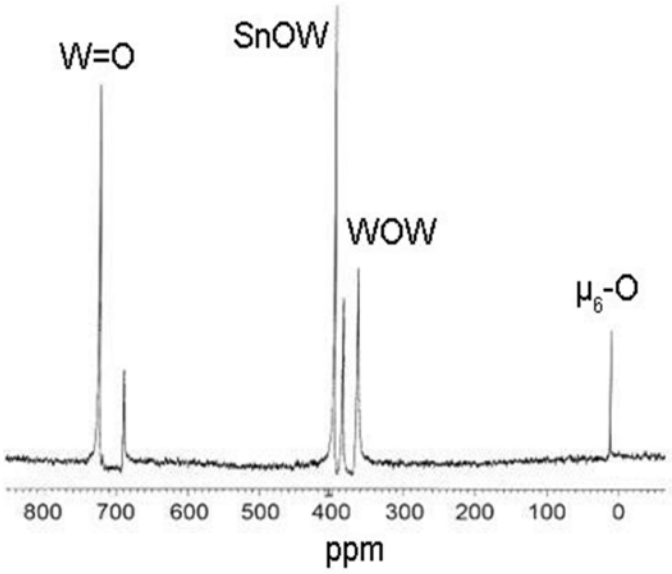

Fig 3.27: ^{17}O NMR spectrum of TBA_3 $[ClSnW_5O_{18}]$.

3.7.2. Single crystal X-ray diffraction

The $(TBA)_3$ **4** can be separated as a single compound and the crystal structure is isostructural with $[(OH)SnW_5O_{18}]^{3-}$. We initially assumed that the water molecule might be coordinated to the tin surface. The charge of anion should have been 2-, if the water molecule was coordinated on the tin surface but XRD revealed that three cations are present in the structure and all the supporting information suggests that it must be $(TBA)_3[ClSnW_5O_{18}]$

3.7.3. ^{119}Sn NMR spectroscopy

The ^{119}Sn NMR spectrum of $(TBA)_3$ **4** showed three resonances with $^2J_{Sn\text{-}W}$ satellite peaks are observed at -610 , -633 and -666 ppm and earlier we have confirmed that -633 and -666 ppm were due to $[(OH)SnW_5O_{18}]^{3-}$ and $[(\mu\text{-}O)(SnW_5O_{18})_2]^{6-}$, respectively. The chloride ion must have come from the tungstate precursors Q_2WO_4 and traces of TBACl impurity present in TBAOH in 1M MeOH solution. The $^2J_{Sn\text{-}W}$ coupling constant value is 47.5 Hz which is quite high compared to $(TBA)_3$ **1** and $(TBA)_3$ **2.** The ^{119}Sn NMR spectrum is shown in the figure 3.28.

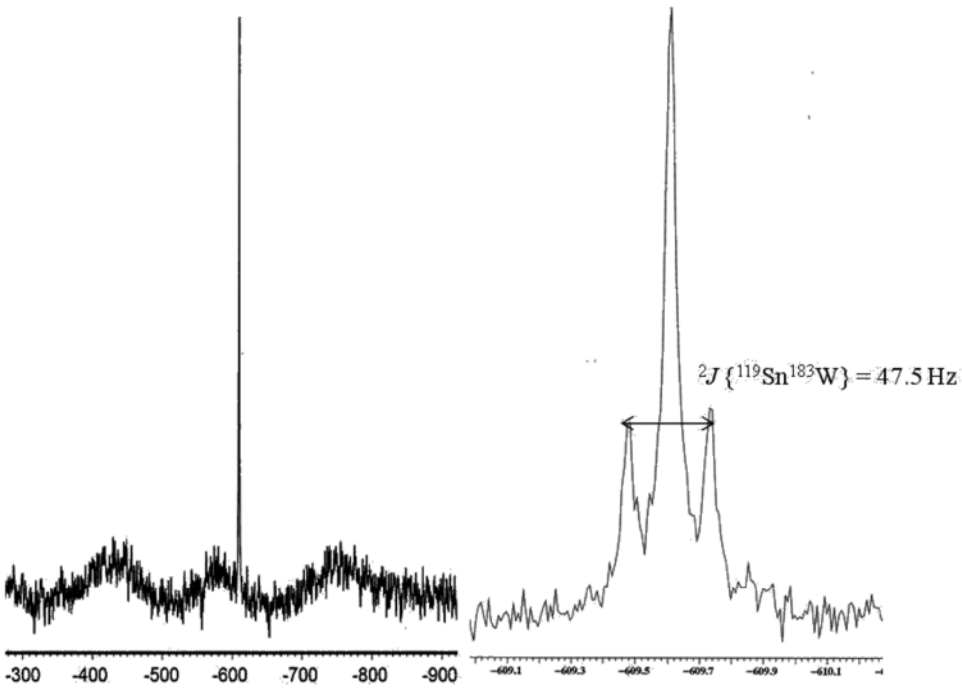

Fig 3.28: ^{119}Sn Spectrum of $(TBA)_3[ClSnW_5O_{18}]$ with an expansion of the resonance to show ^{183}W satellite peaks.

3.7.4. ^{183}W NMR spectroscopy

The ^{183}W NMR was similar to $(TBA)_3$ **1** and it showed two main peaks mainly at δ_W 75.62 and -119.79 ppm along with $^2J_{W\text{-}Sn}$ tin satellite peaks but because of the broadness of the major peaks we were not able to calculate the coupling constant. The ^{183}W NMR spectrum in the figure shows another single peak at 59 ppm due to $Q_2[W_6O_{19}]$. We have assigned the most intense peaks at 75.62 to equatorial and the minor peak at -119.79 to axial tungsten, respectively.

The ^{183}W NMR spectrum of $(TBA)_3$ **4** is shown in the Figure 3.29.

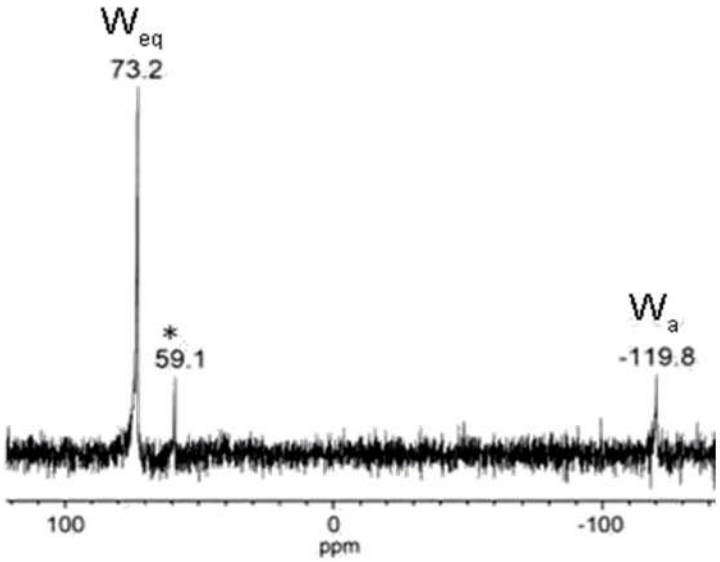

Fig: 3.29: ^{183}W NMR spectrum of $(TBA)_3[ClSnW_5O_{18}]$ [* = $(W_6O_{19})^{2-}$]

3.7.5. Infra red spectroscopy

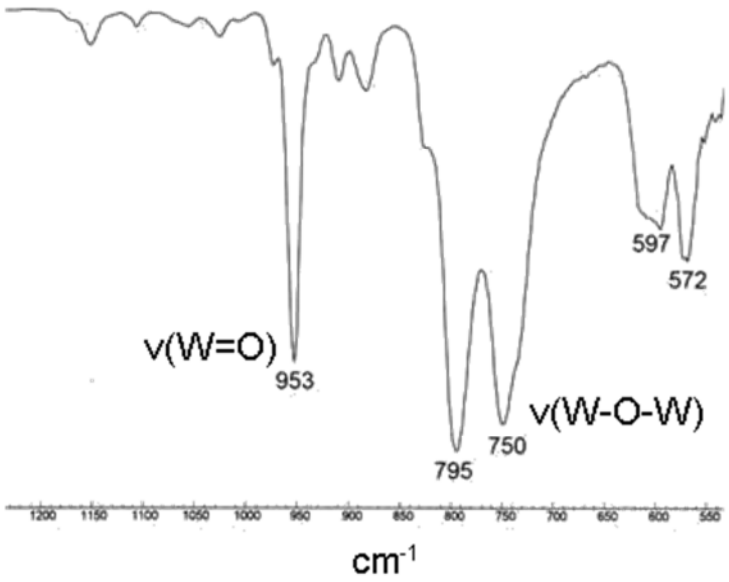

Fig 3.30: Infra red spectrum of $(TBA)_3[ClSnW_5O_{18}]$

The infra red spectrum of $(TBA)_3$ **4** shows three characteristic bands at 953, 795 and 750 cm^{-1}, which were assigned as the W=O, Sn-O-W and W-O-W stretching frequencies, respectively. Because of the highly electronegativity element present on the tin surface and higher charge of the anion, the band frequency values are slightly deviated.

CHN and chloride analysis supports the formulation of $(TBA)_3[ClSnW_5O_{18}]$

3.7.6. Electrospray Mass spectrometry

The negative-ion electrospray mass spectrum of $(TBA)_3[ClSnW_5O_{18}]$ was recorded and is shown in Figure 3.31.

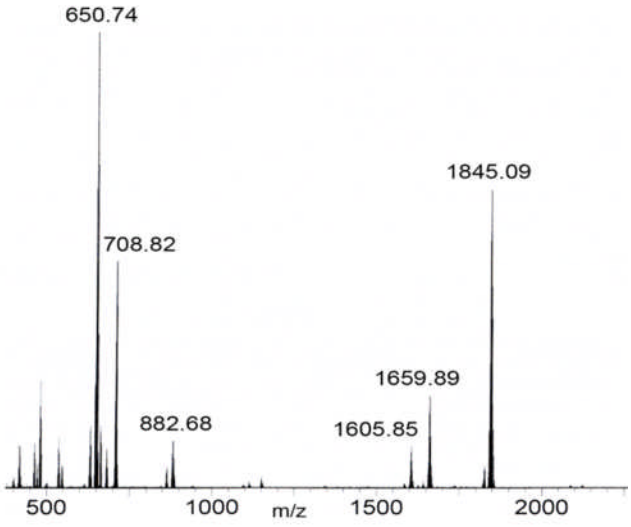

Fig 3.31: Negative ion electrospray mass spectrum of $(TBA)_3[ClSnW_5O_{18}]$

The most intense ion cluster peaks of these spectra were assigned to monomeric species containing the SnW_5O_{18} core although the $[SnW_5O_{18}]^{2-}$ fragment itself has not been observed.

The number of peaks corresponding to the SnW_5O_{18} core indicates this structure has a certain degree of stability in solution and under electrospray conditions. The most intense peak has been observed at 1845.09 m/z and corresponds to $\{(TBA)_2(Cl)SnW_5O_{18}\}^-$ which indicates that the chloride anion is strongly bound to the tin heterometal atom. We have not observed any cluster peaks due to $\{(TBA)_2(OH)SnW_5O_{18}\}^-$ in this mass spectrum which indicates that the chloride ion is not hydrolyzed and is not replaced by any other groups such as OH^-,CH_3CN under ESI MS conditions.

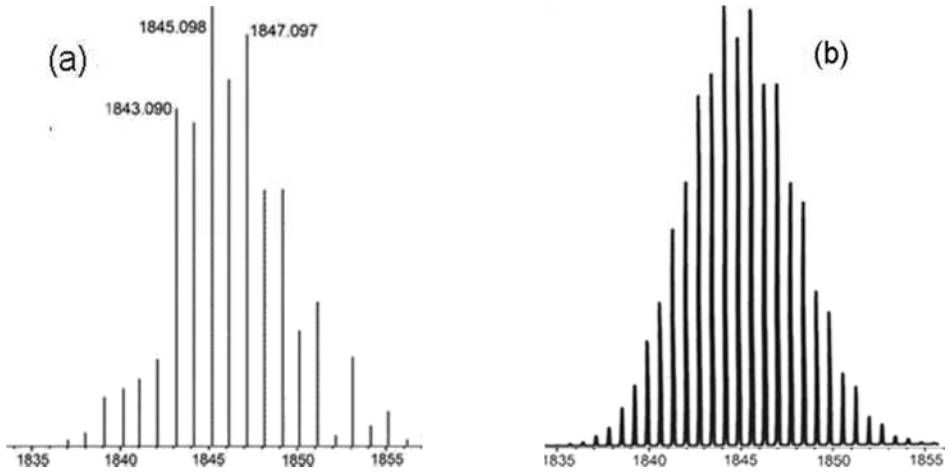

Fig 3.32: a) Peak pattern for the ion cluster assigned to $\{(TBA)_2(Cl)SnW_5O_{18}\}^-$ in the negative ion electrospray mass spectrum of $(^nBu_4N)_3[ClSnW_5O_{18}]$ b) simulated peak pattern for $\{(TBA)_2(Cl)SnW_5O_{18}\}^-$ anion.

3.7.7. Electrochemistry of $[ClSnW_5O_{18}]^{3-}$

The $(TBA)_3$ **4** species has been separated as a pure compound without any $[W_6O_{19}]^{2-}$ impurity. The tetra-n-butyl ammonium tetrafluoroborate (QBF_4) (50 cm^3, 0.005 M) in acetonitrile was freshly prepared and used as supporting electrolyte, The solution of $(TBA)_3$ **4** (25 cm^3, 0.005 M) in QBF_4/ CH_3CN was prepared.

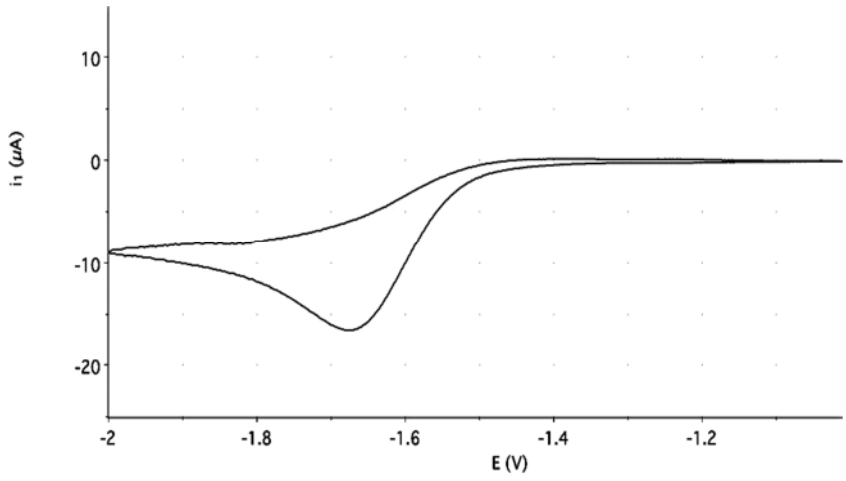

Fig 3.33: Cyclic Voltagram of $(TBA)_3[ClSnW_5O_{18}]$

An irreversible one electron reduction peak was observed at -1.674 V and at this potential the oxidation reaction does not occur. These studies gave useful information

to further explore the reactivity of $(TBA)_3$ **4** in order to develop metathesis reaction towards reduction and halide abstraction reaction. (See section 4.8 in Chapter 4).

3.8. Reaction of $[(MeO)SnW_5O_{18}]^{3-}$ with Concentrated HCl

The aim of producing $[(MeO)SnW_5O_{18}]^{3-}$ was to carry out further experiments to explore the reactivity of the heterometallic site and to introduce various functional groups, and thus to manipulate the anion functionality. The reactivity of $(TBA)_3$ **1** with various aliphatic and aromatic alcohols is discussed separately in Chapter 4.

Previously, four peaks were observed in the ^{119}Sn NMR spectrum when we attempted to synthesise $[(MeO)SnW_5O_{18}]^{3-}$, suggesting that methoxo stannotungstates are very moisture sensitive. It undergoes hydrolysis very rapidly and produces $[(HO)SnW_5O_{18}]^{3-}$. Concentrated hydrochloric acid was reacted with $[(MeO)SnW_5O_{18}]^{3-}$ with the aim of introducing the chloride anion on the tin surface, to generate $[ClSnW_5O_{18}]^{3-}$. When $(TBA)_3$ **1** was treated with an equimolar amount of 12M HCl, the ^{119}Sn NMR spectrum showed two peaks at -610 and 633 ppm and thus we can easily interconvert $(TBA)_3$ **1** to $[ClSnW_5O_{18}]^{3-}$ but also $[OHSnW_5O_{18}]^{3-}$

The same reactivity studies have also been carried out with $[(OH)SnW_5O_{18}]^{3-}$ and its dimer. The end result of this reaction was quite similar to the earlier one. To avoid polyoxometallic cage degradation at higher molar concentration, we used only 5M HCl. The ^{119}Sn NMR spectrum showed one single peak at -610 ppm. We have concluded that $[(MeO)SnW_5O_{18}]^{3-}$ and its derivatives can be easily interconverted to $[ClSnW_5O_{18}]^{3-}$ by treating with HCl.

3.8.1. Other reactions to produce $[ClSnW_5O_{18}]^{3-}$

The $[(HO)SnW_5O_{18}]^{3-}$ is very easy to handle and it remains a monomer in the solid state but is not stable in solution. The aim of this project is to synthesise the linear metal oxo or alkoxo arrays in solution.

$$\mathbf{2\ Q_3[(OH)SnW_5O_{18}] + SnCl_2 \longrightarrow 2\ Q_3[ClSnW_5O_{18}] + Sn(OH)_xCl_{(2-x)}}$$

$$\mathbf{2\ Q_3[(OH)SnW_5O_{18}] + Q_2[SnCl_6] \longrightarrow 2Q_3[ClSnW_5O_{18}] + Q_2[Sn(OH)_xCl_{(6x)}] \quad ----10}$$

We have explored the reactivity of $[(HO)SnW_5O_{18}]^{3-}$ with $SnCl_2$ and $Q_2[SnCl_6]$. The outcome of these reaction was very similar to earlier ones which suggests that the hydroxide group is more labile and it easily undergoes exchange reactions with $SnCl_2$ and $Q_2[SnCl_6]$. The ^{119}Sn NMR spectrum showed two peaks at -610, -21 $\{Sn(OH)_xCl_{(2-x)}\}$ ppm for the $SnCl_2$ reaction and -610, -733 $\{Sn(OH)_xCl_{(6-x)}\}$ ppm for $[SnCl_6]^{2-}$ reaction which confirms that both reactions are producing $[ClSnW_5O_{18}]^{3-}$ and tin halohydroxides. In summary, we can easily prepare chloro stannotungstates from $(TBA)_3$ **1** and its derivatives $(TBA)_3$ **2** by reacting with HCl or chloride resources such as $SnCl_2$ and $TBA_2[SnCl_6]$

3.9. Ligand exchange reactions of $[ClSnW_5O_{18}]^{3-}$

With NaOMe

$$\mathbf{(TBA)_3[ClSnW_5O_{18}] + NaOMe \longrightarrow (TBA)_3[(MeO)SnW_5O_{18}] + NaCl \quad -----11}$$

The aim of this reaction is to produce methoxide functionality on the tin polyoxometalate surface and thus we can easily convert the functional groups by using simple ligand exchange. The crude product from the reaction between $[ClSnW_5O_{18}]^{3-}$ and sodium methoxide shows one single peak at δ_{Sn} -647 ppm in the ^{119}Sn NMR spectrum which suggests that the chloride anion could be easily replaced by methoxide. The white solid separated from the reaction mixture was expected to be NaCl.

With Water

The expected product of reaction between $(TBA)_3[ClSnW_5O_{18}]$ and water is hydroxo stanno polyoxometallates but after being heated overnight $[ClSnW_5O_{18}]^{3-}$ with excess water, the expected product does not form.

Summary

A rational synthetic route has been established for the synthesis of Sn-substituted Lindqvist polyoxometalates. The novel stannotungstates can be prepared by a hydrolytic route from tungstate precursors and the corresponding metal alkoxides similarly to transition metal Lindqvist polyoxometalates as earlier reported. These novel polyoxometllates have been thoroughly studied and fully characterised by single

crystal X-Ray diffraction, CHN analysis and all multinuclear NMR methods. We found that $(TBA)_3$ **1** appears to be very reactive towards moisture and very easily produces hydroxide, which condenses to give a dimer species. The Sn-OMe bond is very reactive towards acids and it easily forms chloro and hydroxo stannotungstates when treated with diluted and concentrated HCl.

The hydrolytic studies of $(TBA)_3$ **1** have also been carried out and the hydrolytic products are characterised by single crystal X-Ray diffraction, CHN analysis and multi nuclear NMR methods. We have found that the hydrolytic product (Sn-OH) is inert to moisture in solid state and most importantly, it is not stable in solution. It undergoes self condensation in solution at room temperature, and then produces dimer species. Sn-OH and Sn-O-Sn bonds are reactive towards acids such as HCl, and readily produces chlorostannotungstates. We observed that, comparatively dimer species are more reactive than hydroxide species.

Finally we have resolved the nature of δ_{Sn} -610 ppm species which appeared in the ^{119}Sn NMR of attempted synthesis of $(TBA)_3$ **1** and $(TBA)_3$ **2** and confirmed that it is due to $(TBA)_3[ClSnW_5O_{18}]$. The Chloride anion possibly might come from TBA_2WO_4 and TBACl in TBAOH (1M MeOH). The Sn-Cl bond is not moisture sensitive and it is very stable at room temperature. $(TBA)_3[ClSnW_5O_{18}]$ can be easily removed by fractional recrystallisation and the ligand exchange reaction studies have also been done with strong base such as sodium methoxide.

Experimental section

Electrospray Mass Spectrometry

ESI mass spectra were recorded on a Waters LCT Premier LC-MS spectrometer in negative ion mode by direct insertion of samples using the following conditions: capillary voltage 5000V; sample cone voltage 35 V; desolvation temperature 20 ˚C; source temperature 90 ˚C. All samples were dissolved in dry acetonitrile and transferred to a sealed septum vial under nitrogen before direct insertion into the spectrometer.

Synthesis of $(TBA)_3[(MeO)SnW_5O_{18}]$

A mixture of TBA_2WO_4 (2.9 g, 3.96 mmol) and $WO(OMe)_4$ (3 g, 9.26 mmol) was dissolved in acetonitrile (20 cm^3) at room temperature and allowed to stir for 1 hr. The golden yellow colour solution was transferred into $Sn(O^tBu)_4$ (1.085 g, 2.64 mmol). The resultant solution was stirred for 2 hrs at 85-90 ^oC before addition of water H_2O (10 % ^{17}O enriched H_2O) (406 μL, 22.44 mmol). After being heated overnight, excess dry methanol (15 cm^3) was added and the solution was stirred for 1 hr at 85- 90 ^oC. At room temperature, all volatile impurities were removed in *vacuo* and redissolved in acetronitrile. A small amount of crystalline $Q_2[W_6O_{19}]$ was removed by filtration before addition of ether layer. The volume of mother liquor was reduced about 30% and dry ether was added. The crude TBA_3 $[(MeO)SnW_5O_{18}]$ product was allowed to settle and carefully the product was removed by filtration. The crude product was heated again with excess dry methanol (20 cm^3) overnight at 85-90 ^oC in the presence of activated 3A molecular sieves. After cooling to room temperature, the pure methanol solution of TBA_3 $[(MeO)SnW_5O_{18}]$ was filtered off and all volatile impurities were removed in v*acuo*. The product was redissolved in saturated acetonitrile again and colourless crystals were formed upon cooling at -30 ^oC. The crystals were washed with ether, dried in *vacuo* and it was used for characterisation.

Yield: 1.996 g, 36.3 %

Data: ^1H NMR (300 MHz, CD_3CN) : δ 3.64 (s, 3H, OC**H**$_3$) $^3J\{^{119}Sn^1H\}$ = 78 Hz, $^3J\{^{117}Sn^1H\}$ = 72 Hz, $^3J\{^{115}Sn^1H\}$ = 66 Hz. ^{13}C NMR (100.53 MHz, CD_3CN): δ 53 (s, O**C**H_3), $^2J\{^{119}Sn^{13}C\}$ = 34.5 Hz. ^{17}O NMR (67.81 MHz, CD_3CN): δ 720, 684 (W=O),

395 (Sn-O-W), 383, 363 (W-O-W) 17 (μ_6-O). ^{119}Sn {^{1}H} NMR (186.85MHz, CD_3CN): δ -647 (s, **Sn**-OMe) $^{2}J\{^{119}Sn^{183W}\}$ = 39 Hz. ^{183}W NMR (20.84 MHz, CH_3CN): δ 76.9 (W_{eq}), -128.1 (W_{ax}) $^{2}J\{^{119}Sn^{183W}\}$ = 39 Hz. FTIR: 2960 m, 2932 m, 2874 m, 1483 s, 1381 m, 1151 m, 1045 m, 951 s,889 m, 790 s, 749 s, 617 w, 562 w, 545 s. Found: C, 27.85; H, 5.39; N, 2.01. $C_{49}H_{111}O_{19}N_3SnW_5$ requires C, 28.2; H, 5.37; N, 2.02 %.

Synthesis of $(TBA)_3$ $[(HO)SnW_5O_{18}]$

The pure $(TBA)_3$ $[(MeO)SnW_5O_{18}]$ (0.938 g, 0.45 mmol) in acetonitrile (10 cm^3) was treated with H_2O (407μL, 3×22.5 mmol) and heated to 85-90 ^{o}C for 30 min. Volatiles were removed, the residue was dissolved in acetonitrile (10 cm^3) and the treatment with water was repeated twice more and heated with a small amount of enriched water at 85-90 ^{o}C for overnight. After cooling to room temperature, volatile impurities were removed in *vacuo* and solid was washed with diethyl ether (20 cm^3) dried in *vacuo*, and then dissolved acetonitrile (2 cm^3) and ether layer 10 (cm^3) was added. The yellow crystals were formed upon slow vapour diffusion. The crystals were washed with ether (3 × 20 cm^3) dried in *vacuo* and it was used for characterisation.

Yield: 0. 893 g, 95.8 %

Data: ^{17}O NMR (67.81 MHz, CD_3CN): δ 719, 683 (W=O), 395 (Sn-O-W), 382, 367 (W-O-W) and) 17 (μ_6-O), -7 (H_2O). ^{119}Sn NMR (186.5 MHz, CD_3CN): δ -633 (s, **Sn**-OH) $^{2}J\{^{119}Sn^{183}W\}$ = 37.4 Hz. ^{183}W NMR (20.84 MHz, CH_3CN): δ 72.2 (W_{eq}), -121.2 (W_{ax}) $^{2}J\{^{119}Sn^{183}W\}$ = 36.7 Hz. FTIR: 3648 s, 2960 m, 2932 m, 2874 m, 1667 vw, 1483 s, 1381 m, 1251 w, 1152 m, 1107 w, 951 s, 906 w, 885 m, 784 s, 748 s, 594 m, 565 m. Found: C, 27.34; H, 5.49; N, 1.99. $C_{48}H_{109}O_{19}N_3SnW_5$ requires C,27.85; H, 5.31; N, 2.03 %.

Attempted Synthesis of $(TBA)_6$[μ-O $(SnW_5O_{18})_2$]

The pure $(TBA)_3$ $[(HO)SnW_5O_{18}]$ in acetonitrile (20 cm^3) heated under reflux for 4 – 5 hrs at 90-100 ^{o}C and distilled very slowly over 4-5 hrs. The crude product was used for characterisation. The attempted synthesis of dimer was not successful due to high solubility, moisture sensitivity and established equilibrium with $(TBA)_3$ $[(HO)SnW_5O_{18}]$.

Data: ^{119}Sn NMR (186.5 MHz, CD_3CN): δ -667 ppm (s), $^2J\{^{119}Sn^{183}W\}$ = 46.1 Hz, $^2J\{^{119}Sn^{117}Sn\}$ = 332.5 Hz. ^{183}W NMR (20.84 MHz, CH_3CN): δ 70.15 (W_{eq}), -131 (W_{ax}), $^2J\{^{119}Sn^{183}W\}$ = 46.1 Hz.

Synthesis of $(TBA)_3[ClSnW_5O_{18}]$

We believe that chloride anion easily comes from TBA_2WO_4 and TBA OH in 1M MeOH. When we attempt to synthesise the TBA_3 $[(HO)SnW_5O_{18}]$ directly, the chloride product was appeared as a major product.

A mixture of TBA_2WO_4 (2.9 g, 3.96 mmol) and $WO(OMe)_4$ (3 g, 9.26 mmol) were dissolved in acetonitrile (20 cm^3) at room temperature and allowed to stir for 1 hr. The golden yellow colour solution was transferred into $Sn(O^tBu)_4$ (1.085g, 2.64 mmol). The resultant solution was stirred for 2 hrs at 85-90 ^oC before addition of water H_2O (10 % ^{17}O enriched H_2O) (453 μL, 25.08 mmol). After being heated overnight, the reaction was stopped. All the volatile impurities were removed in vacuo and again heated with excess water (453 μL) for about 30 min at 85- 90 ^oC. After cooling to room temperature, all volatile impurities were removed in *vacuo* and redissolved in acetronitrile. Significant amount of crystalline $TBA_2[W_6O_{19}]$ was removed by filtration before addition of an ether layer. The volume of mother liquor was reduced about 30% and dry ether was added. The crude product contains $(TBA)_3[(Cl)SnW_5O_{18}]$, $(TBA)_3[(HO)SnW_5O_{18}]$ and $(TBA)_6[(\mu\text{-}O)(SnW_5O_{18})_2]$ and was allowed to settle and carefully it was removed by filtration. The crude product was re-dissolved in saturated acetonitrile again and recrystallising many times. Colourless crystals were formed upon cooling at -30 ^oC. The crystals were washed with ether, dried in *vacuo* and it was used for characterisation.

Yield: 45%

Data: ^{17}O NMR (67.81 MHz, CD_3CN): δ 725, 691 (W=O), 398 (Sn-O-W) 386, 365 (W-O-W), 13.4 (μ_6-O). ^{119}Sn {1H} NMR (186.5 MHz, CD_3CN): δ -609 ppm. $^2J\{^{119}Sn^{183}W\}$ = 47.5 Hz. ^{183}W NMR (20.84 MHz, CH_3CN): 73.2 (W_{eq}), -119.8 (W_{ax}). FTIR (Nujol mull): 2960 m, 2873 m, 1482 s, 1381 w, 1152 s, 953 s, 795 s, 750 s, 597 s, 572 m. Found: C, 27.75; H, 5.58; N,2.2; Cl, 1.69. $C_{48}H_{108}O_{18}N_3SnW_5Cl$ requires C, 27.60; H, 5.21; N, 2.01; Cl, 1.72%.

References

1) M. Filowitz, R. Ho, W. G. Klemperer, and W. Shum, W. *Inorg. Chem*, **1979**, 18, **1**.

2) W. Clegg, M. R. J. Elsegood, R. J. Errington, J. Havelock, *J. Chem. Soc. Dalton Trans*, **1996**, 5, 681-690.

3) R. J. Errington, S. S. Petkar, B. R. Horrocks, A. Houlton, L. H. Lie and S. N. Patole, *Angew. Chem., Int. Ed*, **2005**, 44, 1254.

4) R. J. Errington, S. S. Petkar, P. S. Middleton, W. McFarlane, W. Clegg, R. A. Coxall, and R. W. Harrington, *J.Am.Chem.Soc*, **2007**, 129, 12181-12196.

5) R. J. Errington, L. Coyle, P. S. Middleton, C. J. Murphy, W.Clegg and R. W. Harrington., *J.Clust Sci*, **2010**, *21*, 503–514; L. Coyle, P. S. Middleton, C. J. Murphy, W. Clegg, R. W. Harrington and R. J. Errington, *Dalton Trans*., **2011**, DOI:10.1039/C1DT11256B.

6) R. J. Errington *et.al*., Unpublished results

7) R. J. Errington, G. Harle, W. Clegg, R. W. Harrington, *Eur. J. Inorg. Chem.* **2009**, 5240.

8) B. Krebs, R. Klein, in: M. T. Pope, A. Muller (Eds.), Polyoxometalates From Platonic Solids to Anti-retroviral Activity, Kluwer Academic Publishers, Dordrecht, The Netherlands, **1994**, p. 41.

9) N. Belai, M. T. Pope, *Polyhedron*, **2006**, 25, 2015–2020.

10) P. J. Domaille, *J.Am.Chem.Soc*, **1984**, 106, 7677-7687

11) F. Xin, M. T. Pope, *Organometallics*, **1994**, 13, 4881-4886.

12) F. Hussian, U. Kortz, R. J. Clark, *Inorg. Chem*, **2004**, 10, 3237-3241.

13) D. P. Arnold, E. A. Morrison, *Polyhedron*, **1990**, 9, 1331-1336.

14) D. P. Arnold, J. Blok, *Coordination chemistry reviews*, **2004**, 248, 299-319.

15) M. J. H. Smith, T. Wark, A. Rheingold, J. C. Huffman, *Can. J. Chem*, **1991**, 69, 121-129.

16) M. J. H. Smith, E. Smith and E. N. Duesler, *Inorg.Chem*, **1982**, 28**,** 3399.

17) C. W. Early *Hexametalates as catalysts for photochemical oxidation reactions*, PhD thesis, Illinois State University, **1982**.

18) R. J. Errington, *Advanced practical inorganic and metalorganic chemistry*: Blackie Academic and Professional, London, **1997**.

19) M. Boyer, B. LeMeur, *C. R. Acad. Sci.*, **1975**, C281, 59.

20) J. Zhang, A. M. Bond, D. R. MacFarlane, S. A. Forsyth, M. J. Pringle, A. W. A. Mariotti, A. F. Glowinski, A. G. Wedd, *Inorg. Chem*, **2005**, 44, 5123.

21) S. Himeno, M. Yoshihara, M. Maekawa, *Inorg. Chim. Acta*, **2000**, 298, 165.

22) E. W. Thornton and P. G. Harrison, *J.Chem. Soc.,Faraday Trans.1*, **1975**, 71, 461-472.

23) C. D. Chandeler, J. Caruso and M. J. H. Smith, *Polyhedron*, **1995**, 14, 2491-2497.

24) M. P. Brown, R. Okawara and E. G. Rochow., *Spectrochim.Acta*, **1960**, 16, 595.

25) H. Kriegsmann and S. Pischtschan., *Z.Anorg.Allgem.Chem*, **1962**, 315, 283

26) B. J. Trzeblatowska. J. Hanuza and W. Wojciechowski, *Spectrochim.Acta*, **1967**, 23, 2631-2636.

Chapter 4

Reactivity of $[XSnW_5O_{18}]^{3-}$ (X=MeO, OH, Cl) Polyoxometalates

Chapter 4: Reactivity of $[XSnW_5O_{18}]^{3-}$ (X=MeO, OH, Cl) Polyoxometalates

4.1 Introduction

In order to develop rational synthetic routes to new polyoxotungstates (POMs), a strategy has been adopted in which soluble oxoalkoxoanions formed in the reactions between mononuclear tungstate WO_4^{2-} and metal alkoxides $[M(OMe)_4]$ (where, M = Ti, Zr, Sn) were hydrolysed in organic solvents. Most previously structurally characterised tin-substituted polytungstates have been derived from Keggin or Dawson structural units[1-9], although Lindqvist-type $[XSnW_5O_{18}]^{3-}$ structures are known where X= Ph[10], Me.[11] However, in both of these anions, the Sn-C bonds are inert in nature whereas our goal was to synthesise Lindqvist POM containing reactive Sn-X groups. Having successfully synthesised $(TBA)_3$ **1**, we then studied the chemical reactivity of the Sn-OMe group towards various protic reagents (H_nX).

Errington and his co-workers have systematically studied the reactivity of transition metal alkoxido (RO-) substituted group 4 heterometallic Lindqvist polyoxometalates $(TBA)_3[(RO)TiW_5O_{18}]$[12], $(TBA)_6[\{(MeO)ZrW_5O_{18}\}_2]$[13] in non-aqueous media. These studies gave valid information with regards to understand the reactivity of surface M-X (M=Ti, Zr) functionality in POMs. They have particularly studied hydrolysis and exchange reactions of $[(RO)MW_5O_{18}]^{3-}$ (M=Ti, Zr) with various mondohydric, dihydric phenols and monitored the decomposition of some of the derivatives by ^1H and other multinuclear NMR methods. The alkoxide exchange rate with external methanol has been measured by 2D EXSY NMR spectroscopy for $[(MeO)MW_5O_{18}]^{3-}$ (where M = Ti, Zr) and showed slower exchange reactions than expected.

The reactivity of the Ti-OR bond in $[(RO)MW_5O_{18}]^{3-}$ enables rational manipulation of functionality in titanotungstates and this reactivity also allowed them to attach TiW_5 hexametalates on organic functionalised silicon surfaces which is the first demonstration of the covalent surface immobilisation of polyoxometalates.[14] The systematic synthetic route of $(TBA)_3$ **1** has been already discussed in Chapter 3. This chapter is particularly concerned with the reactivity of Sn-X bonds in tin POMs with various protic reagents HX. (X= RO, ArO)

4.1.1. General information of Sn-polyoxotungstates

The six-coordinate tin heterometal centre in $(TBA)_3$ **1** occupies the pocket of the pentadentate $[W_5O_{18}]^{6-}$ lacunary polyoxometalate 'ligand', and to gain a better understanding of the reactivity of tin in this environment, we have investigated reactions of the Sn–OMe bond with a variety of protic molecules H_nX to give anions $[XSnW_5O_{18}]^{3-}$, including a series of alkoxide and aryloxide derivatives $[(RO)SnW_5O_{18}]^{3-}$, $[(ArO)SnW_5O_{18}]^{3-}$ and $[(^iPrNH_2)_2(\mu\text{-}O)(SnW_5O_{18})_2]^{4-}$.

We have explored reactivity of Sn-X (X=OMe, OH, Cl) bond in Lindqvist POMs with various protic reagents H_nX (X=RO, ArO), hexamethyldisilazane (HMDS) $HN\{(SiMe_3)_2\}$ and diisopropylamine (DIPA) $\{HN[CH(CH_3)_2]_2\}$. It has been observed that Sn^{4+} tends to favour a coordination number of 6 and this is to be expected in all the derivatives of $[(MeO)SnW_5O_{18}]^{3-}$. The counter ion in all derivatives is tetra-n-butylammonium, TBA, $[Bu^n{}_4N]^+$, which ensures organic solubility. $(TBA)_3$ **1** was used as an initial precursor in the synthesis of novel SnW_5 polyoxotungstate family complexes, e.g., $[(L)SnW_5O_{18}]^{3-}$ {L = RO (R=EtO, ^{i}PrO, ^{t}BuO), ArO}. We have carried out all the exchange reactions in acetonitrile with slightly more than an equimolar amount of H_nX.

All of the alkoxido and aryloxido derivatives of $(TBA)_3$ **1** have been thoroughly studied and characterised by single crystal X-Ray diffraction, elemental microanalysis, infra red (Nujol mull), ^{1}H and other multinuclear (^{13}C, ^{119}Sn, ^{17}O, ^{183}W) NMR spectroscopy methods. The hexatungstate $[W_6O_{19}]^{2-}$ and $[ClSnW_5O_{18}]^{3-}$ were invariably formed and present during hydrolysis and synthesis of $(TBA)_3$ **1**. The possible chloride source may be tetra butyl ammonium tungstate $(TBA)_2WO_4$ or tetra butyl ammonium hydroxide (TBAOH) solution. The nature of the $[ClSnW_5O_{18}]^{3-}$ species has been discussed already in Chapter 3. During the course of our study, we have observed that the Sn-Cl bond in chloro stannotungstate is inert to moist air. Based on this, we were that Sn-Cl bond might be more covalent and expected that chloride group is very labile but later we found that it was not. (See section 4.8) Peaks due to impurites are marked with an *asterisk* (*) in the NMR spectra wherever they were found to be present.

We have expected to observe satellite peaks due to coupling to ^{119}Sn, ^{117}Sn in ^{1}H, ^{13}C and ^{183}W NMR spectra for all alkoxido and aryl oxido derivatives. Because of the different concentration, yield and purity of the various samples, we were not able to determine the coupling constants for all the derivatives in multinuclear NMR. However, we discuss here the coupling constants where they were observed. We measured ^{13}C NMR spectra for all the derivatives and were not able to observe the $^{2}J\{^{119}Sn^{13}C\}$, $^{3}J\{^{119}Sn^{13}C\}$ satellite coupling peaks in ^{13}C NMR for all the derivatives, although highly concentrated samples were allowed to run for a long time in the spectrometer to observe satellite coupling peaks. We report some of the $^{2}J\{^{119}Sn^{13}C\}$ coupling constant values here and the values also compared with earlier reported compounds. Similarly, we were not able to see the tin satellite coupling peaks in ^{183}W NMR for all the derivatives but we measured all $^{2}J\{^{119}Sn^{183}W_{eq}\}$ coupling peaks in ^{119}Sn NMR. The $^{2}J\{^{119}Sn^{183}W_{eq}\}$ coupling constants values are carefully measured and the values are depicted in the Table 4.6.

Because of the formation of possible side products $(TBA)_2$ $[W_6O_{19}]$ and $(TBA)_3$ $[Cl\text{-}SnW_5O_{18}]$ in the preparation of $(TBA)_3$ **1**, observed CHN values are slightly deviated from the expected values. Reaction with bulky alcohols and aromatic monohydric phenols gave non-disordered structures. However, in the dihydric phenolic derivatives, excess phenols made hydrogen bonding between two adjacent polyoxometalate cages. In the TBA salt of $[(RO)SnW_5O_{18}]^{3-}$ (R=Me), the methoxido oxygen is covalently bonded to tin metal.

4.2 Results and discussion

4.2.1 Reaction between $[TBA]_3[(MeO)SnW_5O_{18}]$ and ROH (R = Et, ^{i}Pr, ^{t}Bu)

The alkyloxido derivatives of $(TBA)_3$ **1** have been prepared by a simple alcoholysis route. The reactions were carried out between $(TBA)_3$ **1** with a 100 fold excess of respective alcohols in acetonitrile for between 24 and 96 hrs at 85-90 ^{o}C. All the volatile impurities were removed in *vacuo*, and the same procedure was repeated twice further to ensure complete conversion. Once the reaction stopped, the resultant solution was allowed to cool to room temperature, washed with dry ether (2x 20 ml) and the solid was recrystallised from the mother liquor. Colourless crystals were obtained in good yield and were used for NMR characterisation and X-ray crystal structure determination.

$$(^{n}Bu_4N)_3[(CH_3O)SnW_5O_{18}] + ROH \longrightarrow (^{n}Bu_4N)_3[(RO)SnW_5O_{18}] + CH_3OH \qquad \text{----1}$$

R= CH_3CH_2 2
$(CH_3)_2CH$ 3
$(CH_3)_3C$ 4

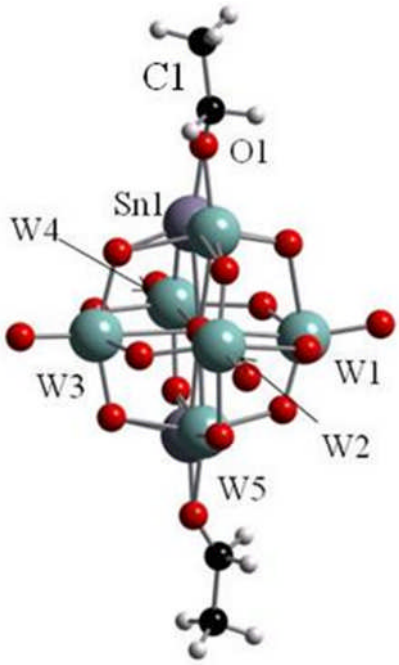

Fig.4.1: Structure of the anion $[(EtO)SnW_5O_{18}]^{3-}$. The colour codes are as follows: W (pale green), O (red), Sn (pale grey), C(black).

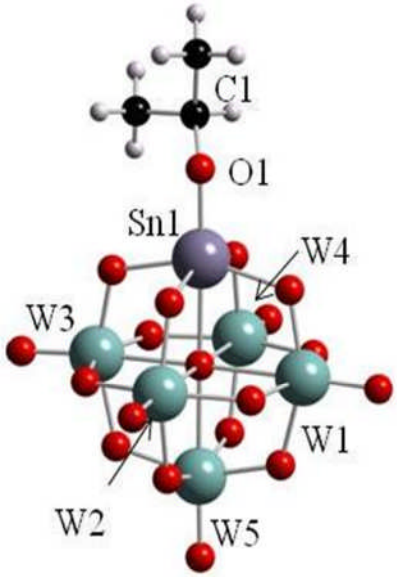

Fig.4. 2: Structure of the anion $[(Pr^{i}O)SnW_5O_{18}]^{3-}$ .The colour codes are as follows: W (pale green), O (red), Sn (pale grey), C(black).

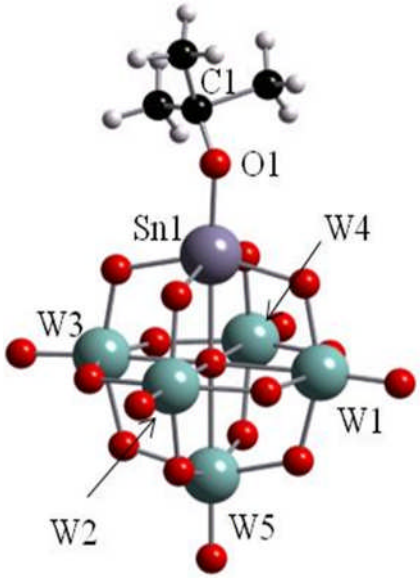

Fig.4. 3: Structure of the anion $[(Bu^{t}O)SnW_5O_{18}]^{3-}$. The colour codes are as follows: W (pale green), O (red), Sn (pale grey), C(black).

Selected bond lengths and bond angles	Compound **2**	Compound **3**	Compound **4**
Sn(1)-O(1)	1.775	1.960	1.976
Sn(1)-C(1)	2.790	2.961	3.025
O(1)-C(1)	1.112	1.349	1.232
Sn(1)-O(c)	2.338	2.255	2.278
Sn(1)-O(1)-C(1)	149.486	126.022	139.925
Sn(1)-O(c)-W(5)	175.425	180.000	180.000
Sn(1)-O(b)-W(1)	114.938	112.730	112.887
Sn(1)-O(b)-W(3)	121.395	113.225	113.002

Table 4.1 : Selected bond lengths (Å) and bond angles (^{o}) of **2**, **3**, **4**

4.2.2 ^{1}H NMR studies of Alkyloxido derivatives

^{1}H NMR Spectra of all alkyloxido derivatives of $(TBA)_3$ **1**, i.e **2**, **3**, **4** showed tin (Sn) satellite coupling peaks. Various concentrations of the NMR sample and the length of accumulation affected the satellite peak intensities, however, we have discussed here some of the satellite peaks coupling constants which we identified in ^{1}H and other multinuclear NMR.

The ^{1}H NMR spectrum of **2** showed a quartet and triplet for ethyl group at δ 3.86 and 1.79 ppm respectively, with tin coupling. We observed only ^{119}Sn satellite coupling for methyl ($-CH_3$) protons which is the highest natural abundance (8.5 %) tin nucleus in earth. $-CH_2$ protons exhibit coupling to ^{119}Sn and ^{117}Sn nuclei. This is possibly due to the proximity of the methylene protons to the tin active center and obviously $^{3}J\{^{1}H^{119}Sn\}$ coupling constant value was larger than $^{4}J\{^{1}H^{119}Sn\}$ coupling. The $^{3}J\{^{1}H^{119}Sn\}$, $^{3}J\{^{1}H^{117}Sn\}$ coupling constant values are 69.6 Hz and 66.6 Hz, respectively. These values can be compared to the structurally related starting precursor i.e $[(MeO)SnW_5O_{18}]^{3-}$ which showed $^{3}J\{^{119}Sn^{1}H\}$ =78 Hz, $^{3}J\{^{117}Sn^{1}H\}$ =72 Hz in the ^{1}H NMR. Hampden smith *et.al* [15] reported that $^{3}J\{^{119}Sn^{1}H\}$ = 36.8 Hz, $^{3}J\{^{117}Sn^{1}H\}$ = 35.6 Hz in $TI[Sn(OEt)_6]_n$ and the value we observed in derivative **2** is largely deviated from the six coordinated tin hexaethoxide anion. Derivative **2** showed

$^4J\{^1H^{119}Sn\}$ = 4.2 Hz but no $^4J\{^1H^{119}Sn\}$ coupling peak was observed in $TI[Sn(OEt)_6]_n$.

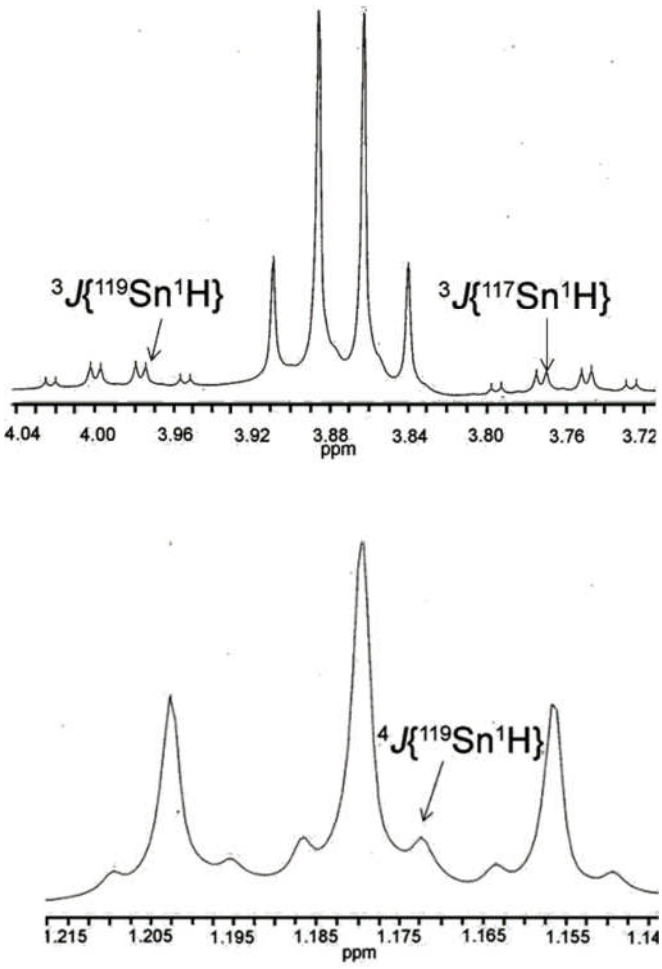

Fig.4.4: Expansion of methylene and methyl proton resonances with tin satellite coupling in the ^1H NMR spectrum of $(TBA)_3$ $[(EtO)SnW_5O_{18}]$

Derivative **3** exhibited a septet and doublet for the isopropyl group at δ 4.23 and 1.16 ppm, respectively along with coupling to ^{119}Sn and the coupling pattern was very similar to **2** which we discussed previously. $^4J\{^1H^{119}Sn\}$ satellite coupling was observed for methyl protons and no $^4J\{^1H^{117}Sn\}$ coupling was identified. In addition, we identified the CH protons to exhibit $^3J\{^1H^{119}Sn\}$ and $^3J\{^1H^{117}Sn\}$ coupling. The $^3J\{^1H^{119}Sn\}$ and $^3J\{^1H^{117}Sn\}$ coupling constant values are 57.3 Hz and 54.9 Hz for the methine proton. This can be compared to the starting material $(TBA)_3$ **1,** $^3J\{^1H^{119}Sn\}$ = 78 Hz, $^3J\{^1H^{117}Sn\}$ = 72 Hz. The four bond tin-proton coupling constant value $^4J\{^{119}Sn^1H\}$ = 3.3 Hz which it was slightly smaller than $^4J\{^{119}Sn^1H\}$ = 4.2 Hz for **2**.

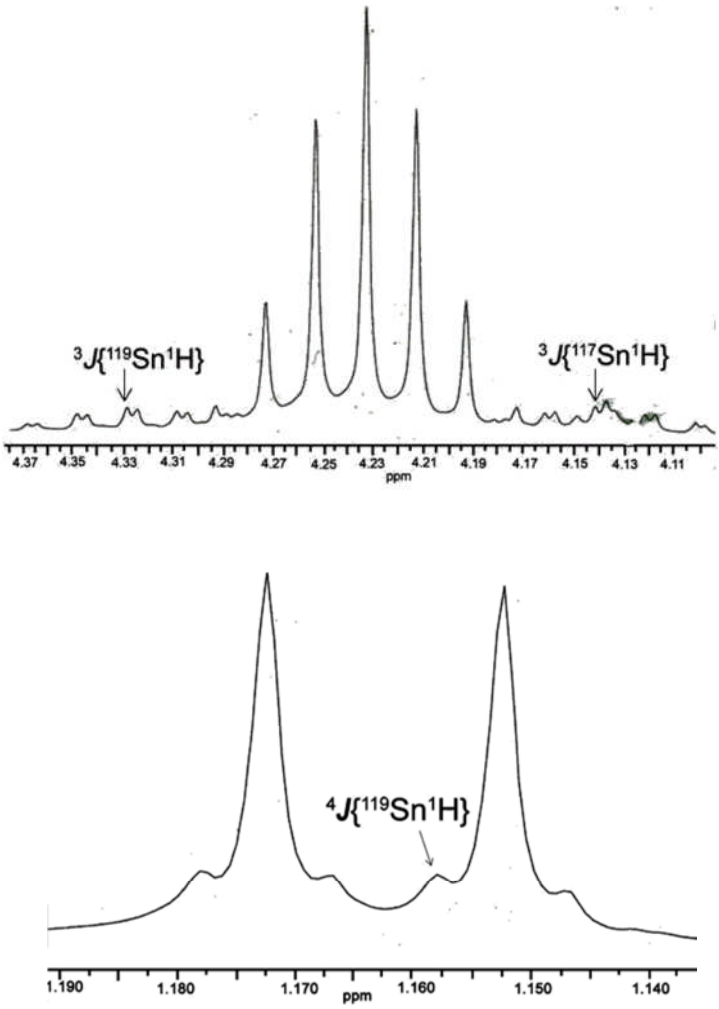

Fig.4.5: Expansion of methylene and methyl proton resonances with tin satellite coupling in the ^{1}H NMR spectrum of $(TBA)_3$ $[(Pr^iO)SnW_5O_{18}]$

Derivative	Proton NMR	$^4J\{^1H^{119}Sn\}$ Hz	$^3J\{^1H^{119}Sn\}$ Hz	$^3J\{^1H^{117}Sn\}$ Hz
2	δ 3.86 (-C***H***$_2$CH$_3$) 1.79 (-CH$_2$C***H***$_3$)	4.2	69.6	66.6
3	δ 4.23 (-C***H***(CH$_3$)$_2$) 1.16 (-CH(C***H***$_3$)$_2$)	3.3	57.3	54.9
4	δ 1.29 (-C(C***H***$_3$)$_3$)	2.4	-	-

Table 4.2: $^nJ\{^1H^{119}Sn\}$ coupling constants for alkoxido derivatives of $(TBA)_3$ $[(RO)SnW_5O_{18}]$ R = Et (**2**), Pr^i (**3**) and Bu^t (**4**).

The ^{1}H NMR spectrum of $(TBA)_3$ **4** depicts one singlet at δ 1.29 ppm for the t-butyl group along with tin coupling. ^{119}Sn satellite peaks were clearly identified and coupling constant value was measured. The $^{4}J\{^{119}Sn^{1}H\}$ coupling constant value is 2.4 Hz which is less than $^{4}J\{^{119}Sn^{1}H\}$ in **2** and **3.** Hampden smith *et.al* reported that $Sn(OBu^{t})_4$ which is monomeric in the solid state and in solution did not show any $^{4}J\{^{119}Sn^{1}H\}$ in non-polar solvents. [16]

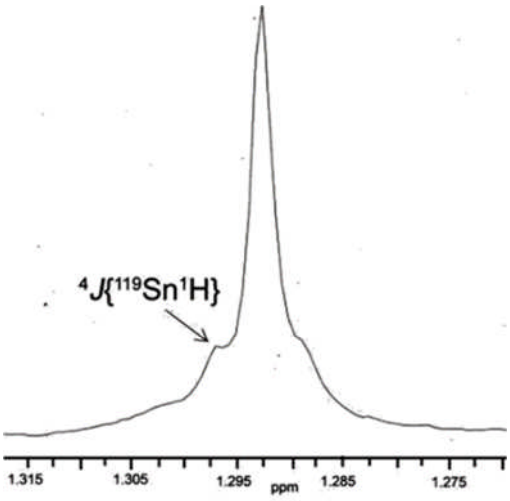

Fig. 4.6: Expansion of t-Butoxide proton resonance with tin satellite coupling in the ^{1}H NMR spectrum of $(TBA)_3[(Bu^{t}O)SnW_5O_{18}]$

4.2.3. ^{13}C NMR studies of Alkyloxido derivatives

Ethoxido derivative **2** showed two ^{13}C resonances for CH_3 and CH_2 at δ 19.94 and 60.6 ppm with ^{119}Sn coupling but no ^{117}Sn coupling was observed. $^{2}J\{^{119}Sn^{13}C\}$ and $^{3}J\{^{119}Sn^{13}C\}$ values are 34.5 Hz and 35.45 Hz respectively which can be compared to $^{2}J\{^{119}Sn^{13}C\}$ = 34.5 Hz for $(TBA)_3$ **1**.

Derivative **3** showed two ^{13}C peaks at δ 26.7 and 66.1 ppm with ^{119}Sn satellite coupling for methyl and methine carbon peaks but no ^{117}Sn coupling was observed. $^{2}J\{^{119}Sn^{13}C\}$ and $^{3}J\{^{119}Sn^{13}C\}$ coupling constant values are 35.5 Hz and 34.5 Hz respectively, which is comparable to $^{2}J\{^{119}Sn^{13}C\}$ = 34.5 Hz in $(TBA)_3$ **1.** Similarly, derivative **4** showed two ^{13}C peaks for methyl and quaternary carbons at δ 32.7 and 71.5 ppm. The quaternary resonance does not exhibit any coupling to tin but the methyl resonance shows ^{119}Sn satellite coupling with $^{3}J\{^{119}Sn^{13}C\}$ of 32.5 Hz. These values can be compared with the parent alkoxides i.e. $Sn(O^{t}Bu)_4$. Hampden-smith *et.al*

reported that both methyl and quaternary resonance in $Sn(O^tBu)_4$ showed ^{119}Sn satellite coupling with $^2J\{^{119}Sn^{13}C\}$ and $^3J\{^{119}Sn^{13}C\}$ of 45 and 27 Hz for terminal butoxide ligands.

Derivative	^{13}C NMR chemical shift	$^2J\{^{119}Sn^{13}C\}$	$^3J\{^{119}Sn^{13}C\}$
2	δ 19.94 (-CH_2***C***H_3) 60.6 (-***C***H_2CH_3)	34.5	35.5
3	δ 26.7 (-CH(***C***$H_3)_2$) 66.1 (-***C***$H(CH_3)_2$)	35.5	34.5
4	δ 32.7 (-C(***C***$H_3)_3$) 71.5 (-***C***$(CH_3)_3$)	-	32.5

Table 4.3: $^nJ\{^{13}C^{119}Sn\}$ coupling constants for alkoxido derivatives of $(TBA)_3$ $[ROSnW_5O_{18}]$ R=Et (**2**), Pr^i (**3**), Bu^t (**4**).

4.2.4. ^{119}Sn NMR studies of Alkyloxido derivatives

Alkoxido derivatives of $(TBA)_3$ **1** showed ^{119}Sn resonances between δ -650 and -670 ppm with ^{183}W satellites. A small impurity peak at δ -610 ppm was present in all of the derivatives. All the alkoxido derivatives showed $^4J\{^{119}Sn^1H\}$ and $^3J\{^{119}Sn^1H\}$ coupling which allowed us to study axial and equatorial $^2J\{^{119}Sn^{183}W\}$ by using INEPT NMR spectroscopy. The INEPT studies of starting precursor $(TBA)_3$ **1** have been discussed in Chapter 3.

During the course of this study, we have found that the impurity peak at δ -610 ppm arises from $[ClSnW_5O_{18}]^{3-}$, which is not very reactive towards acidic substances. The $^2J\{^{119}Sn^{183}W_{eq}\}$ coupling constant value varies from 39 to 49 Hz and depends on the functional group attached to the heterometal tin site. The ^{119}Sn chemical shifts for all the derivatives are shown in the Table 4.6.

$^{2}J\{^{119}Sn^{183}W_{eq}\}$ coupling constant is consistently increasing when introducing the electron donating group on the tin surface in alkyloxido derivatives but whereas it is been observed in the same manner in aryloxido derivatives. Similarly, aryloxido derivatives also show larger coupling constant values but some electronic factors influence the coupling constant values. However the appropriate reason should be investigated by modern computational methods.

4.2.5. ^{17}O and ^{183}W NMR studies

All the derivatives of $(TBA)_3$ **1** shown six characteristic peaks for W=O and Sn-O-W, W-O-W and μ_6 –oxygen in the ^{17}O NMR spectra. These values are compared with the starting precursor and the value is slightly deviated from its original value. The ^{17}O NMR chemical shift directly depends on the charge and functional group attached to heterometal center in POM cage. The ^{17}O NMR data are given in Table 4.9.

All the alkyloxido derivatives shown two peaks for W_{eq}=O and W_{ax}=O in the ^{183}W NMR spectra. The peak appeared at δ 58 ppm was assigned to possible side product $[W_6O_{19}]^{2-}$. The tungsten peaks also shown tin satellite coupling peaks although we measured $^{2}J\{^{119}Sn^{183}W_{eq}\}$ from ^{119}Sn NMR spectra. The ^{183}W NMR data are given in the table 4.10.

4.3. Reaction between $(TBA)_3$ $[(MeO)SnW_5O_{18}]$ with ArOH (Ar=Ph, *p*-CH_3-C_6H_4, *p*-$(CH_3)_3C$-C_6H_4-)

Aryloxido $(TBA)_3[(ArO)SnW_5O_{18}]$ derivatives were prepared by direct reaction between $(TBA)_3$ **1** and the appropriate phenol. All the monohydric phenols gave non-disordered SnW_5 structures but dihydric phenols produced hydrogen bonding between polyoxometalates and free hydroxyl groups on the aromatic ring. The starting material $(TBA)_3$ **1** was reacted with an excess of the phenols in acetonitrile with stirring for 24 - 60 h at 85-90 °C. Reactions with bulkier aromatic phenols usually took longer to replace the methoxide group than simple phenols. All the volatile impuritites were removed in *vacuo*, the solid was washed twice with toluene, then tetrahydrofuran (THF) and diethyl ether and colourless single crystals were obtained from saturated acetonitrile and ether by slow vapour diffusion. These crystals were used for single crystal X-ray structure determination, ^1H NMR spectroscopy, multinuclear NMR spectroscopy and elemental analysis.

$$[Bu^n_4N]_3[(CH_3O)SnW_5O_{18}] + ArOH \longrightarrow [Bu^n_4N]_3[\{ArO\}SnW_5O_{18}] + CH_3OH \quad \text{----2}$$

Ar =	**C_6H_5**	**5**
	4-CH_3- C_6H_4	**6**
	4-$(CH_3)_3C$-C_6H_4	**7**
	3-OH-C_6H_4	**8**
	4-OH-C_6H_4	**9**

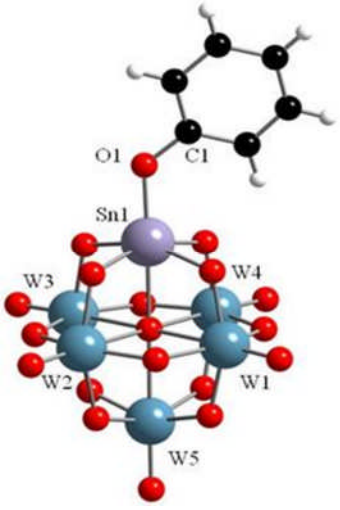

Fig 4.7: Structure of the anion $[(PhO)SnW_5O_{18}]^{3-}$. The colour codes are as follows: W (pale blue), O (red), Sn (pale grey), C(black)

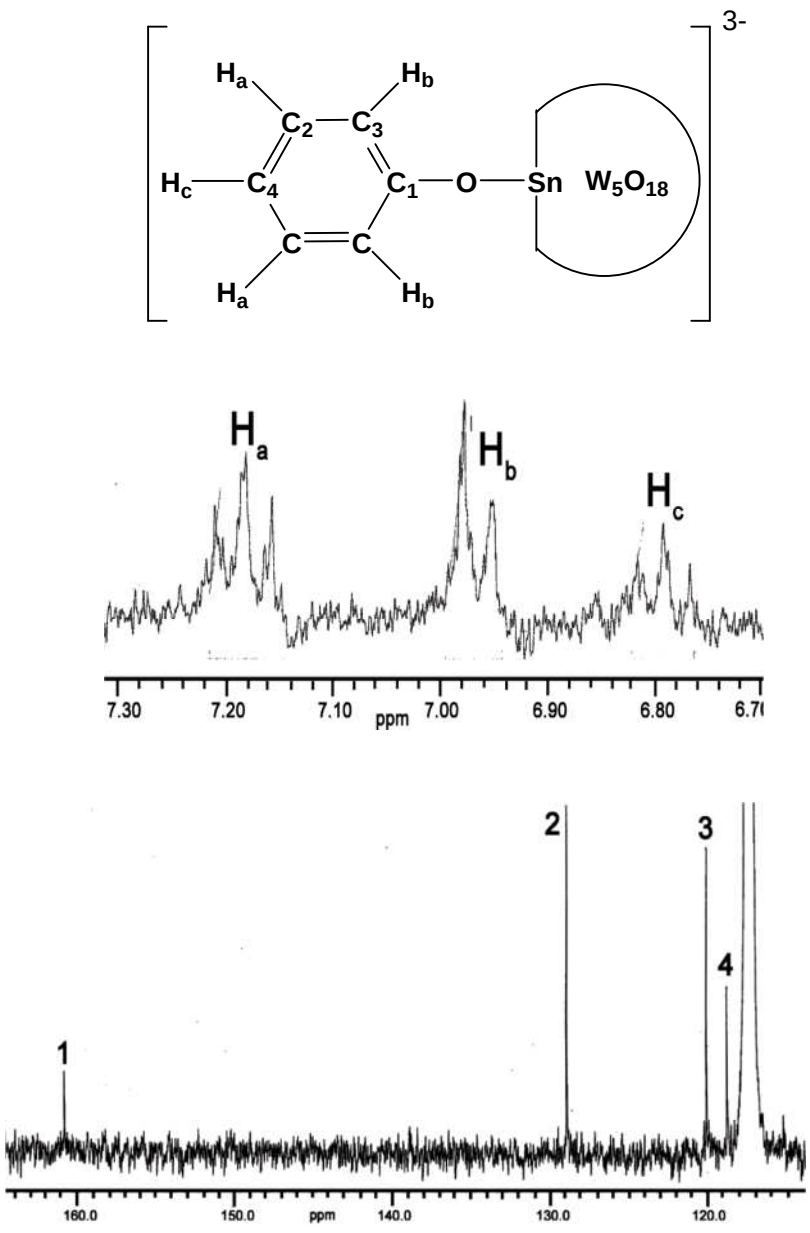

Fig 4.8: ^{1}H and ^{13}C NMR of $(Bu^{n}_{4})_3[(PhO)SnW_5O_{18}]$

The ^{1}H NMR spectrum in Fig. 4.8 shows aromatic peaks at δ 6.8, 7.0 and 7.2 and no peak for Sn-OMe which confirm formation of **5**. The ^{13}C NMR spectrum in Fig. 4.8 shows aromatic carbon peaks at 118.8, 120, 129 and 161 ppm for **5.** $^{2}J\{^{119}Sn^{13}C\}$ and $^{3}J\{^{119}Sn^{13}C\}$ satellite coupling were not observed for the derivatives of **5-9** because of the concentration of the sample and the length of spectrum accumulation. $^{3}J\{^{119}Sn^{13}C\}$ coupling was observed for derivative **5** and the coupling constant value was 31.6 Hz. In general, the ipso carbon was difficult to observe because of a longer relaxation time and we were not able to observe $^{2}J\{^{119}Sn^{13}C\}$ coupling.

The ^{17}O NMR spectrum of aryloxido derivatives were quite similar to the starting material and the chemical shift values are shown in the Table 4.9, but peaks for the side product $[W_6O_{19}]^{2-}$ appeared in all the derivatives. The ^{119}Sn NMR spectrum showed a major peak at -673 ppm along with tungsten satellite coupling. $^2J\{^{119}Sn^{183}W_{eq}\}$ coupling constants were measured for all the derivatives and are shown in the Table 4.6. The ^{183}W NMR spectrum contained (Fig 4.10) two peaks in the ratio 4:1 for W(*eq*) at 76.2 and W(*ax*) at -124 ppm respectively along with tin satellite coupling but because of low sensitivity we have measured $^2J\{^{119}Sn^{183}W\}$ coupling constants only from ^{119}Sn NMR spectra of all the derivatives.

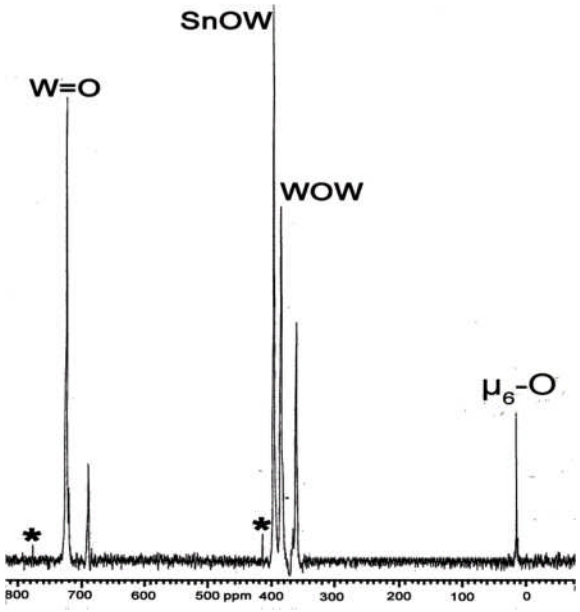

Fig 4.9: ^{17}O spectrum of of $(TBA)_3[(PhO)SnW_5O_{18}]$ [*=$W_6O_{19}]^{2-}$]

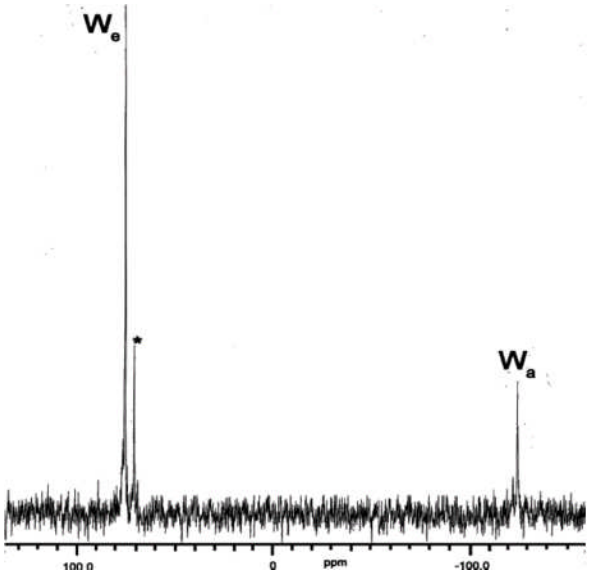

Fig 4.10: ^{183}W NMR spectrum of $(TBA)_3[(PhO)SnW_5O_{18}]$ [*= $(OHSnW_5O_{18})^{3-}$]

Electro-spray ionisation mass spectrometry (ESI-MS) produced results that were consistent with $\{TBA_2[(C_6H_5O)SnW_5O_{18}]\}^{1-}$ aggregate ion at 1903.1 m/z. The line spacing of 1.0 suggested a charge of 1^- for the ion and the m/Z value for the ion is 1904.3. It suggests that Sn-OPh bond is stable compared with the alkoxido derivatives, indicating that aryl oxido derivatives are less susceptible to hydrolysis.

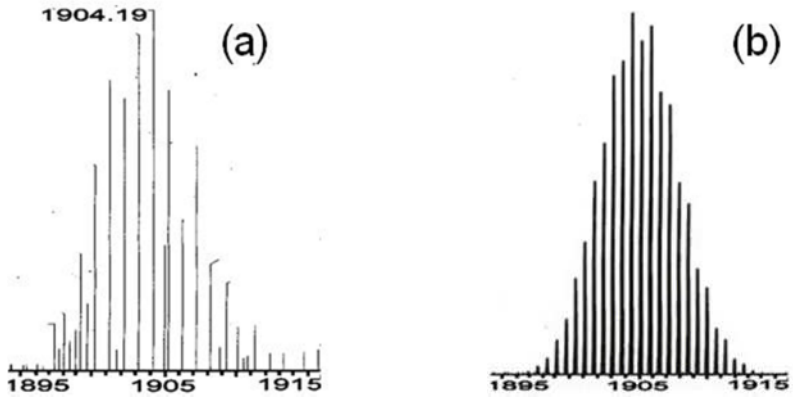

Fig.4.11: a) Peak pattern for the ion cluster assigned to $\{(TBA)_2(C_6H_5O)SnW_5O_{18}\}^-$ in the negative ion electrospray mass spectrum of $(^nBu_4N)_3[C_6H_5OSnW_5O_{18}]$. b) Simulated peak pattern for $\{(TBA)_2(C_6H_5O)SnW_5O_{18}\}^-$ anion.

The aryloxido derivative **6** was prepared by the same alcoholysis route in which the reactants in CH_3CN were heated to 85-90 °C for about 24-36 hrs. The ^1H NMR spectrum of derivative **6** showed two aromatic doublets and a singlet for a *p*-cresol group at δ 6.85, 6.89 and 2.24 ppm and loss of the methoxide peak at δ 3.62 ppm supports the formation of **6**. The ^{13}C NMR spectrum showed aromatic carbon peaks at 119.9, 127.7, 129.3 and 158 ppm and *p*-methyl carbon peak at 19.7 ppm. In addition the *p*- cresol derivative showed both $^2J\{^{119}Sn^{13}C\}$ and $^3J\{^{119}Sn^{13}C\}$ coupling of 36.7 and 30.7 Hz. The ^{119}Sn NMR resonance showed at -674 ppm showed tungsten satellite coupling.

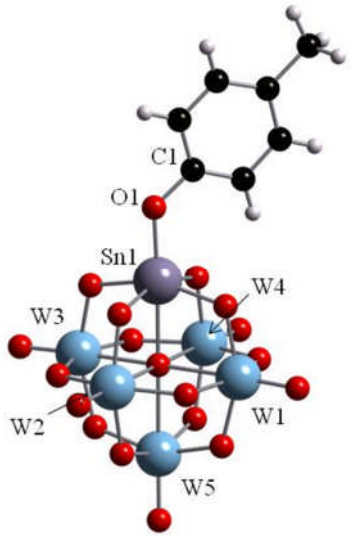

Fig 4.12: Structure of anion $[4\text{-Me-}C_6H_4O\text{-}SnW5O_{18}]^{3-}$. The colour codes are as follows: W (pale blue), O (red), Sn (pale grey), C(black)

The ^{183}W NMR spectrum contained two peaks in a 4:1 ratio for W(*eq*) at 76.2 and W(*ax*) at -122.8 ppm, respectively, along with tin satellite coupling. The ^{17}O NMR spectrum was quite similar to the ^{17}O NMR spectrum of the starting material and chemical shift values are shown in Table 4.9.

Derivative **7** took a long time to form compared to other phenols due to the bulkiness of the reactant. Pale yellow single crystals were obtained at room temperature and were used for further characterisation.

The ^{1}H NMR spectrum showed all aromatic protons and a singlet for the *p*-t-butyl group at δ 1.29 ppm. The ^{13}C NMR spectrum also supports the formation of **7** and showed aromatic carbon peaks at δ 119.4, 125.6, 141.3 and 158.3 ppm and peaks at δ 31.94 and 34.8 ppm for the t-butyl group. In addition ipso and *o*-carbons of *p*- *t*-butyl ligand showed $^{2}J\{^{119}Sn^{13}C\}$ and $^{3}J\{^{119}Sn^{13}C\}$ coupling and the coupling constant values are 38.3 Hz and 31.6 Hz.

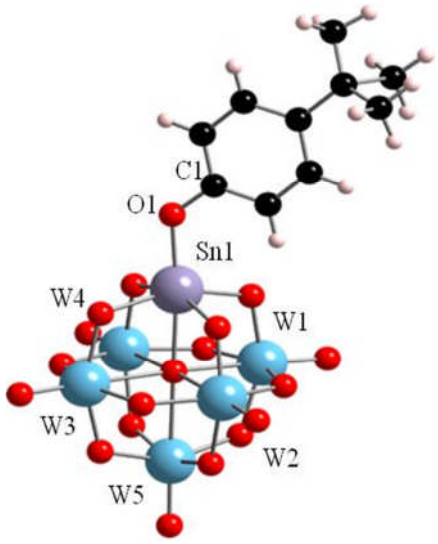

Fig.4.13: Structure of the anion $[(4\text{-}CH_3)_3C\text{-}C_6H_4O\text{-}SnW_5O_{18}]^{3-}$. The colour codes are as follows: W (pale blue), O (red), Sn (pale grey), C(black)

The ^{119}Sn NMR spectrum showed a peak at -673.6 ppm with tungsten satellite coupling. The $^{2}J\{^{119}Sn^{183}W\}$ coupling constant value was measured and is shown in the Table 4.6. The ^{183}W NMR spectrum contained two peaks in a 4:1 ratio for W(*eq*) at 76.2 and W(*ax*) at -121.6 ppm respectively along with tin satellite coupling.

4.4. Reaction between $(TBA)_3$ $[(MeO)SnW_5O_{18}]$ with ArOH (Ar = *m*-OH-C_6H_4, *p*-OH-C_6H_4-)

4.4.1. With resorcinol

Reactions between $(TBA)_3$ **1** and di-functional phenols were explored as a means of introducing reactive OH groups for further structural elaboration and the construction of large supramolecular assemblies from SnW_5 POM building blocks. The reaction stoichiometry was such as to ensure that one of the –OH groups from resorcinol would be left free for further reactions. With regards to the reactivity of $(TBA)_3$ **1**, towards difunctional phenols, we had expected to observe $[(OHC_6H_4O)SnW_5O_{18}]^{3-}$ or $[(\mu\text{-}C_6H_4O)_2(SnW_5O_{18})]^{6-}$. Pale yellow single crystals were obtained by vapour diffusion and were used for characterisation.

The ^{1}H NMR spectrum of derivative **8** exhibited aromatic protons at δ 6.26, 6.46, 6.49, 6.96 ppm. In addition, a broad singlet appeared at δ 6.86 ppm which strongly indicates that the OH site is available for further reaction. ^{13}C NMR spectrum showed aromatic

carbon peaks at δ 162.0, 129.2, 111.9 and 107.0 ppm. The ^{119}Sn NMR spectrum showed a peak at -674 ppm along with tungsten satellite coupling. The $^{2}J\{^{119}Sn^{183}W_{eq}\}$ coupling constant value was measured and coupling constant value is showed in the table 45.6 Hz. The ^{17}O NMR and ^{183}W NMR spectra were similar to other aryloxido derivatives and chemical shift values are given in the Tables 4.9 and 4.10.

4.4.2. Reaction with Hydroquinone

Derivative **9** was prepared by the same route as derivative **8.** The reaction between **3.1** and an equimolar amount of hydroquinone was carried out in acetonitrile at 80 °C for 48-52 hrs. Pale yellow single crystals were obtained but **9** is very soluble in non-polar solvents compared to derivative **8.**

The ^{1}H NMR spectrum of derivative **9** showed peaks in the aromatic region at δ 6.62, 6.68 ppm which confirmed that the phenolic group is present on the tin surface. A broad single peak which appeared at δ 6.46 ppm confirmed that the free –OH group is accessible for further reaction. The ^{13}C NMR spectrum confirmed the formation of derivative **9** and showed peaks at δ 153.67, 149.7, 119.47 and 115.33 ppm. The ^{119}Sn NMR spectrum of **9** showed one single peak at -674 ppm along with tungsten satellite coupling. The $^{2}J\{^{119}Sn^{183}W\}$ coupling constant was 51.2 Hz. and the values are given in the Table 4.6.

We had expected to observe monomeric or dimeric derivatives for both dihydric phenols $[(m\text{-}OHC_6H_4O)SnW_5O_{18}]^{3-}$ **8**, $[(p\text{-}OHC_6H_4O)SnW_5O_{18}]^{3-}$ **9** or $[(\mu\text{-}C_6H_4O)_2(SnW_5O_{18})]^{6-}$ but crystal structures revealed that monomeric structures were formed. In addition, the 'excess' free hydroxyl (OH) group from phenols were involved in hydrogen bonding between the polyoxometalates. Based on this crystllographic structure, we confirmed that W=O site is very basic compared to SnOW site in the polyoxometalate cage.

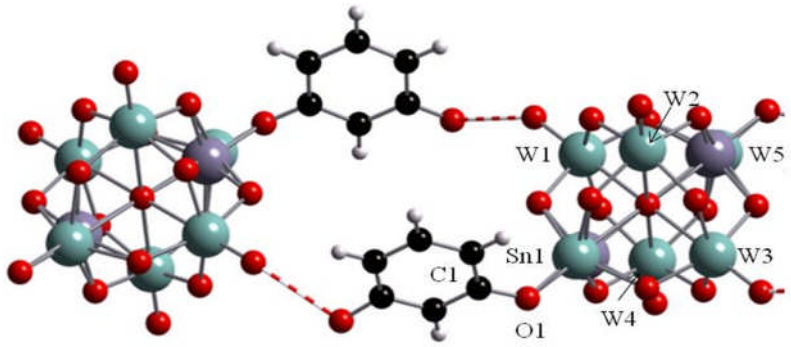

Fig 4.14: Structure of the H-bonded anions $[3\text{-}OH\text{-}C_6H_4O\text{-}SnW_5O_{18}]^{3-}$. The colour codes are as follows: W (green), O (red), Sn (grey), C (black)

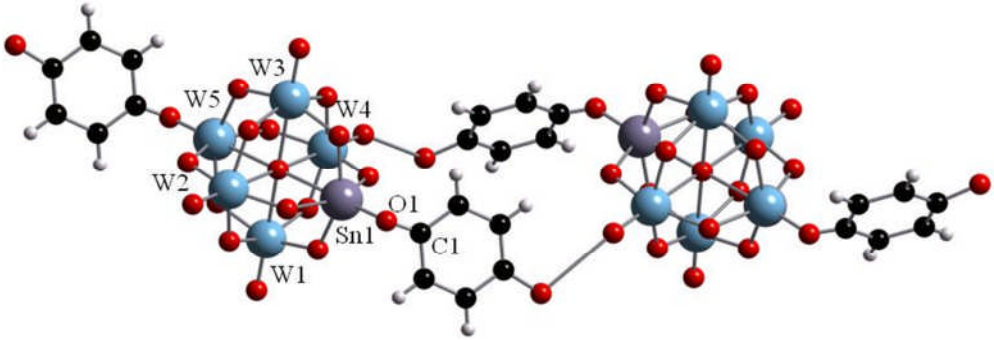

Fig 4.15: H-bonded structure of the anions $[4\text{-}OH\text{-}C_6H_4O\text{-}SnW_5O_{18}]^{3-}$. The colour codes are as follows: W (blue), O (red), Sn (grey), C (black)

Selected bond lengths and angles	Compound **5**	Compound **6**	Compound **7**	Compound **8**	Compound **9**
Sn(1)-O(1)	1.961	1.954	1.955	1.953	1.740
O(1)-C(1)	1.355	1.371	1.328	1.281	1.076
Sn(1)-O(c)	2.338	2.239	2.194	2.169	2.372
Sn(1)-O(1)-C(1)	128.320	129.224	127.558	132.614	133.698
Sn(1)-O(c)-W(5)	180.000	180.000	180.000	175.801	180.000
Sn(1)-O(b)-W(1)	112.692	112.961	113.100	111.437	118.359
Sn(1)-O(b)-W(3)	113.135	112.555	114.369	110.688	116.663

Table 4.4: Selected bond lengths (Å) and bond angles (^{o}) of Aryl oxido derivatives of $(TBA)_3$**1.**

4.5. Reaction between salicyaldehyde and $(TBA)_3[(MeO)SnW_5O_{18}]$ 10

The coordination chemistry of tin in solution is an attractive and multifaceted target for structural studies by means of spectroscopic and diffraction techniques. The main purpose of this reaction is to confirm whether tin expands the coordination number from six or not. The tin atom exhibits 5 to 7 coordination in organotin tropolonato complexes [17] $R_3Sn(trop)$ where R=Bu, Ph but tin polytungstates shown only a six coordination tin site.

Excess salicyaldehyde in acetonitrile was added to a solution of $(TBA)_3$ **1** then the reaction mixture was heated at 80 ºC for 24-36 hrs. Once the reaction colour had turned pale yellow, the solution was allowed to cool to room temperature and washed with diethyl ether (2x20 ml). Pale yellow single crystals were obtained by slow vapour diffusion and these crystals were used for characterisation.

$$[Bu^n{}_4N]_3[(MeO)SnW_5O_{18}] + [2\text{-}(CHO)C_6H_4OH] \longrightarrow [Bu^n{}_4N]_3[\{2\text{-}(CHO)C_6H_4O\}SnW_5O_{18}] + MeOH \quad \text{----3}$$

The ^1H NMR spectrum exhibited all aromatic protons at δ 6.90, 7.24, 7.48, 7.65 ppm and a sharp singlet appeared at δ 10.56 ppm which indicates that the aldehyde proton is present in the POM cage while the ^{13}C NMR spectrum depicts aromatic carbon peaks at δ 164.8, 135.6, 126.65, 122.9 and 119.3 ppm. A sharp singlet appeared at 190.8 which corresponds to the aldehyde carbon. The ^{119}Sn NMR spectrum shows a major peak at -673 ppm along with tungsten satellite coupling. The $^2J\{^{119}Sn^{183}W_{eq}\}$ coupling constant value is 49.0 Hz.

The ^{17}O NMR spectrum was quite similar to the ^{17}O NMR spectrum of the starting material and chemical shift values are shown in the Table 4.9. The ^{183}W NMR spectrum contained two peaks in a 4:1 ratio for W(*eq*) at 79.1 and W(*ax*) at -120.6 ppm respectively along with tin satellite coupling, but because of the low sensitivity of W, we usually measured the coupling constant value from the ^{119}Sn NMR. Elemental analysis supported the data above and the proposed structure $[\{2\text{-}(CHO)C_6H_4O\}\text{-}SnW_5O_{18}]^{3-}$ was confirmed by a single crystal X-ray structure determination.

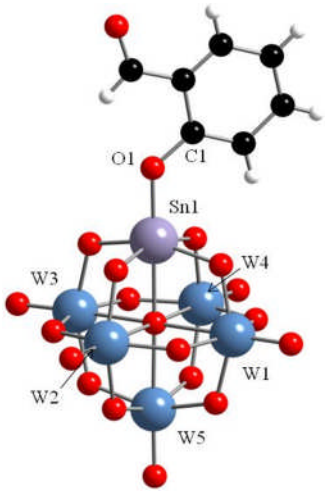

Fig 4.16: Structures of the anion $[2\text{-}CHO\text{-}C_6H_4O\text{-}SnW_5O_{18}]^{3-}$. The colour codes are as follows: W (pale blue), O (red), Sn (pale grey), C (black)

Sn(1)-O(1)	1.961	Sn(1)-O(1)-C(1)	129.196
Sn(1)-C(1)	3.034	Sn(1)-O(c)-W(5)	178.757
O(1)-C(1)	1.386	Sn(1)-O(b)-W(1)	112.255
Sn(1)-O(c)	2.247	Sn(1)-O(b)-W(3)	113.276

Table 4.5: Selected bond lengths (Å) and bond angles (^{o}) of $[2\text{-}CHO\text{-}C_6H_4O\text{-}SnW_5O_{18}]^{3-}$.

Anion [a]	^{119}Sn NMR chemical shift (ppm)	$^{2}J\{^{119}Sn^{183}W_{eq}\}$ (Hz)
$[(MeO)SnW_5O_{18}]^{3-}$ **1**	-647	38.4
$[(EtO)SnW_5O_{18}]^{3-}$ **2**	-651	39.8
$[(^{i}PrO)SnW_5O_{18}]^{3-}$ **3**	-654	39.9
$[(^{t}BuO)SnW_5O_{18}]^{3-}$ **4**	-663	40.3
$[(PhO)SnW_5O_{18}]^{3-}$ **5**	-673	45.6
$[(p\text{-}CH_3\text{-}C_6H_4O)SnW_5O_{18}]^{3-}$ **6**	-674	47.5
$[(p\text{-}C(CH_3)_3\text{-}C_6H_4O)SnW_5O_{18}]^{3-}$ **7**	-673	45.6
$[(m\text{-}OH\text{-}C_6H_4O)SnW_5O_{18}]^{3-}$ **8**	-674	45.6
$[(p\text{-}OH\text{-}C_6H_4O)SnW_5O_{18}]^{3-}$ **9**	-674	51.2
$[(2\text{-}CHO\text{-}C_6H_4O)SnW_5O_{18}]^{3-}$ **10**	-672	48.9
$[(Me_3SiO)SnW_5O_{18}]^{3-}$ **11**	-669	45.6
$[(^{i}Pr_2NH_2)_2(\mu\text{-}O)(SnW_5O_{18})_2]^{4-}$ **12**	-658	39.9

Table 4.6: ^{119}Sn NMR chemical shifts and $^{2}J\{^{119}Sn^{183}W_{eq}\}$ coupling constant values of derivatives of $(TBA)_3$ **1**.

4.6. Attempted preparation of extended metal oxides

The major objective of our project is to synthesise extended metal oxide structures in a controlled manner. Alkoxo functionalised Lindqvist type heterometallic polytungstates $[(RO)MW_5O_{18}]^{3-}$ where M = Ti, Zr and Sn usually have rigid frameworks and were

used as polynuclear building blocks in order to synthesise the extended metal oxide structures. To achieve the target materials, we used a very simple hydrolytic and metathesis method.

4.6.1. Reaction between $[(OH)SnW_5O_{18}]^{3-}$ and $Sn\{N(SiMe_3)_2\}_2$

We were trying to synthesise stepwise, controlled extended metal oxide structures and used $[(OH)SnW_5O_{18}]^{3-}$ as starting precursor. Reaction between $[(OH)SnW_5O_{18}]^{3-}$ and tin bis(trimethylsilylamide) $Sn\{N(SiMe_3)_2\}_2$ provides an unexpected product $[Me_3SiO\text{-}SnW_5O_{18}]^{3-}$, **11**. We expected to observe the formation of POM-Sn^{IV}-O-Sn^{II}-O-Sn^{IV}-POM linkage in solution but it gave the derivative **11**. After heating $[(OH)SnW_5O_{18}]^{3-}$ and $Sn\{N(SiMe_3)_2\}_2$, the solution turned very pale yellow colour. Pale yellow single crystals were obtained from acetonitrile and ether by vapour diffusion and these were used for characterisation and single crystal X-ray structure determination.

$$\mathbf{2\,[^nBu_4N]_3[(HO)SnW_5O_{18}] + Sn\{N(SiMe_3)_2\}_2 \longrightarrow}$$

$$\mathbf{[^nBu_4N]_6[W_5O_{18}Sn\text{-}O\text{-}Sn\text{-}O\text{-}SnW_5O_{18}] + 2\,HN(SiMe_3)_2} \quad \mathbf{----4}$$

The derivative **11** can also be synthesised from the starting precursor $(TBA)_3$ **1**. An attempted functionalisation of $(TBA)_3$ **1** with nitrogen containing ligands such as hexamethyldisilzane (HMDS) favours the formation of derivative **11.** The methoxide protons in $(TBA)_3$ **1** and $[(OH)SnW_5O_{18}]^{3-}$ were expected to be acidic in nature but it proved to be basic in non-aqueous media. Based on this reaction, we have concluded that the O-H and O-C bonds are more reactive than the Sn-O bond.

Mechanism

In an attempt to generate Sn^{IV}–O–Sn^{II} linkages, $[(OH)SnW_5O_{18}]^{3-}$ was reacted with $Sn\{N(SiMe_3)_2\}_2$. However, the product isolated was $(TBA)_3$ **11** which requires N–Si rather than Sn^{II}–N cleavage, *i.e.* Si is more electrophilic than Sn(II) in this reaction. It confirms that the O-H bond shown more basic rather than acidic.

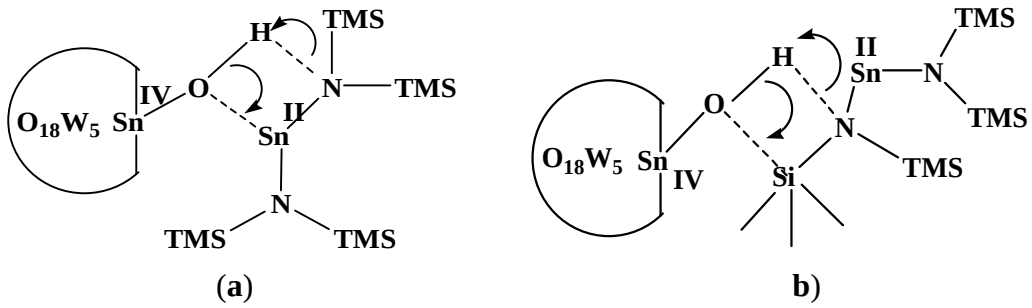

Fig. 4.17: Possible mechanism for the formation of $(TBA)_3$ **11**

A single peak observed at δ 0 ppm along with many satellite peaks in the ^{1}H NMR spectrum confirm the formation of **11**. When we changed the processing parameter of the ^{1}H NMR spectrum we would identify all of the NMR satellites (^{29}Si and ^{119}Sn). The $^{2}J\{^{29}Si^{1}H\}$ and $^{4}J\{^{119}Sn^{1}H\}$ coupling constant values are 6.8 and 1.3 Hz, respectively. In the ^{13}C NMR spectrum we observed trimethylsilyl peak at 21.82 ppm with no satellite peaks. In addition, the ^{29}Si NMR also showed a single peak at 9.9 ppm with ^{119}Sn coupling. The $^{2}J\{^{119}Sn^{29}Si\}$ coupling constant value is 22.5 Hz.

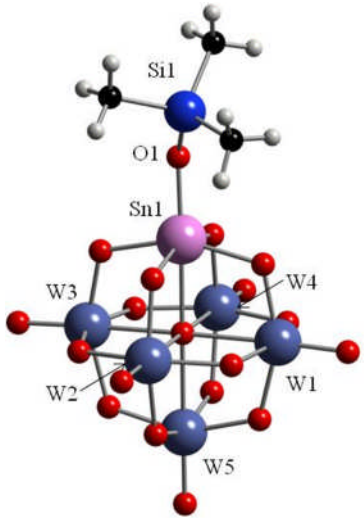

Fig. 4.18: Structure of the anion $[(Me_3SiO)\text{-}SnW_5O_{18}]^{3-}$. The colour codes are as follows: W (pale blue), O (red), Sn (pale pink), Si (dark blue), C(black)

Sn(1) –O(1)	1.937	Sn(1)-O(1)-Si(1)	140.648
Sn(1)-C(1)	3.326	Sn(1)-O(c)-W(5)	179.070
O(1)-C(1)	1.593	Sn(1)-O(b)-W(1)	112.577
Sn(1)-O(c)	2.242	Sn(1)-O(b)-W(3)	113.331

Table 4.7: Selected bond lengths (Å) and bond angles (°) of $[(Me_3SiO)\text{-}SnW_5O_{18}]^{3-}$

The ^{119}Sn NMR spectrum showed a peak at -669 ppm along with tungsten satellites. The $^{2}J\{^{119}Sn^{183}W\}$ coupling constant value is 45.6 Hz. The ^{183}W NMR spectrum showed two peaks in a 4:1 ratio for W(*eq*) at 73.1 and W(*ax*) at -127.9 ppm respectively along with tin satellite coupling.

4.7. Infra-red spectroscopy

The FTIR spectra of pure samples of $(TBA)_3$ **2**, $(TBA)_3$ **3** and $(TBA)_3$ **4** were very similar to the starting material $(TBA)_3$ **1**. The higher anion charge compared with $[W_6O_{19}]^{2-}$ causes bathochromic shifts of *v* (WO) bands and the lower symmetry results in band splitting. So therefore, three strong bands appeared at lower frequency in the region 955-960 cm^{-1} and 749-770 cm^{-1} for W=O and W-O-W frequency and values are compared to 974 cm^{-1}, 814 cm^{-1} for $[W_6O_{19}]^{2-}$. This is due to the higher charge of the tin polyoxometalate structures.

The solid state IR spectrum of $(TBA)_3$ **1** was discussed in Chapter 3 and the band at 620 cm^{-1} was assigned to the Sn-O stretching vibrations. In this chapter, we studied in more detail the alkoxido and aryloxido derivatives in order to assign the Sn-O stretching frequency. The Sn-O stretching frequency was not affected much by the nature of the substituent groups and varies from 625 to 617 cm^{-1}. The maximum value (625 cm^{-1}) was observed for derivative **2** and the lowest (617 cm^{-1}) was observed for derivative **10**. Hampden-Smith *et.al* [17] assigned the strong band appeared at 937 cm^{-1} to the C-O stretching vibrations for $Sn(O^tBu)_4$ but we were not able to assign the C-O stretching frequencies for all of the derivatives due to overlapping of the W=O and C-O stretching vibrations.

In addition, all the aromatic derivatives **5**, **6**, **7**, **8**, **9** and **10** showed aryl stretching vibration *v*(C-H) at 3000 cm^{-1} and stretching vibration *v*(C-C) at 1653 cm^{-1} Derivatives **8** and **9** also showed *v*(O-H) at 3255 cm^{-1} and 3294 cm^{-1} respectively. Carbonyl *v*(C=O) stretching vibration appeared at 1679 cm^{-1} for derivative **10** which indicates that the salicyaldehyde is present on the tin surface. The spectrum of derivative **11** contains a strong band 1243 cm^{-1} which is associated with $Si(CH_3)_3$.

Anion [a]	IR data
$[(MeO)SnW_5O_{18}]^{3-}$ **1**	2960m,2932m, 2874m, 1483s, 1381m, 1151m, 1045m, 951s,889m, 790s, 749s, 617w, 562w, 545s
$[(EtO)SnW_5O_{18}]^{3-}$ **2**	2729m, 2409m, 1655m, 1378s, 1309vw, 1152m, 1097m, 1058m, 1027m, 953s, 885m, 803s, 758s, 625m, 569m, 429s
$[(^{i}PrO)SnW_5O_{18}]^{3-}$ **3**	2728m, 1662w, 1377s, 1152m, 1124w, 1026w, 953s, 884m, 803s, 758s, 623m, 569m, 430s
$[(^{t}BuO)SnW_5O_{18}]^{3-}$ **4**	2727 m, 1669m, 1195s, 1153m, 1056m, 1027m, 952s, 885m, 800s, 755s, 624 m, 564m, 425s
$[(PhO)SnW_5O_{18}]^{3-}$ **5**	2729m, 2303m, 1593m, 1378s, 1282m, 1260s, 1073w, 1027w, 957s, 884m, 804s, 755s, 621m, 608m 572m,
$[(p\text{-}CH_3\text{-}C_6H_4O)SnW_5O_{18}]^{3-}$ **6**	2729m, 1608m, 1508s, 1378s, 1272m, 1258m, 1153w, 1028w, 957s, 885m, 802s, 751s, 619m, 569m, 519w, 431s
$[(p\text{-}C(CH_3)_3\text{-}C_6H_4O)SnW_5O_{18}]^{3-}$ **7**	2727m,, 1603m, 1509s, 1377s, 1256m, 1183m, 1152m, 1108m, 1068w, 1026w, 956s, 884m, 803s, 754s, 696m, 622m, 570s
$[(m\text{-}OH\text{-}C_6H_4O)SnW_5O_{18}]^{3-}$ **8**	3255br, 2728m, 1661w, 1580m, 1377s, 1295w, 1253w, 1142s, 1107w, 1057w, 1026w, 953s, 885w, 899s, 748s, 619m, 569m, 427m
$[(p\text{-}OH\text{-}C_6H_4O)SnW_5O_{18}]^{3-}$ **9**	3294br, 2726m, 1377s, 1307w, 1238w, 1153m, 1027w, 955s, 885w, 805s, 754s, 624m, 570w, 432s
$[(2\text{-}CHO\text{-}(C_6H_4O)SnW_5O_{18}]^{3-}$ **10**	2728m, 1679m, 1597m, 1378s, 1315m, 1247m, 1308vw, 1240m, 1153m, 1027m, 958s, 884m, 802s, 751s, 617m, 573m, 527m, 432s

$[(Me_3SiO)SnW_5O_{18}]^{3-}$ **11**	2728 m, 1669 m, 1243s, 1152 s, 1107 m, 1056m, 1027 m, 952 s, 799 s, 751 s, 622 m, 566 m, 426 bs
$[(^iPr_2NH_2)_2(\mu\text{-}O)(SnW_5O_{18})_2]^{4-}$ **12**	ATR : 2960s, 2874s, 1482s, 1381 m, 1152 m, 953vs, 794s, 750s, 717s, 611s, 567s Nujol-mull: 3435 vw, 2874 s, 2726, m, 1378 m, 1152 m, 952 vs, 798 s, 748 s, 722 s, 614 s, 568s.

Table 4.8: IR data for derivatives of $(TBA)_3$ **1**.

4.8. Crystal structures and mechanism

The crystal structure of **2** is *trans* disordered and the structure is very similar to $(TBA)_3$ **1**. When a bulkier group is bounded to tin, non-disordered crystal structures were obtained. The Sn-O bond distances are varies between 2.79 to 2.97 Å in all alkyloxido derivatives and similarly SnOC bond angles vary between 125° to 150° in all alkyloxido derivatives.

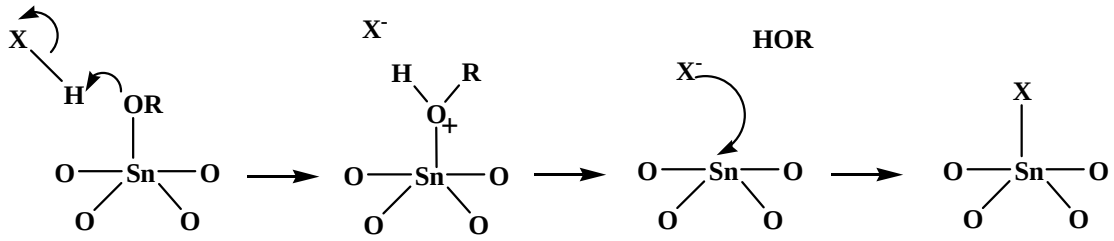

Fig. 4.19: possible mechanism of the reaction between $(TBA)_3$ **1** and HX

Difunctional phenol derivatives such as resorcinol and hydroquinone interact with neighbouring polyoxometalates *via* hydrogen bonding forming extended structures. Interestingly, this involves the terminal W=O [18] rather than bridging SnOW or WOW, which are expected to be more basic and consequently the POMs are organised into chains. This information is slightly contradictory for derivative **12**, for which proton coordinate to cis- SnOW sites rather than W=O sites. (See section 4.8.4) The Sn(1)-O(1) bond lengths varies from 2.164 to 2.337 A° and SnOC bond angles vary between 127.55° to 133.69°.

Anion [a]	W=O	Sn-O-W	W-O-W	μ_6-O
$[(MeO)SnW_5O_{18}]^{3-}$ **1**	720, 684	395	384, 363	17.2
$[(EtO)SnW_5O_{18}]^{3-}$ **2**	725, 684	395	382, 365	17.4
$[(^{i}PrO)SnW_5O_{18}]^{3-}$ **3**	726, 684	396	383, 367	17.7
$[(^{t}BuO)SnW_5O_{18}]^{3-}$ **4**	725, 683	396	382, 368	17.6
$[(PhO)SnW_5O_{18}]^{3-}$ **5**	723, 689	397	385, 361	15.8
$[(p\text{-}CH_3\text{-}C_6H_4O)SnW_5O_{18}]^{3-}$ **6**	722, 688	396	385, 361	15.6
$[(p\text{-}C(CH_3)_3\text{-}C_6H_4O)SnW_5O_{18}]^{3-}$ **7**	723, 689	396	386, 362	16.5
$[(m\text{-}OH\text{-}C_6H_4O)SnW_5O_{18}]^{3-}$ **8**	723, 688	397	386, 362	15.7
$[(p\text{-}OH\text{-}C_6H_4O)SnW_5O_{18}]^{3-}$ **9**	723, 689	398	386, 363	16.7
$[(2\text{-}CHO\text{-}C_6H_4O)SnW_5O_{18}]^{3-}$ **10**	725, 691	399	387, 365	15.3
$[(Me_3SiO)SnW_5O_{18}]^{3-}$ **11**	720, 684	395	383, 368	16.5
$[(^{i}Pr_2NH_2)_2(\mu\text{-}O)(SnW_5O_{18})_2]^{4-}$ **12**	725, 691	398	386, 365	19.5

Table 4.9: ^{17}O NMR data for derivatives of $(TBA)_3$ **1**

Anion [a]	δ_W	
	W (*eq*) [4 W]	W (*ax*) [1 W]
$[(MeO)SnW_5O_{18}]^{3-}$ **1**	76.9	-128.1
$[(EtO)SnW_5O_{18}]^{3-}$ **2**	74.7	-129.6
$[(^{i}PrO)SnW_5O_{18}]^{3-}$ **3**	74.5	-128.3
$[(^{t}BuO)SnW_5O_{18}]^{3-}$ **4**	71.8	-126.7
$[(PhO)SnW_5O_{18}]^{3-}$ **5**	77.4	-124.1
$[(p\text{-}CH_3\text{-}C_6H_4O)SnW_5O_{18}]^{3-}$ **6**	78.9	-122.8
$[(p\text{-}C(CH_3)_3\text{-}C_6H_4O)SnW_5O_{18}]^{3-}$ **7**	76.7	-121.6
$[(m\text{-}OH\text{-}C_6H_4O)SnW_5O_{18}]^{3-}$ **8**	76.5	-123.1
$[(p\text{-}OH\text{-}C_6H_4O)SnW_5O_{18}]^{3-}$ **9**	76.4	-122.8
$[(2\text{-}CHO\text{-}C_6H_4O)SnW_5O_{18}]^{3-}$ **10**	79.1	-120.6
$[(Me_3SiO)SnW_5O_{18}]^{3-}$ **11**	73.1	-127.9
$[(^{i}Pr_2NH_2)_2(\mu\text{-}O)(SnW_5O_{18})_2]^{4-}$ **12**	71.8	-121.7

[a] = as $Bu^{n}_{4}{}^{+}$ salts.

Table 4.10: ^{183}W NMR data for derivatives of $(TBA)_3$ **1**

4.9. Reactions of $[ClSnW_5O_{18}]^{3-}$

During the course of our study, we investigated the reactivity of the Sn-Cl bond with $AgBF_4$, HBF_4, solvents like H_2O, MeOH and Diisopropyl amine (DIPA), in order to develop the metalthesis towards halide abstraction, ligand hydrolysis and aminolysis respectively.

4.9.1. Halide abstraction reaction

Reaction between $AgBF_4$ and $(TBA)_3[ClSnW_5O_{18}]$ were carried out with the aim of removing the chloride anion to generate $[SnW_5O_{18}]^{2-}$ with a vacant coordination site on the tin metal (Sn). The possible outcome was that this site would be occupied by MeCN or possibly another $[SnW_5O_{18}]^{2-}$ anion so dimerising to give the structural analogue of $[\{CoW_5O_{18}H\}_2]^{6-}$ or $[(TiW_5O_{18})_2]^{4-}$.[19]

$$\mathbf{TBA_3[ClSnW_5O_{18}] + AgBF_4 \longrightarrow AgCl + TBABF_4 + TBA_2[SnW_5O_{18}]} \quad \mathbf{----5}$$

A DCM/CH_3CN mixture was used as a solvent and the reaction was left to stir overnight during which time a white solid precipitated and was assumed to be silver chloride (AgCl). The mother liquor was filtered off and examined by ^{119}Sn NMR spectroscopy but it did not show any characteristic peaks. An attempted recrystallisation of the mother liquor gave only $[W_6O_{19}]^{2-}$ product and uncharacterised oily product.

The NMR scale reaction between HBF_4 and $(TBA)_3$ **4** gave a colourless solution. We were expecting that H^+ ion from HBF_4 would coordinate to POM cage initially, followed by elimination of HCl and subsequently produce vacant a coordination site i.e. $[SnW_5O_{18}]^{2-}$. The sample was examined by ^{119}Sn and ^{17}O NMR. We were not able to observe any significant characteristic peaks in the ^{119}Sn NMR spectrum in this reaction and the spectrum was very similar to that of the $AgBF_4$ reaction. The ^{17}O spectrum showed mainly very sharp peaks at δ 415 and 776 ppm due to possible side product $[W_6O_{19}]^{2-}$ with broad peaks at 759, 451 and 426 ppm. From these two reactions we observed some degradation of POM occurring in solution and the leads possible to side product formation of $[W_6O_{19}]^{2-}$. Currently we are investigating the reactivity of $(TBA)_3[ClSnW_5O_{18}]$

4.9.2. Attempted preparation of $[(\mu\text{-}O)(SnW_5O_{18}H)_2]^{4-}$

$$Na \longrightarrow Na^+ + e^-$$

$$[ClSnW_5O_{18}]^{3-} \xrightarrow{e^-} [ClSnW_5O_{18}]^{4-} \longrightarrow Cl^- + [SnW_5O_{18}]^{3-} \quad \text{-----6}$$

Errington and his co-workers have successfully synthesised the titanium $[(TiW_5O_{18})_2]^{4-}$ [20] analogous by halide abstraction route and following hydrolysis of the intermediate, it produced $[(\mu\text{-}O)(TiW_5O_{18}H)_2]^{4-}$. IR spectra showed a characteristic band for this new species and lower charge anions were formed because both protons are on the polyoxometalate cage.

Cyclic Voltammetry studies of $(TBA)_3$ **4,** showed one electron non-reversible reduction peak at -1.672 V and the added electron remains in the POM cage. We expected that Sn atom also to behave in same the manner but an attempted preparation of $[(\mu\text{-}O)(SnW_5O_{18}H)_2]^{4-}$ was not successful.

4.9.3. Reaction between $(TBA)_3$ $[ClSnW_5O_{18}]$ and H_2O, MeOH and PhOH

$$Q_3[ClSnW_5O_{18}] + HOR \longrightarrow Q_3[ROSnW_5O_{18}] \quad \text{----7}$$

$$R = H, Me, Ph$$

The reactivity of the Sn-Cl bond towards water, methanol and phenol has also been studied. Hydrolysis of $(TBA)_3[ClSnW_5O_{18}]$ was expected to produce the new peak at δ -633 ppm in the ^{119}Sn NMR spectrum if Sn-Cl bond undergoes the hydrolysis but excess water does not affect the original chemical shift of the starting material. In spite of this, $[ClSnW_5O_{18}]^{3-}$ readily reacted with excesss methanol at elevated temperatures to produce $[(MeO)SnW_5O_{18}]^{3-}$ along with the side product $[W_6O_{19}]^{2-}$. Based on ${}_pK_a$ values, phenol is more acidic compared to other solvents i.e MeOH and H_2O. We are assuming that $[ClSnW_5O_{18}]^{3-}$ is acidic and reluctant to abstract the proton from phenol but whereas it accept the proton from methanol. However, the reactivity of $[ClSnW_5O_{18}]^{3-}$ has to be investigated.

4.9.4. With diisopropyl amine

The attempted synthesis of an amido functionalised tin polyoxometalates gave the associated species $[(^{i}Pr_2NH_2)_2(\mu\text{-}O)(SnW_5O_{18})_2]^{4-}$ which can also be regarded as a H-bonded amine adduct of the protonated oxo-bridged species $[(\mu\text{-}O)(SnW_5O_{18}H)_2]^{4-}$. This is analogous to a recently characterised titanium analogue $[(\mu\text{-}O)(TiW_5O_{18}H)_2]^{4-}$, which has been structurally characterised and forms the H-bonded THF adduct $[(\mu\text{-}O)(TiW_5O_{18}H)_2(THF)]^{4-}$.

DIPA was reacted easily with chloro tin polyoxometalate at higher temperatures and yielded a pink coloured product, which was investigated by ^{119}Sn NMR spectroscopy. Initially, the tin-amido compound was formed upon reacting $(TBA)_3$ **4** with excess DIPA and a new peak appeared at -647 ppm along with starting material $(TBA)_3[ClSnW_5O_{18}]$ at -610 ppm. We propose that it may be a Sn-amido functionalised POM product which hydrolyses readily in solution to form an oxo-bridged product that interacts with $^{+}H_2NPr^{i}_2$ cations which showed another new peak at -657 in ^{119}Sn NMR spectrum. After being heated at elevated temperature over 72 hrs, only one peak remained at -657 ppm. The new product was successfully recrystallised from acetonirile and ether by vapour diffusion. Pale pink crystals were formed and used for multinuclear NMR spectroscopy characterisation. In conclusion, we propose that an intermediate Sn-amido functionalised POM initially forms with the chemical shift of -647 ppm. This moisture sensitive POM hydrolyse to produce the associated species **12.**

The ^{1}H NMR spectrum of derivative **12** exhibited single broad peak at δ 8.85 ppm which is assigned to the ammonium protons. In addition a triplet and a septet were observed at δ 1.14 and 3.45 ppm corresponding to the isopropyl groups. The ^{13}C NMR spectrum shows isopropyl peaks for the amine at δ 47.39 and 19.09 ppm. The ^{119}Sn NMR spectrum showed a peak at -659 ppm with tungsten satellites. The $^{2}J\{^{119}Sn^{183}W_{eq}\}$coupling constant is 39.0 Hz. In addition, we also observed $^{2}J\{^{119}Sn^{117}Sn\}$ satellite peaks in the ^{119}Sn NMR. The coupling constant was 256 Hz and this can be compared to 333 Hz for $(TBA)_6$ **3.**

Chemical shift values in the ^{17}O NMR spectrum of this novel associated species are shown in Table 4.9. The ^{183}W NMR spectrum contained two peaks in 4:1 for W(*eq*) at 71.8 and W(*ax*) at -121.7 ppm respectively along with tin satellite peaks although the resolution of the spectrum was not enough to measure coupling constants. Elemental analysis supported the data above and the structure was confirmed by single crystal X-ray structure determination.

Derivative **12** showed two SnW_5O_{18} fragments are linked by oxo ligand and SnOSn (154.0 ^{o}) bond is more bent in nature compare to TiOTi (173.1 ^{o}) in $[(\mu\text{-}O)TiW_5O_{18}]^{6-}$ [12] and NbONb (180 ^{o}) in $[(\mu\text{-}O)NbW_5O_{18}]^{5-}$ [21] Interestingly, Sn(1)-O-Sn(1A) bond lengths are not equivalent and the associated species are stabilised by two $Pr^{i}_2NH_2^+$ cation which appeared as a possible side product in solution. These observations provide important insight into protonation-deprotonation events at metal oxide surfaces. Protonation occurred on cis- SnOW sites rather than W=O, WOW sites and possibly proton should have come from $Pr^{i}_2NH_2^+$ cation. A strong band at 717 cm^{-1} (ATR) and 722 cm^{-1} (Nujol-mull) in IR spectrum of derivative **12** was assigned to SnOSn asymmetric stretching frequency. This value can be compared to $[(\mu\text{-}O)SnW_5O_{18}]^{6-}$ which shown SnOSn stretching frequency at 720 cm^{-1} in infra red spectrum. The derivatives **1**-**11** IR does not show strong band at 722 and 717 cm^{-1}.

Proposed mechanism

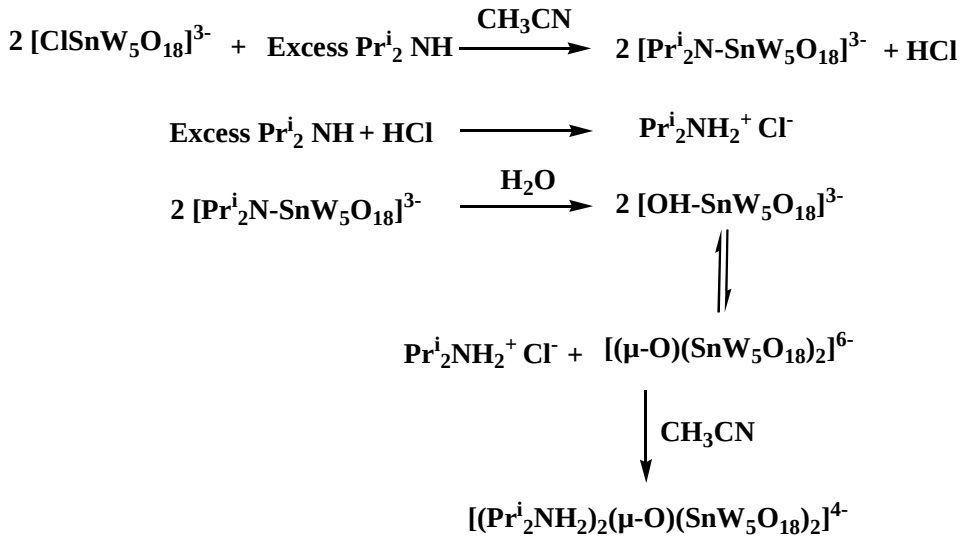

Fig. 4.20: Proposed mechanism of $[(^{i}Pr_2NH_2)_2(\mu\text{-}O)(SnW_5O_{18})_2]^{4-}$ formation

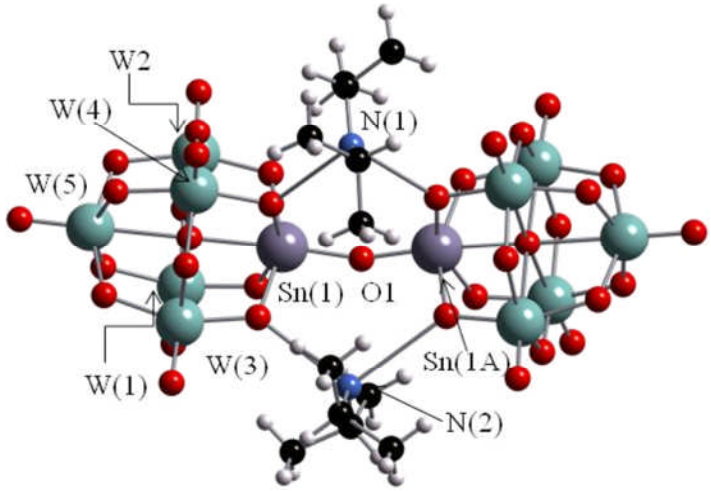

Fig.4. 21: Structure of associated species $[(^{i}Pr_2NH_2)_2(\mu\text{-}O)(SnW_5O_{18})_2]^{4-}$. The colour codes are as follows: W (pale green), O (red), Sn (pale grey), C(black), N(blue).

Sn(1)-O(1)	1.929	Sn(1)-O1-Sn(1A)	154.019
Sn(1A)-O(1)	1.902	Sn(1)-O1-W(5)	180.000
Sn(1)-Sn(1A)	3.733	Sn(1)-Ob-W(1)	113.614
Sn(1)-Oc	2.244	Sn(1)-Ob-W(3)	112.353

Table 4.11: selected bond lengths (Å) and bond angles (°) of $[(^{i}Pr_2NH_2)_2(\mu\text{-}O)(SnW_5O_{18})_2]^{4-}$

4.10. Attempted synthesis of Di-tin tetratungstate species

We attempted the preparation of a di-tin tetratungstate species, in order to provide two reactive sites for extended aggregation to polymerise di-tin tetratungstate species, *via* the organic bridging ligand i.e. $-OC_6H_4O-$ by using resorcinol **8,** hydroquinone **9** or inorganic bridging ligands i.e. O^{2-} by using hydrolysis and condensation. A polymer would form if the di-tin are positioned *cis* or *trans* to one-another in the metal oxide framework Such species are versatile and possibly could be used to prepare extended metal oxide strucutres in solution, but this would require a strict maintenance of the reaction conditions, e.g. the stoichiometry, temperature, and the duration of the reaction. The preparation of such species could provide active polynuclear building blocks and would allow assembling building blocks *via* inorganic ligand, and this kind of building block would create many more varieties of compounds.

Recently, Erringtion and co workers successfully synthesised a *cis* - di titanium tetratungstate species [22] with three methoxide groups $[(MeO)_3Ti_2W_4O_{16}]^{3-}$. Based on the solid state structure, two methoxide groups are directly attached to the titanium metal center and the remaining methoxide group is present on the bridging position. We adapted the same stoichiometry and synthetic conditions in an attempt to synthesise a di-tin-tetratungstate species as shown below.

$$\mathbf{2Sn(O^tBu)_4 + 2[Bu^n{}_4N]_2WO_4 + 2WO(OMe)_4 + 7H_2O \longrightarrow}$$

$$\mathbf{[Bu^n{}_4N]_4[(MeO)_2Sn_2W_4O_{17}] + 14\ ROH} \qquad \text{----8}$$

$$\mathbf{R=Bu^t,\ Me}$$

$Sn(OBu^t)_4$ and TBA_2WO_4 were dissolved in acetonitrile and transferred to tungsten oxymethoxide. The reaction was hydrolysed with 10% ^{17}O-enriched water and was heated at 85-90 °C to form a pale yellow solution. Pale yellow single crystals were obtained by slow vapour diffusion and these were used for characterisation and an X-ray crystal structure determination.

We expected to observe only three signals in the ^{17}O NMR spectrum for a *trans* – $Sn_2W_4O_{16}$ rather than six signals observed in $(TBA)_3$ **1** but the ^{17}O NMR of this novel compound is very similar to $(TBA)_3$ **1**. The ^1H NMR spectrum also showed one single resonance at 3.6 ppm for methoxide protons. Most of the data supports the formation of $(TBA)_3$ **1.** Further work is needed to characterise the products from this reaction.

Summary

The novel heterometallic Lindqvist type POMs with reactive Sn-X (X=MeO, OH, Cl) have been successfully synthesised and reactivity studies been carried out with various alcohols and phenols. All the alkoxido and aryloxido derivatives were characterised by single crystal X-Ray diffraction, ^{1}H and multinuclear NMR spectroscopy, infra red spectroscopy and CHN analysis. Smaller alkyl groups and di functional phenol derivatives gave *trans* disordered structures. However, no disorder is present when we introduce bulkier aliphatic alkoxide or aryloxide groups.

The attempted synthesis of species with extended Sn^{IV}-O-Sn^{II}-O-Sn^{IV} linkages by reacting $(TBA)_3$ $[(OH)SnW_5O_{18}]$ with $Sn\{N(SiMe_3)_2\}_2$ produced the unexpected product $[(Me_3SiO)SnW_5O_{18}]^{3-}$ **11**. The O-H bond in $[(OH)SnW_5O_{18}]^{3-}$ was expected to be acidic but it proved to be basic and it easily react with most acidic sites in $Sn\{N(SiMe_3)_2\}_2$ (Si rather than Sn). However, the mechanism was not completely understood in solution. An attempted synthesis of $[O_{18}W_5Sn\text{-}N(SiMe_3)_2]^{3-}$ by reacting $(TBA)_3$ **1** with $HN(SiMe_3)_2$ leads to the same product **11**.

We are currently investigating the metathesis reactivity of $(TBA)_3[ClSnW_5O_{18}]$ with various lewis acids ($AgBF_4$, HBF_4) and solvents (H_2O, Pyridine) and found that it readily react with $Pr^{i}{}_2NH$, lithium diisopropylamide (LDA). However, the Sn-N bond is moisture sensitive and hydrolyses to give an oxo-bridged specices which interacts with the $^{+}H_2N^{i}Pr_2$ cation to produce the associated species, $[(^{i}Pr_2NH_2)_2(\mu\text{-}O)(SnW_5O_{18})_2]^{4-}$.

Experimental section

Synthesis of $(TBA)_3[(EtO)SnW_5O_{18}]$

$(TBA)_3$ $[(MeO)SnW_5O_{18}]$ (0.778 g, 0.373 mmol) in dry acetonitrile (15-20 cm^3) was treated with 100 fold excess of dry ethanol (2.2 cm^3, 37.3 mmol) and heated at 85-90 ^oC for overnight. Volatiles were removed in *vacuo*, the residue was redissolved in acetonitrile (15-20 cm^3) and the treatment with dry ethanol was repeated twice more. After cooling to room temperature, all volatile impurities were removed in *vacuo*, and the product was washed with dry ether (3×20 cm^3).

Recrystallisation: The crude product (0.747 g) was redissolved in a small amount of acetonitrile (2-3 cm^3) and an ether layer (20 cm^3) was added. Colourless crystals (0.707 g, 90%) formed upon diffusion and were carefully separated by filtration. The crystals were washed with ether (3×20 cm^3), dried under vacuum and were used for characterisation.

Data: ^1H NMR (500 MHz, CD_3CN): δ 1.19, $^4J\{^{119}Sn^1H\}$ = 4.2 Hz, [t, 3H, $OCH_2C\boldsymbol{H_3}$], 3.8 $^3J\{^{119}Sn^1H\}$ = 69.6 Hz, $^3J\{^{117}Sn^1H\}$ = 66.6 Hz, [q, 2H, $OC\boldsymbol{H_2}CH_3$]. ^{13}C $\{^1H\}$ (100.53 MHz, CD_3CN): 19.94, $^2J\{^{119}Sn^{13}C\}$ = 34.5 Hz ($-CH_2\boldsymbol{C}H_3$), 60.6, $^3J\{^{119}Sn^{13C}\}$ = 35.45 Hz, ($-\boldsymbol{C}H_2CH_3$). ^{17}O NMR (67.81 MHz, CD_3CN): δ 725, 684 (W=O), 395 (Sn-O-W) 382, 368 (W-O-W) 17.4 (μ_6-O). ^{119}Sn $\{^1H\}$ NMR (186.5 MHz, CD_3CN): δ -651 ppm. $^2J\{^{119}Sn^{183}W\}$ = 39.8 Hz. ^{183}W NMR (20.84 MHz, CH_3CN): 74.7 ($4W_{eq}$), -129. 6(W_{ax}). FTIR (Nujol mull): 2729m, 2409m, 1655m, 1378s, 1309vw, 1152m, 1097m, 1058m, 1027m, 953s, 885m, 803s, 758s, 625m, 569m, 429s. Elemental analysis Found: C, 27.32; H, 5.41; N, 1.99. $C_{50}H_{113}N_3O_{19}SnW_5$ requires C, 28.61; H, 5.42; N, 2.00.

Synthesis of $(TBA)_3[(^iPrO)SnW_5O_{18}]$

$(TBA)_3$ $[(MeO)SnW_5O_{18}]$ (0.771 g, 0.370 mmol) in dry acetonitrile (15-20 cm^3) was treated with a 100 ~ fold excess of dry isopropanol (2.83 mL, 37 mmol) and heated at 85-90 ^oC overnight. Volatiles were removed in *vacuo*, the residue was redissolved in acetonitrile (15-20 cm^3) and the treatment with dry isopropanol was repeated twice more. After cooling to room temperature, all volatile impurities were removed in vacuo and the residue was washed twice with dry ether.

Recrystallisation: The crude product was redissolved in minimal amount of acetonitrile (2-3 cm^3) and an ether layer (20 cm^3) was added. The pure colourless crystals (0.628 g, 79 %) were formed upon slow vapour diffusion and were carefully separated by filtration. The crystals were washed with ether (3 × 20 cm^3) and dried under vacuum.

Data: ^{1}H NMR (500 MHz, CD_3CN): δ 1.16, $^4J\{^{119}Sn^1H\}$ = 3.3 Hz, (d, 6H, -HC(C***H*****$_3$**$)_2$). 4.23, $^3J\{^{119}Sn^1H\}$ = 57.3 Hz $^3J\{^{117}Sn^1H\}$ = 54.9 Hz, (s, C***H***$(CH_3)_2$). ^{13}C $\{^1H\}$ (100.53MHz, CD_3CN): δ 26.7 (s, HC(***C***$H_3)_2$), $^3J\{^{119}Sn^{13}C\}$ = 34.5 Hz, 66.1 (s, -H***C***$(CH_3)_2$), $^3J\{^{119}Sn^{13}C\}$ = 35.5 Hz. ^{17}O NMR (67.81 MHz, CD_3CN): δ 726, 684 (W=O), 396 (Sn-O-W) 383, 367 (W-O-W) 17.7 (μ_6-O). ^{119}Sn NMR $\{^1H\}$ (186.5 MHz, CD_3CN) : δ -654 ppm $^2J^3J\{^{119}Sn^{183}W\}$= 39.86 Hz. ^{183}W NMR (20.84 MHz, CH_3CN): 74.5 (W_{eq}), -128. 3 (W_{ax}). FTIR (Nujol mull): 2728m, 1662w, 1377s, 1152m, 1124w, 1026w, 953s, 884m, 803s, 758s, 623m,569m, 430s. Elemental analysis: Found: C, 27.87; H, 5.21; N, 2.00. $C_{51}H_{115}O_{19}N_3SnW_5$ requires C, 28.99; H, 5.48; N, 1.98 %

Synthesis of $(TBA)_3[(^tBuO)SnW_5O_{18}]$

$(TBA)_3$ $[(MeO)SnW_5O_{18}]$ (0.749 g, 0.360 mmol) in dry acetonitrile (20 cm^3) was treated with a 100~ fold excess of dry tert- butanol (3.42 mL, 36 mmol) and heated at 85-90 ^oC for overnight. Volatiles were removed under reduced pressure, the residue was redissolved in acetonitrile (20 cm^3) and the treatment with dry tert- butanol was repeated twice more. After cooling to room temperature, all volatile impurities were removed in *vacuo,* and the residue washed twice with dry ether.

Recrystallisation: The crude product (0.723 g) was redissolved in a minimal amount of acetonitrile (3 cm^3) and an ether layer (20 cm^3) was added. The pure colourless crystals (0.576 g, 75.3 %) were formed upon slow vapour diffusion and were carefully separated by filtration. The crystals were washed with ether (3 × 20 cm^3), and dried under vacuum.

Data: ^{1}H NMR (500 MHz, CD_3CN): δ 1.29, $^4J\{^{119}Sn^1H\}$ = 2.4 Hz, (s, 9H, OC(C***H*****$_3)_3$**). ^{13}C $\{^1H\}$ (100.53 MHz, CD_3CN): δ 32.7 (s, OC(***C***$H_3)_3$), δ 71.5 (s, O***C***$(CH_3)_3$), $^3J\{^{119}Sn^{13}C\}$ = 32.5 Hz. ^{17}O NMR (67.81 MHz, CD_3CN): δ 725, 683 (W=O), 396 (Sn-

O-W), 382, 368 (W-O-W)17.6 (μ_6-O). ^{119}Sn {^{1}H} NMR (186.5 MHz, CD_3CN): δ -663 ppm $^2J\{^{119}Sn^{183}W\}$= 40.31 Hz. ^{183}W NMR (20.84 MHz, CH_3CN): 71.8 (W_{eq}), -126. 7 (W_{ax}). FTIR (Nujol mull): 2727 m, 1669m, 1195s, 1153m, 1056m, 1027m, 952s, 885m, 800s, 755s, 624 m, 564m, 425s. Elemental analysis: Found: C, 30.2; H, 5.92; N, 2.01. $C_{52}H_{117}O_{19}N_3SnW_5$ requires: C, 29.37; H, 5.55; N, 1.97 %

$(TBA)_3[(C_6H_5O)SnW_5O_{18}]$

A mixture of phenol (0.035 g, 0.366 mmol) and $(TBA)_3[(MeO)SnW_5O_{18}]$ (0.694 g, 0333 mmol) in acetonitrile (15 cm^3) was stirred for 24 h at 85-90 ^{o}C (oil bath temperature) forming a bright yellow solution. After cooling to room temperature, volatiles were removed *in vacuo,* and the sticky yellow product was washed with THF (2 x 20 cm^3), toluene (2 x 20 cm^3) and ether (2 x 20 cm^3).

Recrystallisation: The pale yellow powder was dissolved in acetonitrile (3 cm^3) and ether (15 cm^3), and was diffused slowly at room temperature to yield yellow single crystals (0.586 g, 82%).

Data: ^{1}H NMR (500 MHz, CD_3CN): δ 6.8, 7.0, 7.2 (5H, $C_6\boldsymbol{H}_5$) ^{13}C {^{1}H} (100.53 MHz, CD_3CN): δ 161, 129, 120 and 118.8 ($\boldsymbol{C}_6H_4$). ^3J {^{119}Sn^{13}C} = 31.6 Hz. ^{17}O NMR (67.81 MHz, CD_3CN): δ 723, 689 (W=O), 397 (Sn-O-W) 385, 361 (W-O-W) 15.8 (μ_6-O). ^{119}Sn {^{1}H} NMR (186.5 MHz, CD_3CN): δ -673 ppm $^2J\{^{119}Sn^{183}W\}$ = 45.56 Hz. ^{183}W NMR (20.84 MHz, CH_3CN): 77.4 (W_{eq}), -124. 1 (W_{ax}). FTIR (Nujol mull): 2729m, 2303m, 1593m, 1378s, 1282m, 1260s, 1073w, 1027w, 957s, 884m, 804s, 755s, 621m,608m 572m, 432s. Elemental analysis: Found: C, 29.42; H, 5.38; N, 1.95. $C_{54}H_{113}O_{19}N_3SnW_5$ requires C, 30.22; H, 5.30; N, 1.96 %

$(TBA)_3[(p\text{-}CH_3\text{-}C_6H_4O)SnW_5O_{18}]$

A solution of *p*-cresol (48.4 mg, 0.448 mmol) in acetonitrile was added to a solution of $(TBA)_3[(MeO)SnW_5O_{18}]$ (0.848 g, 0.407 mmol) in acetonitrile (15 cm^3) via cannula with constant stirring. The resultant solution was heated at 85-90 ^{o}C for about 28-30 hrs. A yellow solution was formed and allowed to cool to room temperature. All the volatile impurities were removed *in vacuo* and the yellow sticky product was washed with ether (2 x 20 cm^3) forming a pale yellow powder.

Recrystallisation: The crude powder (0.784 g) was recrystallised from acetonitrile (2 cm^3) and ether (15 cm^3) by diffusion at room temperature. Yellow single crystals were obtained (0.72 g, 82 %) and X-ray crystal structure determined

Data: ^{1}H NMR (500 MHz, CD_3CN): δ 6.85, 6.89 (4H, $C_6\boldsymbol{H}_4$) 2.24 (s, 3H, $C\boldsymbol{H}_3$) ^{13}C {^{1}H} (100.53 MHz, CD_3CN): 158, 129.3, 127.7, 119.9 ($\boldsymbol{C}_6H_4$) and 19.7 (-$\boldsymbol{C}H_3$) ppm. $^3J\{^{119}Sn^{13}C\}$= 30.7, ^2J $\{^{119}Sn^{13}C\}$ = 30.7. ^{17}O NMR (67.81 MHz, CD_3CN): δ 722, 688 (W=O), 396 (Sn-O-W) 385, 361 (W-O-W) 17.4 (μ_6-O). ^{119}Sn {^{1}H} NMR (186.5 MHz, CD_3CN): δ -674 ppm $^2J\{^{119}Sn^{183}W\}$ = 47.50 Hz. ^{183}W NMR (20.84) MHz, CH_3CN): 78.9 (W_{eq}), -122.8 (W_{ax}). FTIR (Nujol mull): 2729m, 1608m, 1508s, 1378s, 1272m, 1258m, 1153w, 1028w, 957s,885m, 802s, 751s, 619m, 569m, 519w, 431s. Elemental analysis: Found C, 30.29; H, 5.37; N, 2.06 % $C_{52}H_{117}O_{19}N_3SnW_5$ requires C, 30.58; H, 5.36; N, 1.94 %

$(TBA)_3[(p\text{-}Bu^tC_6H_4O)\text{-}SnW_5O_{18}]$

A solution of *p*-t-butyl phenol (0.025 g, 0.166 mmol) in acetonitrile was added to a solution of $(TBA)_3[(MeO)SnW_5O_{18}]$ (0.314 g, 0.151 mmol) in acetonitrile (15 cm^3) via cannula with constant stirring. The resultant solution was heated at 85-90 ^oC for about 64 hrs. A yellow solution was formed and allowed to cool to room temperature. All the volatile impurities were removed *in vacuo* and the yellow sticky product was washed with THF (2 x 20 cm^3), toluene (1 x 20 cm^3) and ether (2 x 20 cm^3) forming a pale yellow powder.

Recrystallisation: The crude powder was recrystallised from acetonitrile (3 cm^3) and ether (15 cm^3) by diffusion at room temperature. Yellow single crystals were obtained (0.269 g, 81 %) and X-ray crystal structure determined.

Data: ^{1}H NMR (500 MHz, CD_3CN): δ 6.83, 6.87, 7.19, 7.33 (4H, $C_6\boldsymbol{H}_4$) 1.29 (s, 9H, $C(C\boldsymbol{H_3})_3$) ^{13}C {^{1}H} (100.53 MHz, CD_3CN): δ 158.3, 141.3, 125.6 and 119.4 ($\boldsymbol{C}_6H_4$) δ 31.94 ($C(\boldsymbol{C}H_3)_3$) and 34.8 ($\boldsymbol{C}(CH_3)_3$). $^2J\{^{119}Sn^{13}C\}$ = 34.51 Hz, 60.6 (-$\boldsymbol{C}H_2CH_3$) ^3J $\{^{119}Sn^{13}C\}$ = 35.45 Hz. ^{17}O NMR (67.81 MHz, CD_3CN): δ 723, 689 (W=O), 396 (Sn-O-W) 386, 362 (W-O-W) 16.5 (μ_6-O). ^{119}Sn {^{1}H} NMR (186.5 MHz, CD_3CN) : δ -673 ppm $^2J\{^{119}Sn^{183}W\}$ = 45.56 Hz. ^{183}W NMR (20.84 MHz, CH_3CN): 76.7 (W_{eq}), -121. 6 (W_{ax}). FTIR (Nujol mull): 2727m,, 1603m, 1509s, 1377s, 1256m, 1183m, 1152m, 1108m, 1068w, 1026w, 956s, 884m, 803s, 754s, 696m, 622m, 570s.

Elemental analysis: Found C, 32.02; H, 5.36; N, 1.99. $C_{58}H_{121}N_3O_{19}SnW_5$ requires C, 31.62; H, 5.53; N, 1.9 %

$(TBA)_3[(m\text{-}HO\text{-}C_6H_4\text{-}O)SnW_5O_{18}]$

A mixture of $(TBA)_3[(MeO)SnW_5O_{18}]$ (0.767 g, 0.368 mmol) and resorcinol (0.045 g, 0.405 mmol) in acetonitrile (15 cm^3) was stirred for 65 h at 85-90 ^oC (oil bath temperature) forming a clear yellow solution. After cooling to room temperature, volatiles were removed in *vacuo* and the sticky yellow product was washed with THF (4 x 20 cm^3) and ether (2 x 20 cm^3).

Recrystallisation: The crude product was dissolved in acetonitrile (5 cm^3) and ether (15 cm cm^3) was allowed to diffuse slowly at room temperature. Golden yellow single crystals (0.619 g, 77.8 %) were obtained and X-ray crystal structure determined.

Data: ^1H NMR (500 MHz, CD_3CN): δ 6.26, 6.46, 6.49, 6.96 (4H,$C_6\boldsymbol{H}_4$), 6.86 (bs, 1H, O***H***) ^{13}C {^1H} (100.53 MHz, CD_3CN): δ 162.0, 129.2, 111.9 and 107.0 ($\boldsymbol{C_6}H_4$). ^{17}O NMR (67.81 MHz, CD_3CN): δ 725, 691 (W=O), 398 (Sn-O-W) 387, 357.6 (W-O-W) 15.3 (μ_6-O). ^{119}Sn {^1H} NMR (186.5 MHz, CD_3CN): δ -672 ppm, $^2J\{^{119}Sn^{183}W\}$ = 48.95 Hz. ^{183}W NMR (20.84 MHz, CH_3CN): 76.5 (W_{eq}), -123.1 (W_{ax}). FTIR (Nujol mull): 3255br, 2728m, 1661w, 1580m, 1377s, 1295w, 1253w, 1142s, 1107w, 1057w, 1026w, 953s, 885w, 899s, 748s, 619m, 569m, 427m. Elemental analysis: Found: C, 29.60; H, 5.3; N, 2.04. $C_{54}H_{113}N_3O_{20}SnW_5$ requires C, 29.99; H, 5.26; N, 1.94 %

$(TBA)_3[(p\text{-}HO\text{-}C_6H_4\text{-}O)SnW_5O_{18}]$

A mixture of $(TBA)_3[(MeO)SnW_5O_{18}]$ (0.603 g, 0.290 mmol) and hydroqunione (0.067 g, 0.609 mmol) in acetonitrile (15 cm^3) was stirred for 91 h at 85-90 ^oC (oil bath temperature) forming a red colour solution. After cooling to room temperature, volatiles were removed in *vacuo* and the sticky product was washed with toluene (2 x 20 cm^3) and ether (2 x 20 cm^3).

Recrystallisation: The crude product was dissolved in acetonitrile (3 cm^3) and acetonitrile/ether mixture layer (15/15 cm^3) was allowed to diffuse slowly at room temperature. Pale yellow single crystals (0.468 g, 74.6%) were obtained and X-ray crystal structure determined.

Data: ^{1}H NMR (500 MHz, CD_3CN): δ 6.62, 6.68 (4H, $C_6\boldsymbol{H}_4$), 6.46 (bs, 1H, O***H***) ^{13}C {^{1}H} (100.53 MHz, CD_3CN): δ 153.67, 149.7, 119.47 and 115.33 ($\boldsymbol{C}_6H_4$). ^{17}O NMR (67.81 MHz, CD_3CN): δ 723, 689 (W=O), 398 (Sn-O-W) 386, 363 (W-O-W) 16.7 (μ_6-O). ^{119}Sn {^{1}H} NMR (186.5 MHz, CD_3CN): δ -674 ppm $^{2}J\{^{119}Sn^{183}W\}$ = 51.24 Hz. ^{183}W NMR (20.84 MHz, CH_3CN): 76.4 (W_{eq}) -122.8 (W_{ax}). FTIR (Nujol mull): 3294br, 2726m, 1377s, 1307w, 1238w, 1153m, 1027w, 955s, 885w, 805s, 754s, 624m, 570w, 432s. Elemental analysis: Found: C, 30.32; H, 5.39; N, 2.01. $C_{54}H_{113}O_{20}N_3SnW_5$ requires C, 29.99; H, 5.26; N, 1.94 %

$[Bu^{n}_4N]_3[(2\text{-}CHO\text{-}C_6H_4O)\text{-}SnW_5O_{18}]$

A solution of salicyaldehyde (0.58 ml, 0.542 mmol) in acetonitrile (5 cm^3) was added to the solution of $(TBA)_3[(MeO)SnW_5O_{18}]$ (0.974 g, 0.467 mmol) in acetonitrile (15 cm^3) *via* cannula with constant stirring. The resultant solution was heated at 85-90 ^{o}C for 48 hrs. A yellow solution formed was allowed to cool and cooled to room temperature. Volatile impurities were removed in *vacuo* and the yellow sticky product was washed with ether (2 x 20 cm^3) forming a very pale yellow powder.

Recrystallisation: The yellow colour crude product (0.708 g) was recrystallised from acetonitrile (2 cm^3) and ether (15 cm^3) by diffusion at room temperature. White colour single crystals were obtained (0.628 g, 61.8 %) and X-ray crystal structure determined.

Data: ^{1}H NMR (500 MHz, CD_3CN): δ 6.90, 7.24, 7.48, 7.65 (4H, $C_6\boldsymbol{H}_4$) 10.56 (s, 1H, -C***H***O) ^{13}C {^{1}H} (100.53 MHz, CD_3CN): 164.8, 135.6, 126.65, 122.9, 119.3 ($\boldsymbol{C}_6H_4$) and 190.8 (-***C***HO). ^{17}O NMR (67.81 MHz, CD_3CN): δ 725, 691 (W=O), 398 (Sn-O-W) 387, 357.6 (W-O-W) 15.3 (μ_6-O). ^{119}Sn {^{1}H} NMR (186.5 MHz, CD_3CN) : δ -672 ppm $^{2}J\{^{119}Sn^{183}W\}$ = 48.95 Hz. ^{183}W NMR (20.84 MHz, CH_3CN): 79.1 (W_{eq}), -120.6 (W_{ax}). FTIR (Nujol mull): 2728 m,1679 m,1597 m,1378 s,1315 m,1247 m,1308 vw,1240 m,1153 m,1027 m,958 s,884 m,802 s,751 s,617 m,573 m,527 m,432 s. Elemental analysis: Found: C, 29.50; H, 5.61; N, 2.1. $C_{55}H_{113}O_{20}N_3SnW_5$ requires C, 30.38; H, 5.24; N, 1.93 %

Synthesis of $(TBA)_3[(Me_3SiO)SnW_5O_{18}]$

a) Slight excess of hexamethyldisilazane (HMDS) (40μL, 0.192 mmol) was added directly to $(TBA)_3$ $[(MeO)SnW_5O_{18}]$ (0.363 g, 0.174 mmol) in acetonitrile by syringe

and the resulting solution was stirred for 58 hrs at 85-90 ^{o}C (oil bath temperature). After cooling to room temperature, volatile impurities were removed in *vacuo*, and the sticky yellow colour product was washed with ether (2 x 20 cm^3)

Recrystallisation: The yellow colour crude product was recrystallised from acetonitrile (3 cm^3) and ether (15 cm^3) by diffusion at room temperature. Yellow single crystals were obtained (0.278 g, 74.5 %) and X-ray crystal structure determined.

b) A solution of $Sn[N(SiMe_3)_2]_2$ (0.088g, 0.200 mmol) in toluene was transferred *via* cannula to solution of $(TBA)_3[(HO)SnW_5O_{18}]$ (0.828 g, 0.400mmol) in acetonitrile. The mixture was stirred for 48 hrs at 85-90 ^{o}C (oil bath temperature) forming a green colour solution. After cooling to room temperature, volatile impurities were removed in *vacuo*, the sticky dark green colour product was washed with ether (2 x 20 cm^3)

Recrystallisation: The green colour crude product was recrystallised from acetonitrile (3 cm^3) and ether (15 cm^3) by diffusion at room temperature. Yellow single crystals were obtained (0.759 g, 88.5 %) and X-ray crystal structure determined.

Data: ^{1}H NMR (500 MHz, CD_3CN): δ 0 (s, 9H, $OSi(C\boldsymbol{H_3})_3$] $^{4}J\{^{119}Sn^{1}H\}$ = 1.3 Hz, $^{2}J\{^{29}Si^{13}C\}$ = 6.8 Hz, $^{1}J\{^{13}C^{1}H\}$= 2.3 Hz. ^{13}C $\{^{1}H\}$ (100.53 MHz, CD_3CN): 21.82 ($-OSi(\boldsymbol{C}H_3)_3$) $^{2}J\{^{119}Sn^{29}Si\}$ = 22.45 Hz. ^{17}O NMR (67.81 MHz, CD_3CN): δ 720, 684 (W=O), 395 (Sn-O-W) 383, 368 (W-O-W) 16.5 (μ_6-O). ^{29}Si NMR (99.36 MHz, CD_3CN): δ 9.9 $^{2}J\{^{119}Sn^{29}Si\}$ = 22.45 Hz. ^{119}Sn $\{^{1}H\}$ NMR (186.5 MHz, CD_3CN) : δ -669 ppm $^{2}J\{^{119}Sn^{183}W\}$ = 45.56 Hz. ^{183}W NMR (20.84 MHz, CH_3CN): 73.18 (W_{eq}), -127.9 (W_{ax}). FTIR (Nujol mull): 2728 m, 1669 m, 1243s, 1152 s, 1107 m, 1056m, 1027 m, 952 s, 799 s, 751 s, 622 m, 566 m, 426 bs. Elemental analysis: Found: C, 27.92; H, 5.39; N, 2.12. $C_{51}H_{117}O_{19}N_3SiSnW_5$ requires C, 28.59; H, 5.50; N, 1.96 %

Reaction between $TBA_3[ClSnW_5O_{18}]$ and $AgBF_4$ in CH_2Cl_2/CH_3CN:

$AgBF_4$ in CH_2Cl_2/CH_3CN was transferred to $(TBA)_3[ClSnW_5O_{18}]$. After addition, white colour precipitate was formed immediately. The mother liquor was filtered and the solid was washed with further MeCN (5mL) and allowed to settle over 72 hrs. The mother liquor again was filtered and combined with earlier, and it was concentrated. All the solvent was removed in *vacuo* and then redissolved in CH_3CN and submitted for ^{119}Sn NMR spectroscopy. Set up for vapour re-crystallisation using CH_3CN/Et_2O.

Data: ATR: 3344 vw, 2963 s, 2875 s, 1665 s, 1483 m, 1382 s, 1051 s, 958 s, 800 s, 706 w, 568 w. $^{119}Sn\{^{1}H\}$ NMR (186.5 MHz, CH_3CN): δ -678, -696 ppm.

Reaction between $[Bu_4^n]_3$ $[ClSnW_5O_{18}]$ and Na/Hg amalagam in MeCN

A solution of $(TBA)_3[ClSnW_5O_{18}]$ in CH_3CN was added to Na/Hg amalgam and stirred. Light green colour was formed initially and it changed light blue in colour upon heating. The resultant solution was allowed to stir at room temperature overnight. All the solvent was removed in *vacuo* and the crude product was washed ether couple of times, and examined by ^{119}Sn NMR spectroscopy.

Data: $^{119}Sn\ \{^{1}H\}$ NMR (186.5 MHz, CD_3CN): δ -609 ppm.

Synthesis of $(TBA)_4[(^{i}Pr_2NH_2)_2(\mu\text{-}O)(SnW_5O_{18})_2]$

A mixture of $(TBA)_3[ClSnW_5O_{18}]$ (0.613 g, 0.294 mmol) and 35 fold excess diisopropyl amine $^{i}Pr_2NH_2$ (1.44 cm^3, 10.274 mmol) in acetonitrile (20 cm^3) was stirred for 52-64 h at 85-90 ^{o}C (oil bath temperature) forming a pale pink solution. After cooling to room temperature, volatiles were removed in *vacuo* and the sticky yellow product was washed with ether (2 x 20 cm^3).

Recrystallisation: The crude pink product was dissolved in acetonitrile (5 cm^3) and ether (15 cm^3) was allowed to diffuse at room temperature. Pale pink colour crystals (0.759, 88.5 %) were obtained and X-ray crystal structure determined.

Data: ^{1}H NMR (500 MHz, CD_3CN): δ 8.85 (bs, 2H, -N**H₂**$CH(CH_3)_2$], 3.45 (sept, 2H, -NH_2C**H**$(CH_3)_2$, 1.14 (t, 12H, -$NH_2CH(C$**H₃**$)_2$). ^{13}C {1H} (100.53 MHz, CD_3CN): 47.39 (-***C***$H(CH_3)_2$) 19.09 (-$CH($***C***$H_3)_2$). ^{17}O NMR (67.81 MHz, CD_3CN): δ 725, 691 (W=O), 398 (Sn-O-W) 386, 365 (W-O-W) 19.5 (μ_6-O). $^{119}Sn\ \{^{1}H\}$ NMR (186.5 MHz, CD_3CN) : δ -659 ppm $^{2}J\{^{119}Sn^{183}W\}$ = 39.86 Hz, $^{2}J\{^{119}Sn^{117}Sn\}$ = 256 Hz. ^{183}W NMR (20.84 MHz, CH_3CN): 71.8 (W_{eq}), -121.7 (W_{ax}). FTIR (Nujol mull): 3435 vw, 2874 s, 2726, m, 1378 m, 1152 m, 952 vs, 798 s, 748 s, 722 s, 614 s, 568s. ATR data: 2960s, 2874s, 1482s, 1381 m, 1152 m, 953vs, 794s, 750s, 717s, 611s, 567s. Elemental analysis: Found: C, 25.92; H, 4.89; N, 2.48. $C_{80}H_{176}N_8O_{37}Sn_2W_{10}$ requires C, 24.52; H, 4.52; N, 2.86 %

Attempted preparation of di- tin tetratungstates

$(TBA)_4[(MeO)_2Sn_2W_4O_{17}]$

Q_2WO_4 (0.535 g, 0.73 mmol) and $Sn(O^tBu)_4$ (0.30 g, 0.73 mmol) in acetonitrile were transferred to $[\{WO(MeO)_4\}_2]$ (0.237 g, 0.73 mmol) in acetonitrile. The resultant solution was stirred for 2 hrs at 85-90 °C. ^{17}O-enriched water (210 μL, 11.66 mmol) was added to reaction mixture for partial hydrolysis and the solution was stirring for 24 hrs at 85-90 °C (oil bath temperature). The reaction was stopped and cooled to room temperature.

Recrystallisation: At room temperature the volume of the mother liquor was reduced to 50 % and ether layer (33 cm^3) was allowed to diffuse slowly into the solution to obtain single colourless crystals (3.89 g, 61%).

Data: ^{1}H NMR (500 MHz, CD_3CN): δ 3.64 (s, 3H, -OC***H*$_3$**), ^{119}Sn {^{1}H} NMR (186.5 MHz, CD_3CN): δ -647 ppm. ^{17}O NMR (67.81 MHz, CD_3CN): δ 720, 684, 396, 382, 363, 17.

References

1) R. Cao, K. P. O'Halloran, D. A. Hillesheim, K. I. Hardcastle and C. L. Hill. *Cryst Eng Comm*, **2010**, 12, 1518-1525

2) W. H. Knoth, P. J. Domaille and R. D. Farlee, *Organometallics*, 1985, 4, 62–68

3) F. Xin, M. T. Pope, G. J. Long and U. Russo, *Inorg. Chem*, **1996**, 35, 1207–1213

4) G. Sazani, M. H. Dickman and M. T. Pope, *Inorg. Chem*, **2000**, 39, 939–943.

5) F. Hussain and U. Kortz, *Chem. Commun*, **2005**, 1191–1193.

6) F. Hussain, M. Reicke and U. Kortz, *Eur. J. Inorg. Chem*, **2004**, 2733–2738.

7) F. Xin and M. T. Pope, *Organometallics*, **1994**, 13, 4881–4886.

8) L. F. Piedra-Garza, M. H. Dickman, O. Moldovan, H. J. Breunig and U. Kortz, *Inorg. Chem*, **2009**, 48, 411–413.

9) S. Reinoso, M. H. Dickman, A. Praetorius, L. F. Piedra-Garza and U. Kortz, *Inorg. Chem*, **2008**, 47, 8798–8806

10) M. T. Pope and A. Muller *Polyoxometalates: From Platonic Solids to Anti-retroviral Activity*, ed., Kluwer, Dordrecht, The Netherlands, 1994.

11) N. Belai and M. T. Pope., *Polyhedron*, **2006**, 25, 2015-2020.

12) R. J. Errington, S. S. Petkar, P. S. Middleton, W. McFarlane, W. Clegg, R. A. Coxall, and R. W. Harrington, *Dalton Trans*, **2007**, 5211

13) R. J. Errington, S. Petkar, P. S. Middleton, W. McFarlane, W. Clegg, R. A. Coxall, and R. W. Harrington, *J. Am. Chem. Soc*, **2007**, 129, 12181–12196.

14) E. L.Torres, A. R. Cowley, J. R. Dilworth, *Inorganic chemistry communications*, **2007**, 10, 724-727.

15) M. J .H. Smith, E. Smith and E. N. Duesler, *Inorg.Chem*., **1982**, *28***,** 3399.

16) M. J. H. Smith, T. Wark. A. Rheingold, J. C. Huffman, *Can. J. Chem.* **1991**, *69*, 121-129.

17) C. C. Camacho, R. Contreras, H. North, M. Bechmann, A. Sebald, W. Milius and B. Wrackmeyer. *Magn.Reson.Chem*, **2002**, 40, 31-40.

18) a) J. A. Fernandez, X. Lopez and J. M. Poblet, *J. Mol. Catal. A: Chem*, **2007**, 262, 236 b) X. Lopez, C. Bo and J. M. Poblet, *J. Am. Chem. Soc*, **2002**, 124, 12574.

19) R. J. Errington *et. al*, Unpublished results.

20) R. J. Errington *et. al*, Unpublished results.

21) W. Clegg, M. R. J.Elsegood, R. J. Errington and J. Havelock, *J.Chem.Soc.,Dalton Trans.*, **1996**, 681-690.

22) R. J. Errington *et. al*, Unpublished results.

Chapter 5

Immobilisation of Titanium Alkoxides and SnW_5 Polyoxometalates on Functionalised Si(111) Surfaces

Chapter 5: Immobilisation of Titanium Alkoxides and SnW_5 Polyoxometalates on Functionalised Si(111) Surfaces.

5.1. Introduction

The self assembly of organic monolayers on surfaces has developed much in the past 25 years, although self assembled inorganic monolayers have received much less attention. Several groups around the world have been investigating the incorporation of POMs onto surface confined structures. This chapter describes the preliminary studies of the immobilisation of mononuclear metal alkoxides and alkoxo derivatised Lindqvist polyoxometalates ~ 30% hydroxy functionalised silicon surfaces.

Klemperer *et.al* [1] initially developed an approach to construct monolayers of POMs on various surfaces. They prepared monolayers by immersing the Au(111) and Ag(111) surfaces in to acidic solutions of silicotungstate $[SiW_{12}O_{40}]^{4-}$ and characterised the products by Scanning Tunnelling Microscopy (STM). This was followed by Errington *et.al* [2], who successfully attached mono functionalised alkoxido TiW_5 Lindqvist type POMs on functionalised silicon surfaces. These POM species were obtained by hydrolytic aggregation of metal alkoxides, and were readily accessible for surface reactions as confirmed by reacting with various protic reagents (H_nX). These species easily react with robust, alkanol derivatised Si(111) surfaces, and provided the first demonstration of covalent attachment of POMs to a Si surface. The basic principle was that reactive POMs easily bind to functionalised surfaces with small molecule elimination.[3]

Ordered monolayers have been obtained on silver and gold surfaces by adsorption from solution, whilst evaporative deposition has also been used to produce catalytically active POM layers on highly orientated pyrolytic graphite (HOPG).[4] Coranado *et.al* reported that hybrid organic POM multilayer magnetic structures could be synthesised by using Langmuir–Blodgett techniques [5] while electrostatic layer-by-layer assembly has produced very robust structures. Langmuir-Blodgett deposition of monolayers from a gas-liquid interface to a planar, substrate support, provide well-ordered, closely packed mono- and multilayer systems. However, monolayers of this type tend to be mechanically unstable, held together by weak van der Waals forces.[6] V.Cabuil *et.al* [7] reported the covalent attachment of thiol derivatised POMs on gold nanoparticles.

Our interest is to develop low energy methods to assemble metal oxide networks on functionalised surfaces by using a surface sol-gel process which it relates to Atomic Layer Deposition. (ALD)

5.2. Atomic Layer Deposition

ALD is one of the processes used for the formation of oxide thin films on surfaces and has received much attention recently because of the potential application in various fields such as micro electronics, optics. etc. ALD had already been developed and introduced worldwide with the name Atomic Layer Epitaxy (ALE) in the late 1970's. It was originally developed for fabrication of polycrystalline luminescent ZnS:Mn and amorphous Al_2O_3 insulator films for electroluminescent flat panel displays.[8] ALD method is a special modification of Chemical Vapour Deposition (CVD) with the distinct feature that film growth takes places in cyclic manner and breaks the CVD reaction into two half reactions, keeping the precursor materials separate during the reaction. The growth of material layers by ALD consist of four consecutive steps. [9]

1) Exposure of the first precursor,

2) purge the reaction chamber,

3) Exposure of the second precursor, and

4) a further purge the reaction chamber.

These four steps are repeated many times as required for the desired film thickness. The film thickness obtained per cycle may depend on the size of the precursor molecule. Monolayer growth per cycle easily can be achieved when expose the small molecules to reaction chamber and in addition the number of adsorption sites also affects the amount of molecules adsorbed.

Precursor chemistry plays a key role in ALD. Generally precursors must of course be volatile in nature and thermally should be stable but they may be gases, liquids or solids. The precursor molecules chemisorbs or react with the surface groups saturatively, and after the formation of the chemisorbed layer no further adsorption takes place. [10] The desired ALD reactions should have a large negative ΔG value, but unfortunately thermodynamic data are available only for a limited number of precursors.

5.2.1. Types of precursors

The number of precursors and reactions used in ALD is high as can be seen from the recent reviews made by M. Leskala *et.al* [9,11] and the precursors can be classified into two types.

a) Non-metallic precursor e.g: H_2O, H_2S, NH_3 and AsH_3.

b) Metallic precursor e.g: metal halides, metal alkyls, metal alkoxides and metal β – diketonates.

Both precursors show different features and properties. The non-metallic precursors are usually hydrides and no difficulty in volatility and thermal stability. Reactivity at low temperatures and formation of suitable surface species for the metal precursor to be anchored, are properties of H_2O and H_2S has already established and has been reported several times. Metal halides especially chlorides have been widely used for ALD process. Various group around the world introduced many different types of metal precursors such as metal β – diketonates, [12,13] cyclopentadienyl [14, 15] in ALD and they have been used in deposition of both alkaline earth titanate and sulphide films.

As we mentioned earlier, our interest is to develop low energy methods to assemble metal oxide networks on functionalised surfaces by using a surface sol-gel process. Metal alkoxides $Ti(OPr^i)_4$, bulk metal oxoalkoxides i.e. $Ti_{12}O_{16}(OPr^i)^{16}$ and reactive POM, $[(MeO)SnW_5O_{18}]^{3-}$ have been used for this work. Here we are developing methods for chemisorption of the mononuclear functional alkoxido POMs, metal alkoxides to Si surfaces. In this approach, it is assumed that Si-O-M bonds will be relatively stable compared to C-O-M bonds and further surface sol-gel process would be carried out on Si surfaces. This process not only controls the thickness limit of the conventional sol-gel method but also helps us to design the internal structure of the layer.

In our efforts, we are trying to synthesise the single, monolayer metal oxide network on ~ 30% OH-functionalised Si (111) surfaces and only preliminary studies of surface chemistry is discussed in the following section, and due to lack of time, we could not able to do reactivity studies of polynuclear metal oxoalkoxides i.e. $Ti_{12}O_{16}(OPr^i)_{16}$.

5.3. Results and discussion

Precursors

$Ti(OPr^i)_4$ was used for preliminary studies of metal alkoxide immobilisation and was purchased from Sigma Aldrich. The monoalkoxido derivatised Lindqvist type POM was synthesised by hydrolytic aggregation method as discussed in Chapter 3, and the mono functional alkoxido group is readily available to make covalent attachment on ~ 30% functionalised Si(111) surface, however, initial experiments only have been carried out with these precursors, which have characterised by atomic force microscopy (AFM).

5.3.1. Synthesis of ~ 30% OH functionalised Si(111) surfaces

Y.J.Chabal *et.al* [16] reported that immersion of atomically smooth H/Si(111) surfaces in neat anhydrous CH_3OH at 65 ^oC for 12 hrs yielded high quality surfaces with ~30% of a monolayer Si-OCH_3 moieties, each being surrounded by six nearest-neighbour Si-H sites. The distance between the surface Si atoms was calculated as 3.8 Å. At elevated temperatures, methoxo groups easily coordinate to H-functioanlised Si (111) surface though the effects of steric hindrance from surrounding surface Si-H sites, only 33% surface Si-OCH_3 monolayer coverage was observed. Treatment of the Si-OCH_3 monolayer with 40% aq HF solution provides F-Si(111) layers, which can interconverted by immersion in water, to OH/Si monolayers. These OH/Si(111) wafers were used as a template for these studies.

5.3.2. Reaction with metal alkoxides

$Ti(OPr^i)_4$ (5 mM) was diluted in toluene (20 cm^3) and was heated with ~ 30% hydroxyl functionalised Si(111) surface. After being heated for two hrs at elevated temperatures, the Si(111) was washed with dry toluene (20 cm^3) twice. The Si(111) was carefully analysed by AFM. The elevated temperatures (80 ^oC) aided in attaching one of the alkoxide groups on to the Si(111) surface and the rate of hydrolysis was expected to be very slow compare to hydrolysis in solution. Further hydrolysis of free alkoxide groups on the surface leads reactive M-OH groups. We are assuming that a metal oxide network will be formed if we allow M-OH sites to react further with metal alkoxides. The systematic representation of metal oxide formation is shown in the

Figure 5.1 and the AFM image was taken after reaction of Si(111) surface with metal alkoxide, and shown in the Figure 5.2.

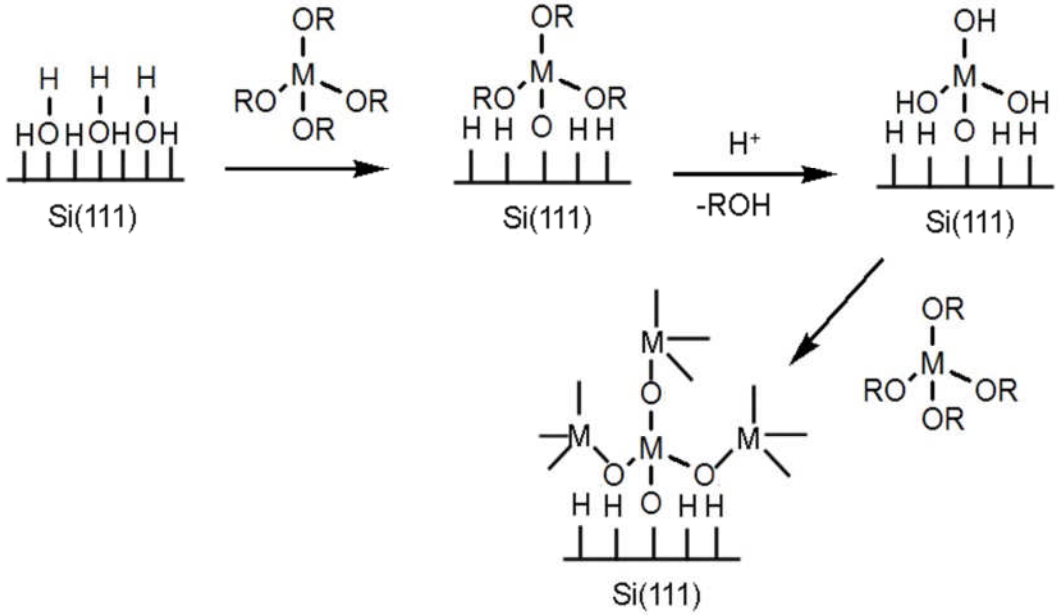

Fig. 5.1: Possible mechanism for the metal oxide formation on ~30% hydroxyl functionalised Si(111) surfaces. $M(OR)_4$ where M=Ti.

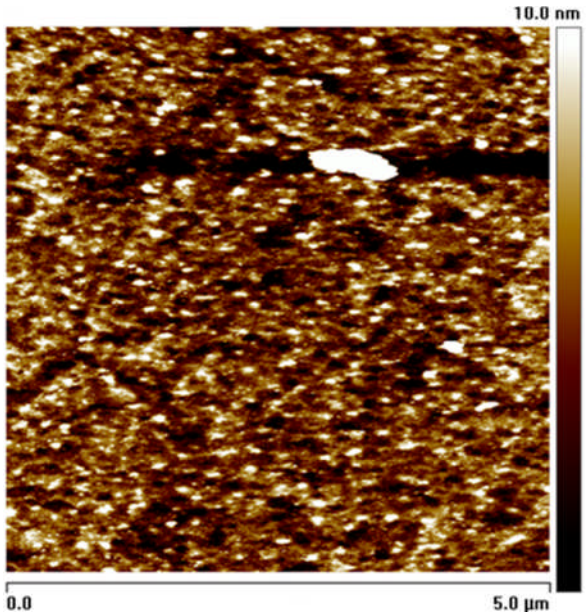

Fig 5.2: AFM image of $Ti(OPr^i)_4$ on Si(111) surfaces.

rms roughness = 3.38 nm (over 5x5 μm^2 area)

mean roughness = 1.94 nm (over 5x5 μm^2 area)

The AFM image showed dense coverage of the surface with numerous spots of varying size (white features densely populating the AFM image), suggesting that one or more alkoxide groups may be hydrolysed by surface OH groups. At the atomic level, chemical modification of the surface occurs through the formation of Si-C, Si-O occasionally Si-N bonds. The stability of these 'first bonds' determines the stability of the interface and the electrical performance. The Si-O bond is very stable compared to the Si-C bond from a thermodynamic point of view and chemical functionalisation based on Si-O linkages are ubiquitous in surface adsorbed monolayer (SAM) applications.[17] Errington *et.al* [2] successfully attached the heterometallic Lindqvist $[(MeO)TiW_5O_{18}]^{3-}$ POM onto undecanol derivatised Si(111) surface and found that the C-O-Ti bond is not particularly stable at high temperatures towards trace hydrolysis. In our efforts, we tried to attach the metal alkoxides to Si(111) surfaces through Si-O-M linkages, where we expected a stronger bond to Ti metal center to be formed. However the mechanism of stepwise adsorption and hydrolysis is not yet clearly understood.

5.3.3. Reaction with polyoxometalate

The ~30% OH-Si(111) wafers were prepared according to literature procedure and were used as a template for POM studies.

A similar type of reaction was carried out at elevated temperatures with methoxo derivatised tin POMs. The schematic representation of attachment of POMs on Si surfaces is shown in the following equation and Figure 5.3

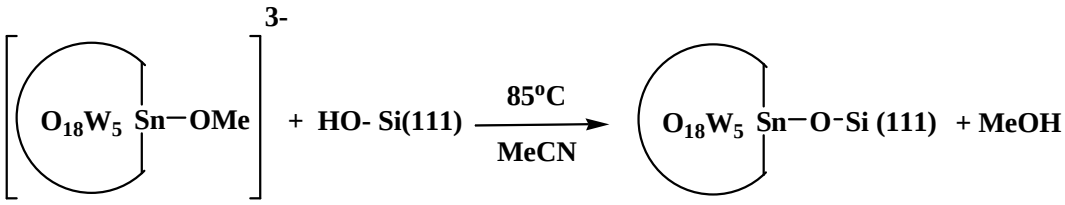

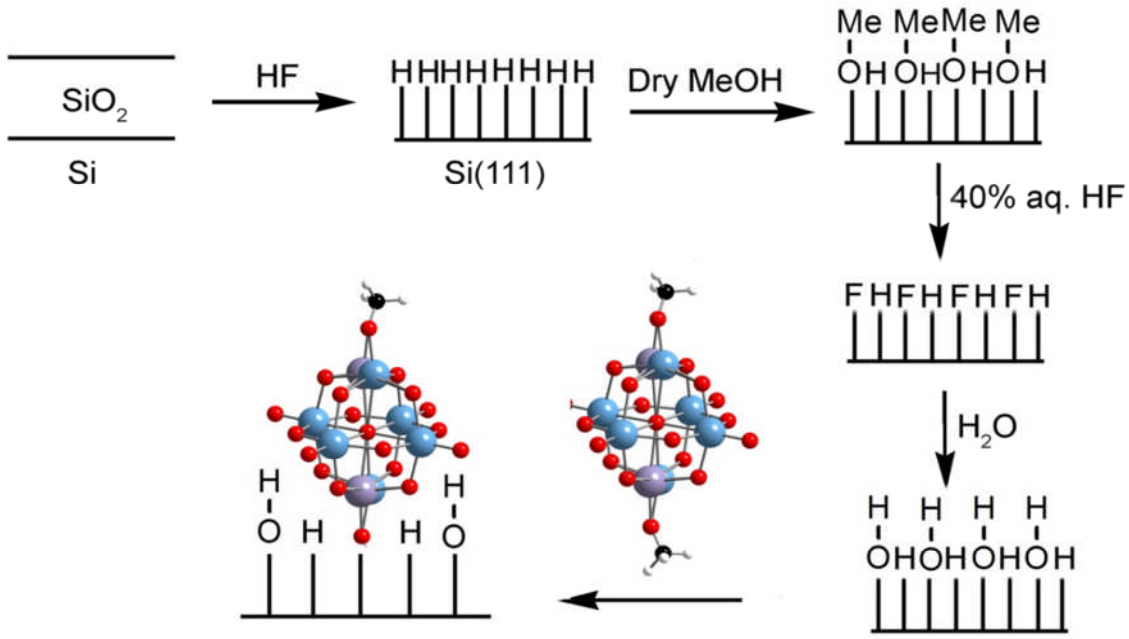

Fig 5.3: Schematic representation of chemisorptions of $[(MeO)SnW_5O_{18}]^{3-}$ on OH-Si(111) surfaces.[**Note**: $[(MeO)SnW_5O_{18}]^{3-}$ anion was *trans* disordered]

We might expect the POMs to be more visible by scanning probe microscopy and to reflect the density of OH groups on the surface. At elevated temperatures (85-90 ^oC), the methoxido tin POMs were allowed to react with OH functionalised Si (111) surfaces and polyoxometalates are expected to attach to the Si surfaces. $(TBA)_3$ **1** undergoes exchange reactions with protic reagents (H_nX) and produces various aliphatic and aromatic derivatives. The methoxido tin polytungstate easily reacted with OH functionalised Si (111) surfaces and was expected to form a strong bond to Si surfaces with elimination of methanol.

After heating 10 µM solutions of $[(MeO)SnW_5O_{18}]^{3-}$ with OH/Si(111) surfaces at elevated temperatures for about 2 hrs, the Si wafers were then washed with excess CH_3CN, dried under N_2, before characterisation by AFM.

AFM images showed extensive coverage of the OH/Si(111) surface by particulate structures, assumed to be stannotungstates. Cross section analysis of the particulates, showed them to range in height from 12-14 nm.

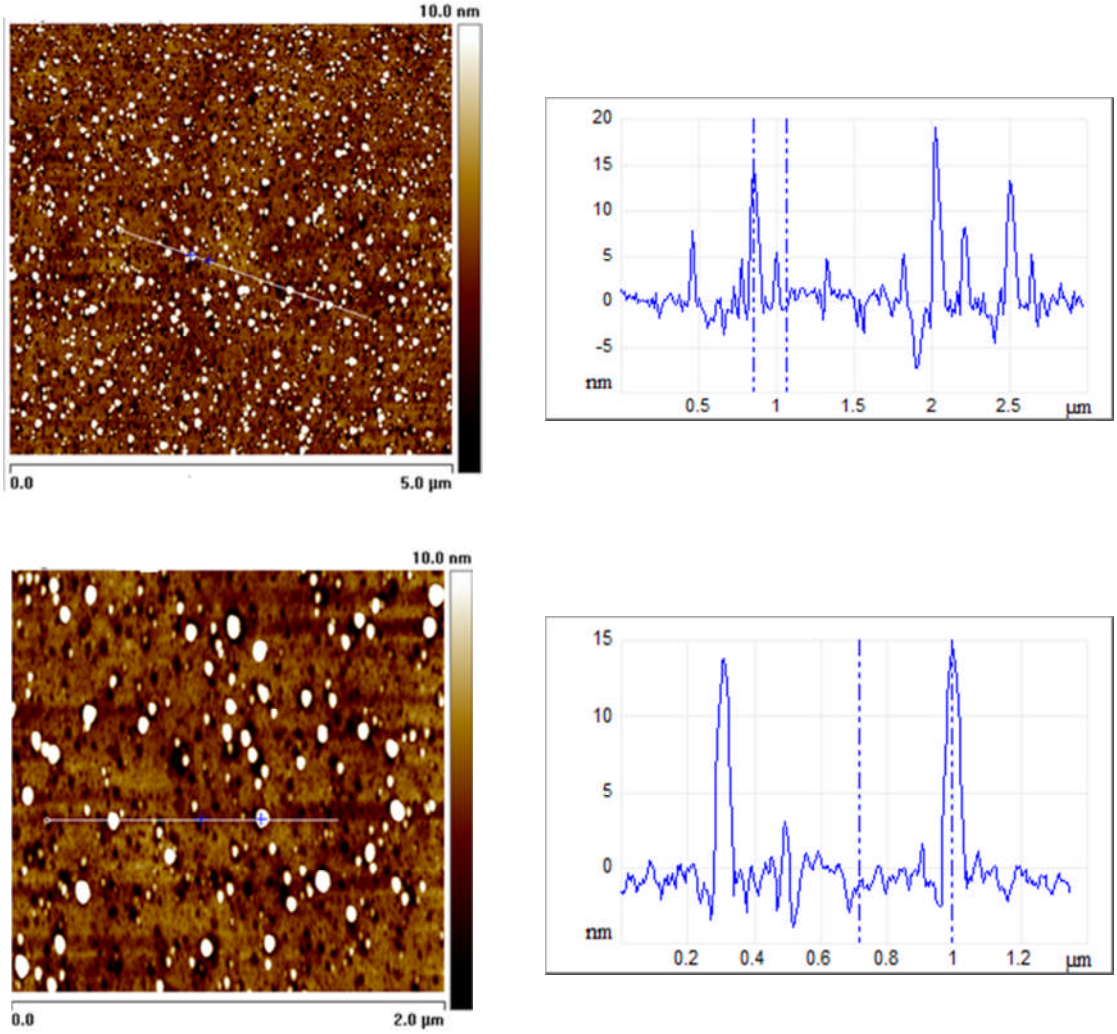

(a) (b)

Fig 5.4: AFM image of $[(MeO)SnW_5O_{18}]^{3-}$ on Si(111) surfaces a) 5 µm and 2 µm b) Cross section of images.

Note the values related to surface roughness stated here will be slightly increased due to the pitted nature of the underlying substrate (*i.e.* the dark brown patches in the image will most likely be pits/holes in the substrate)

rms square roughness = 2.40 nm (measured over 5x5 μm^2 area)

mean roughness = 1.41nm (measured over 5x5 μm^2 area)

The molecular diameter of anion **1** is ~ 8 Å from the X-ray crystal structure determination. White coloured spots were observed in Figure 5.4 and were assumed to be $[(MeO)SnW_5O_{18}]^{3-}$. Cross section of these spots suggested to us that the distance between the POM and the surface is 12-14 nm. Some dense spots were observed in all the AFM images. The possible reason could be that because of width of the AFM tip

the cross section value of POMs are higher than expected (8 Å). However, the complete mechanism is not yet clearly understood.

5.4. Synthesis of $Ti_{12}O_{16}(OPr^i)_{16}$

Klemperer *et.al* [18] successfully synthesised α–$Ti_{12}O_{16}(OPr^i)_{16}$ cluster molecule which was readily made by adding titanium iso-propoxide to an aqueous iso-propanol solution, followed by heating at 90-115 ^oC for at least 54 hrs. In our experiments, removal of solvents followed by recrystallisation in hexanes yielded 18-21% of the α_1 cluster. This material has characteristic ^{17}O and ^{13}C NMR spectra and single crystal X-Ray diffraction which can be used to identify it from the α_1-$Ti_{12}O_{16}(OPr^i)_{16}$ cluster and related $Ti_{11}O_{13}(OPr^i)_{18}$. The $Ti_{12}O_{16}(OPr^i)_{16}$ contains 6 coordinate Ti atoms and the other half are 5 coordinate. Each molecule contains two μ_3-O lignads that bridge three 6 coordinate Ti atoms, 12 μ-O lignads that bridge one 6 coordinate and two 5 coordinate Ti atoms, and two μ_2-O lignads that bridge two 6-coordinate Ti atoms. Further it also contains four μ_2-(OPr^i)- ligands that bridge two 6-coordiante Ti atoms and 12-terminally- bonded (OPr^i) ligands.

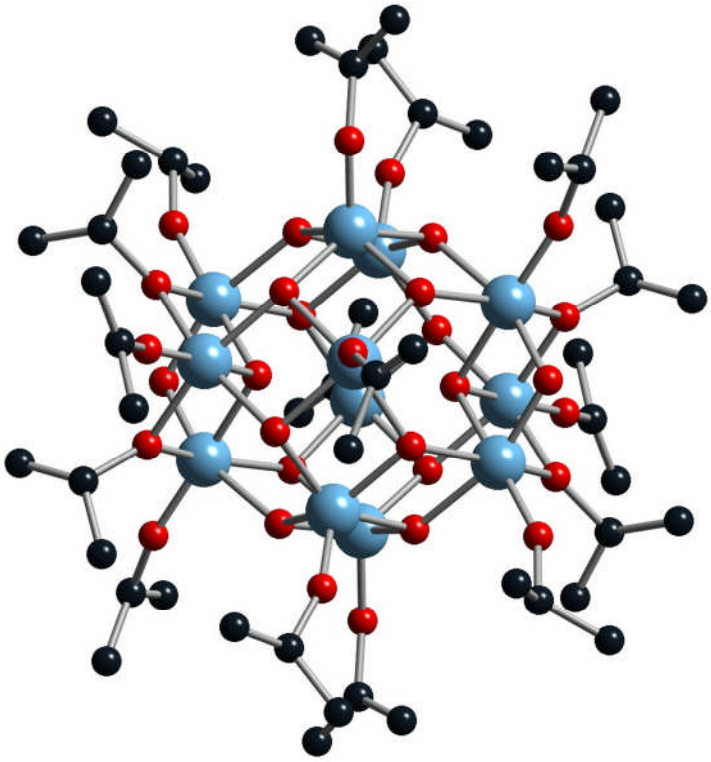

Fig: 5.5. Crystal structure of $Ti_{12}O_{16}(OPr^i)_{16}$ molecule. The colour codes are as follows: Ti (blue), O (red), C(black).

Klemperer *et.al* confirmed that the surface atlkoxo groups were readily available for exchange reaction. Errington *et.al* [19] carried out preliminary experiments to replace surface alkoxo groups by aromatic phenols, however phenol did not replace the isopropoxo group. Instead, phenol coordinated on the cluster surface and the crystal structure was not refined due to high degree of disorder of the isopropoxy groups.

Generally, 5 coordinate Ti atoms are expected to be more reactive than 6 coordinate Ti atoms. In reactions with ~30% OH functionalised Si(111) surface one or two 5 coordinate Ti atoms would be expected to react with the Si surface. In principle, stepwise hydrolysis could then be performed at the immobilised Ti_{12} units on the Si surfaces in order to synthesise a metal oxide network.

Experimental section

Synthesis of ~ 30% OH functionalised surface

The silicon wafers (phosphorus-doped, n-type, 1-12 Ω cm resistivity, 0.1 deg. miscut angle, Virginiac semiconductors InC, VA) with <111> orientation, were cut into (1 cm x 1 cm) pieces and cleaned with acetone and deionized water (Millipore, 18 MΩ cm) for 2 minutes each. A clean oxide layer was formed by immersing the silicon chips in freshly prepared 'pirhana' solution (1:4 v/v conc. H_2SO_4 and 30% H_2O_2) for 1 hr at 80 °C. The chips were placed vertically for etching 40% w/v aqueous NH_4F for 15 minutes. After this purging with N_2 removed the oxide over the silicon surface and hydrogen terminated surface was formed. The chips were dried under N_2 then further treated with dry methanol ($15cm^3$) for 12 hrs. The MeO-Si(111) chips were dried under N_2 again then vertically placed for etching 40% HF for 15 minutes. The methoxy layer was then reacted with HF, fluoride layer was formed. This is followed by, the F-Si(111) chips were further treated with deionized water for 2 minutes (Millipore, 18 MΩ cm) and blown dry with N_2 and was used for subsequent surface reactions.

Reacting $Ti(OPr^i)_4$ with ~30% functionalised (111) Si-OH in acetonitrile

A solution of excess $Ti(OPr^i)_4$ (0.5 ml, 1.7 mmol) in acetonitrile was prepared and 20 cm^3 of alkoxide solution was added to ~ 30 % OH functionalised silicon (111) - OH chips. The reaction was refluxed for 2 hrs at 85- 90 °C (oil bath temperature). The chips were taken out of the reaction mixture at an ambient temperature and washed with dry acetonitrile and further dried under N_2 before AFM characterisation.

Reacting $[(MeO)SnW_5O_{18}]^{3-}$ with ~30% functionalised (111) Si-OH in acetonitrile

A solution of $[(MeO)SnW_5O_{18}]^{3-}$ **3.1** (0.002 g, 10 μ mol) in acetonitrile was prepared and 20 cm^3 of stock solution **3.1** was added to ~ 30 % OH functionalised silicon (111) - OH chips. The reaction was heated under reflux for 2 hrs at 85- 90 °C (oil bath temperature). The chips were taken out of the reaction mixture at an ambient temperature and washed with dry acetonitrile and further dried under N_2 before AFM characterisation.

Preparation of α_1 – $[Ti_{12}O_{16}(OPr^i)_{16}]$

$Ti(OPr^i)_4$ (12.0 g, 42.2 mmol) was added slowly down the side of a schlenk flask onto a solution of iso-propanol (16 cm^3) and water (0.78 cm^3, 43.3 mmol) resulting in a two-layer system. The flask was then shaken vigorously for *ca* 30 seconds to obtain a hazy suspension. After one week the suspension was heated to 100-115 ^oC for 54 hrs before removing the solvents under vacuum to obtain clear, colourless oil. Extraction with hexanes (20 cm^3) and storage at -30 ^oC for two weeks yielded a colourless crystalline solid. This was collected by filtration, washed with acetone N_2 cooled hexanes and dried in *vacuo*.

Yield: 1.32 g, 21.1 %.

Data: **FTIR:** 2960s, 2830s, 1455 (sh), 1445s, 1370s, 1360s, 1325m, 1160(sh), 1130s, 1010s, 950m, 850m, 680(br), 565s, 515s and 465s cm^{-1}. **NMR:** (CD_5CD_3, 500 MHz) 5.64 (mult, 5H), 5.20-4.80 (multiplets, 11H), 2.20-1.80 (doublets, 40H) and 1.80-1.40 (doublets, 55H). ^{13}C (CD_5CD_3, 100.53 MHz): 81.29, 80.93, 80.52, 78.07, 77.26, 27.23, 26.93, 26.61, 26.47, 26.09 and 25.92.

References

1) W. G. Klemperer and C. G. Wall, *Chem.Rev*, **1998**, 98, 297-306.

2) R. J. Errington, S.S.Petkar, B. R. Horrocks, A. Houlton, L. H. Lie, and S. N. Patole., *Angew. Chem. Int. Ed*, **2005**, 44, 1254 –1257.

3) A. R. Pike, B. R. Horrocks, A. Houlton, *Angew. Chem. Int. Ed.* **2002**, 41, 4.

4) a) B. Keita, L. Nadjo, *Surf. Sci. Lett*. **1991**, 254, L443. b) M. S. Kaba, I. K. Song, D. C. Duncan, C. L. Hill, M. A. Barteau, *Inorg. Chem*.,**1998**, 37, 398. c) M. A. Barteau, J. E. Lyons, I. K. Song, *J. Catal*, **2003**, 216, 236.

5) E. Coronado and C. J.G. Garcla., *Chem.Rev*, **1998,** 98, 273-296.

6) S. Liu, G. D. Kurth, B. Bredenkotter, D. Volkmer, *J. Am. Chem. Soc*. **2002**, 124, 12 279.

7) a) C. R. Mayer, S. Neveu, V. Cabuil, *Angew. Chem.* **2002**, 114, 519; b) *Angew. Chem. Int. Ed*., **2002**, 41, 501.

8) T. Suntola, J. Antson, U.S.Patent 4,058,430, **1977**.

9) M. Ritala, M. Leskela in *Handbook of Thin Film Materials, Vol.1* (Ed: H.S.Nalwa), Academic Press, San Diego, **2001**, pp.103-106.

10) M. Leskela and M. Ritala, *Thin Solid Films*, **2002**, 409, 138-146.

11) M. Leskela and M. Ritala, J.Phys.IV 9, 1999, pp.8-837.

12) M. Putkonen, T. Sajavaara, L-S. Johansson, L. Niinisto, *Chem,Vap.Depos*, **2001**, 7, 44.

13) M. Nieminen, M. Putkonen and L. Niinisto, *Appl.Surf.Sci*, **2001**, 174, 155.

14) M. Vehkamaki, T. Hatanpaa, T. Hanninen, M. Ritala, M. Leskela, *Electrochem.Solid state Lett*, **1999**, 2, 504.

15) J. Ihanus, T. Hanninen, T. Hatanpaa, T. Aaltonen, I. Mutikainen, T. Sajavaara, J. Keininen, M. Ritala and M. Leskela, *Chem.Mater.,* **2002**, 12, 14 (5), 1937-1944.

16) D. J. Michalak, S. R. Amy, D. Aureau, M. Dai, A. Esteve and Y. J. Chabal, *Nature materials*, **2010**, 9, 266-271.

17) D. J. Michalak, S. R. Amy, A. Esteve and Y. J. Chabal, *J.Phys.Chem.C,* **2008**, 112, 11907-11919.

18) V. W. Day, T. A. Eberspacher, W. G. Klemperer and C. W. Park., *J.Am.Chem.Soc,* **1993**, 115, 8469-8470.

19) R. J. Errington and J. Ridland *et.al*, Unpublished results.

Appendix

Crystallographic Data

$PhCH_2N(CH_3)_3[Sn_2(OMe)_9]$

Chemical formula (total)	$C_{19}H_{43}NO_9Sn_2$	
Formula weight	666.92	
Temperature	150(2) K	
Radiation, wavelength	MoKα, 0.71073 Å	
Crystal system, space group	triclinic, $P\bar{1}$	
Unit cell parameters	a = 8.0314(2) Å	α = 82.878(2)°
	b = 11.5736(3) Å	β = 81.018(2)°
	c = 15.0665(5) Å	γ = 77.938(2)°
Cell volume	1346.69(7) $Å^3$	
Z	2	
Calculated density	1.645 g/cm^3	
Absorption coefficient μ	1.898 mm^{-1}	
F(000)	672	
Crystal colour and size	colourless, 0.40 × 0.40 × 0.30 mm^3	
Reflections for cell refinement	13635 (θ range 3.0 to 29.5°)	
Data collection method	Oxford Diffraction Gemini A Ultra diffractometer thick-slice ω scans	
Index ranges	h −10 to 10, k −16 to 14, l −20 to 20	
Completeness to θ = 26.0°	99.8 %	
Reflections collected	22253	
Independent reflections	6677 (R_{int} = 0.0264)	
Reflections with $F^2>2\sigma$	5422	
Absorption correction	semi-empirical from equivalents	
Min. and max. transmission	0.5174 and 0.5998	
Structure solution	direct methods	
Refinement method	Full-matrix least-squares on F^2	
Weighting parameters a, b	0.0245, 0.0067	
Final R indices [$F^2>2\sigma$]	R1 = 0.0207, wR2 = 0.0460	
R indices (all data)	R1 = 0.0301, wR2 = 0.0478	
Goodness-of-fit on F^2	1.021	
Largest and mean shift/su	0.002 and 0.000	

$\{Nb(OMe)_4Cl\}_2$

Chemical formula (total)	$C_8H_{24}Cl_2Nb_2O_8$	
Formula weight	504.99	
Temperature	150(2) K	
Radiation, wavelength	MoK α, 0.71073 Å	
Crystal system, space group	triclinic, $P\bar{1}$	
Unit cell parameters	a = 7.1498(6) Å	α = 98.304(7)°
	b = 7.8674(7) Å	β =109.699(7)°
	c = 8.8750(7) Å	γ =107.039(8)°
Cell volume	432.66(6) $Å^3$	
Z	1	
Calculated density	1.938 g/cm^3	
Absorption coefficient μ	1.660 mm^{-1}	
F(000)	252	
Crystal colour and size	colourless, 0.32 × 0.20 × 0.20 mm^3	
Reflections for cell refinement	2610 (θ range 2.8 to 29.5°)	
Data collection method	Oxford Diffraction Gemini A Ultra diffractometer thick-slice ω scans	
θ range for data collection	2.8 to 29.5°	
Index ranges	h –7 to 9, k –10 to 10, l –12 to 11	
Completeness to θ = 26.0°	99.9 %	
Reflections collected	3664	
Independent reflections	2013 (R_{int} = 0.0264)	
Reflections with $F^2>2\sigma$	1772	
Absorption correction	semi-empirical from equivalents	
Min. and max. transmission	0.6186 and 0.7325	
Structure solution	direct methods	
Refinement method	Full-matrix least-squares on F^2	
Weighting parameters a, b	0.0306, 0.0000	
Data / restraints / parameters	2013 / 0 / 96	
Final R indices [$F^2>2\sigma$]	R1 = 0.0258, wR2 = 0.0606	
R indices (all data)	R1 = 0.0319, wR2 = 0.0622	

Goodness-of-fit on F^2	1.051
Extinction coefficient	0.0090(14)
Largest and mean shift/su	0.000 and 0.000
Largest diff. peak and hole	0.47 and –0.47 e $Å^{-3}$

$Sb(O^iPr)_5.NH_3$

Chemical formula (total)	$C_{15}H_{38}NO_5Sb$	
Formula weight	434.21	
Temperature	150(2) K	
Radiation, wavelength	MoKα, 0.71073 Å	
Crystal system, space group	monoclinic, $P12_1/n1$	
Unit cell parameters	a = 8.64700(10) Å	α = 90°
	b = 19.5728(2) Å	β=94.3750(10)°
	c = 12.7405(2) Å	γ = 90°
Cell volume	2150.00(5) $Å^3$	
Z	4	
Calculated density	1.341 g/cm^3	
Absorption coefficient μ	1.302 mm^{-1}	
F(000)	904	
Crystal colour and size	colourless, 0.34 × 0.30 × 0.30 mm^3	
Reflections for cell refinement	10335 (θ range 2.9 to 29.4°)	
Data collection method	Xcalibur, Atlas, Gemini ultra	
	thick-slice ω scans	
θ range for data collection	2.9 to 29.5°	
Index ranges	h –8 to 11, k –26 to 18, l –14 to 17	
Completeness to θ = 26.0°	99.8 %	
Reflections collected	12712	
Independent reflections	5193 (R_{int} = 0.0168)	
Reflections with $F^2>2\sigma$	4609	
Absorption correction	semi-empirical from equivalents	
Min. and max. transmission	0.6659 and 0.6961	
Structure solution	direct methods	
Refinement method	Full-matrix least-squares on F^2	
Weighting parameters a, b	0.0223, 0.4349	
Data / restraints / parameters	5193 / 0 / 222	
Final R indices [$F^2>2\sigma$]	R1 = 0.0163, wR2 = 0.0403	
R indices (all data)	R1 = 0.0203, wR2 = 0.0411	
Goodness-of-fit on F^2	1.033	

Extinction coefficient	0.00110(17)
Largest and mean shift/su	0.001 and 0.000
Largest diff. peak and hole	0.38 and –0.33 e $Å^{-3}$

$(TBA)_3[(MeO)SnW_5O_{18}]$

Chemical formula (total)	$C_{49}H_{110}N_3O_{19}SnW_5$	
Formula weight	2083.34	
Temperature	150(2) K	
Radiation, wavelength	MoKα, 0.71073 Å	
Crystal system, space group	monoclinic, C12/c1	
Unit cell parameters	a = 29.5923(8) Å	α = 90°
	b = 18.6180(3) Å	β =113.067(3)°
	c = 27.2820(7) Å	γ = 90°
Cell volume	13829.2(6) $Å^3$	
Z	8	
Calculated density	2.001 g/cm^3	
Absorption coefficient μ	8.701 mm^{-1}	
F(000)	7976	
Crystal colour and size	colourless, 0.42 × 0.40 × 0.40 mm^3	
Reflections for cell refinement	15286 (θ range 3.0 to 28.5°)	
Data collection method	Xcalibur, Atlas, Gemini ultra	
	thick-slice ω scans	
θ range for data collection	3.2 to 26.0°	
Index ranges	h –29 to 36, k –22 to 19, l –33 to 33	
Completeness to θ = 26.0°	97.3 %	
Reflections collected	31417	
Independent reflections	13241 (R_{int} = 0.0344)	
Reflections with $F^2>2\sigma$	8975	
Absorption correction	semi-empirical from equivalents	
Min. and max. transmission	0.1211 and 0.1285	
Structure solution	direct methods	
Refinement method	Full-matrix least-squares on F^2	
Weighting parameters a, b	0.0547, 0.0000	
Data / restraints / parameters	13241 / 306 / 736	
Final R indices [$F^2>2\sigma$]	R1 = 0.0418, wR2 = 0.0941	
R indices (all data)	R1 = 0.0748, wR2 = 0.1027	

Goodness-of-fit on F^2	1.007
Largest and mean shift/su	0.007 and 0.000
Largest diff. peak and hole	5.59 and –5.23 e $Å^{-3}$

$(TBA)_3[OHSnW_5O_{18}]$

Chemical formula (total)	$C_{48}H_{104}N_3O_{19}SnW_5$	
Formula weight	2065.28	
Temperature	150(2) K	
Radiation, wavelength	MoKα, 0.71073 Å	
Crystal system, space group	monoclinic, $P12_1/c1$	
Unit cell parameters	a = 24.1538(3) Å	α = 90°
	b = 16.9306(2) Å	β = 97.6760(10)°
	c = 16.6864(2) Å	γ = 90°
Cell volume	6762.56(14) $Å^3$	
Z	4	
Calculated density	2.029 g/cm^3	
Absorption coefficient μ	8.896 mm^{-1}	
F(000)	3940	
Crystal colour and size	colourless, 0.24 × 0.20 × 0.20 mm^3	
Reflections for cell refinement	30703 (θ range 2.8 to 28.5°)	
Data collection method	Xcalibur, Atlas, Gemini ultra	
	ω scans	
θ range for data collection	2.8 to 28.6°	
Index ranges	h –30 to 30, k –19 to 22, l –21 to 21	
Completeness to θ = 26.0°	98.7 %	
Reflections collected	61780	
Independent reflections	14719 (R_{int} = 0.0339)	
Reflections with $F^2>2\sigma$	10546	
Absorption correction	semi-empirical from equivalents	
Min. and max. transmission	0.2240 and 0.2692	
Structure solution	direct methods	
Refinement method	Full-matrix least-squares on F^2	
Weighting parameters a, b	0.0321, 16.3735	
Data / restraints / parameters	14719 / 0 / 706	
Final R indices [$F^2>2\sigma$]	R1 = 0.0340, wR2 = 0.0687	
R indices (all data)	R1 = 0.0622, wR2 = 0.0737	
Goodness-of-fit on F^2	1.022	

Largest and mean shift/su	0.003 and 0.000
Largest diff. peak and hole	1.29 and –1.18 e $Å^{-3}$

$(TBA)_3$ $[(EtO)SnW_5O_{18}]$

Chemical formula (total)	$C_{50}H_{113}N_3O_{19}SnW_5$	
Formula weight	2098.37	
Temperature	150(2) K	
Radiation, wavelength	MoKα, 0.71073 Å	
Crystal system, space group	monoclinic, C12/c1	
Unit cell parameters	a = 29.6464(14) Å	α = 90°
	b = 18.5757(5) Å	β =127.269(8)°
	c = 31.5454(16) Å	γ = 90°
Cell volume	13824.8(10) $Å^3$	
Z	8	
Calculated density	2.016 g/cm^3	
Absorption coefficient μ	8.705 mm^{-1}	
F(000)	8048	
Crystal colour and size	colourless, 0.40 × 0.40 × 0.40 mm^3	
Reflections for cell refinement	22056 (θ range 3.0 to 28.5°)	
Data collection method	Xcalibur, Atlas, Gemini ultra	
	thick-slice ω scans	
θ range for data collection	3.0 to 28.5°	
Index ranges	h –39 to 39, k –21 to 23, l –38 to 39	
Completeness to θ = 26.0°	98.3 %	
Reflections collected	49465	
Independent reflections	14992 (R_{int} = 0.0575)	
Reflections with $F^2>2\sigma$	10271	
Absorption correction	semi-empirical from equivalents	
Min. and max. transmission	0.1284 and 0.1284	
Structure solution	direct methods	
Refinement method	Full-matrix least-squares on F^2	
Weighting parameters a, b	0.0418, 353.2295	
Data / restraints / parameters	14992 / 15 / 759	
Final R indices [$F^2>2\sigma$]	R1 = 0.0536, wR2 = 0.1138	
R indices (all data)	R1 = 0.0877, wR2 = 0.1228	

Goodness-of-fit on F^2	1.027
Largest and mean shift/su	0.098 and 0.002
Largest diff. peak and hole	1.83 and –1.74 e $Å^{-3}$

$(TBA)_3[(Pr^iO)SnW_5O_{18}]$

Chemical formula (total)	$C_{51}H_{115}N_3O_{19}SnW_5$	
Formula weight	2112.40	
Temperature	150(2) K	
Radiation, wavelength	MoKα, 0.71073 Å	
Crystal system, space group	monoclinic, $P2_1/c$	
Unit cell parameters	a = 29.7267(5) Å	α = 90°
	b = 37.2181(9) Å	β = 67.165(2)°
	c = 27.2009(5) Å	γ = 90°
Cell volume	27735.7(10) $Å^3$	
Z	16	
Calculated density	2.024 g/cm^3	
Absorption coefficient μ	8.679 mm^{-1}	
F(000)	16224	
Reflections for cell refinement	47507 (θ range 2.9 to 29.6°)	
Data collection method	Xcalibur, Atlas, Gemini ultra	
	thick-slice ω scans	
θ range for data collection	2.9 to 25.0°	
Index ranges	h –31 to 35, k –37 to 44, l –31 to 32	
Completeness to θ = 25.0°	99.8 %	
Reflections collected	148110	
Independent reflections	48754 (R_{int} = 0.0743)	
Reflections with $F^2>2\sigma$	30714	
Absorption correction	semi-empirical from equivalents	
Min. and max. transmission	0.39927 and 1.00000	
Structure solution	direct methods	
Refinement method	Full-matrix least-squares on F^2	
Weighting parameters a, b	0.1000, 0.0000	
Data / restraints / parameters	48754 / 262 / 1445	
Final R indices [$F^2>2\sigma$]	R1 = 0.0892, wR2 = 0.2199	
R indices (all data)	R1 = 0.1428, wR2 = 0.2393	
Goodness-of-fit on F^2	1.390	
Largest and mean shift/su	0.001 and 0.000	

$(TBA)_3[(Bu^tO)SnW_5O_{18}]$

Chemical formula (total)	$C_{52.50}H_{118}N_{3.50}O_{19}SnW_5$	
Formula weight	2140.44	
Temperature	150(2) K	
Radiation, wavelength	MoKα, 0.71073 Å	
Crystal system, space group	monoclinic, $P12_1/c1$	
Unit cell parameters	a = 24.8325(6) Å	α = 90°
	b = 33.8943(8) Å	β = 91.325(3)°
	c = 16.9063(4) Å	γ = 90°
Cell volume	14225.9(6) $Å^3$	
Z	8	
Calculated density	1.999 g/cm^3	
Absorption coefficient μ	8.462 mm^{-1}	
F(000)	8236	
Crystal colour and size	colourless, 0.43 × 0.20 × 0.20 mm^3	
Reflections for cell refinement	21781 (θ range 2.9 to 28.6°)	
Data collection method	Xcalibur, Atlas, Gemini ultra	
	thick-slice ω scans	
θ range for data collection	3.0 to 25.0°	
Index ranges	h –29 to 28, k –39 to 40, l –15 to 20	
Completeness to θ = 25.0°	99.8 %	
Reflections collected	79374	
Independent reflections	24983 (R_{int} = 0.0729)	
Reflections with $F^2>2\sigma$	14564	
Absorption correction	semi-empirical from equivalents	
Min. and max. transmission	0.1217 and 0.2824	
Structure solution	direct methods	
Refinement method	Full-matrix least-squares on F^2	
Weighting parameters a, b	0.0485, 22.2258	
Data / restraints / parameters	24983 / 6 / 1470	
Final R indices [$F^2>2\sigma$]	R1 = 0.0561, wR2 = 0.1071	
R indices (all data)	R1 = 0.1168, wR2 = 0.1203	

Goodness-of-fit on F^2	1.020
Largest and mean shift/su	0.001 and 0.000
Largest diff. peak and hole	3.31 and –2.30 e $Å^{-3}$

$(TBA)_3$ [$(PhO)SnW_5O_{18}$]

Chemical formula (total)	$C_{54}H_{113}N_3O_{19}SnW_5$	
Formula weight	2146.41	
Temperature	150(2) K	
Radiation, wavelength	MoKα, 0.71073 Å	
Crystal system, space group	orthorhombic, $P2_12_12_1$	
Unit cell parameters	a = 16.5832(3) Å	α = 90°
	b = 17.7461(3) Å	β = 90°
	c = 23.6843(3) Å	γ = 90°
Cell volume	6969.98(19) $Å^3$	
Z	4	
Calculated density	2.045 g/cm^3	
Absorption coefficient μ	8.636 mm^{-1}	
F(000)	4120	
Crystal colour and size	colourless, 0.34 × 0.30 × 0.30 mm^3	
Reflections for cell refinement	16683 (θ range 2.8 to 28.5°)	
Data collection method	Oxford Diffraction Gemini A Ultra diffractometer ω scans	
θ range for data collection	2.8 to 28.6°	
Index ranges	h –22 to 22, k –23 to 18, l –31 to 24	
Completeness to θ = 28.6°	87.9 %	
Reflections collected	42652	
Independent reflections	14595 (R_{int} = 0.0521)	
Reflections with $F^2>2\sigma$	11100	
Absorption correction	semi-empirical from equivalents	
Min. and max. transmission	0.1573 and 0.1815	
Structure solution	direct methods	
Refinement method	Full-matrix least-squares on F^2	
Weighting parameters a, b	0.0070, 0.0000	
Data / restraints / parameters	14595 / 20 / 750	
Final R indices [$F^2>2\sigma$]	R1 = 0.0317, wR2 = 0.0414	
R indices (all data)	R1 = 0.0531, wR2 = 0.0439	

Goodness-of-fit on F^2	0.848
Absolute structure parameter	0.475(5)
Largest and mean shift/su	0.002 and 0.000
Largest diff. peak and hole	1.11 and −1.26 e $Å^{-3}$

$(TBA)_3$ [(*p*-CH_3-C_6H_4O)SnW_5O_{18}]

Chemical formula (total)	$C_{55}H_{115}N_3O_{19}SnW_5$	
Formula weight	2160.44	
Temperature	150(2) K	
Radiation, wavelength	MoKα, 0.71073 Å	
Crystal system, space group	orthorhombic, Pnma	
Unit cell parameters	a = 23.7204(3) Å	α = 90°
	b = 17.1487(3) Å	β = 90°
	c = 17.1872(2) Å	γ = 90°
Cell volume	6991.31(17) $Å^3$	
Z	4	
Calculated density	2.053 g/cm^3	
Absorption coefficient μ	8.610 mm^{-1}	
F(000)	4152	
Reflections for cell refinement	17370 (θ range 2.8 to 28.6°)	
Data collection method	Xcalibur, Atlas, Gemini ultra	
	thick-slice ω scans	
θ range for data collection	2.8 to 28.6°	
Index ranges	h –30 to 31, k –21 to 21, l –21 to 21	
Completeness to θ = 28.6°	89.8 %	
Reflections collected	41634	
Independent reflections	8322 (R_{int} = 0.0461)	
Reflections with $F^2>2\sigma$	5756	
Absorption correction	semi-empirical from equivalents	
Min. and max. transmission	0.31465 and 1.00000	
Structure solution	direct methods	
Refinement method	Full-matrix least-squares on F^2	
Weighting parameters a, b	0.0334, 0.0000	
Data / restraints / parameters	8322 / 271 / 458	
Final R indices [$F^2>2\sigma$]	R1 = 0.0348, wR2 = 0.0674	
R indices (all data)	R1 = 0.0653, wR2 = 0.0714	
Goodness-of-fit on F^2	1.026	

Largest and mean shift/su	0.002 and 0.000
Largest diff. peak and hole	1.68 and –2.08 e $Å^{-3}$

$(TBA)_3$ [(*p*-$(CH_3)_3C$-C_6H_4O-SnW_5O_{18}]

Chemical formula (total)	$C_{58}H_{121}N_3O_{19}SnW_5$	
Formula weight	2202.52	
Temperature	150(2) K	
Radiation, wavelength	MoKα, 0.71073 Å	
Crystal system, space group	orthorhombic, $Pna2_1$	
Unit cell parameters	a = 24.9650(5) Å	α = 90°
	b = 16.9285(3) Å	β = 90°
	c = 17.7849(4) Å	γ = 90°
Cell volume	7516.3(3) $Å^3$	
Z	4	
Calculated density	1.946 g/cm^3	
Absorption coefficient μ	8.011 mm^{-1}	
F(000)	4248	
Crystal colour and size	colourless, 0.32 × 0.30 × 0.30 mm^3	
Reflections for cell refinement	30618 (θ range 2.9 to 28.5°)	
Data collection method	Xcalibur, Atlas, Gemini ultra	
	thick-slice ω scans	
θ range for data collection	2.9 to 26.0°	
Index ranges	h –26 to 30, k –19 to 20, l –18 to 21	
Completeness to θ = 26.0°	99.4 %	
Reflections collected	53971	
Independent reflections	13452 (R_{int} = 0.0346)	
Reflections with $F^2>2\sigma$	11639	
Absorption correction	semi-empirical from equivalents	
Min. and max. transmission	0.1837 and 0.1973	
Structure solution	direct methods	
Refinement method	Full-matrix least-squares on F^2	
Weighting parameters a, b	0.0316, 50.0316	
Data / restraints / parameters	13452 / 389 / 775	
Final R indices [$F^2>2\sigma$]	R1 = 0.0340, wR2 = 0.0758	
R indices (all data)	R1 = 0.0445, wR2 = 0.0788	

Goodness-of-fit on F^2	1.031
Absolute structure parameter	0.030(10)
Largest and mean shift/su	0.026 and 0.002
Largest diff. peak and hole	1.38 and –1.26 e $Å^{-3}$

$(TBA)_3$ [(*p*-OH -C_6H_4O-SnW_5O_{18}]

Chemical formula (total)	$C_{54}H_{111}N_3O_{20}SnW_5$	
Formula weight	2160.40	
Temperature	293(2) K	
Radiation, wavelength	MoKα, 0.71073 Å	
Crystal system, space group	monoclinic, C2/c	
Unit cell parameters	a = 30.9218(11) Å	α = 90°
	b = 15.1562(5) Å	β = 125.800(3)°
	c = 18.4269(6) Å	γ = 90°
Cell volume	7004.3(4) $Å^3$	
Z	4	
Calculated density	2.049 g/cm^3	
Absorption coefficient μ	8.595 mm^{-1}	
F(000)	4144	
Reflections for cell refinement	10683 (θ range 2.9 to 28.5°)	
Data collection method	Xcalibur, Atlas, Gemini ultra	
	thick-slice ω scans	
θ range for data collection	3.0 to 28.5°	
Index ranges	h –40 to 41, k –17 to 20, l –23 to 22	
Completeness to θ = 26.0°	97.8 %	
Reflections collected	23089	
Independent reflections	7448 (R_{int} = 0.0552)	
Reflections with $F^2>2\sigma$	3951	
Absorption correction	semi-empirical from equivalents	
Min. and max. transmission	0.49033 and 1.00000	
Structure solution	direct methods	
Refinement method	Full-matrix least-squares on F^2	
Weighting parameters a, b	0.0999, 166.5487	
Data / restraints / parameters	7448 / 26 / 321	
Final R indices [$F^2>2\sigma$]	R1 = 0.0823, wR2 = 0.1995	
R indices (all data)	R1 = 0.1495, wR2 = 0.2300	
Goodness-of-fit on F^2	1.037	

Largest and mean shift/su	0.015 and 0.001
Largest diff. peak and hole	2.88 and –2.46 e $Å^{-3}$

$(TBA)_3$ [(*m* -OH -C_6H_4O-SnW_5O_{18}]

Chemical formula (total)	$C_{54}H_{113}N_3O_{20}SnW_5$	
Formula weight	2162.41	
Temperature	150(2) K	
Radiation, wavelength	MoKα, 0.71073 Å	
Crystal system, space group	monoclinic, C12/c1	
Unit cell parameters	a = 30.594(4) Å	α = 90°
	b = 15.4851(10) Å	β = 125.17(2)°
	c = 18.135(2) Å	γ = 90°
Cell volume	7023.5(14) $Å^3$	
Z	4	
Calculated density	2.045 g/cm^3	
Absorption coefficient μ	8.572 mm^{-1}	
F(000)	4152	
Crystal colour and size	colourless, 0.50 × 0.40 × 0.40 mm^3	
Reflections for cell refinement	7737 (θ range 2.8 to 29.5°)	
Data collection method	Oxford Diffraction Gemini A Ultra diffractometer thick-slice ω scans	
θ range for data collection	2.8 to 29.6°	
Index ranges	h –38 to 37, k –19 to 21, l –24 to 20	
Completeness to θ = 26.0°	97.8 %	
Reflections collected	29274	
Independent reflections	8498 (R_{int} = 0.0662)	
Reflections with $F^2>2\sigma$	4099	
Absorption correction	semi-empirical from equivalents	
Min. and max. transmission	0.0995 and 0.1308	
Structure solution	direct methods	
Refinement method	Full-matrix least-squares on F^2	
Weighting parameters a, b	0.0756, 0.0000	
Data / restraints / parameters	8498 / 303 / 439	
Final R indices [$F^2>2\sigma$]	R1 = 0.0530, wR2 = 0.1254	
R indices (all data)	R1 = 0.1297, wR2 = 0.1483	

Goodness-of-fit on F^2	0.937
Largest and mean shift/su	0.004 and 0.000
Largest diff. peak and hole	2.52 and –1.76 e $Å^{-3}$

$(TBA)_3$ [(2-CHO -C_6H_4O-SnW_5O_{18}]

Chemical formula (total)	$C_{55}H_{113}N_3O_{20}SnW_5$	
Formula weight	2174.42	
Temperature	293(2) K	
Radiation, wavelength	MoKα, 0.71073 Å	
Crystal system, space group	orthorhombic, Pnma	
Unit cell parameters	a = 23.4632(8) Å	α = 90°
	b = 17.1341(7) Å	β = 90°
	c = 17.4416(5) Å	γ = 90°
Cell volume	7011.9(4) $Å^3$	
Z	4	
Calculated density	2.060 g/cm^3	
Absorption coefficient μ	8.587 mm^{-1}	
F(000)	4176	
Reflections for cell refinement	14949 (θ range 2.9 to 29.6°)	
Data collection method	Xcalibur, Atlas, Gemini ultra	
	thick-slice ω scans	
θ range for data collection	2.9 to 25.0°	
Index ranges	h –27 to 27, k –20 to 20, l –20 to 20	
Completeness to θ = 25.0°	99.8 %	
Reflections collected	49058	
Independent reflections	6390 (R_{int} = 0.1788)	
Reflections with $F^2>2\sigma$	5432	
Absorption correction	semi-empirical from equivalents	
Min. and max. transmission	0.41108 and 1.00000	
Structure solution	direct methods	
Refinement method	Full-matrix least-squares on F^2	
Weighting parameters a, b	0.0000, 1194.7222	
Data / restraints / parameters	6390 / 217 / 429	
Final R indices [$F^2>2\sigma$]	R1 = 0.1089, wR2 = 0.2265	
R indices (all data)	R1 = 0.1232, wR2 = 0.2371	
Goodness-of-fit on F^2	1.120	

Largest and mean shift/su	0.001 and 0.000
Largest diff. peak and hole	3.70 and –6.39 e $Å^{-3}$

$(TBA)_3$ [$(Me_3SiO\text{-}SnW_5O_{18}$]

Chemical formula (total)	$C_{104}H_{237}N_9O_{36}Si_2Sn_2W_{10}$	
Formula weight	4322.09	
Temperature	150(2) K	
Radiation, wavelength	MoKα, 0.71073 Å	
Crystal system, space group	monoclinic, $P12_1/c1$	
Unit cell parameters	a = 24.9945(7) Å	α = 90°
	b = 33.9960(12) Å	β = 91.299(3)°
	c = 16.8769(4) Å	γ = 90°
Cell volume	14336.8(8) $Å^3$	
Z	4	
Calculated density	2.002 g/cm^3	
Absorption coefficient μ	8.413 mm^{-1}	
F(000)	8320	
Crystal colour and size	colourless, 0.32 × 0.20 × 0.20 mm^3	
Reflections for cell refinement	22013 (θ range 2.8 to 28.6°)	
Data collection method	Oxford Diffraction Gemini A Ultra diffractometer thick-slice ω scans	
θ range for data collection	2.8 to 25.0°	
Index ranges	h –25 to 29, k –34 to 40, l –20 to 20	
Completeness to θ = 25.0°	99.7 %	
Reflections collected	72430	
Independent reflections	25173 (R_{int} = 0.0953)	
Reflections with $F^2>2\sigma$	14673	
Absorption correction	semi-empirical from equivalents	
Min. and max. transmission	0.1738 and 0.2840	
Structure solution	direct methods	
Refinement method	Full-matrix least-squares on F^2	
Weighting parameters a, b	0.0719, 671.6777	
Data / restraints / parameters	25173 / 0 / 1484	
Final R indices [$F^2>2\sigma$]	R1 = 0.0789, wR2 = 0.1792	
R indices (all data)	R1 = 0.1450, wR2 = 0.2080	

Goodness-of-fit on F^2	1.026
Largest and mean shift/su	0.352 and 0.002
Largest diff. peak and hole	4.37 and –2.68 e $Å^{-3}$

$(TBA)_4[(^iPr_2NH_2)_2(\mu\text{-}O)(SnW_5O_{18})_2]$

Chemical formula (total)	$C_{80}H_{176}N_8O_{37}Sn_2W_{10}$	
Formula weight	3918.17	
Temperature	150(2) K	
Radiation, wavelength	MoKα, 0.71073 Å	
Crystal system, space group	monoclinic, $P12_1/n1$	
Unit cell parameters	a = 25.548(2) Å	α = 90°
	b = 18.6365(10) Å	β = 108.982(6)°
	c = 27.6337(13) Å	γ = 90°
Cell volume	12441.4(14) $Å^3$	
Z	4	
Calculated density	2.092 g/cm^3	
Absorption coefficient μ	9.665 mm^{-1}	
F(000)	7392	
Crystal colour and size	colourless, 0.50 × 0.40 × 0.40 mm^3	
Reflections for cell refinement	16973 (θ range 2.5 to 26.8°)	
Data collection method	Xcalibur, Atlas, Gemini ultra	
	thick-slice ω scans	
θ range for data collection	2.5 to 26.8°	
Index ranges	h –21 to 31, k –23 to 22, l –34 to 25	
Completeness to θ = 26.0°	95.1 %	
Reflections collected	44901	
Independent reflections	23641 (R_{int} = 0.0410)	
Reflections with $F^2>2\sigma$	18175	
Absorption correction	semi-empirical from equivalents	
Min. and max. transmission	0.0857 and 0.1130	
Structure solution	direct methods	
Refinement method	Full-matrix least-squares on F^2	
Weighting parameters a, b	0.0439, 141.5065	
Data / restraints / parameters	23641 / 0 / 1260	
Final R indices [$F^2>2\sigma$]	R1 = 0.0461, wR2 = 0.1064	
R indices (all data)	R1 = 0.0711, wR2 = 0.1224	

Goodness-of-fit on F^2	1.078
Largest and mean shift/su	0.017 and 0.000
Largest diff. peak and hole	2.68 and –2.86 e $Å^{-3}$